TECHNISCHE UNIVERSITÄT WIEN
Vienna | Austria

Diplomarbeit

Mechanistic investigations of chain transfer reagents

performed at

Institute of Applied Synthetic Chemistry

Technische Universität Wien

under the supervision of

Univ. Prof. Dipl.-Ing. Dr. techn. Robert Liska

and

Univ. Ass. Dipl.-Ing. Dr. techn. Christian Gorsche

by

Markus Kury

Karlsdorf 29, 9851 Lieserbrücke

Danksagungen

Zuallererst möchte ich mich bei meinem Professor Robert bedanken. Danke, für die vielen Möglichkeiten, die du mir in den letzten Jahren in deiner Arbeitsgruppe gegeben hast. Beginnend mit der Bachelorarbeit, über Tutorendienste im Otech Labor, den Besuch von Konferenzen bis hin zur Verfassung meiner Diplomarbeit werde ich immer gerne auf diese schönen und lehrreichen Jahre zurückblicken. Danke, für die großartige Betreuung und das super Arbeitsklima.

Ein besonderer Dank gilt auch meinem Zweitbetreuer Christian, der immer für mich da war, wenn ich Fragen hatte. Danke, für deine Unterstützung, deine Geduld und die ausgezeichnete Betreuung.

Weiters möchte ich mich bei meinem Bacheloranten Jakob, meiner Wahlpraktikantin Maria und bei Markus bedanken, die mir bei meiner praktischen Laborarbeit tatkräftig unter die Arme gegriffen und somit meine Arbeit ungemein erleichtert haben.

Danke auch an Anastasiya und Thomas, die für mich zahlreiche Maldi-TOF-MS Messungen und mechanische Tests durchgeführt haben und mir ihre Expertise in ihren Fachgebieten zu Verfügung gestellt haben.

Außerdem möchte ich mich auch bei Konzi und Mia für die vielen Diskussionen und für ihre Ratschläge zu vielen verschiedenen Themen bedanken.

Besonders möchte ich mich bei der gesamten Arbeitsgruppe MC bedanken. Danke für eure Unterstützung, für das enorm gute Arbeitsklima und für viele wirklich unvergessliche Momente.

Zwei besonderen Menschen, denen ich danken möchte, sind mein lieber Opa und meine liebe Oma, die meinen Studienabschluss leider nicht mehr miterleben kann. Danke, dass ihr mich Zeit meines Lebens immer unterstützt und mir immer ein sicheres Heim geboten habt.

Mein letzter Dank gebührt meiner Schwester Michi, meiner Mama und meinem Papa. Danke, dass ihr mich immer unterstützt und gefördert habt und dass ihr es mir ermöglicht habt mein Studium abzuschließen.

Kurzfassung

Photopolymere werden heutzutage in vielen Industriebereichen eingesetzt. Typische Anwendungen sind Beschichtungen, Tinten, Klebstoffe, Fotolacke, medizinische Anwendungen (z.B. Biomaterialien und Dentalfüllungen), und Stereolithographie. Die Herstellung durch freie radikalische Photopolymerisation führt zu Vorteilen wie zum Beispiel schnelles Aushärten, die Möglichkeit 3D Sturkturen drucken zu können, und gute mechanische Eigenschaften hinsichlich Härte, Steifheit, und Wärmeformbeständigkeit. Trotzdem führt freie radikalische Polymerisation, durch ihren unkontrollierten Mechanimus, zu Materialien niedriger Schlagzähigkeit, die durch polymerisationsinduzierte Schrumpfspannung und inhomogene Netzwerkarchitekturen hervorgerufen werden. Diese Nachteile führen zur Nachfrage an Zusatzstoffe, die eine Regulierung der Netzwerkstrukturen ermöglichen.

Der literaturbekannte Stand der Technik zur Regulierung von Polymernetzwerken ist „Thiol-ene“ Chemie. Thiole agieren als Kettentransferreagenzien, welche die kinetische Kettenläge kürzen und zu einem homogeneren Polymernetzwerk beitragen. Dennoch wird der Einsatz von Thiol-ene Chemie durch die niedrige Lagerstabilität der Formulierungen, dem starken Geruch und der Entstehung von flexiblen Thioetherbrücken limitiert. Kürzlich wurde eine neue Technik „Addition-fragmentation chain transfer“ (AFCT) für Photopolymere publiziert. AFCT Reagenzien basierend auf β-Allylsulfonen und Vinylsulfonatestern in Methacrylaten zeigen ähnliche Verbesserungen bezüglich Netzwerkregulierung und Schlagzähigkeit, wie Thiole. Vorteilhaft jedoch sind die deutlich verbesserte Lagerbeständigkeit, die vernachlässigbare Geruchsbelästigung, sowie die Erhaltung eines hohen E-Moduls.

Diese Arbeit beinhaltet eine umfangreiche Studie zur Untersuchung der Regulierungs-fähigkeit von monofunktionellen AFCT Reagenzien mit monofunktionellen Monomeren auf Basis von Methacrylaten, Vinylestern und Acrylaten, welche anhand verschiedener Analysenmethoden (Photoreaktor, GPC, Maldi-TOF-MS) gemessen wurden. Nachdem sich Vinylsulfonatester als vielversprechendes Kettentransferreagenz zur Regulierung von Acrylaten hervorgetan hatten, wurde eine ausführliche Studie über die Netzwerkregulierung von Divinylsulfonatestern in Diacrylaten mit Hilfe von RT-NIR Photorheologie, DMTA, Zugversuchen, Dynstat Schlagzähigkeitsversuchen, Lagerbeständigkeitstestungen, und Quellexperimenten durchgeführt. Weiters wurde ein Dithiol als Vergleichsketten-transferreagenz herangezogen, um die Vorteile von AFCT Regulierung aufzuzeigen. Als Resultat konnte gezeigt werden, dass AFCT regulierte Diacrylatnetzwerke zu homogeneren Netzwerkarchitekturen führen, welche im Besonderen verbesserte mechanische Eigenschaften z.B. erhöhte Schlagzähigkeit ohne E-Modulverlust bei Raumtemperatur aufweisen.

Abstract

Nowadays, photopolymers are widely used in industries. Typical applications of photopolymers are coatings, inks, adhesives, photoresists, medical applications (e.g. biomaterials and dental fillings), and stereolithography. Advantages of free radical photopolymerization are economically friendly processing (ambient conditions), rapid curing, the ability of 3D structuring, and beneficial mechanical properties such as high hardness, rigidity, and heat deflection temperature. Nevertheless, free radical photopolymerization suffers from its uncontrolled curing mechanism yielding materials with low toughness due to polymerization induced shrinkage stress and inhomogeneous network architectures. These drawbacks demonstrate the need for additives, which enable the regulation of the final network structure.

The state-of-the-art approach in literature for regulating the radical network formation is thiol-ene chemistry. Thiols act as chain-transfer reagents, shorten the kinetic chain length, and therefore lead to more homogeneous networks. However, low storage stability, strong odor, and the formation of flexible thio-ether bridges leading to soft materials represent limitations of thiol-ene chemistry. Another new reported technique is addition-fragmentation chain transfer (AFCT). β-Allyl sulfones and vinyl sulfonate esters as AFCT reagents in methacrylic resins are able to show similar improvements in terms of network regulation and toughness. Beneficially, storage stability is much improved, odor pollution is negligible, and modulus at room temperature is not sacrificed. Moreover, the exchange of activating and leaving group makes it possible to tune AFCT reagents towards certain monomers.

An extensive study was launched to investigate the regulating abilities of different monofunctional AFCT reagents (β-allyl sulfones and vinyl sulfonate esters) with monofunctiontal methacrylates, vinyl esters, and acrylates by means of photoreactor, GPC, and Maldi-TOF-MS measurements. After discovering vinyl sulfonate esters to represent the most promising candidate for acrylate regulation, a detailed study about network regulation of divinyl sulfonate esters in diacrylate-based resins was conducted including RT-NIR photorheology, DMTA, tensile test, Dynstat impact resistance test, storage stability, and swellability. Besides that, a dithiol was used to compare and highlight the benefits of AFCT regulation. As a result, AFCT-regulated diacrylate networks exhibit more homogeneous networks coming along with improved mechanical properties like increased toughness without losing modulus at room temperature.

Table of Content

Introduction

In the last decades photopolymers gained in importance.[1-2] Nowadays, many industrial applications are inconceivable without the concept of radical photopolymerization. Major fields of application are:

- Coatings[3]
- Inks[4]
- Adhesives[5]
- Photoresists[6]
- Biomaterials[7-10]
- Dental fillings[11-12]
- Stereolithography[9, 13-14]

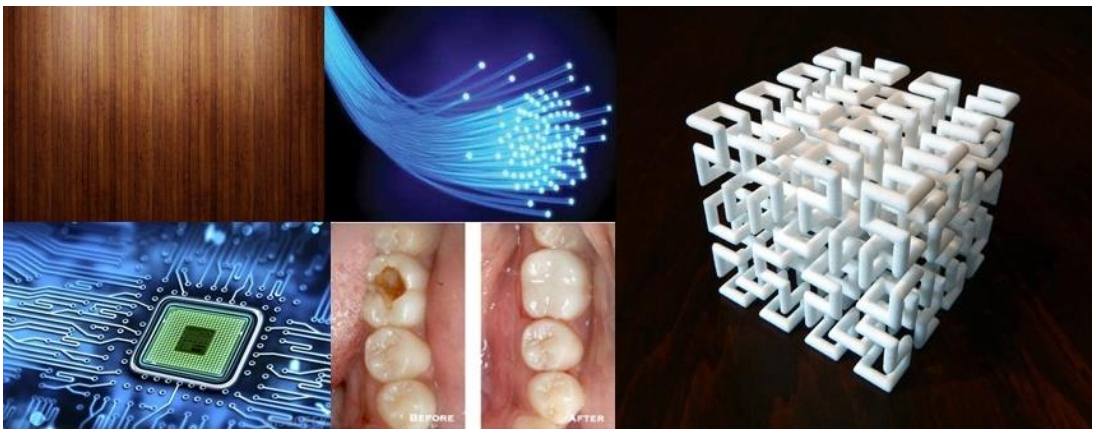

Figure 1: Application of photopolymers as wood coatings[15], glass fiber coatings[16], 3D structures[17], photoresists[18] and dental fillings[19]

The advantages of radical photopolymerization are the rapid curing speed, the solvent-free curing conditions, low production and energy costs, and beneficial mechanical properties like high hardness, rigidity, and heat deflection temperature.[20-22] Drawbacks are higher material costs than e.g. alkyds, polyesters or epoxies and high acquisition costs for UV curing systems.

Generally, photopolymerizable resins consist of a photoinitiator (**PI**), oligomers, reactive diluents, and additional additives depending on the application.[23] The reaction mechanism itself is a free radical polymerization (chain growth reaction), which can be described in three steps (Figure 2):

The first step is an initiation step ①. During this step radicals are formed, which then start a chain growth reaction. After the initiation, the propagation ② takes place. In this step monomer units with reactive double bonds (**DB**s) are rapidly added to the chain. Finally, the

free radical polymerization is stopped in the termination step ③, where two radicals (either from a growing chain or initiator radicals) react by combination (a) or disproportionation (b).[24]

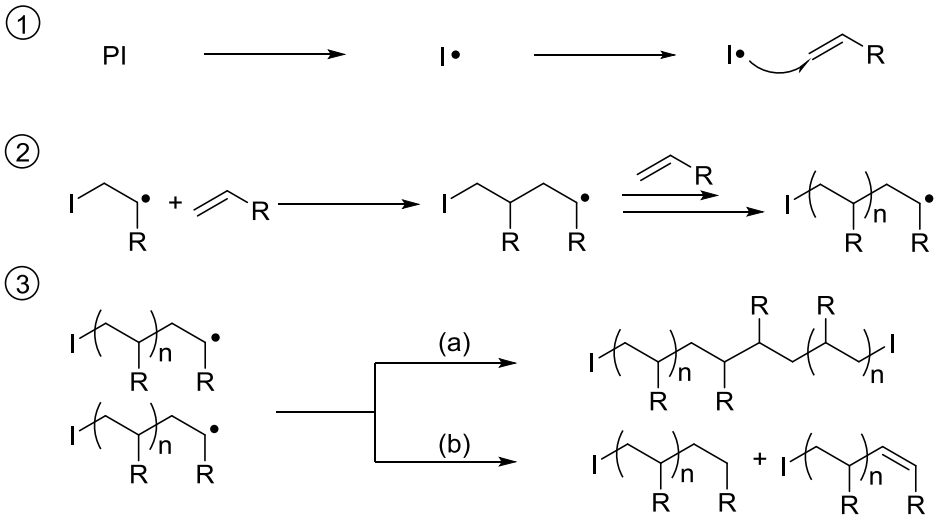

Figure 2: Reaction scheme of a free radical polymerization including ① initiation, ② propagation, and ③ termination ((a) combination and (b) disproportionation)

For enabling photopolymerization, the first crucial prerequisite is a PI. When irradiated with light in the UV/Vis range, a PI generates radicals, which can then start the polymerization process. Basically, PIs can be classified into[25]:

- Type I PI
- Type II PI

Typical type I PIs are hydroxy alkyl ketones (e.g. Irgacure 2959), benzoyl phosphine oxides (e.g. BAPO), dialkoxyacetophenones or benzilketals.[25] A very efficient type I PI used in fillings for dental application is germanium-based Ivocerin.[26] As can be seen in Figure 3, the benzoyl moiety is the most commonly used for type I PIs.

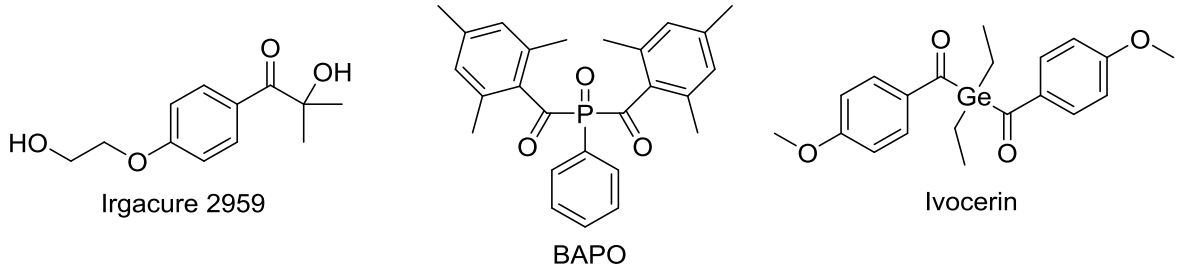

Figure 3: Variety of type I PIs: Irgacure 2959, BAPO (Irgacure 819), and Ivocerin

One of the most important commercially available type II PI system is campherquinone/ dimethylaminobenzoic acid ethyl ether (CQ/DMAB). This initiator system is also applied in curing dental composites. Moreover, benzophenone derivatives together with tertiary amines can be used.[25]

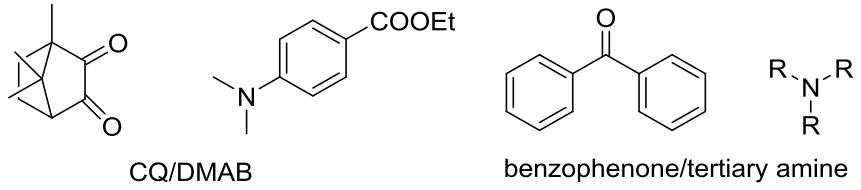

Figure 4: Typical type II PIs: CQ/DMAB and benzophenone/tertiary amine

Generally, the difference between type I and type II PIs is the chemical mechanism of radical formation. Type I PIs react to UV/Vis irradiation with a unimolecular α-cleavage (fragmentation) of the chemical bond next to the carbonyl carbon, while type II PIs need a coinitiator to undergo a bimolecular reaction in the form of an electron-proton transfer for providing radicals.

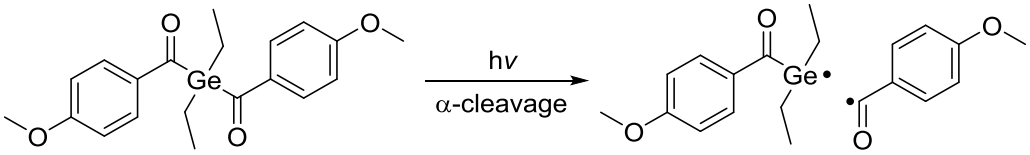

Figure 5: Decay mechanism of type I PI Ivocerin

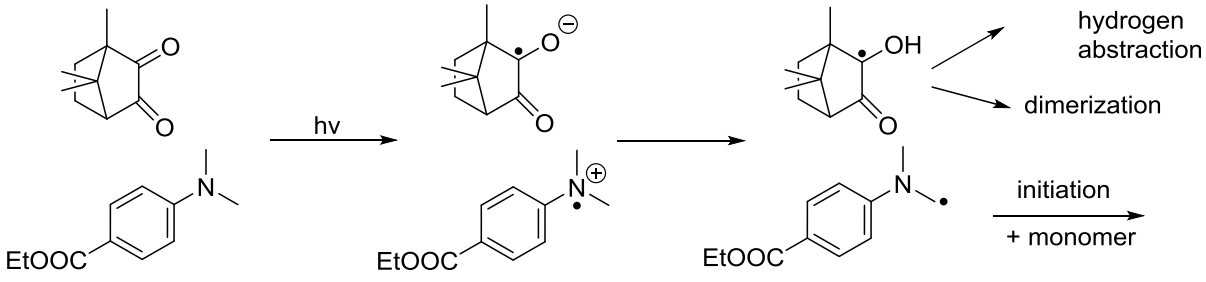

Figure 6: Mechanism of radical formation of type II PI CQ/DMAB

Type I PIs are characterized by a higher reactivity because of the formation of two radicals, which can initiate the polymerization. Hence, a lower concentration of type I PIs is necessary. On the other hand, type II PIs are less reactive but cheaper and less sensitive towards oxygen inhibition.[27-28]

After successful initiation, the monomers are attacked by the radical species starting polymerization. Depending on the functionality of the monomers, chains (monofunctional monomers) or networks (multifunctional monomers) can be formed.

In radical photopolymerization especially two types of monomers are applied[29]:

- Acrylates (**ACs**)
- Methacrylates (**MAs**)

AC-based monomers are able to undergo radical polymerization at high reaction rates even at room temperature and represent thus ideal candidates for photopolymerization.[30-31] Typical photo-curable AC resins consisting of multifunctional monomers can be seen in Figure 7 below.

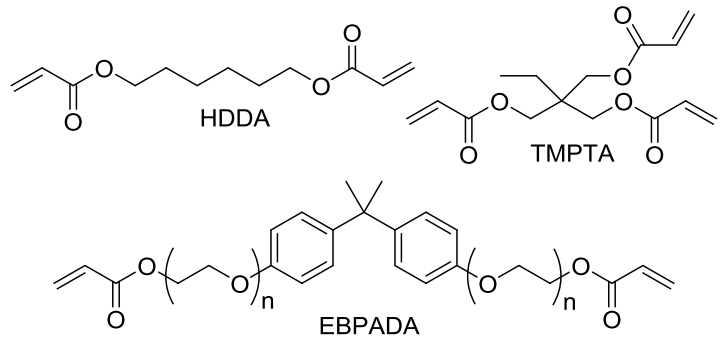

Figure 7: Typical AC monomers in photopolymerization like 1,6-hexanediol diacrylate (HDDA), trimethylolpropane triacrylate (TMPTA) or ethoxylated bisphenol-A diacrylate (EBPADA)

Compared with ACs, MAs suffer from lower reactivity. However, their much lower toxicity and good heat deflection temperature make them perfectly applicable for dental resins.[11] Some examples for compounds used in dental restorative processes are shown in Figure 8.

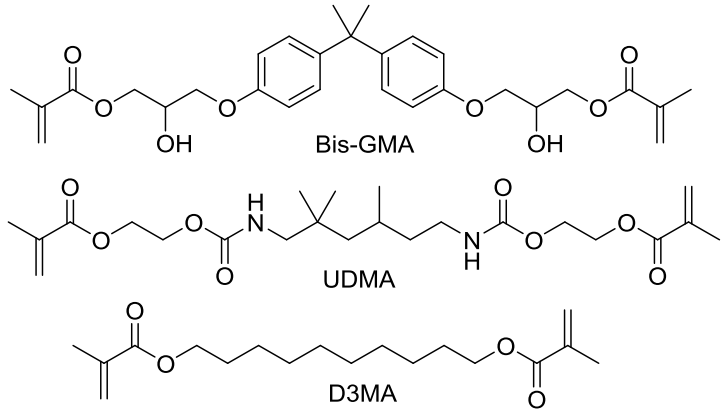

Figure 8: Typical MA compounds used in dental applications like bisphenol A-glycidyl methacrylate (Bis-GMA), urethane dimethacrylate (UDMA) or 1,10-decanediol dimethacrylate (D3MA)[11]

Another advantage of ACs and MAs is their easy synthesis from alcohols with (meth)acrylic acid.[29]

A rather new approach in radical photopolymerization is the utilization of vinyl esters (**VEs**) as a monomeric compound. Concerning reactivity, VEs are in between ACs and MAs, but they show less toxic behavior and can therefore be assumed to be future candidates for materials in medicine.[8-9, 32] Unfortunately, the availability of commercial VEs is limited.

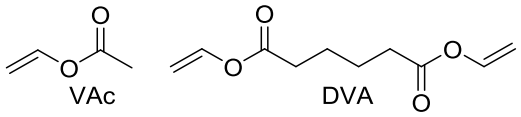

Figure 9: Vinyl acetate (VAc) is the most important representative of VEs and divinyl adipate (DVA) is the only commercially available multifunctional VE

Nowadays, the most important application of VEs is the polymerization of poly vinyl acetate (**PVA**). PVA is used as binder for adhesives and dyes. Aside from that, it can be hydrolyzed to give poly vinyl alcohol, which finds widespread utilization in industry and is an FDA-approved chemical.

Network architecture

Photopolymerization of multifunctional monomers is a very complex process. The polymer network architecture of the final polymer, thus its mechanical and physical properties depend on the nature of monomers, the PI concentration, and the chosen curing conditions.

Fundamentally, free radical polymerization is a chain growth reaction resulting in rather long kinetic chain lengths.[33] This means that rather long polymer chains are generated at low DB conversions (**DBC**s) leading to early gelation. At the gel point the resin system changes its aggregate state from liquid to solid. Before reaching the gel point, the resin is able to flow due to its liquid nature and therefore mechanical energy arising from polymerization can be dissipated. When becoming solid, the limited mobility of the chains leads to shrinkage causing stress in the cured material.[34] Moreover, a decrease of the average kinetic chain length can be observed. This decrease can be explained by the increase of radical concentration that can be linked to the reduction of termination reactions arising from limited mobility of active growing polymer chains in the solid gel. The impact on the polymer architecture is a high irregularity in regard to the distances of crosslinks. As a result, the inhomogeneous networks formed by photopolymerization exhibit very brittle behavior and poor toughness.[35]

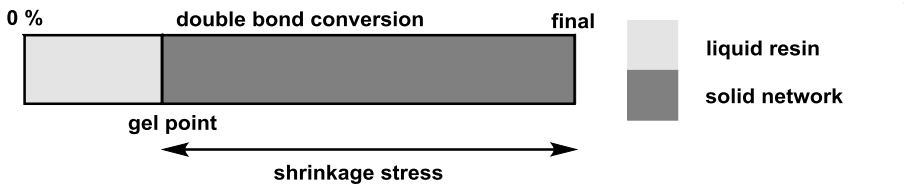

Figure 10: Connection between gel point and shrinkage stress

These problems can be attributed to the uncontrolled curing mechanism of free radical photopolymerization leading to inhomogeneous and strongly crosslinked networks.[36] For epoxy resins similar problems have been reported. To overcome these issues, several different strategies were developed. By adding rubber[37], block copolymers[38-39], nano particles[40] or core shell particles[41], the mechanical properties significantly improved. Unfortunately, these approaches may show limitations when applied to radical photopolymerization because of occurring phase separation[42]. In addition, the viscosity of the resins increased, mechanical properties like hardness and stiffness were sacrificed and adhesion between polymer matrix and added particles was poor.

Mechanical properties can also be improved by adding polar monomers like urethane groups that can build hydrogen bridges.[43] Another possibility is to add monofunctional monomers that lower the viscosity delaying gelation.[44]

However, they are not able to prevent the formation of inhomogeneous networks. Furthermore, radical ring-opening polymerization was reported to be an appropriate strategy to decrease shrinkage stress, since cyclic monomers show a smaller shrinkage volume than vinyl monomers.[45]

A strategy to tackle shrinkage stress and low toughness is the implementation of chain transfer reagents (**CTA**s). In radical polymerization, chain transfer describes a process in which the active radical of a growing polymer chain is transferred by a CTA to start a new polymer chain. For determining the ability of undergoing a chain transfer, the chain transfer constant ($\mathbf{C_{tr}} = k_{tr}/k_p$) can be adducted. The C_{tr} describes the ratio between the rate constant of the chain transfer reaction ($\mathbf{k_{tr}}$) and the rate constant of the propagation reaction ($\mathbf{k_p}$) that are depending on many different influences such as monomer reactivity, functionality of the CTA, reaction temperature, radical initiation, solvent, and conversion.

CTAs were early used in polymerization to lower the average molecular weight of linear polymers. Especially thiols were used.[46] Thiols possess a weak S-H bond, so the hydrogen can easily be abstracted. This explains the high reactivity towards macroradicals. Moreover, the generated thiyl radical is reactive enough to reinitiate a new growing chain without retarding polymerization.[47]

At the present day, the most significant and versatile technique for regulating free radical photopolymerization is thiol-ene chemistry.[48-50] Thiols are known to be potent hydrogen donors and to form very reactive thiyl radicals, which react with DBs in an anti-Markownikov manner.

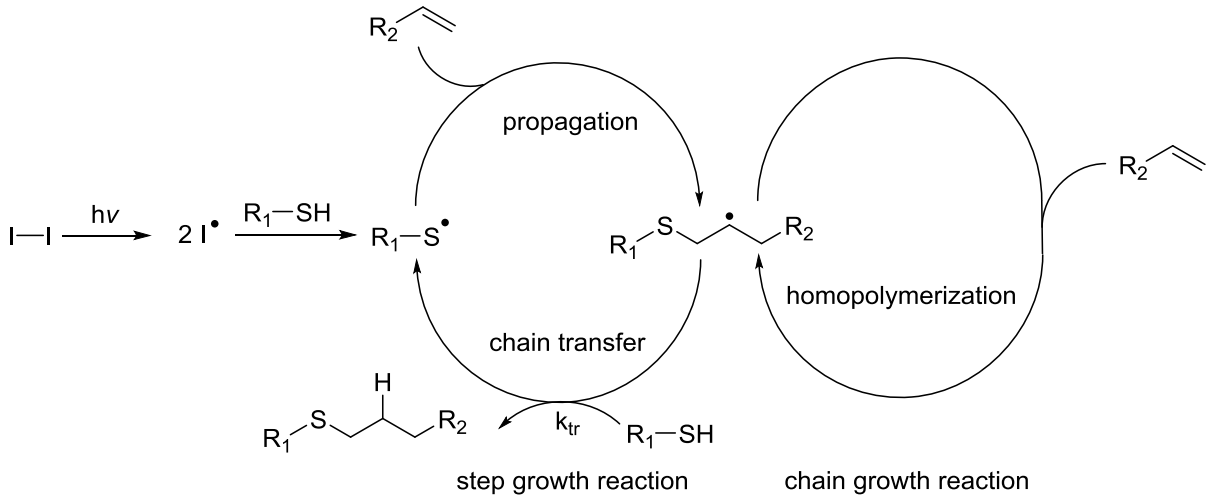

Figure 11: Thiol-ene mixed step growth/chain growth mechanism

The rate constant of chain transfer is highest for electron-rich unsaturated carbon-carbon bonds like norbornenes or vinyl ether and much lower for ACs or MAs.

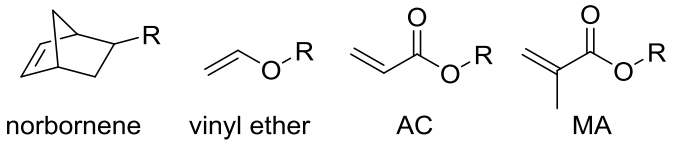

Figure 12: Electron-rich ene compounds (norbornene and vinyl ether) and ene compounds with low electron density (AC and MA)

Table 1: Chain transfer constants for different ene compounds

vinyl compound	C_{tr}
norbornene[51]	1.00
vinyl ether[51]	0.83
methacrylate[52]	0.26
acrylate[51]	0.08

As can be seen in Figure 11[50], electron density at the ene also influences the thiol-ene mechanism. While electron-rich enes like norbornenes and vinyl ethers undergo step growth reaction, electron-poor enes like ACs and MAs tend to a mixed step growth/ chain growth mechanism. For MA and AC the given C_{tr}s mean that propagation is preferred over chain transfer. Thus, active polymer chains are formed, before being terminated by hydrogen

abstraction from a thiol and the generated thiyl radical can initiate a new chain. In comparison with homopolymerization this mechanism results in shorter kinetic chain lengths.

When applied to multifunctional thiol-ene systems these shorter kinetic chain lengths are responsible for shifting the gel point to higher DBC, resulting in more uniform crosslinks, reduced shrinkage stress, and higher final DBC. Mechanical properties of the material like a sharper glass transition and higher impact resistance can be obtained. On the other hand, the formed thio-ether bridges reduce the hardness of the material that can be attributed to their flexibility.

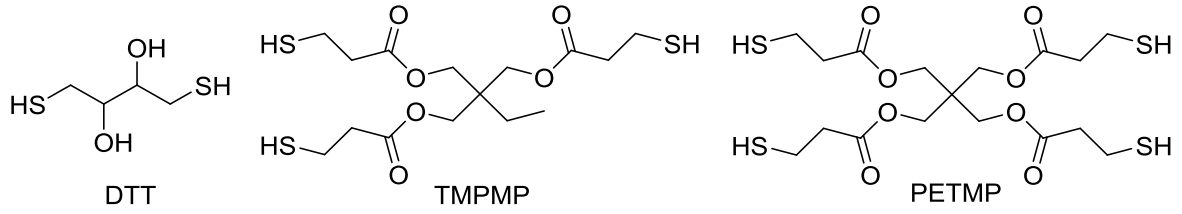

Figure 13: Typical thiols used in thiol-ene photopolymerization like water-soluble dithiothreitol (DTT), trimethylolpropane tris(3-mercaptopropionate) (TMPMP) and pentaerythritol tetrakis(3-mercapto-propionate) (PETMP)

Another advantage of thiol-ene chemistry is that it provides a strategy to reduce oxygen inhibition.[27, 46, 53] In homopolymerization, the reaction with oxygen radicals is preferred over the propagation reaction. Unfortunately, the so formed peroxy radical is not reactive enough to propagate the polymerization reaction leading to lower DBC and tacky surfaces. Regarding thiol-ene chemistry, the propagating polymer chain is also prone to add an oxygen diradical. Unlike homopolymerization, the formed peroxy radical can now abstract the hydrogen of the thiol creating a more reactive thiyl radical that can reinitiate the polymerization.

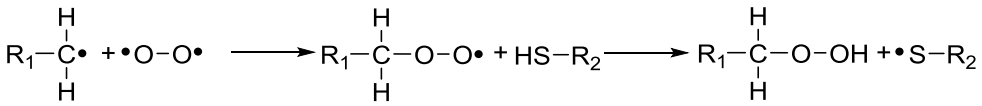

Figure 14: Mechanism, which shows the mitigation of oxygen inhibition by means of thiol-ene addition

Even though thiol-ene chemistry offers doubtlessly several advantages, there are also two major drawbacks. The strong odor of the thiols[54] and the poor storage stability of the formulations[55] pose serious problems for industrial application.

Other techniques used for regulation of free radical polymerization for linear polymers were discovered in the 1980s. Especially reversible addition-fragmentation chain transfer (**RAFT**)[56] and atom-transfer radical polymerization (**ATRP**)[57] are nowadays used to synthesize polymers with a narrow molecular weight distribution. Major applications are end-group modification and the synthesis of block copolymers.[58-59] However, these techniques suffer from a significant decrease of polymerization rates. Moreover, RAFT reagents strongly absorb in the UV/Vis region and ATRP uses metal catalysts, which are difficult to remove after polymerization.

Addition-fragmentation chain transfer (**AFCT**)[36, 60-61] reagents are also potential candidates for regulating free radical polymerization. Compared with RAFT and ATRP, the AFCT approach does not show strong retardation and absorbance of UV/Vis light is acceptable for possible application in photocuring.[62]

Irreversible addition-fragmentation chain transfer (**AFCT**) was firstly reported in the 1980s to provide a way for controlling free radical polymerization of monofunctional monomers.[63-65] AFCT similar to thiol-ene chemistry is turning a chain growth reaction into a mixed chain growth/ step growth-like reaction. While the thiol-ene mechanism is based on hydrogen abstraction, AFCT mechanism is similar to propagation of free radical polymerization.

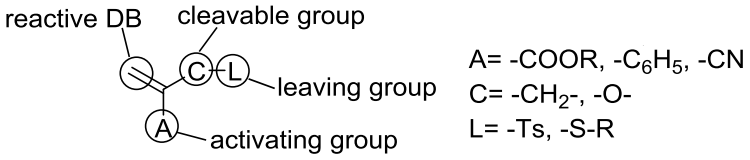

Figure 15: General structure of an AFCT reagent consisting of a DB, a leaving group and an activating group

Principally, an AFCT reagent[44, 56] consists of a reactive DB an activating group **A**, a cleavable group **C** (methylene or oxygen), and a leaving group **L**. A defines the reactivity of the DB of the AFCT reagent, while the leaving group should be a molecule that forms a reinitiating radical.

A general mechanism for AFCT reagents can be seen in Figure 16[62]. During the first step, the radical of a growing polymer chain attacks the unsaturated carbon-carbon bond of the AFCT reagent and undergoes an addition reaction. An intermediate radical is formed, which on the one hand can perform a back reaction to regenerate the starting species or on the other hand fragments via β-scission to give a reactive leaving group radical that can then reinitiate a new chain.

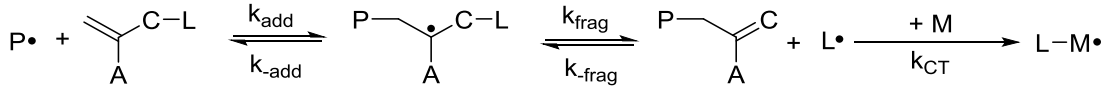

Figure 16: General mechanism of AFCT-regulated free radical polymerization

Theoretically, propagation of the intermediate radical is possible, even though unlikely because of steric hindrance. However, the stability of the intermediate radical is influenced by the activating group. The more stable the radical is, the slower the fragmentation occurs. Hence, too stable intermediate species can result in significant retardation of the polymerization.

As already discussed for thiol-ene chemistry, the C_{tr} also plays an important role in AFCT regulated polymerization and can be seen as measure for compatibility of AFCT reagents and chosen monomer resins. For a better understanding of the influence of the C_{tr} on the polymerization, it makes sense to consider the following cases[62]:

- $C_{tr} < 1$: in this case homopolymerization and hence chain growth reaction is preferred, leading to polymers with a broad molecular weight distribution. Applied to multifunctional monomer systems, inhomogeneous networks due to the lack of regulation can be expected.
- $C_{tr} > 1$: this implies that chain transfer is preferred. Especially at the beginning of the polymerization, polymers with low molecular weights are formed. After some time the favored consumption of AFCT reagents leads to exhaustion. Thus, the regulation in the system decreases and chain growth reaction becomes the decisive factor yielding in high molecular weights with a broad distribution.
- $C_{tr} \sim 1$: the chosen monomer and the AFCT reagent show good co-reactivity. This leads to a steady and uniform incorporation resulting in a consistent consumption of monomer and AFCT reagent. Equal consumption also guarantees efficient and uniform regulation throughout the whole polymerization process. Concerning network formation, more homogeneous networks can be expected.

A major advantage of AFCT reagents in comparison with thiol-ene chemistry is that by varying the activating group, the reactivity of the used AFCT reagent can be adapted to the reactivity of the monomer system of choice. This tunability provides a powerful tool to influence the C_{tr} towards a certain monomer.

Like thiols, AFCT reagents can also be used for network regulation when using multifunctional monomers. As already pointed out, shrinkage stress mainly arises from

gelation (solidification) in an early stage of polymerization at low DBC. Employing AFCT strategy in multifunctional resins shortens the kinetic chain length of the growing polymer back bones and can hence move the gel point to higher DBC.[36] This shift of gelation allows the resin to remain in liquid aggregate up to higher DBC and thus formed mechanical energy can dissipate in the resin, which finally ends in significantly reduced shrinkage stress.

Compared with homopolymerization, the more homogeneous network of AFCT-regulated reactions show improved mechanical behavior. As an example, the glass transition is much sharper, because regular networks exhibit a more defined glass transition. Besides that, more homogeneous networks largely contribute to an increase in impact resistance, which is a measure for toughness.[36, 61, 66]

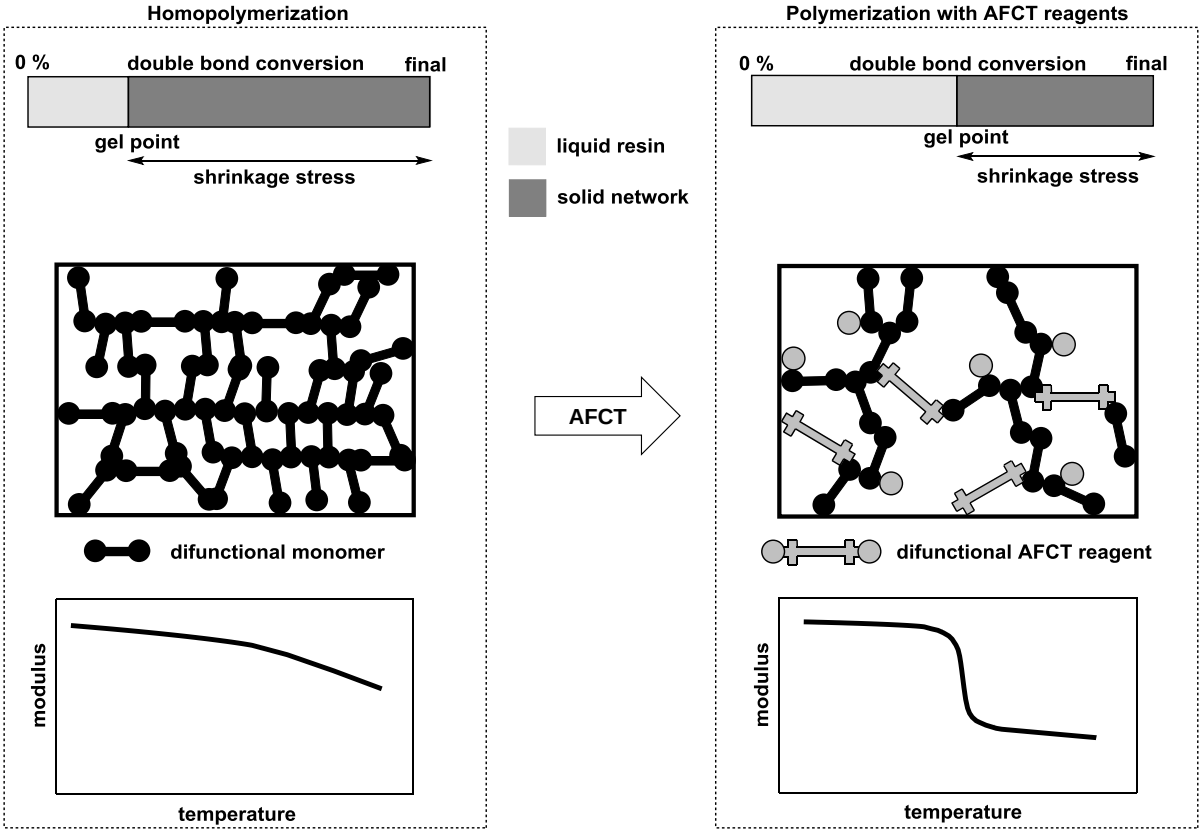

Figure 17: Illustration of advantages of AFCT-regulated photopolymerization of difunctional networks in comparison with homopolymerization

Objective

Nowadays, free radical photopolymerization is an important technique in industry for curing liquid resins for a wide range of application. Rapid curing speed, cured materials of high hardness and the possibility of 3D structuring are the main features of photopolymerization technology. But there are also current challenges, like the formation of high shrinkage stress and poor material toughness, arising from insufficient network regulation that need to be approached.

A well-known strategy therefore is thiol-ene chemistry, which mitigates shrinkage stress and increases the toughness of the cured polymers. An undesired side effect of thiol-ene chemistry represents the significant softening of the photopolymerized materials due to the formation of flexible thioether bridges. In addition, strong odor pollution and poor storage stability of the formulations come along with the employment of thiols.

Recently, addition fragmentation chain transfer (AFCT) was reported to embody a new concept for regulating photopolymerization based on methacrylic monomers, ending up with more homogeneous photocured polymer networks. These more homogeneous networks exhibit reduced stress emerging from shrinkage and considerably improved toughness without sacrificing hardness and modulus at room temperature. Concerning storage stability, the substitution of thiols by AFCT reagents leads to much more stable formulations, and odor issues can be solved. Until now, only reports about AFCT-regulated MA networks were published.

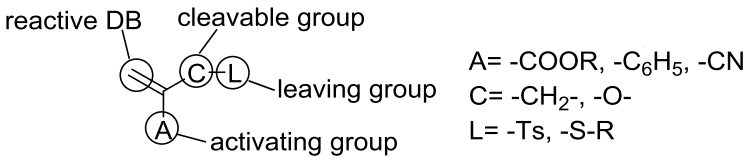

Since AFCT reagents are tunable towards certain monomers by exchanging cleavable, leaving, and activating group, one major task of this work is to find new appropriate AFCT reagents for methacrylates, acrylates and vinyl esters. Especially acrylates are in the focus of this study, because they represent the largest market volume in the field of photopolymerizable resins.

For identifying potential AFCT reagents, the chain transfer constant (C_{tr}) plays an important role. In order to guarantee homogeneous network formation with all its advantages, the C_{tr} should be around 1. Therefore, a new and easy-to-handle method should be developed by using photoreactor, ^{1}H NMR spectroscopy, GPC, and Maldi-TOF-MS as analytical devices. This should enable the monitoring of monomer/ AFCT reagent regulation throughout a whole

polymerization process from low to high DBC. An ideal result would be the consistent and equal consumption of monomer and AFCT reagent during the whole polymerization.

After narrowing down the choice of suitable monomer/ AFCT reagents for homogeneous network formation by means of the new established screening method, these systems should be tested in a wide-ranging study about network regulation including testing procedures like RT-NIR-photorheology, DMTA, tensile tests, Dynstat impact resistance test, nanointendation, swellability, and storage stability. Moreover, the study should contain a comparison with an appropriate thiol to highlight the merits of AFCT chemistry by contrast with thiol-ene chemistry.

General Part

1 State of the art

AFCT reagents in crosslinking methacrylates

Addition-fragmentation chain transfer (AFCT) reagents were first mentioned to regulate free radical polymerization in the late 1980s.[63, 65] In the first years AFCT was mainly used for molecular weight control of linear polymers (styrene[64] and methacrylates (MAs)[67]) for synthesizing hyperbranched polymers[68] or for end-group functionalization.[64, 69-70]

As already discussed in the Introduction, an AFCT reagent consists of a reactive DB, an activating group A, a cleavable group C (mostly -O-, -CH_2-), and a leaving group L. In radical polymerization, the radical of a growing polymer chain can add to the double bond (DB) creating an intermediate state, which can then undergo fragmentation by eliminating the leaving group radical. This radical can then reinitiate a new chain and propagate polymerization.

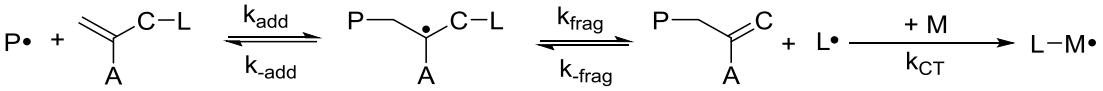

Figure 18: Schematic AFCT reaction mechanism

Applied to photopolymerized networks, AFCT regulation leads to a shift of the gel point to higher DBC reducing shrinkage stress within the material and to more homogeneous networks improving the toughness of the material and.

The first application of AFCT reagents in photopolymerization was reported by *Bowman et al.* in 2010.[71] In this case, AFCT was used in combination with thiol-ene chemistry for modifying an ethoxylated bisphenol-A dimethacrylate network. As chain transfer agents (**CTA**s) an allyl sulfide (AFCT reagent) in conjunction with the tetrathiol PETMP (thiol-ene reaction) were utilized.

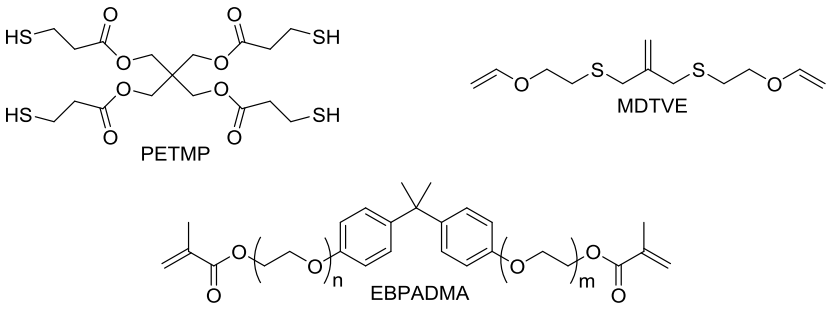

Figure 19: Chemicals used for first photopolymerized AFCT-regulated dimethacrylate networks: monomer: EBPADMA, thiol: PETMP, and AFCT reagent: MDTVE

In order to compare the impact of the MDTVE AFCT mechanism upon photopolymerization and mechanical properties of the cured MA material, formulations of different ratios of PETMP-EBPADMA with AFCT reagent MDTVE and without AFCT reagent were mixed to determine polymer network structure and polymerization-induced shrinkage stress.

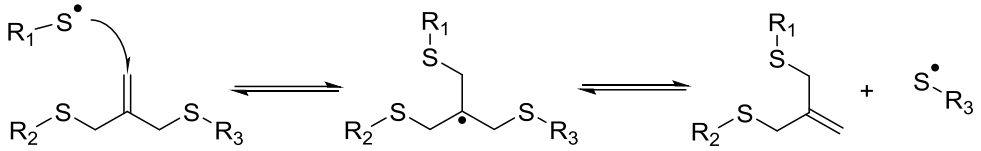

Figure 20: Schematic AFCT mechanism of allyl sulfides

Concerning shrinkage stress, a clear tendency was observed. The higher the MA ratio with respect to the AFCT reagent in the formulation was, the more shrinkage stress was formed. On the other hand, the higher the allyl sulfide amount of the formulation, the less shrinkage stress occurred (up to 75% less shrinkage stress). These findings clearly point out the potential of AFCT reagents for reducing shrinkage stress in photopolymerized materials based on MA. However, allyl sulfides do not possess activating groups, which makes the employment of thiol in the resin inevitable.

Since tunability of activating and leaving group is one major advantage of AFCT-reagents, another interesting approach was the analysis of β-allyl sulfones with different activating groups and their influence on network regulation performed by *P. Gauss.*[34]

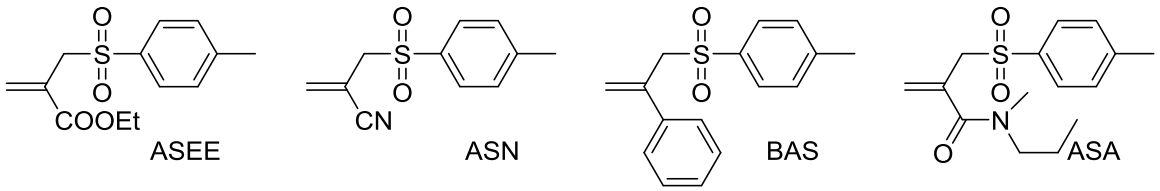

Figure 21: 2-Ethyl-2-(tosylmethyl)acrylate (ASEE), 2-(tosylmeth)acrylonitrile (ASN), 2-(tosylmethyl)styrene (BAS), and N-methyl-N-propyl-2-(tosylmethyl)acrylamide (ASA);

To gain more information about the reactivity and regulation abilities of β-allyl sulfones as AFCT reagents, AFCT reagents with different activating groups (Figure 21) were analyzed by means of photo-DSC, ^{1}H NMR spectroscopy, and GPC. Moreover, laser flash photolysis (LFP) was carried out in order to determine the addition rate constants (k_{add}) of an initiator radical to AFCT reagents with different activating groups and methacrylate monomers such as benzyl methacrylate (BenzMA) and methyl methacrylate (MMA).

Table 2: Determined k_{add} for MA monomers and β-allyl sulfones

Compound	k_{add} [10^7 L mol^{-1} s^{-1}]
BenzMA	4.2
MMA	4.0
ASEE	3.2
ASA	0.8
ASN	2.9
BAS	4.9

Table 2 demonstrates that the k_{add} for MAs ~4.0 x 10^7 M^{-1} s^{-1}. While ASEE (ester activating group), ASN (nitrile activating group), and BAS (phenyl activating group) exhibited k_{add}s close to MA, k_{add} of ASA ~0.8 x 10^7 M^{-1} s^{-1} was rather low. Combining photo-DSC and GPC results, showed that AFCT reagent with a k_{add} similar to MAs showed the best reactivity and regulating performance. Especially, ASEE with a k_{add} of 3.2 x 10^7 M^{-1} s^{-1} showed good performance.

After mechanistic studies, β-allyl sulfones were employed to modify MA networks by *Gorsche.*[36, 61] As matrix a 1:1 mixture of UDMA/D3MA (**2M**) was used, which is a typical resin for dental materials[11].

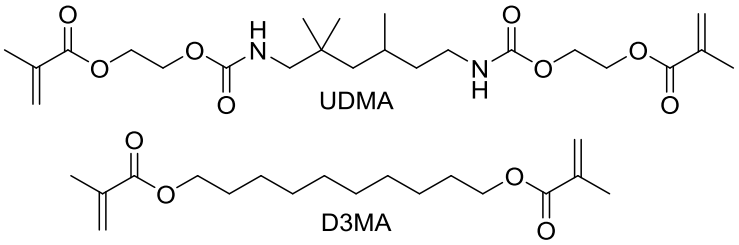

Figure 22: Urethanedimethacrylate (UDMA) and 1,10-decanediol dimethacrylate (D3MA) used as mixture in molar ratio of 1:1 (2M)

In order to highlight the effect of AFCT-regulated photopolymerization, one monofunctional **MAS** and one difunctional AFCT reagent **DAS** were compared with a dithiol **EDT**.

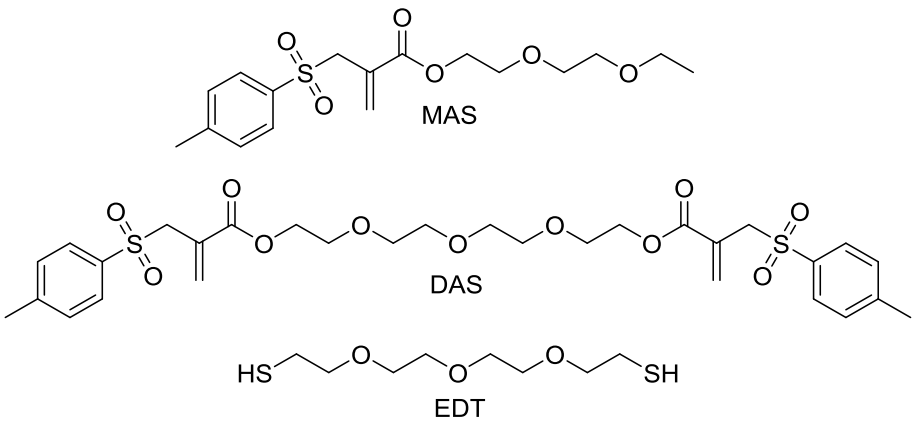

Figure 23: Mono-β-allyl sulfone (MAS), di-β-allyl sulfone (DAS), and tetra(ethylene glycol) dithiol (EDT)

Once again, Laser flash photolysis (**LFP**) showed that the addition rate constant k_{add} for MAS (2.84 ± 0.04) x 10^7 M^{-1} s^{-1} is in the range of methyl methacrylate (**MMA**) (~4.0 x 10^7 M^{-1} s^{-1}). Moreover, β-scission was suggested to be the major pathway for the chain transfer step.

For reactivity and mechanical tests, formulations consisting of different ratios of chain transfer reagents (CTAs) were mixed. Photo-DSC and ^{1}H NMR measurements investigated the reactivity of these systems. The addition of β-allyl sulfones slightly reduced the photoreactivity of the formulations ending in longer curing periods retarding the reaction in comparison with homopolymerization. Beneficial was the enhanced total DBC of AFCT-regulated resins.

Concerning network regulation, DMTA results illustrated the possibility of tuning mechanical and thermal properties of polymers by changing the amount of added AFCT reagents. An increase in AFCT reagents lowered the glass transition temperature (**T_g**) of the cured resins and sharpened the glass transition.

In order to ascertain the potential of AFCT reagents as network modifier, a comparative study with a thiol-ene system was performed. Photo-DSC experiments revealed the faster photopolymerization of thiol formulations compared with the homopolymerization and especially with the β-allyl sulfone formulations. However, RT-NIR-photorheology exposed that adding AFCT reagent enables the formed network to reduce shrinkage stress up to 50% compared to homopolymerization, while the addition of dithiol only yielded in 25% less shrinkage stress. This observation can be attributed to the shift of gel point to higher DBC. Studying the measured data, the DBC at gel point (**DBC_{gp}**) for AFCT-regulated formulations was significantly higher than for thiol-regulated formulations leading to greater reduction of shrinkage stress for β-allyl sulfones compared with dithiols.

DMTA analysis results pointed out that EDT networks showed lower T_g values and lower storage moduli at room temperature (**G'_{20}**) than DAS networks, which can be explained by the formation of flexible thio-ether bridges.

For testing hardness, nanoindentation was performed. As expected, the hardness of the EDT regulated networks significantly dropped with increasing dithiol amount due to the flexible thio-ether bridges in the material. On the other hand, the hardness of AFCT-photopolymerized networks only declines a bit in comparison with homopolymerization and then remains rather constant.

Finally, Dynstat impact resistance tests confirmed the homogeneous network formation comes along with a significant increase in impact strength. This time, thiol- and β-allyl sulfone-modified networks showed a similar increase in value.

Until shortly, β-allyl sulfones were one of the most important and versatile representatives of AFCT reagents in photopolymerization. However, they suffered from retarding effects, which lower the reaction speed and limit their applicability for 3D printing. Recently, a new breakthrough in AFCT reagent design was published by *C. Gorsche.*[66]

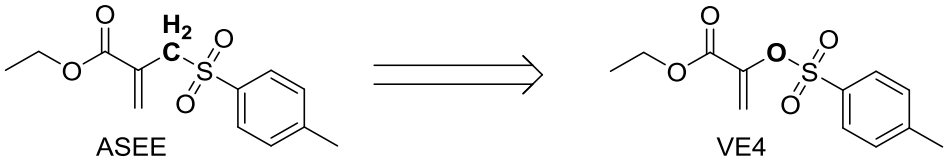

Figure 24: Structural difference between β-allyl sulfone ASEE and vinyl sulfonate ester VE4

The methylene group of the β-allyl sulfone ASEE next to the DB was substituted by an oxygen atom to give the vinyl sulfonate ester VE4. This small modification of the structure of the AFCT reagent has an enormous impact on the fragmentation mechanism. As can be seen in Figure 25, β-allyl sulfones form new DBs after fragmentation. These DBs can then further react with radical species to form low reactive tertiary radicals **T**, which can delay the polymerization and create more crosslinks within the network. These additional crosslinks can cause a more inhomogeneous polymer network. Another possibility would be the addition of an already eliminated sulfonyl radical **S** to a new β-allyl sulfone leading to an intermediate radical (**INT**). In this case, fragmentation as well as back reaction would regenerate the starting AFCT reagent retarding the polymerization.

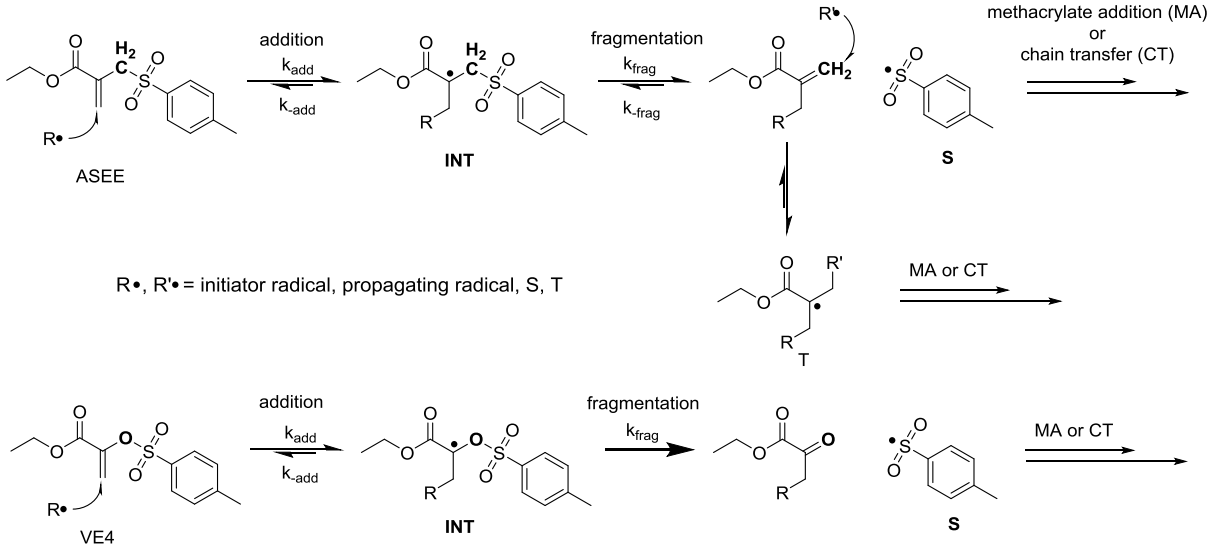

Figure 25: Comparison of reaction mechanism including potential side reactions between β-allyl sulfone ASEE and vinyl sulfonate ester VE4

By introducing an O instead of a CH_2 group, a non-reactive carbonyl bond is formed upon fragmentation, which could make the reaction irreversible and shifts the equilibrium towards

fragmentation. Besides that, low reactive tertiary radicals would not be formed anymore, which would accelerate polymerization as well.

In order to prove these assumptions a variety of experiments were carried out. Photoreactivity was measured *via* photo-DSC measurements comparing ASEE and VE4 resulting in a much faster reaction of VE4, even faster than homopolymerization. RT-FTIR analysis exhibited a significantly higher DBC_{final} for VE4 compared to ASEE-based formulation. Mechanical DMTA tests exhibited a similar regulation for both AFCT formulations, but VE4 showed a higher G'_{20}. Finally, Dynstat impact resistance tests confirmed higher toughness of vinyl sulfonate ester-regulated dimethacrylate networks.

Summarizing, AFCT technique has become a serious alternative to thiol-ene chemistry for regulating photopolymerizable MA networks. While first approaches with allyl sulfides were yet conducted in combination with thiols, β-allyl sulfones and vinyl sulfonate esters represent good candidates for regulating MA networks without the employment of thiols.

Regulating acrylate network formation

Concerning acrylates (**AC**s), no approach with AFCT reagents in photopolymerization of crosslinking monomers has been published by now. Since network regulation of ACs is of great interest in photopolymerization, thiol-ene chemistry represents nowadays the state-of-the-art method.

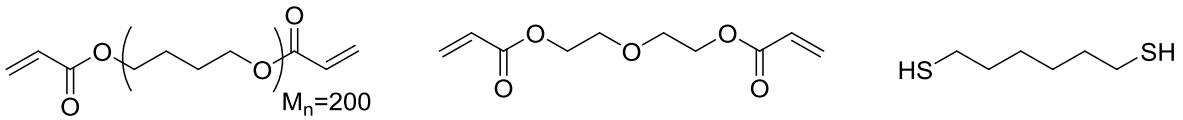

Figure 26: Polyethylene glycol(200) diacrylate (PEG200DA), diethylene glycol diacrylate (DEGDA), 1,6-hexane dithiol (dithiol);

In 2001 *Bowman et al.* [72] reported the sufficient regulation of diacrylate networks by using a dithiol (1,6-hexane dithiol) and polyethylene glycol(200) diacrylate (**PEG200DA**) (Figure 26). By increasing the stoichiometric ratio of dithiol in the PEGDA resin, the T_g was shifted to lower temperatures, the glass transition was sharpened, and the rubbery modulus decreased, which is a consequence of a decreasing crosslinking density in the material. Moreover, reactivity studies were performed by means of RT-FTIR. These studies indicated that in an AC-thiol system (diethylene glycol diacrylate-dithiol) a decrease of the thiol ratio leads to an increase in thiol conversion, while the acrylate conversion always remains at conversion >90%.

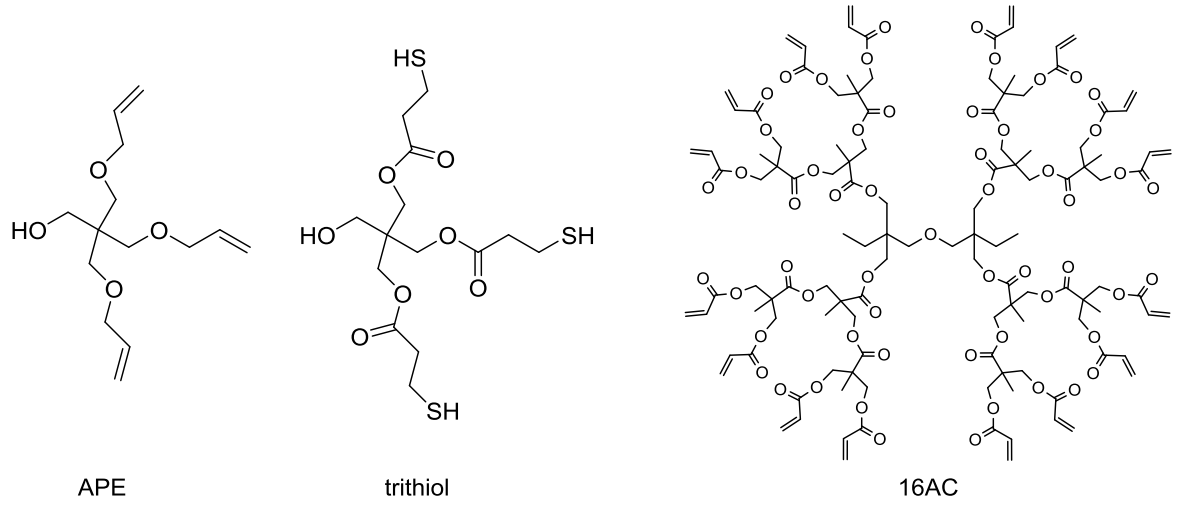

Figure 27: Triallyl ether (APE), trithiol, and 16-functional AC (16AC);

Hoyle et al. [73] carried out a study with a thiol-ene formulation consisting of a triallyl ether, a trithiol, and a 16-functional AC (16AC) (Figure 27). Again, different compositions of AC-thiol samples were prepared to perform DMA and DSC analysis. Like *Bowman et al.*, an increasing amount of thiol in the AC matrix shifted the T_g to lower temperatures and the glass transition became sharper indicating a uniform network matrix, while the homopolymer exhibited a broad tanδ plot specifying a heterogeneous network matrix. Finally, thin polymer films were fabricated to perform a Tinius Olsen impact test. While the neat AC matrix showed no energy absorbance due to its brittle behavior, the thiol-modified network exhibited an energy absorbance of 68%.

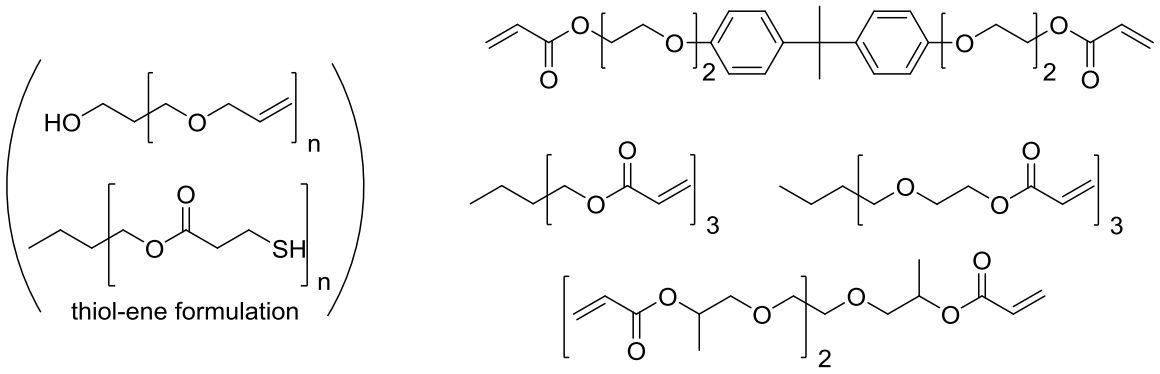

Figure 28: Thiol-ene formulation mixed with a variety of different ACs;

In 2007 *Gould et al.* [74] published an extensive study about ternary thiol-ene/AC photopolymers highlighting mechanical properties. A thiol-ene system was mixed with different multifunctional ACs (Figure 28) and DSC, DMA, and impact absorbance tests were conducted. Again, DSC and DMA results demonstrated a shift of the T_g to lower temperatures, a narrower glass transition, and a more homogeneous network, when increasing the thiol content in the network. Moreover, an increasing thiol ratio in the AC matrix also led to better impact energy absorption.

Regulating vinyl ester network formation

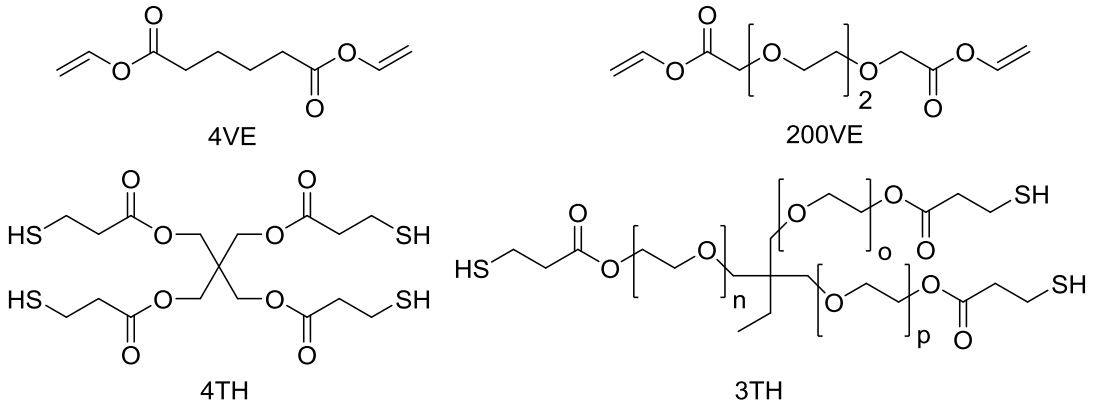

Figure 29: Divinyl adipate (4VE), 3,6,9-trioxanundecanedioic acid divinyl ester (200VE), pentaerythritol tetra(3-mercaptopropionate) (4TH), and ethoxylated trimethylolpropane tri(3-mercaptopropionate) (3TH) (n + o + p = 7.2);

Concerning VEs, *A. Mautner* [8] reported thiol-ene chemistry to be a sufficient tool to enhance network properties of difunctional VE networks. First of all, reactivity studies by means of photo-DSC indicated that the reactivity of VEs is ranged between the highly reactive ACs and the rather low reactive MAs. One problem of VEs during the polymerization process is the formation of highly reactive radicals with low resonance stabilization. Hence, the highly reactive radicals are prone to hydrogen abstraction, which can terminate the reaction. A strategy to tackle this issue is thiol-ene chemistry by providing thiols with easy abstractable hydrogens, which generate new thiyl radicals, which can reinitiate the photopolymerization. Moreover, RT-FTIR revealed that the DBC of VEs is boasted in the presence of thiols. Alamar Blue Assay testified that another advantage of VEs is their low toxicity in comparison with ACs and MAs. However, examination of the G'_{20} values revealed that the addition of thiols gives material with lower G'_{20} due to the flexible thio-ether bridges. Nevertheless, the impact resistance of the thiol-modified VEs was significantly increased.

Potential AFCT reagents for methacrylates, vinyl esters, and acrylates

In order to find new AFCT reagents, literature was searched and a feature article from *Moad*, *Rizzardo*, and *Thang* published in 2008 was found.[56] The publication deals with radical addition-fragmentation chemistry in polymer synthesis for linear polymers comprising reversible addition-fragmentation chain transfer (**RAFT**) and AFCT chemistry. For different AFCT reagents the chain transfer constants ($\mathbf{C_{tr}}$s) for methyl methacrylate (**MMA**), methyl acrylate (**MAC**), and vinyl acetate (**VAc**) are given. As already mentioned in the introduction, the C_{tr} is the relation between the transfer rate constant ($\mathbf{k_{tr}}$) and the propagation rate constant ($\mathbf{k_p}$) ($C_{tr} = k_{tr}/k_p$). An ideal AFCT reagent possesses a $C_{tr} \sim 1$. This means that the

monomer and the AFCT reagent are consumed at the same rate leading to constant molecular weights of the formed polymer during the whole polymerization process.

A selection of AFCT reagents, which were reported to possess a C_{tr} close to 1 for vinyl esters and acrylates, are illustrated in Figure 30.

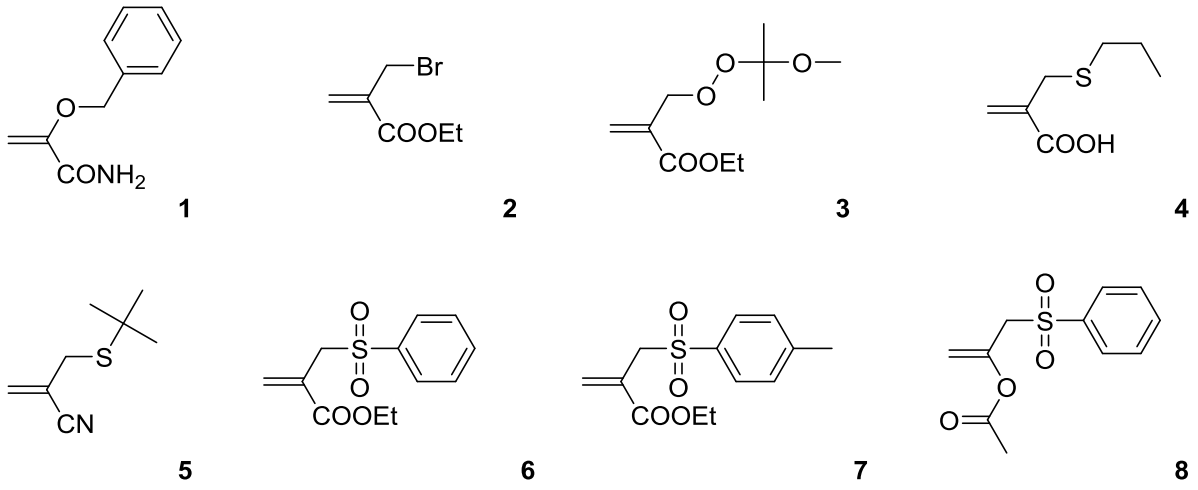

Figure 30: AFCT reagents with promising C_{tr}

AFCT reagent **1** represents a vinyl ether with an amino carbonyl activating group. As can be seen in Table 3, **1** has a C_{tr} of 1.1 in MAC, which would almost perfectly fit for the regulation of acrylates. Unfortunately, significant retardation was reported for compound **1** as well.

AFCT reagent **2**, an allyl halide with an ethyl ester activating group, was reported to have a C_{tr} of 2.3 in MAC and a C_{tr} of 1.5 in MMA. However, AFCT reagent **2** has already been used for modifying methacrylate-based networks by *Matsumoto et al.*[68] In this case, dimethacrylates with AFCT reagent **2** were polymerized to low conversions by means of thermal initiation and formed oligomers were analyzed using Maldi-TOF-MS to identify the oligomeric species formed by AFCT mechanism. Nevertheless, the leaving halogen radical is prone to cause unwanted side reaction.

AFCT reagent **8,** an allyl peroxide, with a C_{tr} of 1.3 in vinyl acetate seems to be a perfect candidate for VE regulation. On problem about allyl peroxides is that the reactivity of the oxygen leaving radical towards DBs is usually low, so an efficient reinitiation by the leaving group cannot be guaranteed.

AFCT reagents **4** and **5** are allyl sulfides, which represent another group of AFCT reagents and have already been used in photopolymerization for regulating methacrylate-based networks.[75] Regarding C_{tr} for MAC of 1.5 and 1.6, they show that the consumption of AFCT reagent would be slightly preferred.

AFCT reagents **6**-**8** are β-allyl sulfones. As already mentioned before, β-allyl sulfone **7** (ASEE) has already been used to successfully modify methacrylate networks in photopolymerization yielding material with enhanced mechanical properties.[36, 61] The good regulating abilities of **7** in methacrylates can be explained by a C_{tr} of 1.1 of **7** in MMA. Concerning acrylates, structure **6** exhibits a C_{tr} of 1.1 in MAC. This can be seen as evidence for good regulating abilities in acrylates. Particularly interesting for vinyl esters is β-allyl sulfone **8**. With a C_{tr} of 2.8 in VAc, structure **8** exhibits one of the values closest to 1. One explanation for that could be the different activating group similar to the vinyl ester moiety compared with structure **6** and **7**.

Table 3: Overview of C_{tr} of AFCT reagents in different monomers

AFCT reagent	**C_{tr} for monomer**		
	MMA	MAC	VAc
1	0.5	1.1	-
2	1.5	2.3	-
3	0.05	0.46	1.3
4	0.27	1.49	-
5	1.35	1.6	~60
6	0.72	1.1	-
7	1.1	2.3	-
8	0.06	0.2	2.8

Summarizing, β-allyl sulfones and allyl sulfides can be considered as potential candidates to regulate MAs, ACs, and VEs. The reason for that is that these classes of substances are known from literature to possess a C_{tr} ~1 in the corresponding monomers. Moreover, α-vinyl sulfonates should also be taken into consideration, since they have been reported to efficiently regulate MA networks.

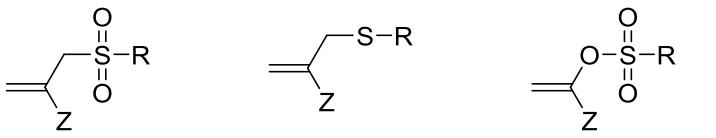

β–allyl sulfone β–allyl sulfide α–vinyl sulfonate

Figure 31: General structure of β-allyl sulfones, β-allyl sulfides, and α-vinyl sulfonates

2 Kinetic studies of addition-fragmentation chain transfer reagents

2.1 Screening addition-fragmentation chain transfer reagents in the photoreactor

As already mentioned in the objective, the photoreactor analysis tool should provide an easy-to-handle and quick method for determining the regulating abilities of a chosen monomer/addition-fragmentation chain transfer (**AFCT**) reagent system. In order to guarantee sufficient regulation, the chain transfer constant ($\mathbf{C_{tr}}$) of AFCT reagents towards a monomer should be around 1, which leads to an equal and steady consumption of AFCT reagents throughout the whole polymerization process.

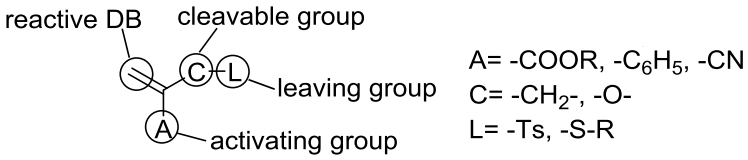

Figure 32: Schematic structure of an AFCT reagent

Since one of the major advantages of AFCT reagents is their tunability of activating group (**A**), cleavable group (**C**), and leaving group (**L**), photoreactor is a new method that makes it easy to compare the influence on regulation of radical photopolymerization when changing activating, cleavable or leaving groups.

In the photoreactor different monomers together with AFCT reagents in a deuterated solvent, which is not forming radicals upon UV/Vis irradiation, and a photoinitiator (**PI**) can be placed and irradiated for predetermined irradiation times. Then samples can be taken for the chosen irradiation times and analyzed by means of ^{1}H NMR spectroscopy. From the decrease of the double bonds (**DB**) of the monomer and the AFCT reagent double bond conversion (**DBC**)-time diagrams can be prepared, which contain information about the co-reactivity of the monomer/AFCT reagent system.

In the first step a broad photoreactor screening will be conducted, where the reactivity of various AFCT reagents towards methacrylates (**MA**s), vinyl esters (**VE**s) and acrylates (**AC**s) will be tested. As model monomers for the photoreactor screening, lauryl methacrylate (**LMA**), vinyl laurate (**LVE**), and lauryl acrylate (**LAC**) were used, due to their low volatility, their comparable M_w, and their similar alkyl chains.

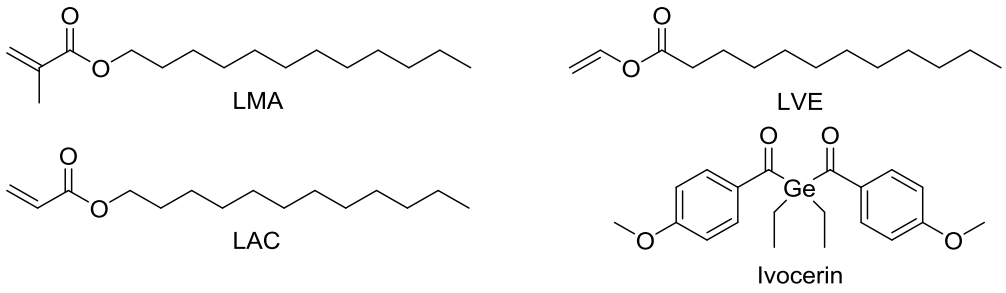

Figure 33: Aliphatic model monomers with reactive methacrylate (LMA), vinyl ester (LVE), and acrylate (LAC) groups used in the photoreactor screening study; As PI Ivocerin was applied;

One crucial selection criterion for model monomers is that they provide a least one chemical group, whose signal in the ^{1}H NMR spectrum does not change during the photopolymerization process. This chemical group can then be used as internal standard to calculate the DBC. In order to prove the stability of the reference signal, dimethyl terephthalate was used as internal standard, which did not take part in the photopolymerization and whose four aromatic protons gave a signal at 8.01 ppm.

For LMA, LVE, and LAC the methyl group at the end of the aliphatic chain was used as internal reference. Signal stability was proven by integration of the singlet at 8.01 ppm and the triplet at 0.80 ppm. Over time no significant changes of the signal were observed.

In order to gain more information, a variety of different AFCT reagents was provided. As can be seen in Figure 34, mainly β-allyl sulfones with different activating groups (ASEE, ASN, BAS, TSAP) should be measured, since β-allyl sulfones are known for sufficiently regulating MA networks[34] and have been reported to possess C_{tr} ~1[56].

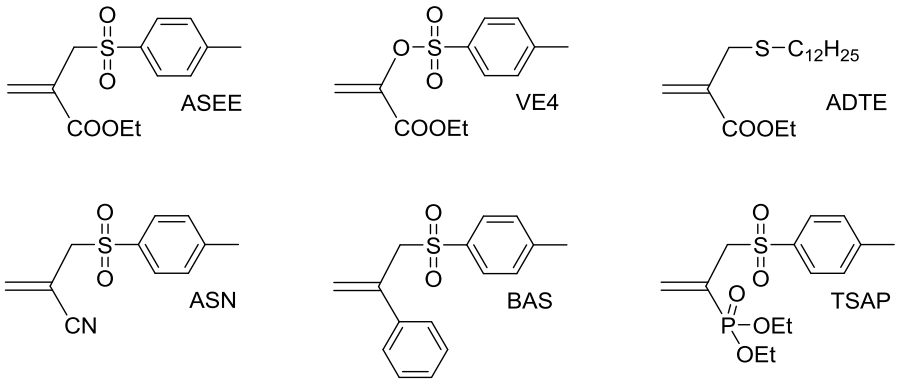

Figure 34: Structure of all tested AFCT transfer reagent

β-Allyl sulfones consist of a methylene group between the reactive DB and the tosyl (**Ts**) leaving group. ASEE possesses ethyl ester, ASN a nitrile, BAS a phenyl, and TSAP a diethyl phosphonate activating group. Besides that, ADTE with a thiol leaving group and recently reported VE4 with oxygen instead of a methylene group between the DB and Ts group should be screened as well.

From the DBC-time diagrams certain key figures, which can characterize the reaction speed and the co-reactivity of a monomer/ AFCT reagent system, can be derived. As indication for the reaction speed of the photopolymerization, the monomer/ AFCT reagent system is compared with the homopolymerization. Hence, the total amount of DBs in the system arising from the monomer and the AFCT reagent is considered to represent 100% of the DBs.

The first key figure, describing the relation between the conversion rate of AFCT-regulated reaction and the conversion rate of the homopolymerization, is the *relative reactivity* $\mathbf{r_R}$, which can be derived by dividing the slope of the summarized DBC-time curve of AFCT-regulated reaction ($\mathbf{R_{reg}}$ [% s^{-1}]) by the slope of the homopolymerization ($\mathbf{R_{homo}}$ [% s^{-1}]) (Eq.1). Therefore, the first measuring points in the linear range of the DBC-time curves are used. The relation of the conversion rates (R) in % s^{-1} indicates, if a reaction is faster (r_R >1), slower (r_R < 1), or as fast (r_R = 1) as homopolymerization. Since AFCT regulation should be applied to rapid 3D printing processes, values for r_R around 1 or >1 are desirable.

$$r_R = \frac{R_{reg}}{R_{homo}} \ (Eq. 1)$$

Another key figure, the *relative double bond conversion* $\mathbf{r_{DBC}}$ can be calculated by dividing the DBC at the end ($\mathbf{DBC_{end}}$) of the AFCT-regulated reaction ($\mathbf{DBC_{reg}}$) by the DBC_{end} of the homopolymerization ($\mathbf{DBC_{homo}}$) (Eq. 2). r_{DBC} gives information, whether the DBC_{end} of the AFCT-regulated reaction or the homopolymerization is higher or lower. This figure can be important, since reaction speed could change during the photopolymerization and r_R only takes the first measuring points at low and medium DBC into account, while the region of higher DBCs is neglected.

$$r_{DBC} = \frac{DBC_{reg}}{DBC_{homo}} \ (Eq. 2)$$

In terms of co-reactivity, the monomer DBC-time curve and the AFCT reagent DBC-time curve are correlated. This time, the slope of the AFCT DBC-time curve ($\mathbf{r_{AFCT}}$ [% s^{-1}]) is divided by the slope of monomer DBC-time curve ($\mathbf{r_{monomer}}$ [% s^{-1}]) to give the *co-reactivity factor* $\mathbf{f_{co}}$ (Eq. 3). In order to provide uniform and equal AFCT regulation during the whole photopolymerization the ideal co-reactivity of an AFCT reagent/ monomer system can be described by an f_{co} of 1, while a formulation with f_{co} < 1 prefers homopolymerization and a formulation with f_{co} > 1 leads to favored consumption of AFCT reagent.

$$f_{co} = \frac{r_{AFCT}}{r_{monomer}} \ (Eq. 3)$$

Since the slopes of $r_{monomer}$ and r_{AFCT} only comprise the first measuring points at low and medium DBCs, the *double bond conversion factor* $\mathbf{f_{DBC}}$ is introduced to give weight to co-reactivity phenomenon that might occur at higher DBCs. Again, f_{DBC} is calculated by dividing the DBC_{end} of the AFCT reagent ($\mathbf{DBC_{AFCT}}$) by DBC_{end} of the monomer ($\mathbf{DBC_{monomer}}$) (Eq. 4). Like f_{co}, an equal DBC_{end} for the monomer and the AFCT reagent is preferable complying with an f_{DBC} of 1.

$$f_{DBC} = \frac{DBC_{AFCT}}{DBC_{monomer}} \ (Eq. 4)$$

Thus, characterizing an ideal AFCT reagent by means of the beforehand explained key figures would lead to reaction speed parameters r_R and $r_{DBC} \geq 1$ and co-reactivity parameters of f_{co} and f_{DBC} of 1.

However, it has to be mentioned that all these parameters are depending on the concentration of AFCT reagent added to the monomer resins. This means that a change in concentration usually comes along with a change of reaction speed and co-reactivity.

For evaluating the co-reactivity of an AFCT reagent with a monomer, a photoreactor was used. A photoreactor consists of a two necked round bottom flask, where 400 mg of a monomer/ AFCT reagent resin (consisting of 80 mol% monomer and 20 mol% AFCT reagent) and additional 3 mol% of PI Ivocerin are dissolved in deuterated benzene under argon atmosphere. By irradiating and taking samples from the formulation at predetermined irradiation times, a decrease of the DB signals of the monomer and the AFCT reagent can be observed when analyzed by means of ^{1}H NMR. This decrease correlates with the conversion of the considered species. By plotting DBC against time, conversion-time diagrams can be obtained. Ideally, the consumption rate of the monomer and the AFCT reagent should be equally to guarantee good regulation.

2.1.1 Regulating methacrylates *via* addition-fragmentation chain transfer

As already mentioned in the State of the art, all known AFCT reagents in photopolymerization were synthesized to regulate MA networks for increasing toughness and reducing shrinkage stress. Thus, most of the following screened AFCT reagents are expected to show a good co-reactivity with MAs. As model monomer compound for MAs lauryl methacrylate has been selected.

Generally, homopolymerization is the first indicator, how reactive a monomer system is and is later on used as reference for the AFCT-regulated LMA reactions.

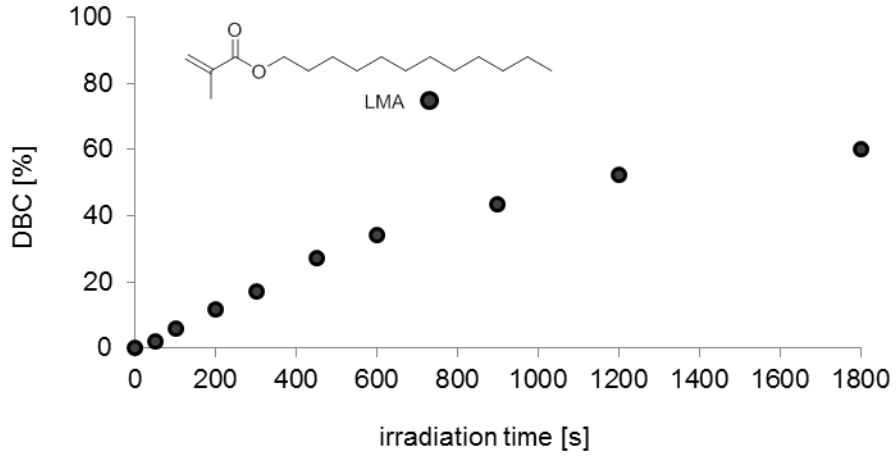

Figure 35: Homopolymerization of LMA ● in the photoreactor

As can be seen in Figure 35, the homopolymerization of LMA leads to a DBC_{homo} of 60% after 1800 s of irradiation, which is a rather low value compared to bulk polymerization, taking the high amount of 3 mol% PI into account. The rather low conversion can be explained by the diluting effect of deuterated benzene.

For determining the slopes of all LMA reaction, the first 6 measured points (after 0, 50, 100, 200, 300, 450, and 600 s of irradiation) were picked and a linear regression curve was calculated, which led to a R_{homo} of 0.058 % s^{-1} for the LMA homopolymerization.

According to the Alfrey-Price theory, which is dealing with relative relativities in vinyl copolymerization, MAs are vinyl compound that show a good resonance stabilization of a radical. In agreement with this theory, MAs should preferably copolymerize with other vinyl compounds that are able to lead to good resonance stabilized radicals.[76] This is important, since the addition of the growing macroradical to an AFCT reagent can be considered as a kind of copolymerization. However, the Alfrey-Price theory does not predict the influence on reaction speed.

First candidate of the photoreactor screening is the β-allyl sulfone ASEE with an ethyl ester activating group, which has already been reported to show excellent regulating properties for MAs.[34, 36, 61] Like all other measurements in the screening section, the ratio of monomer to AFCT reagent was chosen to be 80 mol% to 20 mol%. Figure 36 highlights the very fast photopolymerization of the ASEE-regulated formulation (0.069 % s^{-1}), leading to an r_R of 1.20 and an acceleration of AFCT-regulated reaction compared to homopolymerization. Moreover, the DBC_{reg} is increased to 65% resulting in an r_{DBC} of 1.08. Regarding co-reactivity, a remarkably uniform and equal consumption of LMA and ASEE can be observed. This is confirmed by an f_{DBC} and an f_{co} of 1.00. All key figures clearly point out that ASEE represents an ideal AFCT reagent for regulating MAs, which is not surprising since the ester activating group of ASEE can stabilize the radical and therefore shows good co-reaction with LMA.

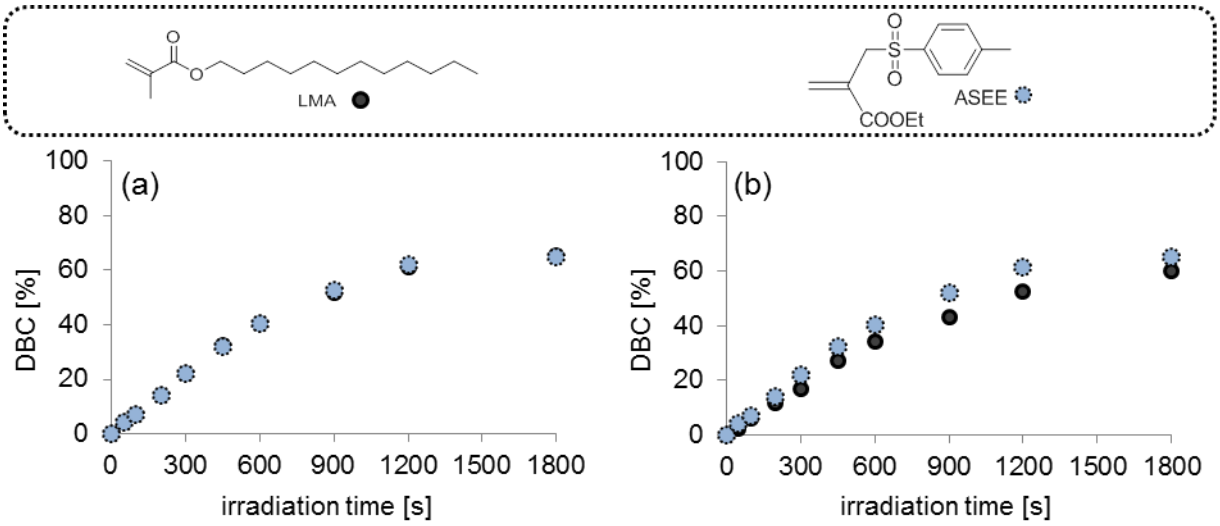

Figure 36: (a) Co-reactivity DBC-time diagram of 80 mol% LMA ● and 20 mol% ASEE ● and (b) DBC-time curve of homopolymerization ● and total DB amount of AFCT-regulated formulation ●

The same holds true for the α-vinyl sulfonate VE4 with an ethyl ester activating group, whose superior regulating abilities in MAs have already been reported.[66] In Figure 37 the DBC-time diagram of the homopolymerization and AFCT-regulated reaction exhibit an acceleration of the AFCT-regulated reaction (r_R= 1.25) ending up in a DBC_{reg} of 66% (r_R = 1.10). In respect of co-reactivity, the LMA slope (r_{LMA}) and the VE4 slope (r_{VE4}) are in the same range and lead to an f_{co} of 0.92. Moreover, similar DBC_{end}s for LMA and VE4 can be reached (f_{DBC} = 0.97). This is not surprising since the diethyl ester activating group is again stabilizing the radical.

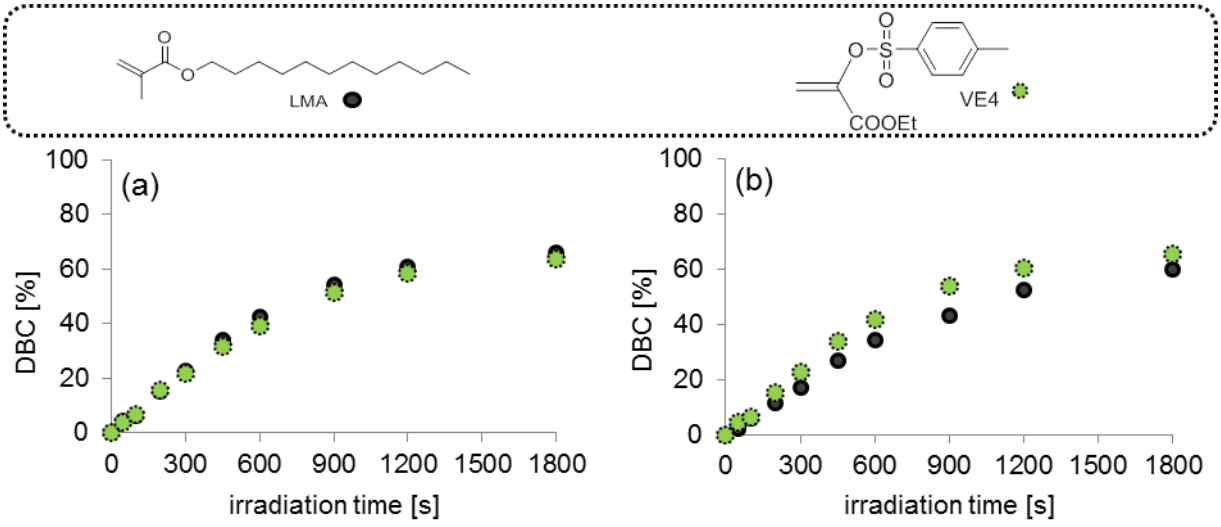

Figure 37: (a) co-reactivity DBC-time diagram of 80 mol% LMA ● and 20 mol% VE4 ● and (b) DBC-time curve of homopolymerization ● and total DB amount of AFCT-regulated formulation ●

Changing the leaving group to an allyl sulfide, ADTE (Figure 38) as AFCT regulator in LMA leads to a slight retardation of the AFCT-regulated photopolymerization (r_R = 0.89) and in a lower DBC_{reg} (r_{DBC} = 0.83). In regard to co-reactivity, LMA is slightly preferred consumed emerging in a higher DBC_{LMA} than DBC_{ADTE} (f_{DBC} = 0.81) and a steeper slope of the LMA

curve (f_{co} = 0.79). As already discussed before, the rather good co-reactivity can once again be attributed to the ester activating group because of its good resonance stabilization.

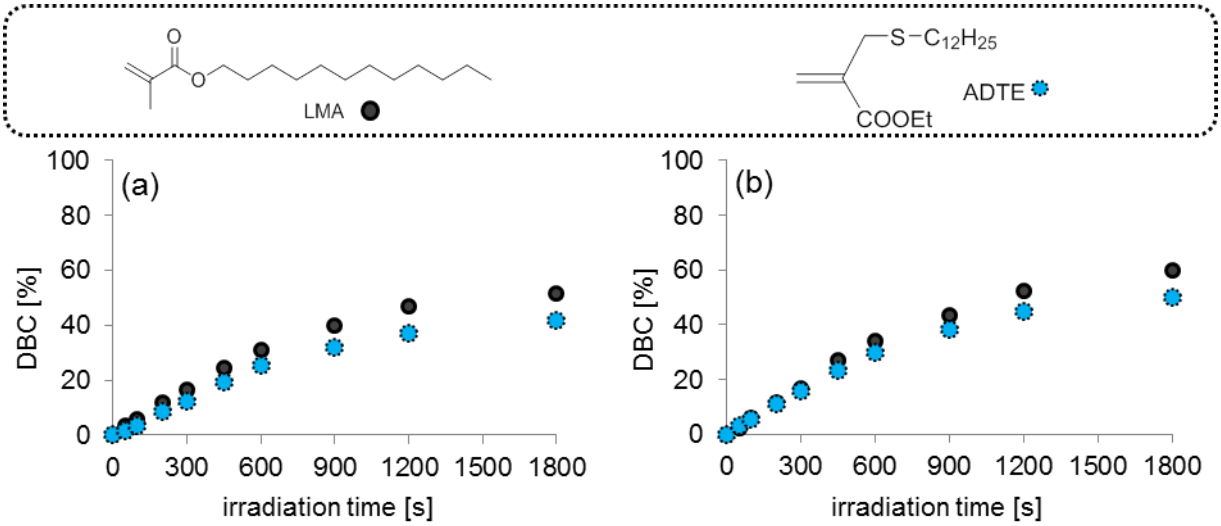

Figure 38: (a) Co-reactivity DBC-time diagram of 80 mol% LMA and 20 mol% ADTE and (b) DBC-time curve of homopolymerization and total DB amount of AFCT-regulated formulation

In Figure 39 the DBC-time diagrams of the β-allyl sulfone with nitrile activating group ASN is illustrated. ASN has already been published to be an AFCT reagent for regulating MAs[34] and nitrile groups are known for their rather good resonance stabilization of radicals. Regarding reaction speed, ASN exhibits retardation, which can be confirmed by r_{DBC} of 0.73 and r_R of 0.82. On the other hand, the co-reactivity is with an f_{co} of 0.99 close to 1. Nevertheless, DBC_{ASN} is with 55% significantly higher than DBC_{LMA} with 42% resulting in an f_{DBC} of 1.31. This development can be explained by the reduced consumption of LMA at higher DBCs.

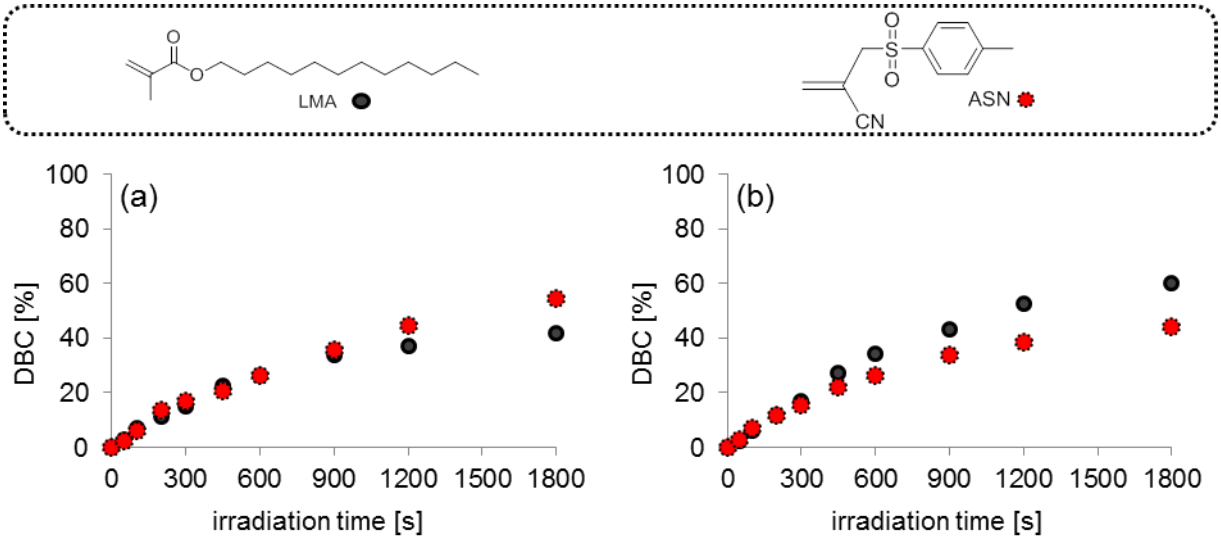

Figure 39: (a) Co-reactivity DBC-time diagram of 80 mol% LMA and 20 mol% ASN and (b) DBC-time curve of homopolymerization and total DB amount of AFCT-regulated formulation

β-Allyl sulfone with phenyl activating group BAS has also been reported to regulate MAs. The DBC-time diagram for BAS can be seen in Figure 39. In the matter of reaction speed, the slope of R_{reg} is clearly flatter than R_{homo} (r_R = 0.60). Besides that, DBC_{reg} with 37% is reduced as well in comparison with DBC_{homo} with 60% (r_{DBC} = 0.62). In regards to co-reactivity, the consumption of BAS is preferred (f_{co} = 1.31) and DBC_{BAS} is higher than DBC_{LMA} (f_{DBC} = 1.37). The rather good co-reactivity can be attributed to resonance stabilizing ability of the phenyl group.

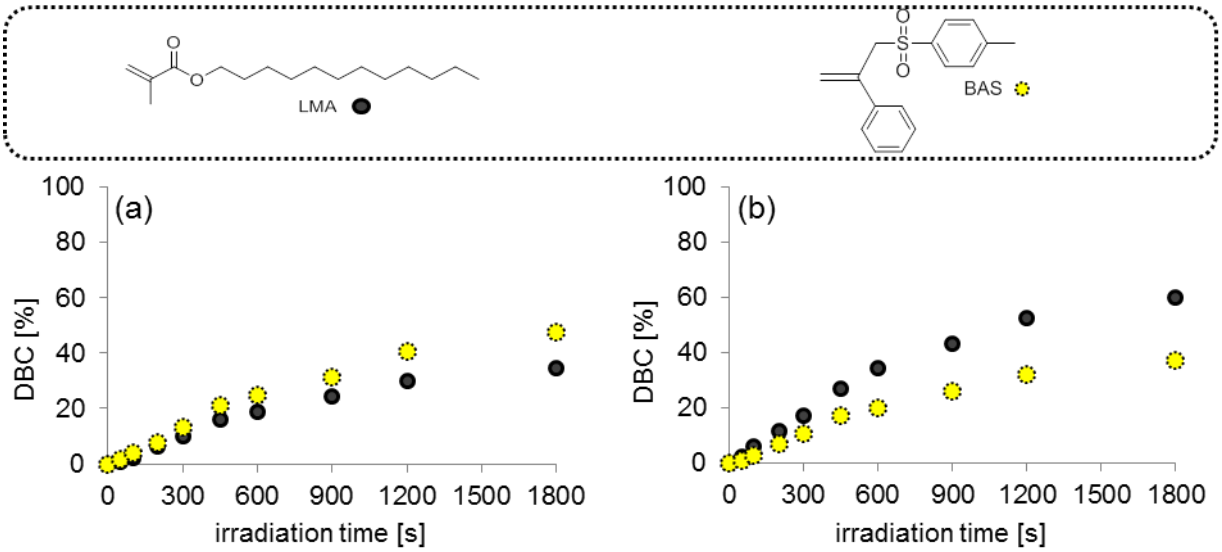

Figure 40: (a) co-reactivity DBC-time diagram of 80 mol% LMA ● and 20 mol% BAS ● and (b) DBC-time curve of homopolymerization ● and total DB amount of AFCT-regulated formulation ●

Finally, the last measured system contained TSAP as AFCT reagent with a diethyl phosphonate activating group. As can be seen in Figure 41, the AFCT-regulated reaction is slower compared to homopolymerization (r_R = 0.81) yielding a DBC_{reg} of 42%, which is significantly lower than the DBC_{homo} of 60%. Co-reactivity between LMA and TSAP shows with an f_{co} of 0.17 the lowest value for all measured AFCT reagents in MA, since TSAP is barely consumed. As a consequence, DBC_{TSAP} remains particularly low (f_{DBC} = 0.15).

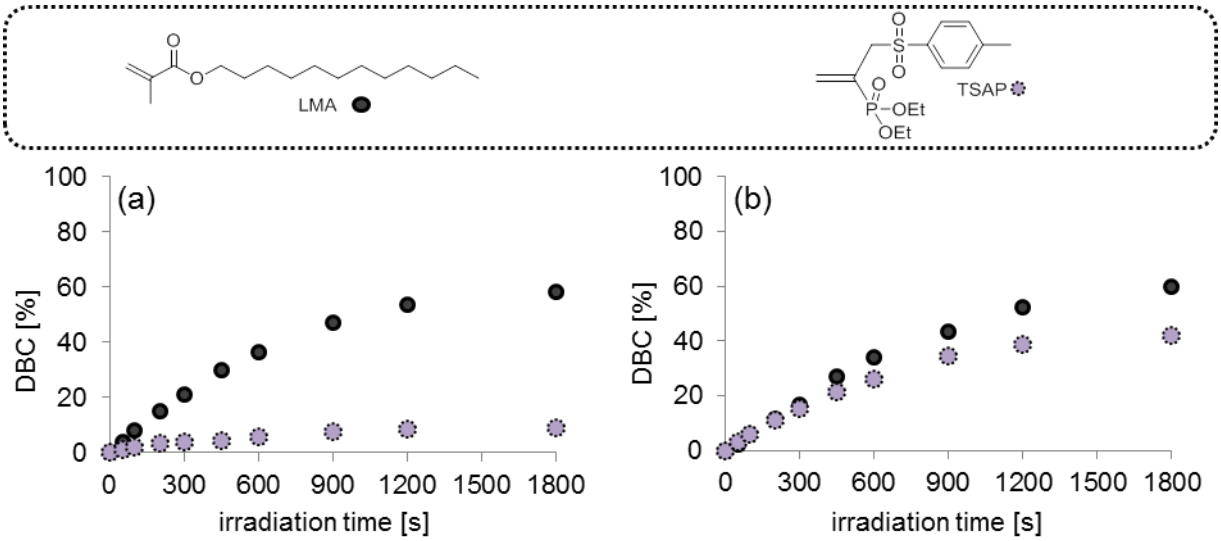

Figure 41: (a) co-reactivity DBC-time diagram of 80 mol% LMA ● and 20 mol% TSAP ● and (b) DBC-time curve of homopolymerization ● and total DB amount of AFCT-regulated formulation ●

When taking a look at Figure 42 picturing the key figures for the photopolymerization speed, it can be seen that the β-allyl sulfone ASEE and the α-vinyl sulfonate VE4 (both with ethyl ester activating group) in LMA lead to an acceleration of photopolymerization. All other AFCT reagents show retardation in comparison to LMA homopolymerization. However, the allyl sulfide ADTE (also with ethyl ester activating group) only exhibits slight retardation.

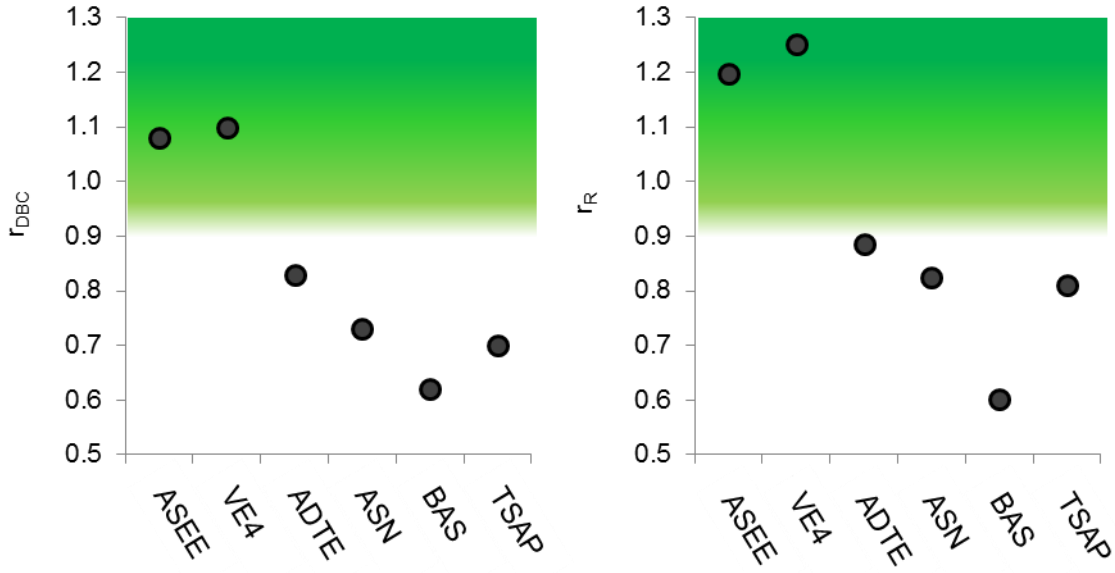

Figure 42: Overview of photopolymerization relative reactivity key figures of AFCT reagents in LMA

In terms of co-reactivity Figure 43 illustrates that ASEE and VE4 also possess an ideal co-reactivity of 1 or close to 1 in MAs. Another AFCT reagent with a co-reactivity factor f_{co} ~1 is ASN, which in the first phase of the photopolymerization shows equal consumption rates of LMA and ASN, but finally ends up with a distinctive higher AFCT DBC. In case of ADTE, homopolymerization is slightly preferred (f_{DBC}, f_{co} ~ 0.8). BAS with the phenyl activating group

and TSAP with the diethyl phosphonate activating group are out of the range of required co-reactivity.

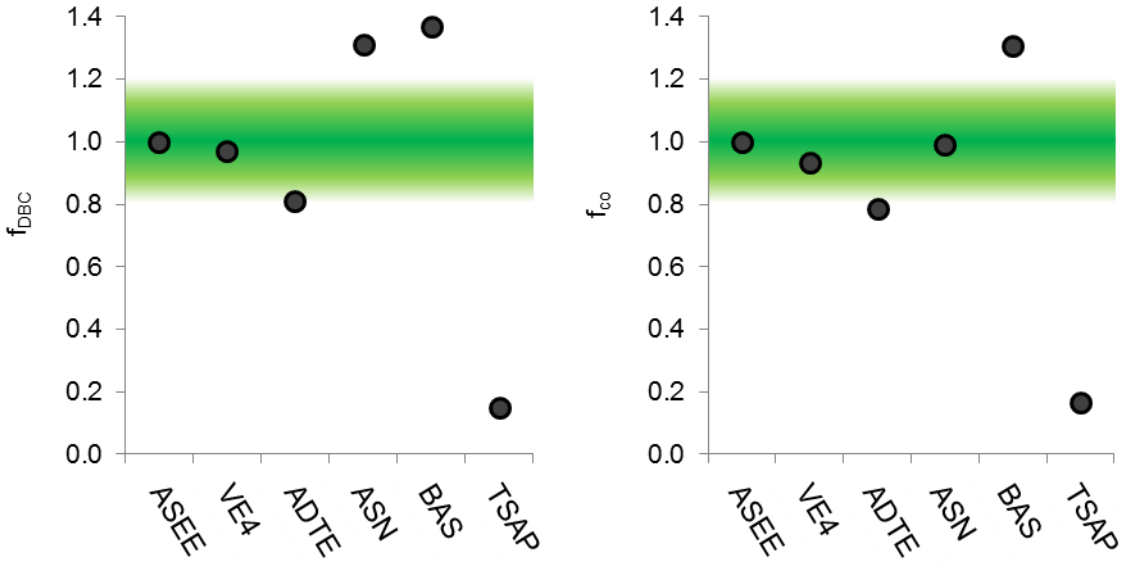

Figure 43: Overview of photopolymerization co-reactivity key figures of AFCT reagents in LMA

Eventually, β-allyl sulfone ASEE and vinyl sulfonate ester VE4 meet the requirement for applicable AFCT reagent showing enhanced photopolymerization rates and good co-reactivity. Moreover, allyl sulfide ADTE delivers results, which are always slightly outside of the required range.

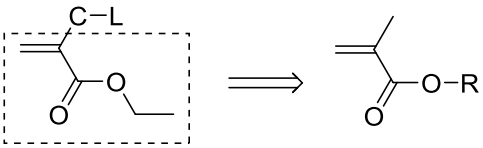

ASEE: C= CH_2, L= Ts
VE4: C= O, L= Ts
ADTE: C= CH_2, L= S-$C_{12}H_{25}$

MA

Figure 44: Structural similarity of AFCT reagents ASEE, VE4, and ADTE with MAs

A short structure analysis of the discussed AFCT reagents indicates that the good regulating abilities towards MAs mainly arise from their activating groups, which are similar to MAs. This similarity in structure leads to similarity in chemical reactivity and therefore to equal and uniform consumption in the conversion-time diagram. This can be substantiated by the fact that ester groups lead to good radical resonance stabilization. Therefore, good co-reactivity can be awaited. The slower reaction of ADTE can be assumed to evolve from the different leaving group influencing fragmentation.

Table 4: Collected results for LMA and tested AFCT reagents

Formulation	*Homopolym. vs. total DBC*					*DBC of monomer and AFCT*			
Composition	**DBC_{end}** [%]	**r_{DBC}** [ ]	**R** [% s^{-1}]	**r_R** [ ]	Monomer AFCT	**DBC_{end}** [%]	**f_{DBC}** [ ]	**r** [% s^{-1}]	**f_{co}** [ ]
neat LMA	60	-	0.058	-	LMA	60	-	0.058	-
LMA + ASEE	65	1.08	0.069	1.20	LMA ASEE	65 65	1.00	0.070 0.070	1.00
LMA + VE4	66	1.10	0.073	1.25	LMA VE4	66 64	0.97	0.073 0.069	0.93
LMA + ADTE	50	0.83	0.051	0.89	LMA ADTE	52 42	0.81	0.054 0.042	0.79
LMA + ASN	44	0.73	0.048	0.82	LMA ASN	42 55	1.31	0.048 0.047	0.99
LMA + BAS	37	0.62	0.035	0.60	LMA BAS	35 48	1.37	0.033 0.043	1.31
LMA + TSAP	42	0.7	0.047	0.81	LMA TSAP	58 9	0.15	0.065 0.011	0.17

2.1.2 Regulating vinyl esters *via* addition-fragmentation chain transfer

In order to provide low toxic tough materials for bioapplications, VEs should also be tested in the photoreactor for being regulated by means of AFCT reagents. The regulation abilities should be evaluated by using key figures, which characterize photopolymerization speed and co-reactivity. For determining the slopes of the DBC-time curves, 7 measuring points (after 0, 50, 100, 200, 300, 450, and 600 s of irradiation) were picked and linear regression curves were calculated, from which the parameters r_R and f_{co} were derived.

Again, homopolymerization of LVE was used as a reference photoreaction for later comparison with AFCT-regulated reactions. As illustrated in Figure 45, the homopolymerization of LVE reaches a DBC_{homo} of 44% after 1800 s of irradiation at a r_{LVE} of 0.058 % s^{-1}, which exactly corresponds with the slope of r_{LMA}. However, the homopolymerization of LVE DBC_{homo} is significantly lower than the DBC_{homo} of lauryl methacrylate (60%). However, LVE are known to provide poor resonance stabilization for radicals.

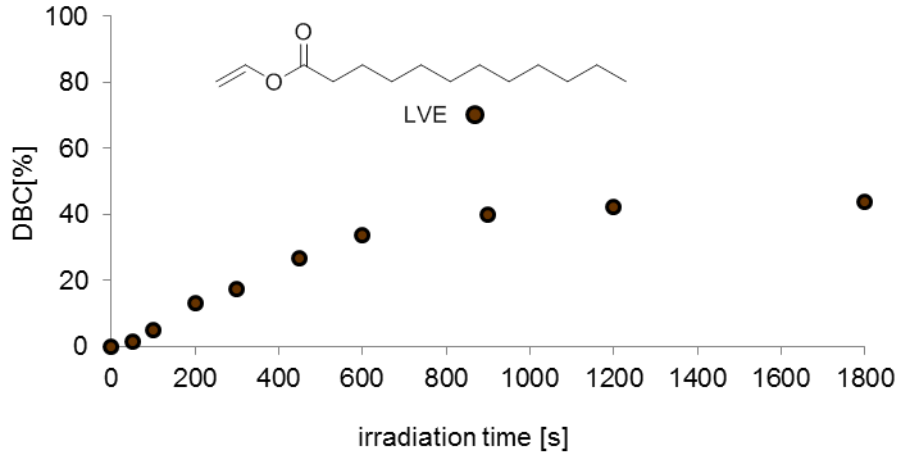

Figure 45: Homopolymerization of LVE ● in the photoreactor

The following analyzed AFCT-regulated photopolymerizations consist again of 80 mol% LVE and 20 mol% AFCT reagent with 3 mol% of PI Ivocerin. Beginning with β-allyl sulfone with an ethyl ester activating group ASEE, the AFCT-regulated reaction shows retardation in comparison with homopolymerization (r_R = 0.82) and additionally ending up with lower DBC_{reg} (31%). Moreover, poor homogeneous co-reactivity is found (f_{DBC} = 4.94, f_{co} = 4.85).

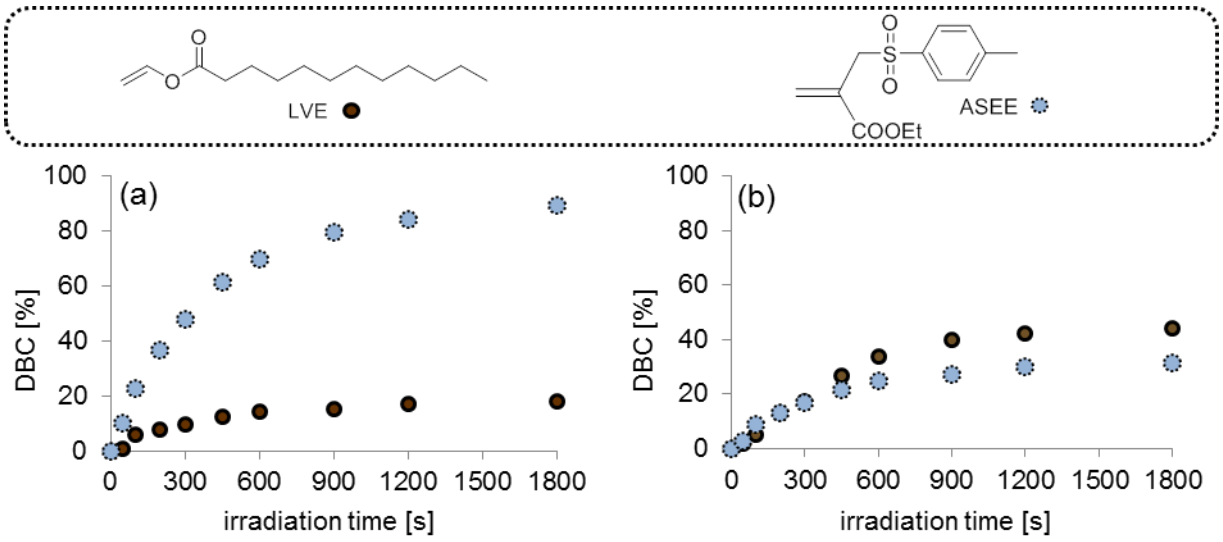

Figure 46: (a) Co-reactivity DBC-time diagram of 80 mol% LVE ● and 20 mol% ASEE ● and (b) DBC-time curve of homopolymerization ● and total DB amount of AFCT-regulated formulation ●

At first glance, the vinyl sulfonate ester VE4 exhibits a faster reaction than the LVE homopolymerization with an r_R of 1.16 and a r_{DBC} of 0.95. By taking a look at the co-reactivity diagram, it can be seen that this acceleration arises from the very fast consumption of VE4 with a r_{VE4} ~0.2 % s^{-1} representing the steepest slope measured in all LVE formulation (f_{co} = 6.30). The high r_{DBC} can also be explained by the full conversion of VE4, while the VE conversion with 28% remains low (f_{DBC} = 3.57). An explanation for this behavior might be given by the fact that the monomer reactivity for vinyl esters is relatively low due to the poor resonance stabilization of the intermediate radical.

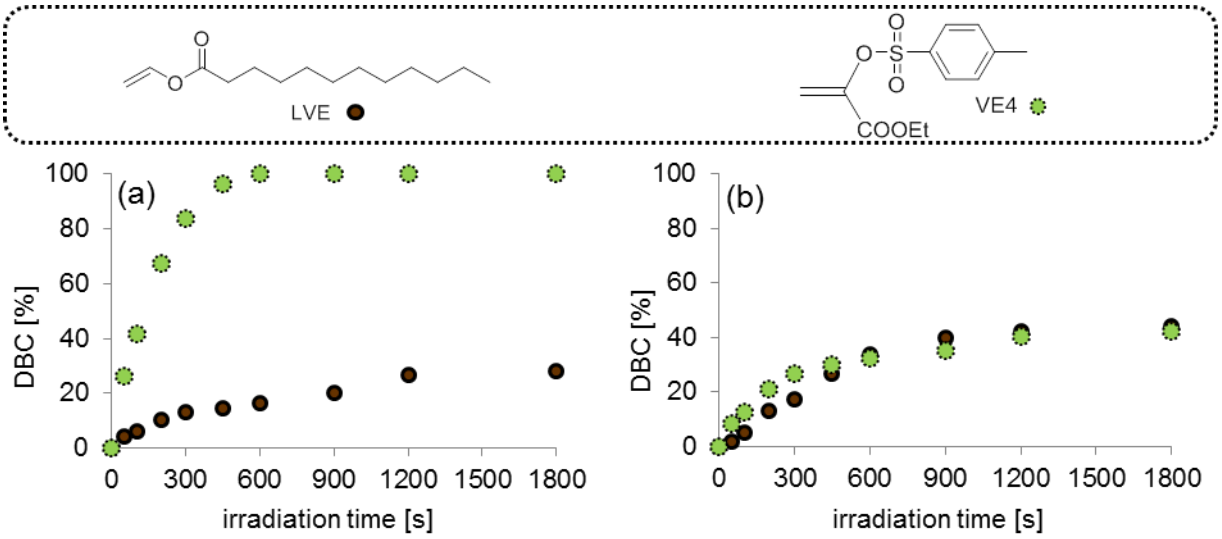

Figure 47: (a) Co-reactivity DBC-time diagram of 80 mol% LVE ● and 20 mol% VE4 ● and (b) DBC-time curve of homopolymerization ● and total DB amount of AFCT-regulated formulation ●

In Figure 48 the allyl sulfide ADTE in LVE shows significant retardation in comparison with homopolymerization (r_R = 0.49) and a significant lower DBC_{reg} of 24%. Concerning consumption of LVE and ADTE, ADTE is preferred consumed, while the LVE conversion remains below 10% (f_{DBC} = 9.56). Hence, f_{co} for the LVE/ ADTE system represents with 13.67 the highest value measured in this screening study.

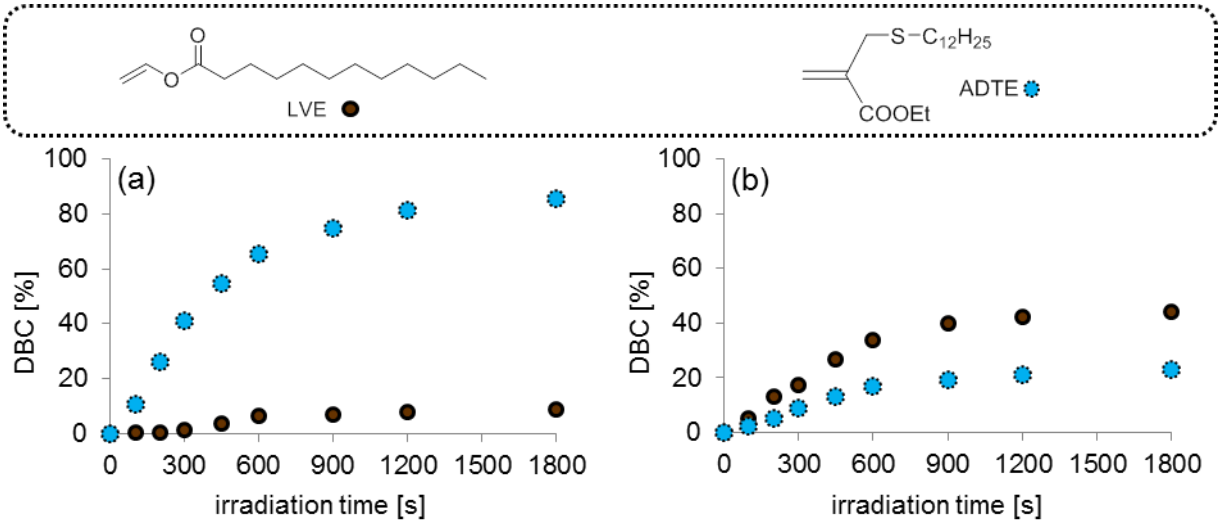

Figure 48: (a) co-reactivity DBC-time diagram of 80 mol% LVE ● and 20 mol% ADTE ● and (b) DBC-time curve of homopolymerization ● and total DB amount of AFCT-regulated formulation ●

The next AFCT reagent that was analyzed in a VE formulation was the β-allyl sulfone ASN. As can be seen in Figure 49, the AFCT-regulated reaction is slower than the LVE homopolymerization (r_R = 0.54) leading to low DBC_{reg} (r_{DBC} = 0.61). Once again, the AFCT

reagent ASN is preferably consumed (f_{co} = 8.20) reaching high DBC_{ASN} of 79%, while the LVE conversion remains below 20%.

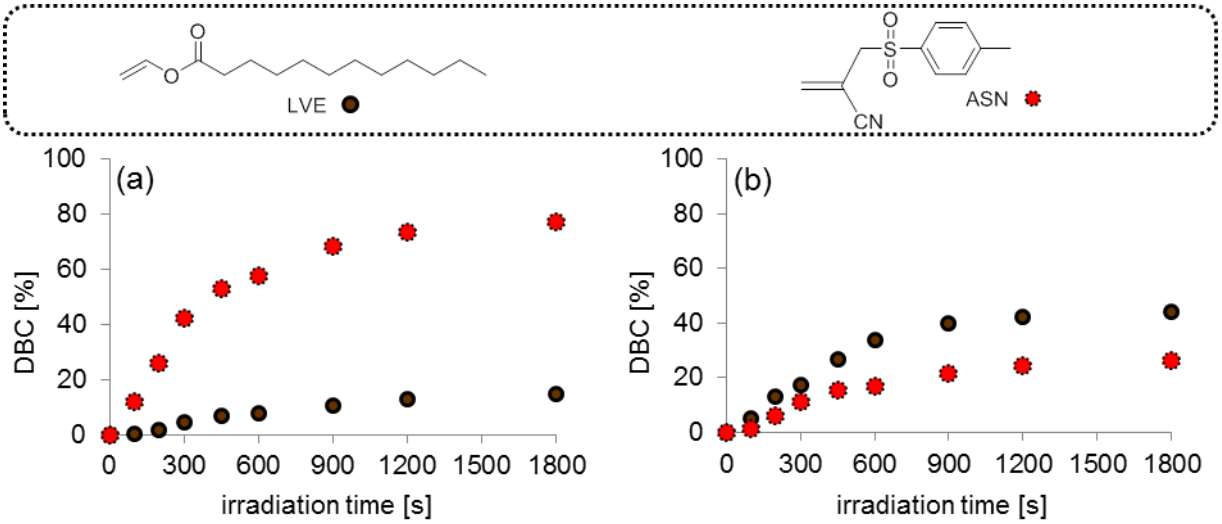

Figure 49: (a) Co-reactivity DBC-time diagram of 80 mol% LVE ● and 20 mol% ASN ● and (b) DBC-time curve of homopolymerization ● and total DB amount of AFCT-regulated formulation ●

The β-allyl sulfone with a phenyl activating group BAS in Figure 50 exhibits the slowest reaction for LVE regulation (r_R = 0.35) with the lowest r_{DBC} (0.32). Moreover, no homogeneous consumption of LVE and BAS can be observed. BAS is preferably consumed (f_{co} = 10.26) yielding a DBC_{BAS} of 49%, while DBC_{LVE} does not exceed 5%.

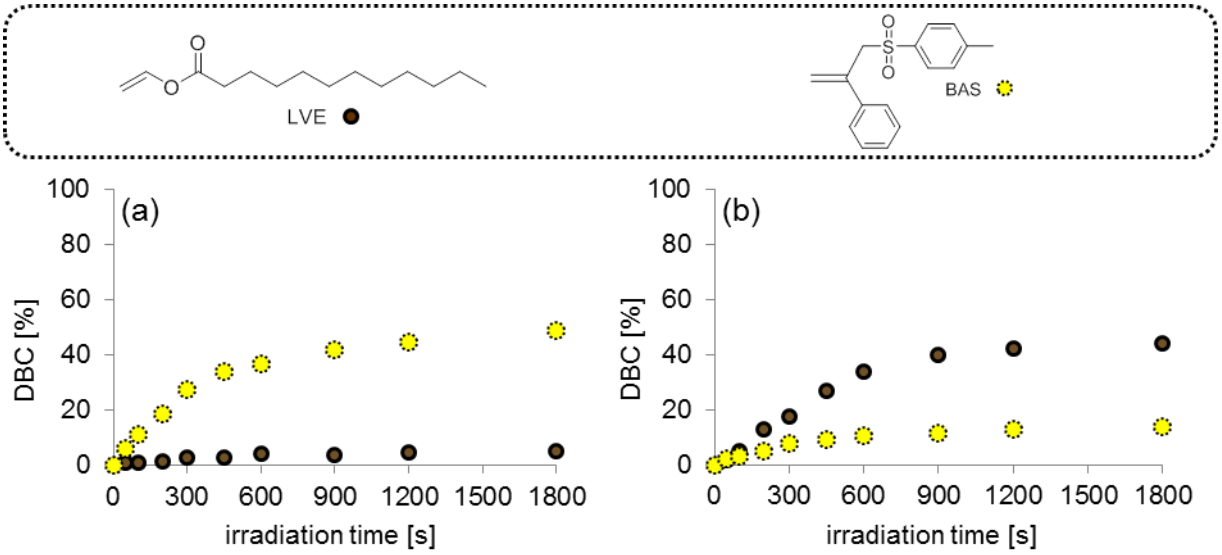

Figure 50: (a) Co-reactivity DBC-time diagram of 80 mol% LVE ● and 20 mol% BAS ● and (b) DBC-time curve of homopolymerization ● and total DB amount of AFCT-regulated formulation ●

Eventually, the β-allyl sulfone TSAP with a diethyl phosphonate activating group was investigated in LVE (Figure 51). The AFCT-regulated reaction is significantly slower than the

homopolymerization of LVE (r_R = 0.40). Moreover, the DBC_{reg} reaches with 22% only half of the DBC_{homo}. Besides that, a much favored consumption of TSAP can be seen (f_{co} = 6.91) resulting in low DBC_{LVE} of 11%.

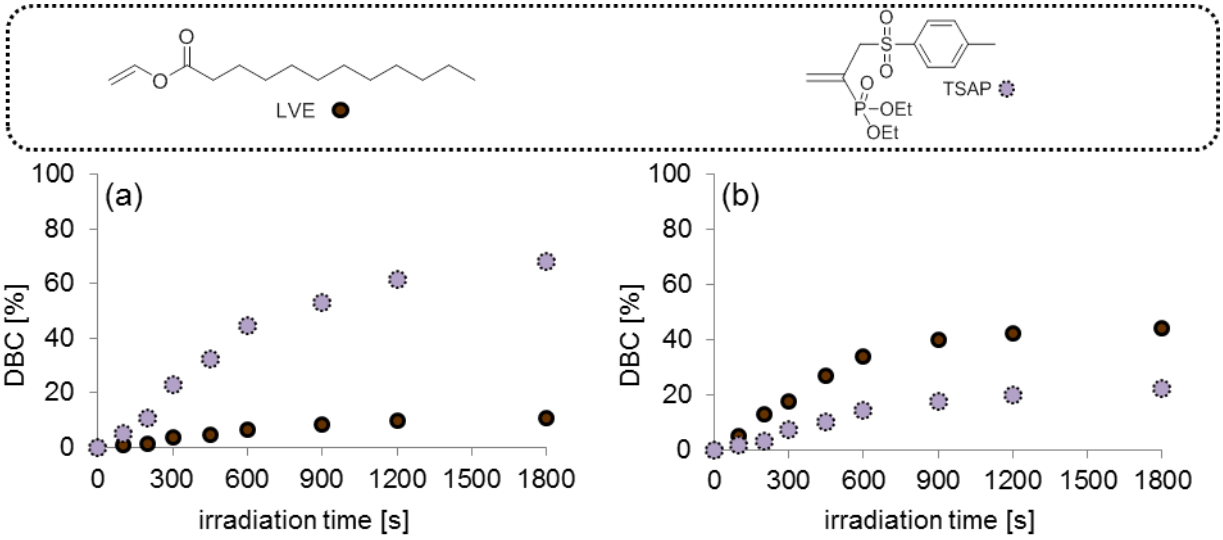

Figure 51: (a) co-reactivity DBC-time diagram of 80 mol% LVE ● and 20 mol% TSAP ● and (b) DBC-time curve of homopolymerization ● and total DB amount of AFCT-regulated formulation ●

In order to review the regulating properties of tested AFCT reagents, the four key figures were collected and plotted in diagrams. Considering reaction speed parameters, only VE4 does not seem to show retardation. As already discussed before, the reason for the high reaction speed is the rapid consumption of the AFCT reagent, while DBC_{LVE} remains low. However, all other tested AFCT reagents show significantly slower reaction compared to LVE homopolymerization.

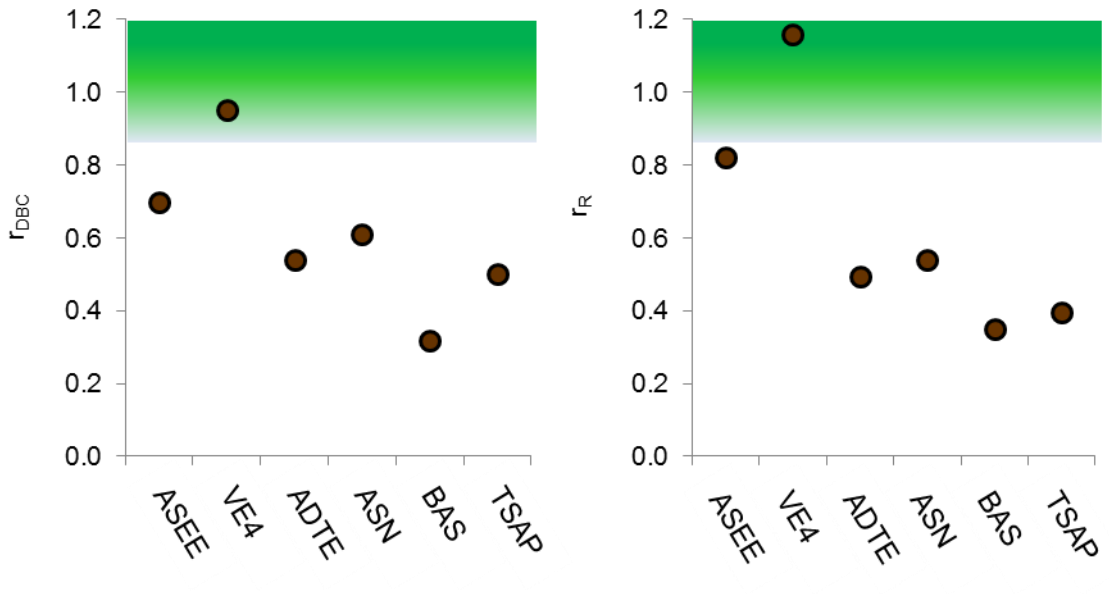

Figure 52: Overview of photopolymerization relative reactivity key figures of AFCT reagents in LVE

Co-reactivity parameters illustrated in Figure 53, clearly demonstrate that the consumption of all tested AFCT reagents in LVE is obviously preferred. No displayed co-reactivity factor f_{co} is close to 1. One explanation for this could be the bad resonance stability that LVE provides for radicals, while most tested activating groups are moieties that provide good resonance stability.

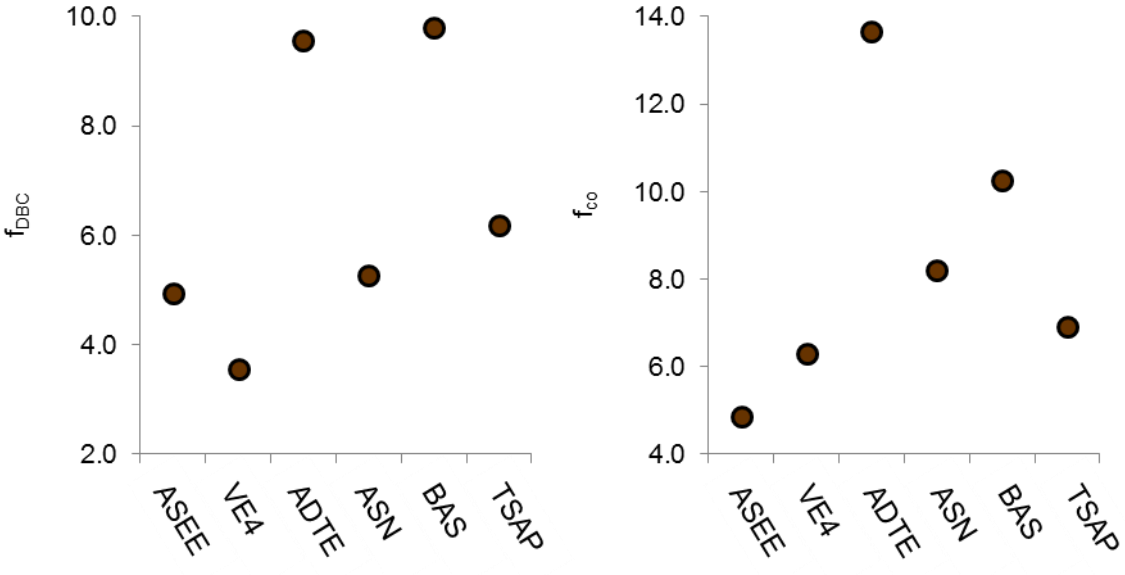

Figure 53: Overview of photopolymerization co-reactivity key figures of AFCT reagents in LVE

As a consequence, new AFCT reagents with suitable activating groups for VEs need to be found, since the concepts of ester, nitrile, phenyl, and phosphonate activating groups do not meet the requirements.

Table 5: Collected results for LVE and AFCT reagents

Formulation	*Homopolym. vs. total DBC*					*DBC of monomer and AFCT*			
Composition	**DBC_{end}** [%]	**r_{DBC}** [ ]	**R** [% s^{-1}]	**r_R** [ ]	Monomer AFCT	**DBC_{end}** [%]	**f_{DBC}** [ ]	**r** [% s^{-1}]	**f_{co}** [ ]
Neat LVE	44	--	0.058	-	LVE	44	-	0.058	-
LVE+ASEE	31	0.70	0.047	0.82	LVE ASEE	18 89	4.94	0.027 0.133	4.85
LVE+VE4	42	0.95	0.067	1.16	LVE VE4	28 100	3.57	0.033 0.209	6.30
LVE+ADTE	24	0.54	0.029	0.49	LVE ADTE	9 86	9.56	0.009 0.118	13.67
LVE+ASN	27	0.61	0.031	0.54	LVE ASN	15 79	5.27	0.013 0.110	8.20
LVE+BAS	14	0.32	0.020	0.35	LVE BAS	5 49	9.80	0.007 0.072	10.26
LVE+TSAP	22	0.50	0.023	0.40	LVE TSAP	11 68	6.18	0.011 0.073	6.91

2.1.3 Regulating acrylates *via* addition-fragmentation chain transfer

By far the largest group of monomers in radical photopolymerization is represented by ACs. Many industrial applications e.g. coatings, adhesives, and resins for stereolithography are based on AC chemistry. Thus, finding an AFCT reagent for regulating AC networks would be of great interest.

In order to compare the co-reactivity and the reaction speed of AFCT-regulated reactions in ACs, parameters were evaluated. Therefore, regression curves were calculated for all measuring points in the first 100 s of irradiation in the photoreactor. The slopes of these curves were then used to determine the key figures r_R and f_{co}.

In Figure 54 the homopolymerization of LAC is illustrated, which will be used as reference reaction for comparison with AFCT regulated reactions. As can be seen at first glance, LAC is way more reactive than LMA and LVE. With a DBC_{LAC} of 100% and a R_{homo} of 0.708 % s^{-1} the LAC homopolymerization is more than 12 times faster than LMA and LVE. Due to the high reactivity and fast reaction, a shorter total irradiation time of 900 s and shorter sampling times were chosen to cover the whole conversion range. However, ACs are also reported to exhibit rather good resonance stability for radicals with respect to copolymerization.

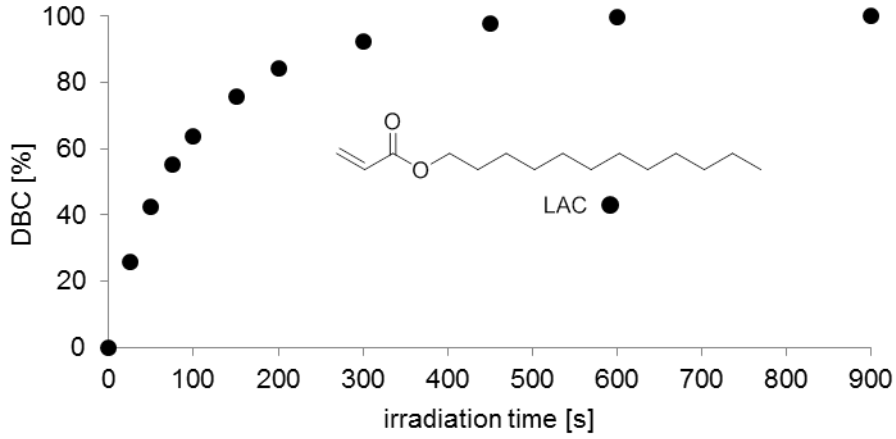

Figure 54: Homopolymerization of LAC ● in the photoreactor

First of all, the β-allyl sulfone ASEE with an ester activating group is measured. The ratio in the photoreactor of LAC to AFCT reagent was 80 mol% to 20 mol% with additional 3 mol% of PI Ivocerin. This ratio was used for all following AFCT reagent screenings. As can be seen in Figure 55, the LAC homopolymerization is much faster characterized by an r_R of 0.45 and reaches a higher DBC_{end} (r_{DBC} = 0.81). Regarding co-reactivity, ASEE is preferably consumed (f_{co} = 1.60) also leading to higher DBC_{ASEE} than DBC_{LAC} (f_{DBC} = 0.81). These findings match the already published C_{tr} of ASEE in MAC of 2.3[56].

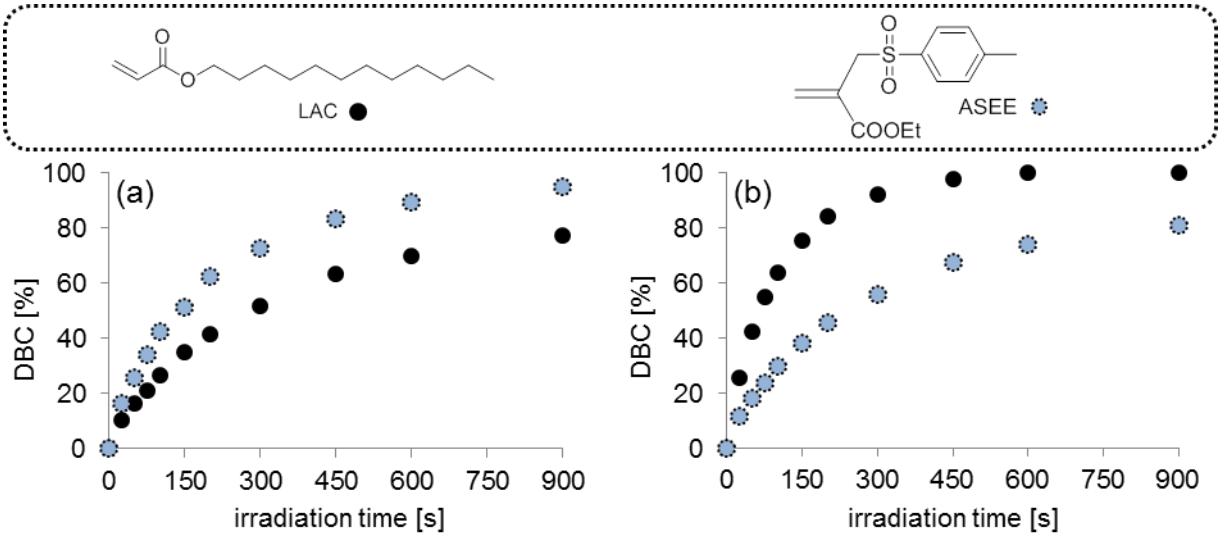

Figure 55: (a) Co-reactivity DBC-time diagram of 80 mol% LAC ● and 20 mol% ASEE ● and (b) DBC-time curve of homopolymerization ● and total DB amount of AFCT-regulated formulation ●

In Figure 56 the DBC-time curves of α-vinyl sulfonate VE4 with an ester activating group in LAC are depicted. The AFCT-regulated reaction is as fast as LAC homopolymerization with an r_R of 1.02 and a r_{DBC} of 1.00. This is particularly striking, since LAC homopolymerization is already very fast. Considering co-reactivity, similar curve shapes can be observed. Even though the consumption of VE4 is slightly preferred, it stays in the same range like LAC,

resulting in an f_{co} of 1.18 and an f_{DBC} of 1.00. This good co-reactivity can be attributed to the good resonance stabilization of radicals of the ester activating group of VE4.

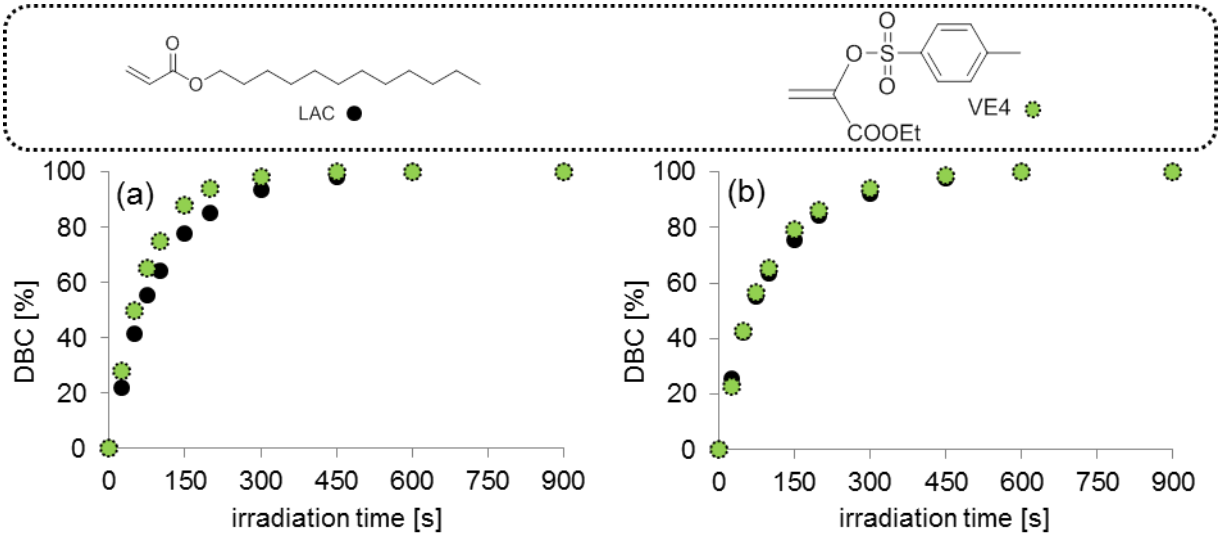

Figure 56: (a) Co-reactivity DBC-time diagram of 80 mol% LAC ● and 20 mol% VE4 ● and (b) DBC-time curve of homopolymerization ● and total DB amount of AFCT-regulated formulation ●

Next candidate for testing was the allyl sulfide ADTE with an ester activating group. In Figure 57 it can be seen, that the homopolymerization of LAC is considerably faster than the AFCT-regulated reaction (r_R = 0.29, r_{DBC} = 0.77). With respect to co-reactivity, ADTE is consumed at higher rates than LAC (f_{co} = 1.54) and also reaches a higher DBC_{end} (f_{DBC} = 1.19).

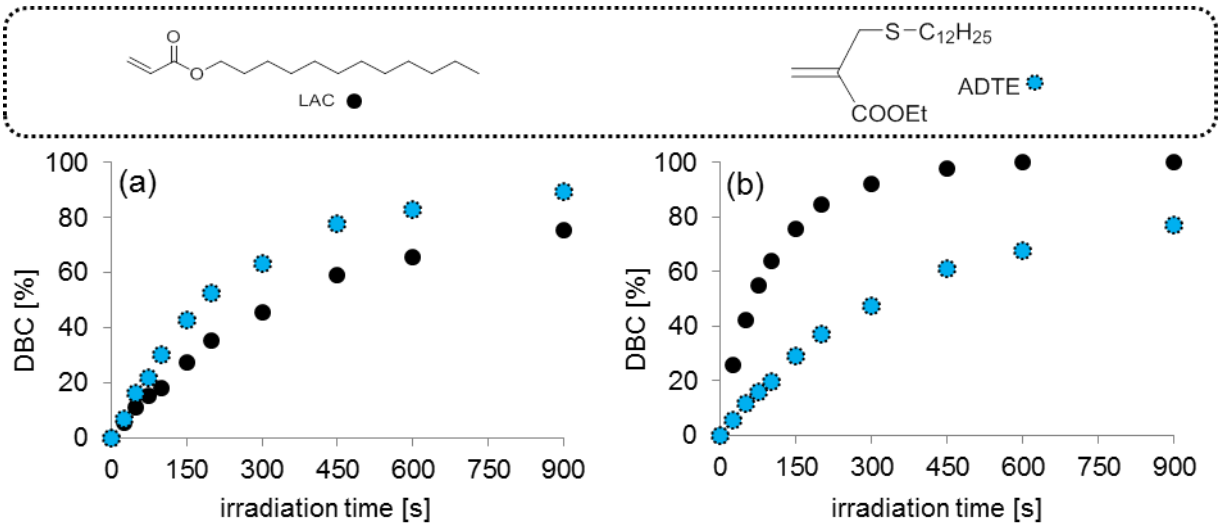

Figure 57: (a) Co-reactivity DBC-time diagram of 80 mol% LAC ● and 20 mol% ADTE ● and (b) DBC-time curve of homopolymerization ● and total DB amount of AFCT-regulated formulation ●

As represented in Figure 58, β-allyl sulfone ASN with a nitrile activating group exhibits significant retardation in comparison with LAC homopolymerization (r_R = 0.14). Also DBC_{reg} is much lower than DBC_{homo} (r_{DBC} = 0.57). Concerning co-reactivity, ASN reacts faster than LAC (f_{co} = 1.72) and leads to a higher DBC_{end} (f_{DBC} = 1.44).

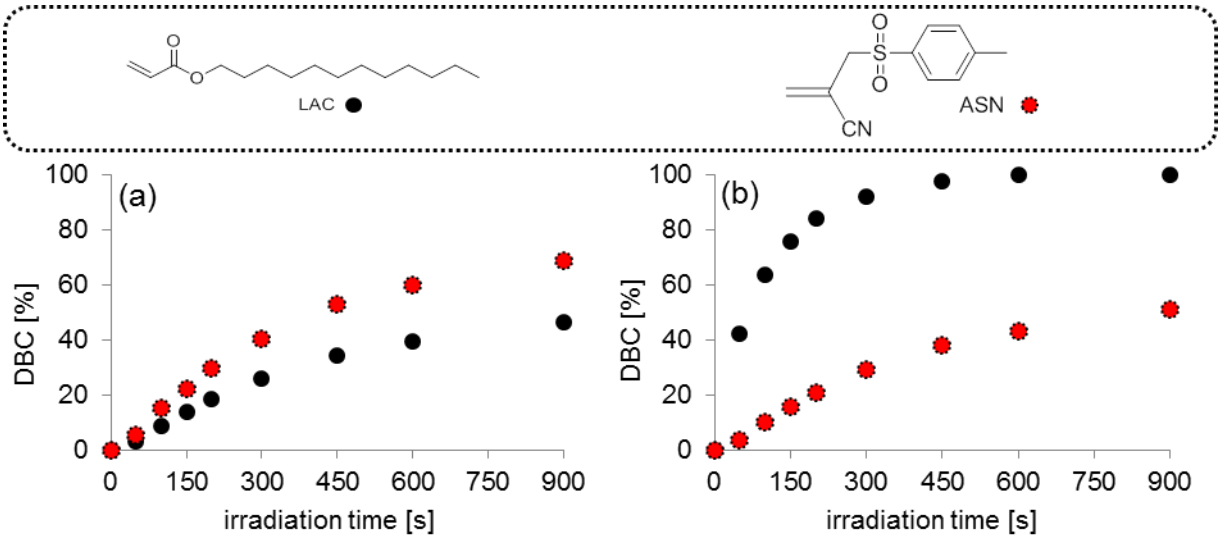

Figure 58: (a) Co-reactivity DBC-time diagram of 80 mol% LAC ● and 20 mol% ASN ● and (b) DBC-time curve of homopolymerization ● and total DB amount of AFCT-regulated formulation ●

Changing the activating group of the β-allyl sulfone to a phenyl moiety (BAS) (Figure 59) leads to an even slower reactivity rate (r_R = 0.10) and lower DBC_{reg} (r_{DBC} = 0.39). In regard to co-reactivity, BAS is preferably consumed resulting in the highest deviation from the targeted reactivity range (f_{co} = 3.73). Consequently, the DBC_{BAS} is significantly higher than DBC_{LAC} after 900 s of irradiation (f_{DBC} = 2.19).

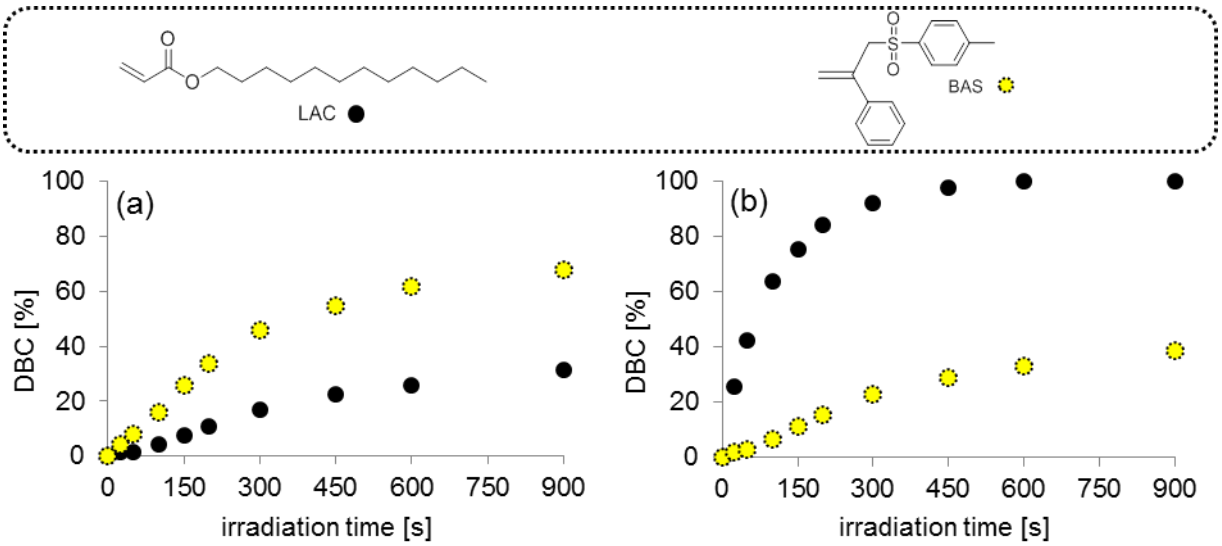

Figure 59: (a) Co-reactivity DBC-time diagram of 80 mol% LAC ● and 20 mol% BAS ● and (b) DBC-time curve of homopolymerization ● and total DB amount of AFCT-regulated formulation ●

Finally, the β-allyl sulfone TSAP with a diethyl phosphonate activating group was screened. Unlike the other β-allyl sulfone systems tested so far in LAC, TSAP-regulated photopolymerization shows preferred consumption of LAC, while TSAP is consumed slower. In this case, AFCT-regulated photopolymerization is not as slow as the beforehand tested β-allyl sulfones (r_R = 0.73), finally yielding a high DBC_{reg} (r_{DBC} = 0.93). However, taking a look at co-reactivity key figures demonstrates that LAC consumption is much more preferred (f_{co} = 0.29, f_{DBC} = 0.65).

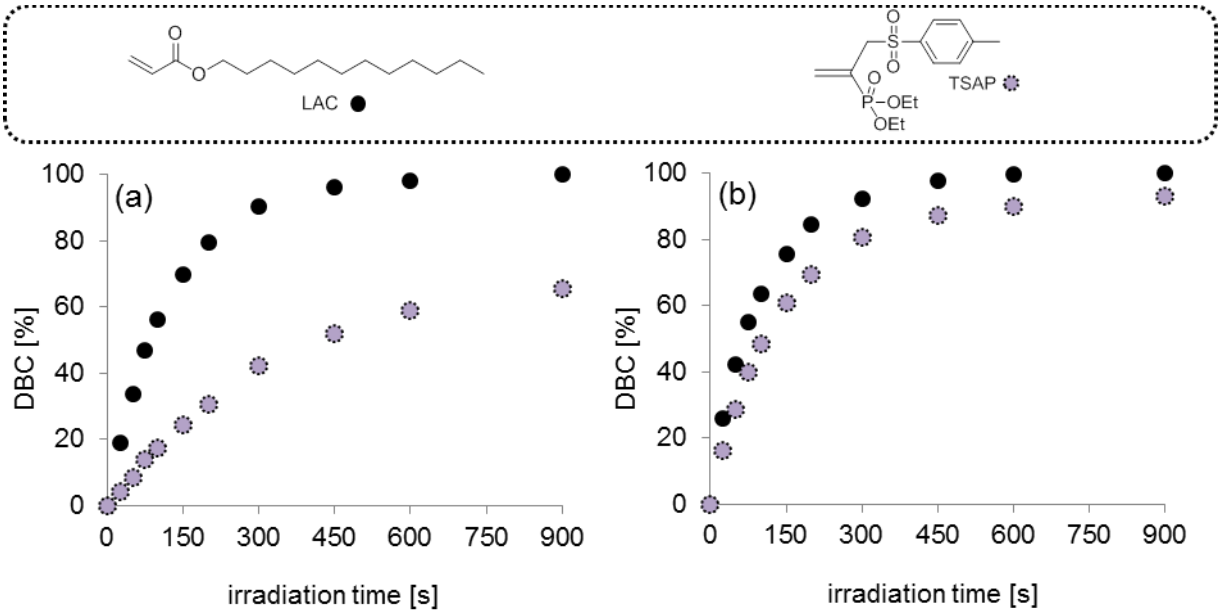

Figure 60: (a) Co-reactivity DBC-time diagram of 80 mol% LAC ● and 20 mol% TSAP ◌ and (b) DBC-time curve of homopolymerization ● and total DB amount of AFCT-regulated formulation ◌

Summarizing, an overview about all tested AFCT reagents in LAC and their extracted key parameters is given in Figure 61 and Figure 62. Discussing photopolymerization speed key figures of tested AFCT reagents in LAC, it can be seen that only the vinyl sulfonate ester VE4 is able to keep the reaction rate at the level of homopolymerization and reaches DBC_{homo} values as well. TSAP with the phosphorous activating group also reaches considerable conversion values, because of a high DBC_{LAC}. However, r_R is already significantly reduced. The addition of all other AFCT reagents to the LAC formulation results in significant retardation of the photopolymerization.

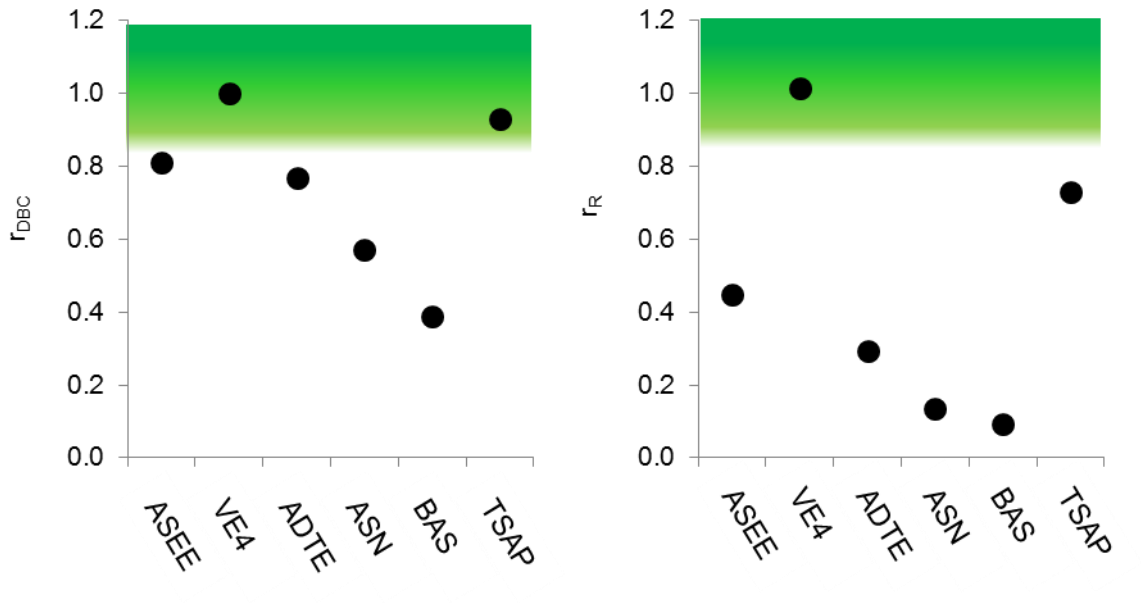

Figure 61: Overview of photopolymerization relative reactivity key figures of AFCT reagents in LAC

By means of Figure 62 statements about the co-reactivity can be made. The vinyl sulfonate ester VE4 and LAC are both completely consumed during the photopolymerization leading to a r_{DBC} of 1.00. Concerning co-reactivity factor f_{co}, VE4 is the only AFCT reagent within the required range. TSAP, which has shown a rather high reaction speed, is clearly outside the targeted area. However, ASEE and ADTE with their ester activating group, show with a r_{DBC} ~1.2 and an f_{co} ~1.5 preferring AFCT reagent over LAC consumption.

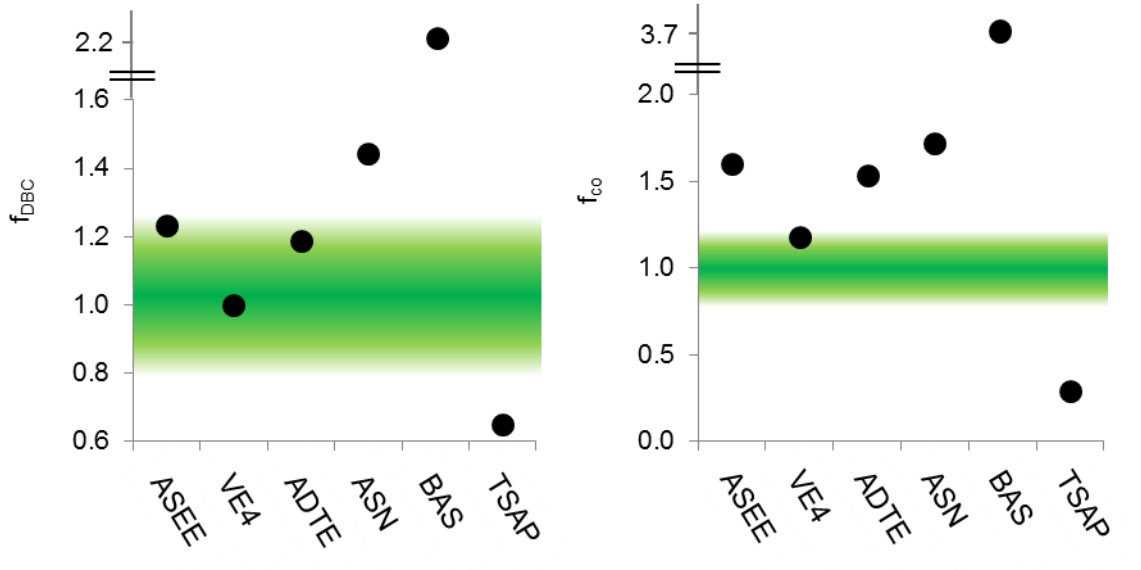

Figure 62: Overview of photopolymerization co-reactivity key figures of AFCT reagents in LAC

Remaining β-allyl sulfones ASN and especially BAS do not exhibit good co-reactivity (f_{co} >1.5).

One reason for the good regulation can be found in the structural similarity of VE4 and ACs. The ester activating group of VE4 essentially corresponds with an AC group, which can provide similar resonances stabilities for radicals. Nonetheless, this statement would also be true for β-allyl sulfone ASEE and allyl sulfide ADTE, which exhibit significant retardation and poorer co-reactivity, though.

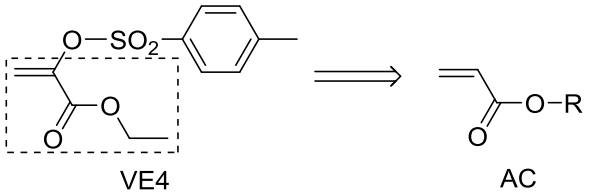

Figure 63: Structural similarity of AFCT reagent VE4 with ACs

The only difference between VE4 and ASEE is the oxygen instead of the methylene group. This structural distinction comes along with a change in mechanism (State of the art), which suggests that the fragmentation of the VE4 intermediate might be the decisive reaction step leading to such a difference in reactivity towards acrylates.

Table 6: Collected results for LAC and AFCT reagents

Formulation	***Homopolym. vs. total DBC***					***DBC of monomer and AFCT***			
Composition	**DBC_{end}** [%]	**r_{DBC}** [ ]	**R** [% s^{-1}]	**r_R** [ ]	Monomer AFCT	**DBC_{end}** [%]	**f_{DBC}** [ ]	**r** [% s^{-1}]	**f_{co}** [ ]
Neat LAC	100	-	0.708	-	LAC	100	-	0.708	-
LAC+ASEE	81	0.81	0.318	0.45	LAC ASEE	77 95	1.23	0.283 0.453	1.60
LAC+VE4	100	1.00	0.718	1.02	LAC VE4	100 100	1.00	0.703 0.831	1.18
LAC+ADTE	77	0.77	0.208	0.29	LAC ADTE	75 89	1.19	0.196 0.301	1.54
LAC+ASN	57	0.57	0.096	0.14	LAC ASN	52 75	1.44	0.084 0.145	1.72
LAC+BAS	39	0.39	0.067	0.10	LAC BAS	31 68	2.19	0.043 0.159	3.73
LAC+TSAP	93	0.93	0.515	0.73	LAC TSAP	100 65	0.65	0.603 0.176	0.29

2.2 New addition-fragmentation chain transfer reagents for vinyl esters and acrylates

2.2.1 3-(Phenylsulfonyl)prop-1-en-2-yl acetate (BVE)

Since no appropriate AFCT reagent was found so far for regulating VEs, a new AFCT reagent with the ability to regulate VEs should be synthesized. As discussed in General Part 2.1.1 and 2.1.3 for MAs and ACs, the similarity of the activating group is decisive for an equal and homogeneous consumption of the monomer and the AFCT reagent.

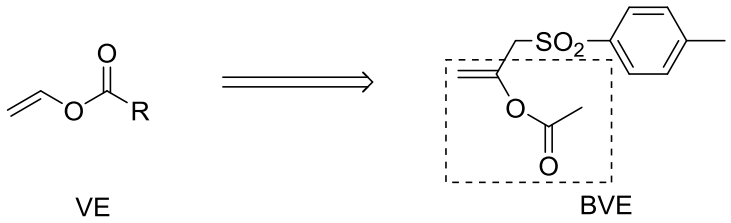

Figure 64: β-allyl sulfone with VE activating group

As shown in Figure 64, the new approach is to synthesize a new AFCT reagent with an activating group resembling a VE. Besides, this structure has already been reported to possess a C_{tr} of 2.8[56] in VAc. If the new AFCT reagent BVE acts in the reaction similar as ASEE and VE4, BVE should exhibit the desired regulation of VEs.

2.2.1.1 Synthesis of 3-(phenylsulfonyl)prop-1-en-2-yl acetate (BVE)

BVE was synthesized in a three step synthesis. Starting from an equimolar amount of thiophenol and propargyl bromide in dry THF catalyzed with Et_3N, 94% of the first product were isolated. A similar synthesis procedure was already reported by *Gotoh et al.*[77]

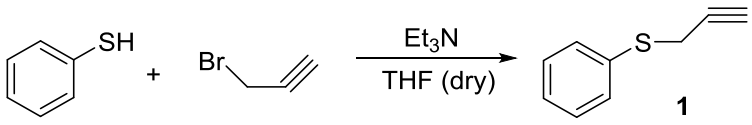

The second synthesis step was carried out in dry DMF using 2.8 eq. Oxone® with its $KHSO_5^-$ species for oxidizing 1.0 eq. **1** yielding in 90% of the sulfonyl product **2**.

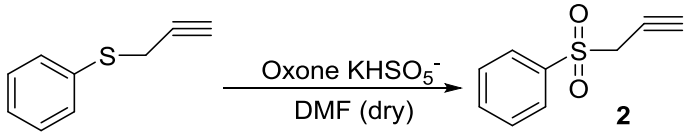

Finally, BVE was synthesized from the sulfonyl product **2** (1.0 eq.) of the second step in DMSO with sodium acetate (18.0 eq.) and acetic acid (4.8 eq.) as already reported by *Stirling et al.*[78] During the concentration of the dissolved product, white crystals precipitated, which were washed with cold ether to give a yield of 63% of the desired BVE.

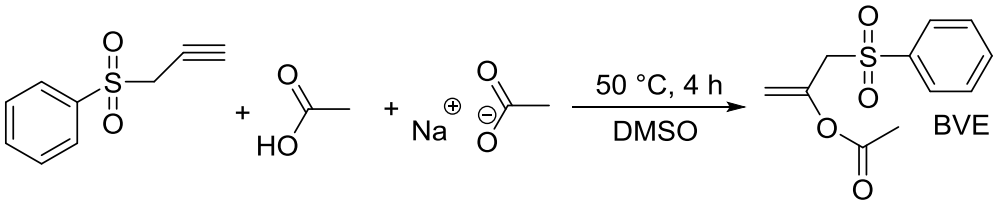

2.2.1.2 Studying reactivity of 3-(phenylsulfonyl)prop-1-en-2-yl acetate (BVE)

The isolated product was then used to carry out further photoreactor experiments for determining the co-reactivity of BVE with LMA, LVE, and LAC. Therefore, a formulation consisting of 80 mol% LMA and 20 mol% BVE with additional 3 mol% Ivocerin was analyzed. The irradiation times for the different monomers correspond with the times in the Section 2.1 as well as the calculation of the key figures r_{DBC}, r_R, f_{DBC}, and f_{co}.

Figure 65 illustrates the photoreaction of LMA with BVE. Concerning reaction speed, the AFCT-regulated reaction is slowed down in comparison with homopolymerization (r_{DBC} = 0.68, r_R = 0.66). Co-reactivity is exceptionally poor, which is confirmed by an f_{DBC} of 0.04 and an f_{co} of 0.05. Hence, BVE is not suitable for regulating MAs.

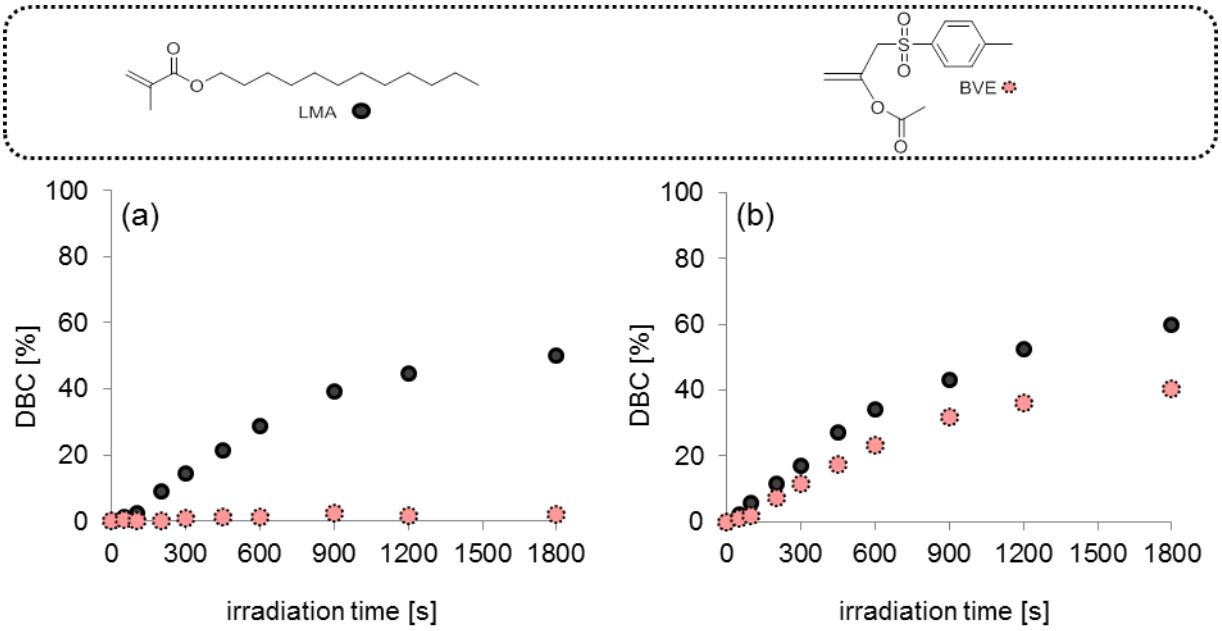

Figure 65: (a) Co-reactivity DBC-time diagram of 80 mol% LMA ● and 20 mol% BVE ● and (b) DBC-time curve of homopolymerization ● and total DB amount of AFCT-regulated formulation ●

Particularly interesting is the photopolymerization of LVE and BVE in Figure 66. Photopolymerization speed is significantly slower, which is expressed by an r_{DBC} of 0.45 and an r_R of 0.32. The co-reactivity plot exhibits a preferred consumption of BVE leading to an f_{co} of 1.75 and an f_{DBC} of 1.76. Even though, BVE exhibits the best co-reactivity with LVE measured so far, significant retardation makes possible future application unlikely.

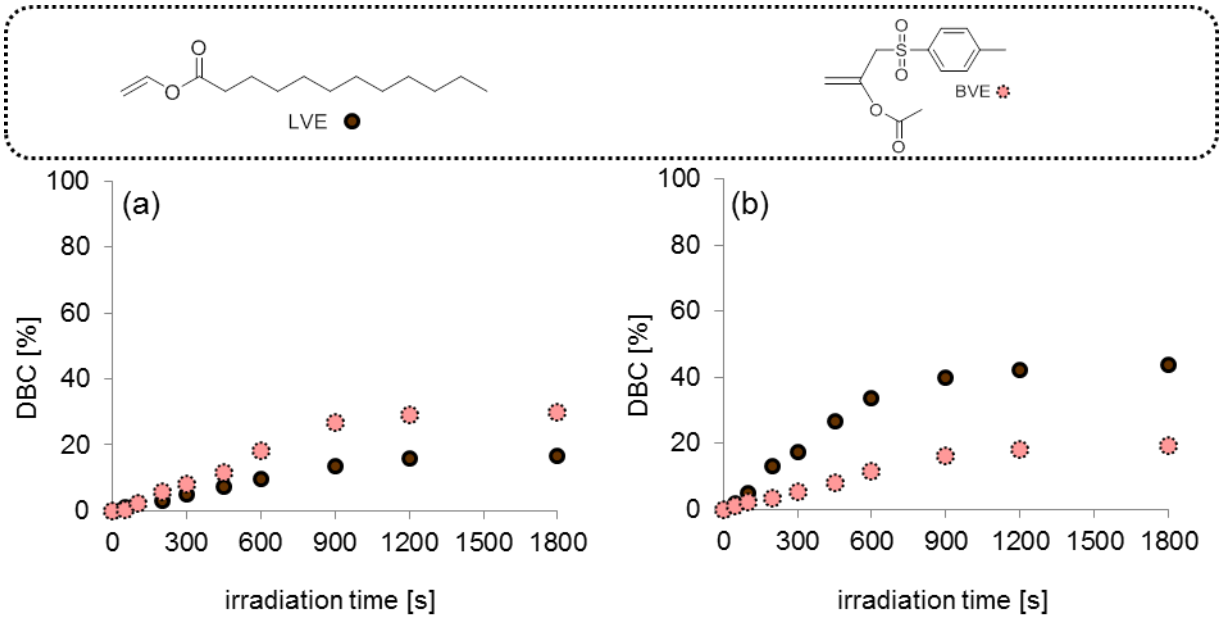

Figure 66: (a) Co-reactivity DBC-time diagram of 80 mol% LVE ● and 20 mol% BVE ● and (b) DBC-time curve of homopolymerization ● and total DB amount of AFCT-regulated formulation ●

Regarding BVE regulation of LAC, the AFCT-regulated reaction shows a high DBC_{reg} (r_{DBC} = 0.93), which mainly arises because of the high DBC_{LAC} of 100%. However, the analysis of the slopes of the DBC-time curves exhibits retardation of the AFCT-regulated reaction (r_R = 0.66). Finally, the co-reactivity plot reveals that co-reactivity between LAC and BVE is rather poor (f_{co} = 0.38, f_{DBC} = 0.21). These results exclude BVE as candidate for regulating AC networks.

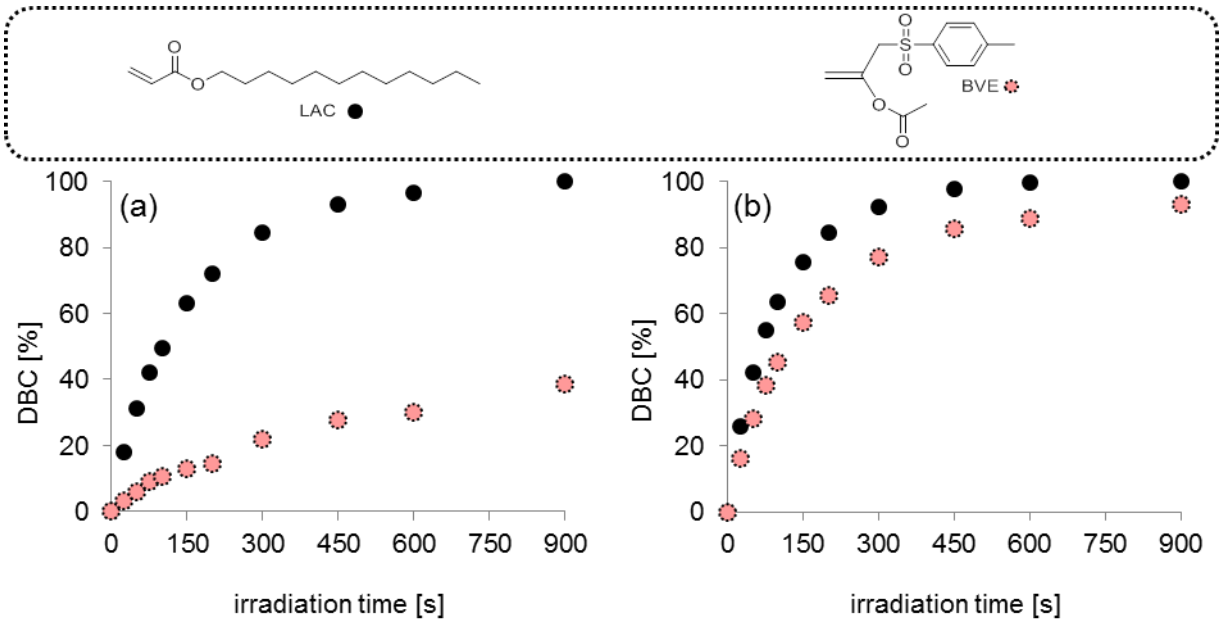

Figure 67: (a) Co-reactivity DBC-time diagram of 80 mol% LAC ● and 20 mol% BVE ● and (b) DBC-time curve of homopolymerization ● and total DB amount of AFCT-regulated formulation ●

It has to be summarized that BVE was not found to be an ideal candidate to regulate MAs, VEs or ACs.

2.2.2 Ethyl 2-((4-methylphenyl)sulfonamido)acrylate (TAA)

In literature, β-allyl sulfone ASEE[36, 61] and α-vinyl sulfonate VE4[66] are already known to regulate MA-based networks in photopolymerization yielding more homogeneous networks with enhanced mechanical properties. Additionally, beforehand conducted photoreactor screening study discovered the regulating abilities of VE4 in ACs. The structural difference between VE4 and ASEE is the oxygen group instead of the methylene group (Figure 68). In order to find new AFCT reagents, the influence of nitrogen in position of the methylene and oxygen group upon AFCT regulation would be interesting.

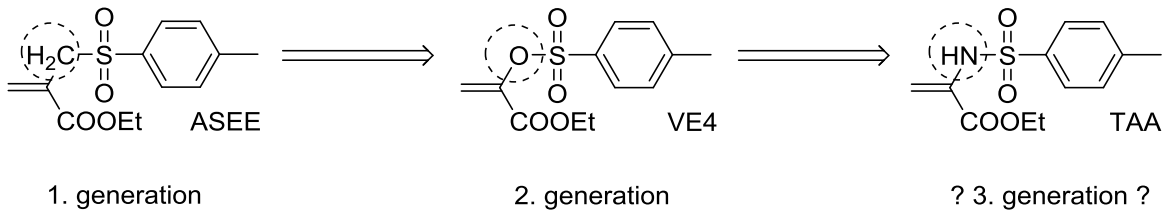

Figure 68: Depiction of different generations of AFCT reagents

2.2.2.1 Synthesis of Ethyl 2-((4-methylphenyl)sulfonamido)acrylate (TAA)

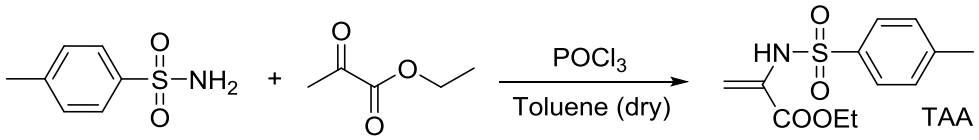

The synthesis of TAA was performed in one step, which was published by Y. Yonezawa *et al.*[79] before. Phosphorus oxychloride (1.1 eq.) was added to a suspension of p-toluenesulfonamide (7.0 eq.) and ethyl pyruvate (7.0 eq.) in dry toluene and was stirred 20 h at 80 °C to give a crude product, consisting of white crystals and an orange matrix. According to the paper the yield for this reaction should be 51% after column chromatography with benzene as solvent. Solubility tests of the crude product exhibited, that the white crystals could be separated from the orange syrup-like matrix with cold ether. It was possible to isolate a quantity of white TAA crystals with a yield of 48%.

The characterization of the product was done by NMR analysis. ^{1}H NMR shows almost all expected hydrogen signals. Surprisingly the expected two DB signals for TAA are overlapping, but the integration gives 2 H coinciding with the target structure. Moreover, a

^{13}C NMR was measured, that also shows all expected signals. In order to assure that the desired molecule structure was successfully synthesized, the performed HSQC spectrum finally indicates that the 2 H at 5.62 ppm are coupling with the C atom at 106.7 ppm. Hence, the structure of the target molecule is confirmed.

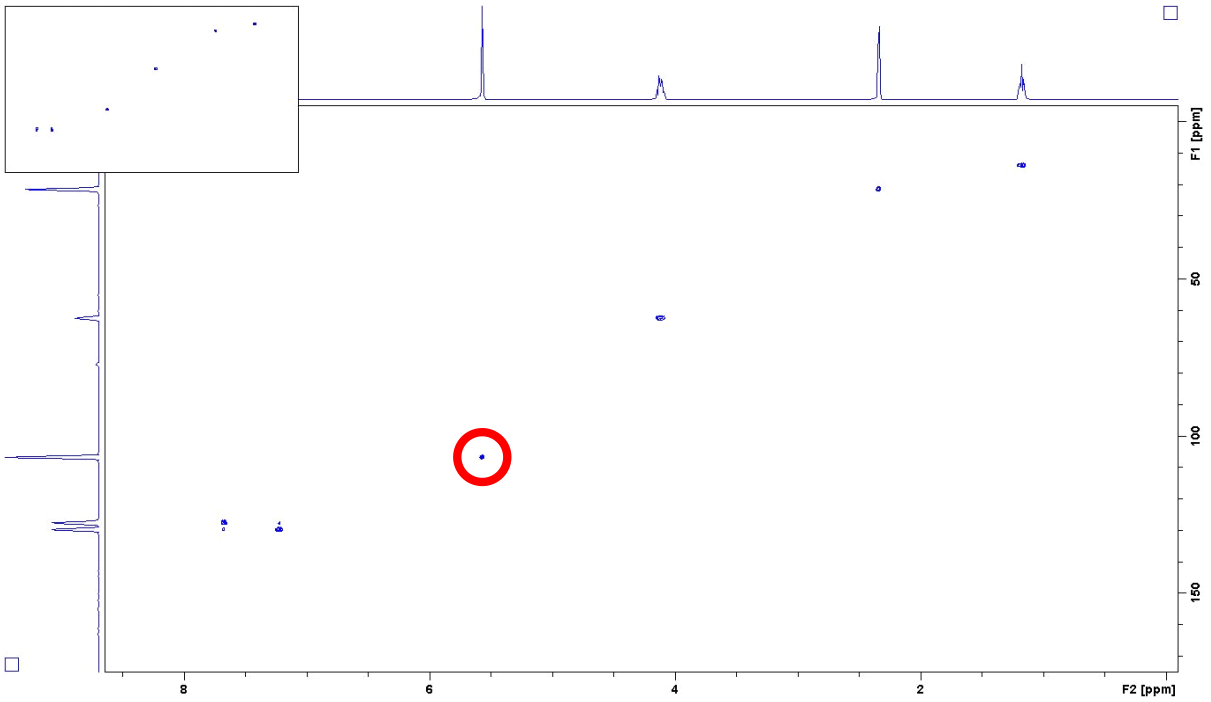

Figure 69: HSQC Spectrum: The red circle indicates the coupling of the carbon atom at 106.7 ppm and the two hydrogen atoms at 5.62 ppm.

2.2.2.2 Studying the reactivity of Ethyl 2-((4-methylphenyl)sulfonamido)acrylate (TAA)

For photo-DSC a formulation of BenzMA with 1 w% PI Ivocerin and a mixture of 80 mol% BenzMA and 20 mol% TAA with 1 w% Ivocerin were prepared. The general idea of the photo-DSC experiment is to polymerize BenzMA once without and once in the presence of CTA monitoring the generated polymerization heat and afterwards perform ^{1}H NMR to determine the DBC. For reproducibility reasons the measurements for both formulations were carried out three times. The results for the average values of the photo-DSC experiment can be seen in Table 7.

Table 7: Average results for neat BenzMA formulation and for BenzMA/TAA mixture

formulation	t_{max} [s]	h_{max} [mW mg^{-1}]	$t_{95\%}$ [s]	Δ H [J/g]
BenzMA	23.8	1.985	128.1	139.2
BenzMA/TAA	19.1	0.563	120.7	28.4

The value for the reaction heat ΔH for the pure BenzMA formulation is with 139.2 J/g significantly higher than for the BenzMA/TAA mixture with 28.2 J/g.

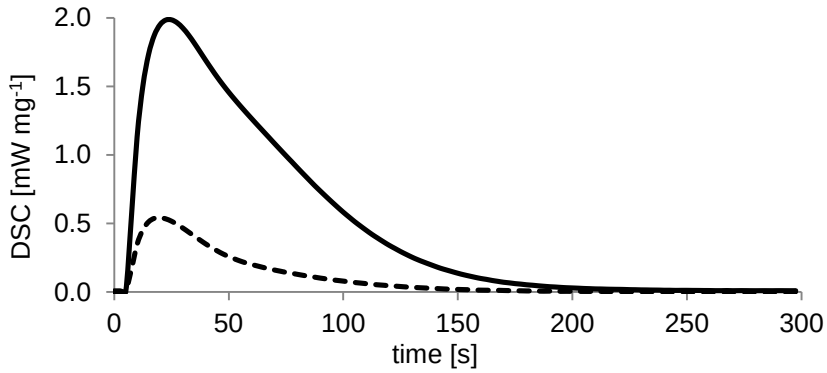

Figure 70: Photo-DSC Plot of pure BenzMA (——) with 1 w% Ivocerin and a mixture of BenzMA (80 mol%)/ TAA (20 mol%) (- - -) with 1 w% Ivocerin

Only through ^{1}H NMR spectroscopy the overall conversion of each DB for this specific formulation can be determined. Therefore, the methylene group of BenzMA at 5.18 ppm was considered to be the best internal reference. During the polymerization the signals for methylene peak are slightly shifted upfield ~ 4.68 ppm, which need to be considered for later interpretation.

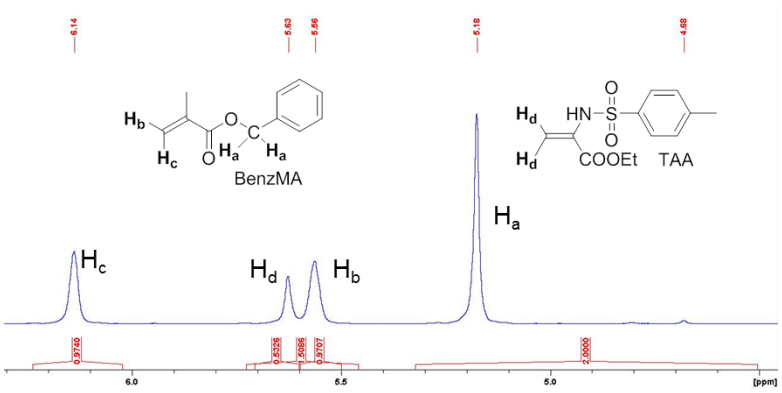

Figure 71: Spectrum of uncured BenzMA/TAA formulation and corresponding signals for calculation of DBC

Basically, the integrals of monomer DBs at 6.14 and 5.56 ppm decrease during polymerization. This decrease directly correlates with the conversion. The same principle applies for the integral of TAA DB at 5.63 ppm, when it is consumed during polymerization.

As can be seen in Figure 71, the TAA and one BenzMA peak are slightly overlapping. Thus, both peaks at 5.63 and 5.56 ppm were integrated and the area of the second BenzMA peak at 6.14 ppm was subtracted from the area of the two peaks to finally get the integral for the hydrogens of TAA. The calculated DBC for the photocured neat BenzMA was only 43%. By dividing ΔH of the neat BenzMA by the DBC_{BenzMA} determined by ^{1}H NMR and multiplying this term by the molecular weight of BenzMA gives a ΔH_0 value for BenzMA of 57 kJ mol^{-1}. This figure perfectly corresponds with the ΔH_0 for BenzMA of 56 kJ mol^{-1} known from literature[80].

For the mixture of BenzMA and TAA the DBC of BenzMA is around 2% and the DBC for TAA is 13%.

Table 8: Average Results for DBC calculated from ^{1}H-NMR

formulation	DBC_{BenzMA} [%]	DBC_{TAA} [%]
BenzMA	43.0	-
BenzMA/TAA	1.9	13.3

According to the ^{1}H NMR interpretation TAA is preferably consumed even though there is a surplus of BenzMA in the formulation. For determining the $DBC_{photo\text{-}DSC}$ the results for ΔH in Table 7 and DBC_{NMR} in Table 8 can be used. Therefore following equations are used:

$$\Delta H_{0,BenzMA} = \frac{\Delta H_{BenzMA}}{DBC_{NMR}} \quad (1)$$

$$DBC_{photo-DSC} = \frac{\Delta H_{BenzMA}}{\Delta H_{0,BenzMA} \frac{m_{BenzMA}}{m_{total}}} \quad (2)$$

ΔH_{BenzMA} corresponds with the value 139.2 J g^{-1} and is divided by the DBC_{NMR} of BenzMA pure 43.0% (Table 8) to give $\Delta H_{0,BenzMA}$. m_{total} and m_{BenzMA} match with the total mass of the mixture and the mass of BenzMA in the mixture. The calculated value for the $DBC_{photo\text{-}DSC}$ for BenzMA in the formulation with TAA is 3.3% which perfectly correlates with the DBC_{NMR} of BenzMA of 1.9%. As found previously for active CTAs, TAA seems not to contribute to the heat of polymerization.

Obviously, TAA is preferably consumed by the formed radicals, whereas the BenzMA DBs are nearly not attacked, even though there is a fourfold surplus of BenzMA DBs in the mixture. Another interesting aspect is that according to the results no sulfonyl radicals seem to be formed by an AFCT mechanism. Hence, it can be concluded that TAA cannot be used as AFCT reagent.

3 In depth kinetic and mechanistic studies of thiols, β-allyl sulfones, and α-vinyl sulfonates in acrylates

Nowadays, ACs represent by far the largest and most important group of radical cured photopolymers. The unregulated free radical photopolymerization of ACs leads to inhomogeneous, brittle networks and shrinkage stress in the material. The state-of-the-art method for regulating free radical photopolymerization of ACs is thiol-ene chemistry, whose application comes along with drawbacks such as strong odor, low storage stability, and the formation of flexible thio-ether bridges yielding soft material. These disadvantages of thiol-ene chemistry stimulate the demand for alternative methods for modifying AC-based networks. Considering beforehand conducted photoreactor screening study, vinyl sulfonate ester VE4 has shown great co-reactivity with ACs without retarding photopolymerization. Thus, more details about the regulating ability of vinyl sulfonate ester VE4 in ACs should be gained and compared with a model thiol MT. Moreover, the already from literature known and second best performing β-allyl sulfone ASEE should be tested in ACs as well.

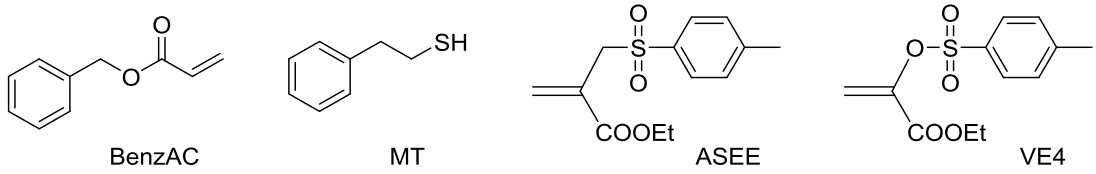

BenzAC MT ASEE VE4

Figure 72: Monomer BenzAC, thiol MT, β-allyl sulfone ASEE, and vinyl sulfonate ester VE4

Besides photoreactor measurements, GPC, and Maldi-TOF-MS should provide more detailed information about the AFCT mechanism. Eventually, the kinetic influence of CTA concentration should also be investigated by varying the CTA ratio in the formulations (0, 5, 10, 20, and 35 mol%). As monomer BenzAC was taken, which was distilled before usage to remove the inhibitor. Moreover, BenzAC-based oligomers and polymers provide phenyl side, which can absorb UV-light energy. This can be beneficial for later conducted Maldi-TOF-MS measurements.

3.1 Free radical homopolymerization of acrylates

First of all, the unregulated homopolymerization of BenzAC was measured in the photoreactor as reference for the later conducted BenzAC/ CTA formulations. After the ^{1}H NMR spectroscopy, GPC measurements were performed to observe the development of the molecular weight distribution during the polymerization.

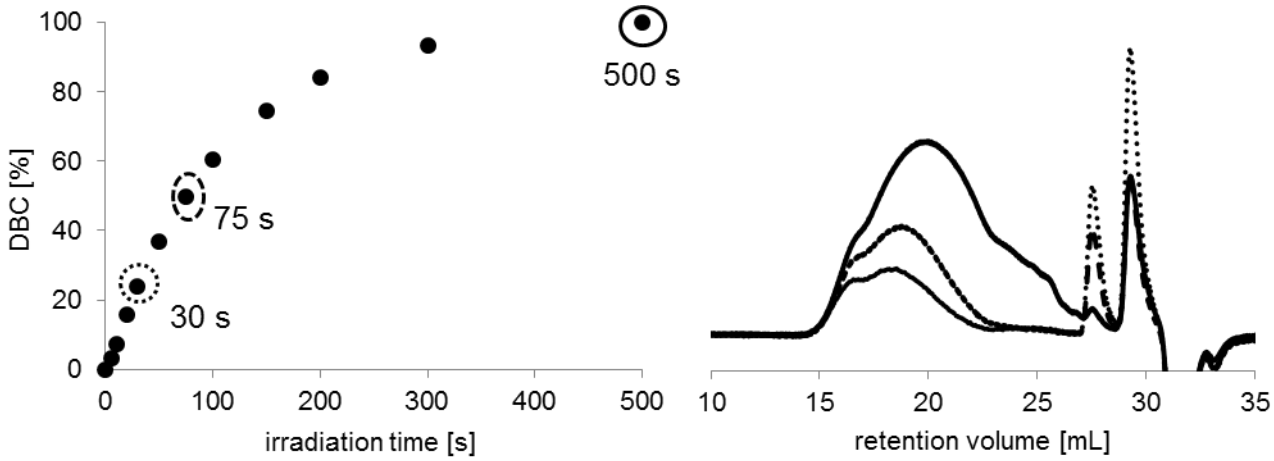

Figure 73: Conversion curve and molecular weight distribution for 30 s (▪▪▪▪▪▪), 75 s (▬▬▬), and 500 s (▬▬▬) for the homopolymerization of BenzAC (●)

As can be seen in Figure 73, homopolymerization reaches 100% DBC (**DBC_{homo}**) after 500 s of irradiation, which indicates a fast polymerization process. In order to cover lower DBCs as well, shorter irradiation intervals were chosen. For determining the regression curve of the BenzAC homopolymerization, the first 8 measuring points were used (0, 5, 10, 20, 30, 50, 75, and 100 s of irradiation). Its slope R_{homo} was calculated to be 0.654 % s^{-1}. Moreover, three samples after 30 s (low DBC), 75 s (medium DBC), and 500 s (high DBC) irradiation were picked from the photoreactor curve and GPC measurements were conducted.

Table 9 reveals that homopolymerization of BenzAC leads to massive variation of the polydispersity index (**Đ**), which is not expected for free radical polymerization. Since the samples after 30 s and 500 s show similar Đ values, it can be assumed that for the sample after 75 s an unknown error occurred. Moreover, it can be seen that the molecular weight (M_n) decreases, if the sample after 30 s of irradiation (7,200 Da) is compared with the sample after 500 s of irradiation (4,000 Da). This can be explained by the increase of termination reactions in the late stage of photopolymerization. However, the unregulated reaction ends up with 100% conversion and a M_n ~4,000 Da exhibiting a broad molecular weight distribution with Đ ~7.6.

Table 9: Results for BenzAC homopolymerization

irradiation time	**conversion**	**GPC**	
	BenzAC [%]	M_n [Da]	Đ
30 s	24	7,200	7.90
75 s	50	9,300	5.26
500 s	100	4,000	7.62

3.2 Regulating acrylates *via* thiols

Thiol-ene chemistry is nowadays the state-of-the-art method for regulating ACs. To determine the regulating ability of thiols in ACs, the thiol MT was chosen as model thiol. The main reason for selecting MT for this in depth study was that the signal of its methylene group next to the sulfur (2.8 ppm) did not overlap during photopolymerization with new formed signals in the ^{1}H NMR spectrum. When the thiyl radical reacts with a DB forming a thio-ether bridge the signal is shifted upfield and the initial methylene signal decreases. This decrease is proportional to the conversion of MT.

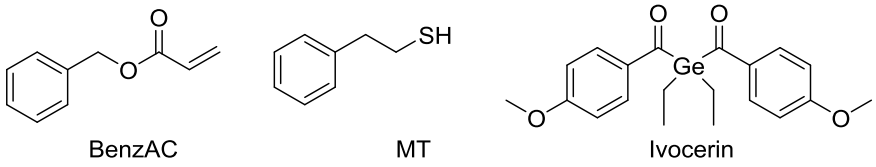

Figure 74: Monomer BenzAC, thiol MT, and PI Ivocerin

In order to determine the regulating abilities of MT with respect of different thiol concentrations in ACs, photoreactor experiments with thiol concentrations of 5, 10, 20, and 35 mol% were investigated. After ^{1}H NMR spectroscopy, GPC measurements of the NMR samples taken after 30, 75, and 500 s of irradiation were conducted. Additionally, Maldi-TOF-MS analysis of the sample containing 20 mol% MT was carried out.

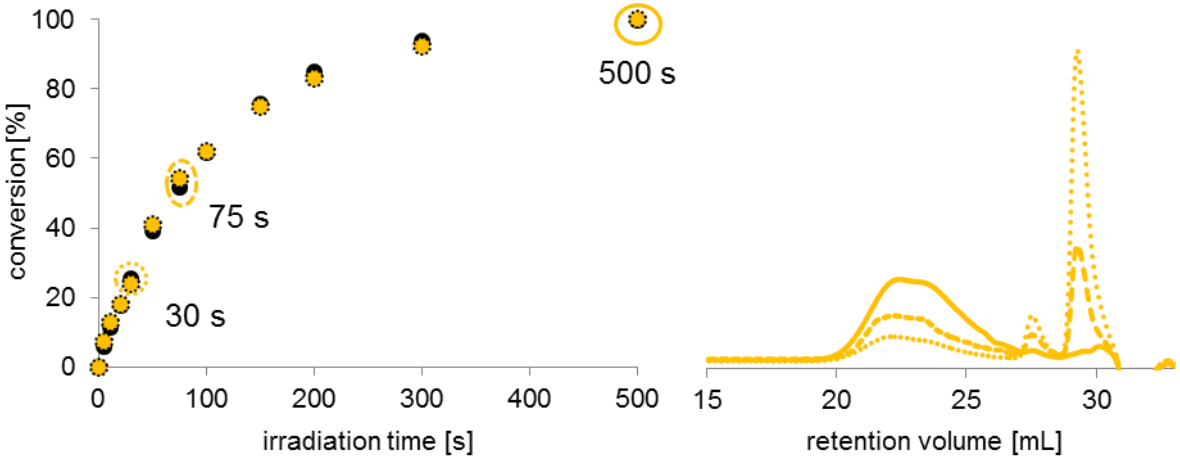

Figure 75: Conversion curve and molecular weight distribution for 30 s (·····), 75 s (– – –), and 500 s (——) for AC formulation consisting of 95 mol% BenzAC (●) and 5 mol% MT (●)

For the AC formulation containing 5 mol% thiol (Figure 75), a DBC_{reg} of 100% was reached (r_{DBC} = 1.00). Moreover, the AFCT-regulated reaction is as fast as the homopolymerization (r_R = 1.04). In terms of co-reactivity an equal and steady consumption of BenzAC and MT throughout the whole photopolymerization process can be observed (f_{DBC} = 1.00, f_{co} = 1.02). The same consumption rates of BenzAC and thiol result in good regulation during

photopolymerization leading to constant Đ values ~1.9 and M_ns between 1700 and 1950 Da (Table 10).

Table 10: Results for BenzAC 95 mol% and MT 5 mol%

irradiation time	conversion		GPC	
	BenzAC [%]	MT [%]	M_n [Da]	Đ
30 s	25	24	1,950	1.95
75 s	52	54	1,900	1.92
500 s	100	100	1,700	1.92

When raising the thiol content to 10 mol%, the reaction speed of the AFCT-regulated reaction remains in the range of homopolymerization (r_{DBC} = 0.98, r_R = 0.95). Concerning co-reactivity, Figure 76 depicts equal consumption of MT and BenzAC (f_{co} = 0.95) until the end of photopolymerization, where less thiol is consumed (f_{DBC} = 0.88).

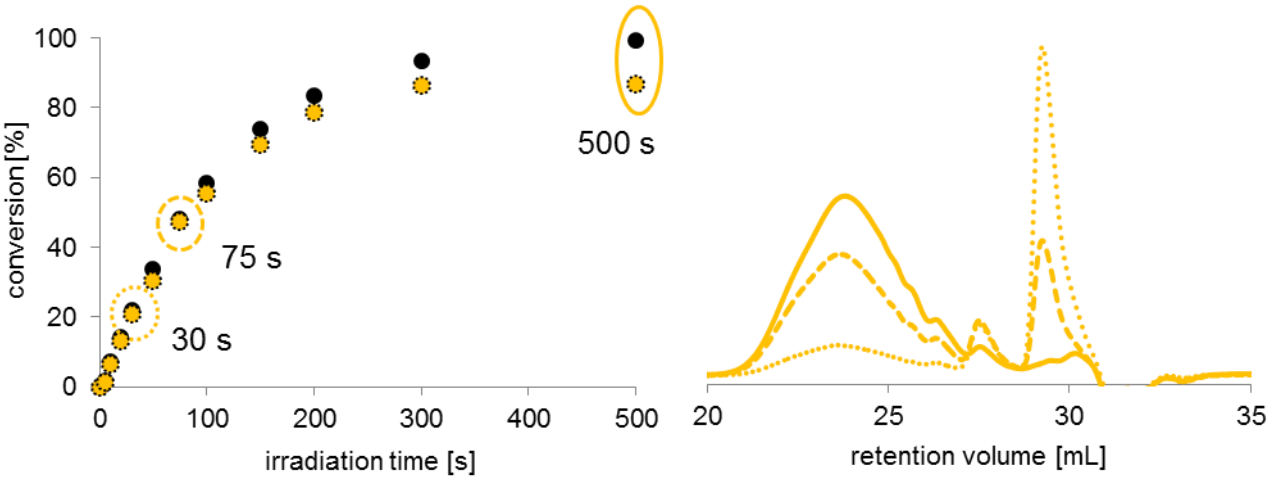

Figure 76: Conversion curve and molecular weight distribution for 30 s (·····), 75 s (– – –), and 500 s (——) for AC formulation consisting of 90 mol% BenzAC (●) and 10 mol% MT (●)

Regarding regulation, Table 11 points out that constant Đ ~1.6 were obtained during polymerization. M_ns were measured in the range between 1,250 and 1,300 Da. Compared to the formulation containing 5 mol% thiol, this is a significant decrease in molecular weight and a clear narrowing of the molecular weight distribution.

Table 11: Results for BenzAC 90 mol% and MT 10 mol%

irradiation time	conversion		GPC	
	BenzAC [%]	MT [%]	M_n [Da]	Đ
30 s	22	21	1,250	1.64
75 s	48	47	1,300	1.61
500 s	100	87	1,250	1.59

Adding 20 mol% of MT to the AC formulation does not influence the reaction speed of AFCT-regulated compared to homopolymerization (r_{DBC} = 0.97, r_R = 0.96). Nevertheless, co-reactivity becomes worse leading to an f_{co} of 0.77 and an f_{DBC} of 0.85.

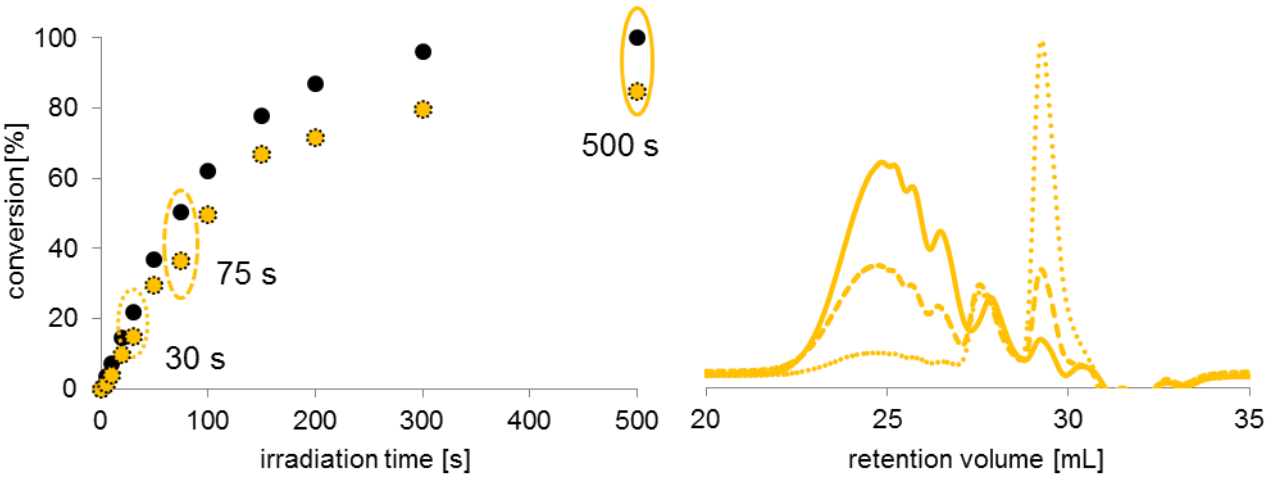

Figure 77: Conversion curve and molecular weight distribution for 30 s (·····), 75 s (– – –), and 500 s (——) for AC formulation consisting of 80 mol% BenzAC (●) and 20 mol% MT (●)

GPC results in Figure 77 and Table 12 prove that the 20 mol% thiol formulation exhibits the expected better regulation with Đ ~1.35 and smaller M_ns between 800 and 850 Da than the 10 mol% thiol formulation.

Table 12: Results for BenzAC 80 mol% and MT 20 mol%

irradiation time	**conversion**		**GPC**	
	BenzAC [%]	MT [%]	M_n [Da]	Đ
30 s	22	15	850*	1.37
75 s	50	36	850*	1.38
500 s	100	84	800*	1.34

*outside of calibration range (890 – 177,000 Da)

Finally, a formulation containing 35 mol% MT was analyzed. Photopolymerization speed key figures exhibit that the reaction rate remains high compared to BenzAC homopolymerization (r_R = 0.92, r_{DBC} = 0.93). As can be seen in Figure 78, the consumption of BenzAC becomes even more preferred than the thiol (f_{co} = 0.65) ending up in a final thiol conversion of 79% (f_{DBC} = 0.79).

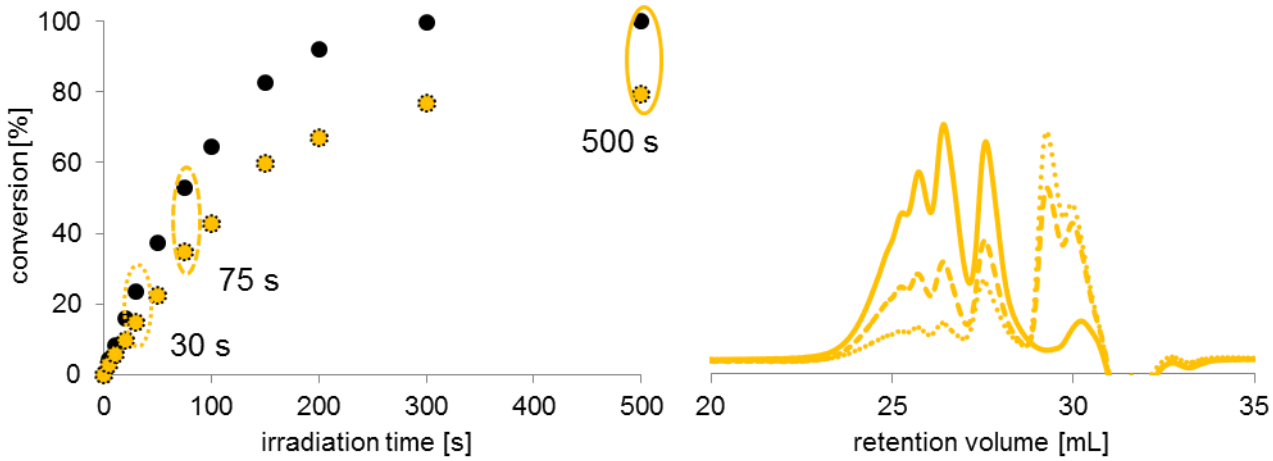

Figure 78: Conversion curve and molecular weight distribution for 30 s (⋯⋯), 75 s (– – –), and 500 s (——) for AC formulation consisting of 65 mol% BenzAC (●) and 35 mol% MT (●)

However, GPC measurements show that the regulation at different DBCs during the photopolymerization is rather constant and the molecular weight distribution becomes narrower with Đ values ~1.2 and the M_ns lower 600 - 650 Da.

Table 13: Results for BenzAC 65 mol% and MT 35 mol%

irradiation time	**conversion**		**GPC**	
	BenzAC [%]	MT [%]	M_n [Da]	Đ
30 s	24	15	650*	1.22
75 s	53	35	600*	1.23
500 s	100	79	600*	1.23

*outside of calibration range (890 – 177,000 Da)

As a short summary, the key figure for photopolymerization speed (r_{DBC}, r_R), co-reactivity (f_{DBC}, f_{co}), and photopolymerization regulation (Đ) are pictured in Figure 79, Figure 80, and Figure 81.

Figure 79 addresses key figure for photopolymerization speed depending on thiol concentrations. DBC_{reg} and R_{reg} values are all in the range of homopolymerization leading to r_{DBC} and r_R around 1. However, it can be observed that an increase in thiol concentration slightly decreases reaction speed.

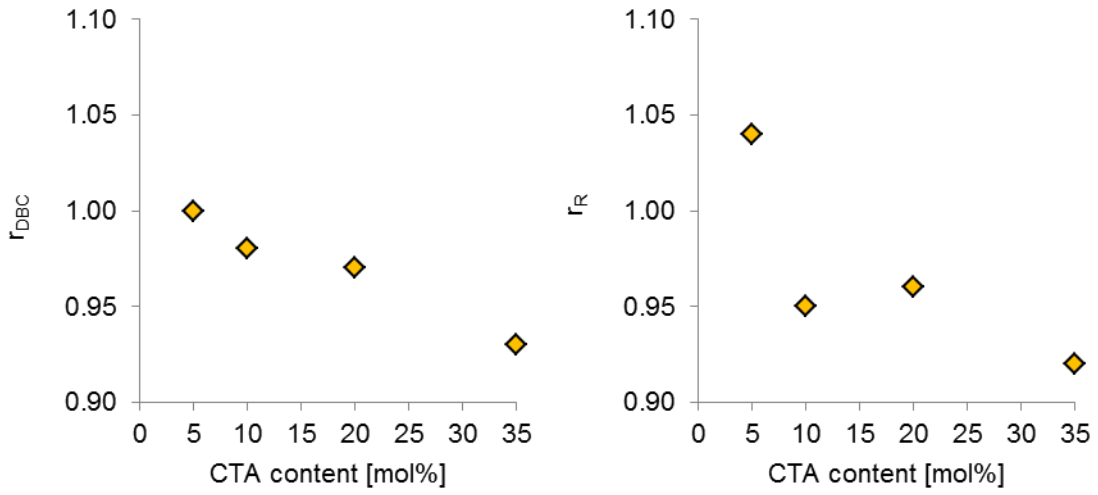

Figure 79: Photoreactor key figures characterizing photopolymerization relative reactivity of thiols (◆) at different concentrations;

In Figure 80 co-reactivity parameters are highlighted. Concerning end conversion, the thiol conversion decreases with increasing thiol content in the AC formulation. Same holds true for the co-reactivity factor f_{co}. Adding 5 mol% of thiol in the BenzAC leads to an almost perfect co-reactivity, while increasing the thiol content to 20 mol% or more significantly decreases the co-reactivity preferring BenzAC homopolymerization over copolymerization.

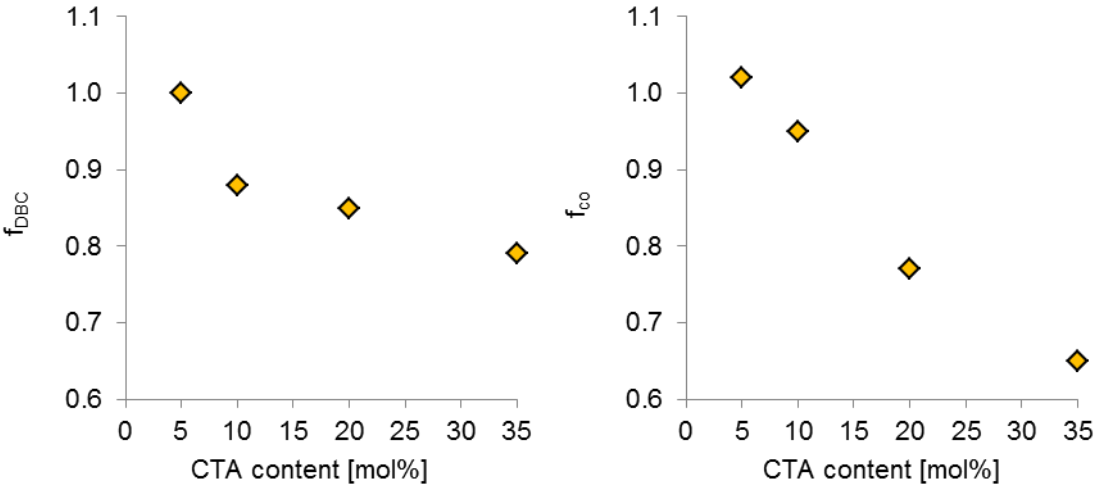

Figure 80: Photoreactor key figures characterizing co-reactivity of thiols (◆) at different concentrations;

In order to make a statement about regulation abilities of thiols, the Đ values are plotted against thiol concentration. First of all, it can be seen that adding only 5 mol% of thiol decreases the Đ value from 7.6 to ~1.9, which clearly indicates regulation of the free radical photopolymerization. By raising the thiol concentration, Đ decreases further indicating better regulation. At 35 mol% of thiol in the BenzAC formulation a Đ value of ~1.2 can be reached.

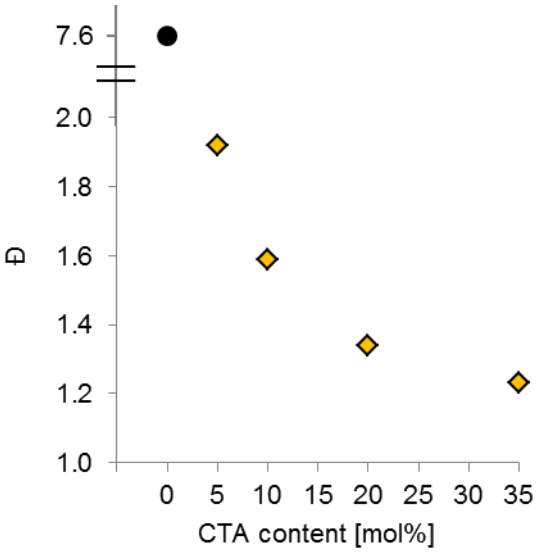

Figure 81: Development of Đ after 500 s of irradiation with increasing thiol (◇) concentration [homopolymerization (●)];

Summarizing, thiol-ene chemistry for regulating ACs in photopolymerization results in good co-reactivity and regulation especially at low thiol concentrations, without slowing down the reaction rate.

Table 14: Collected results for thiol-regulated BenzAC

Formulation	***Homopolym. vs. total DBC***					***DBC of monomer and CTA***			
BenzAC : Thiol	**DBC_{end}** [%]	**r_{DBC}** [ ]	**R** [DBC s^{-1}]	**r_R** [ ]	Monomer CTA	**DBC_{end}** [%]	**f_{DBC}** [ ]	**r** [DBC s^{-1}]	**f_{co}** [ ]
100% : 0%	100	-	0.654	-	BenzAC	100	-	0.654	-
95% : 5%	100	1.00	0.679	1.04	BenzAC Thiol	100 100	1.00	0.678 0.694	1.02
90% : 10%	98	0.98	0.620	0.95	BenzAC Thiol	99 87	0.88	0.622 0.593	0.95
80% : 20%	97	0.97	0.626	0.96	BenzAC Thiol	100 85	0.85	0.657 0.503	0.77
65% : 35%	93	0.93	0.602	0.92	BenzAC Thiol	100 79	0.79	0.686 0.445	0.65

In order to gain information about the oligomeric species formed during photopolymerization, Maldi-TOF-MS measurements were conducted for the 80 mol% BenzAC and 20 mol% MT formulation.

Before starting the interpretation of Maldi-TOF-MS measurements, it has to be mentioned that Maldi-TOF-MS does not represent an analytical technique, which provides quantitative information. Hence, all results shown here have to be considered as qualitative information only. This mainly arises from two facts. First of all, different polymers or oligomers might

exhibit different abilities to be ionized and therefore, some species might be ionized in lager quantity resulting in a higher peak in the mass spectrum. The second reason is that the higher the molecular weight of a polymer of similar ionizing potential, the more difficult ionization becomes. So Maldi-TOF-MS should only be used for polymers with a rather narrow molecular weight distribution. That is the reason why, no Maldi-TOF-MS analysis was performed with the unregulated free radical homopolymerization.

Generally, Maldi-TOF-MS analysis was conducted for the samples taken after 30, 75, and 500 s. However, the MS spectra did not exhibit the formation or disappearance of new peaks during the photopolymerization.

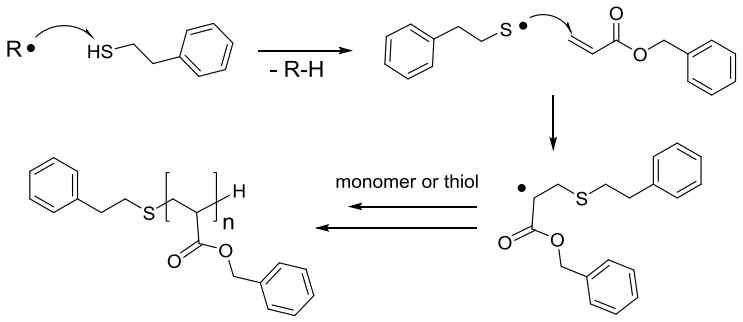

Figure 82: Thiol-ene regulation mechanism ending up with the most expected oligomer species

Concerning thiol-regulation, the main oligomers expected from thiol-ene regulation mechanism in the BenzAC/MT system are illustrated in Figure 82. As can be seen in Figure 83, the sodium adduct of the suggested main oligomer species represent the highest peaks in the mass spectrum. These findings confirm the regulating mechanism suggested for thiols in Figure 82.

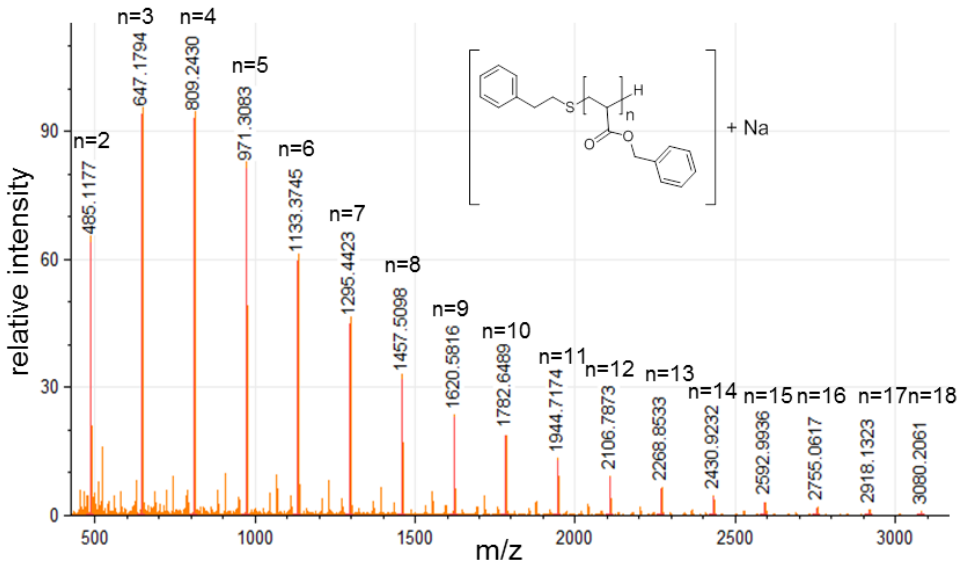

Figure 83: Maldi-TOF spectrum highlighting the main sodium adduct of MT regulated BenzAC;

Comparing the most intensive peaks of the mass spectrum with the M_n determined by means of GPC measurements, it can be seen that M_n ~800 Da corresponds rather well with the most intensive mass peak at 809 Da.

Moreover, traces of following species were found in the mass spectrum (Figure 84). Structure of species **1** arises from a polymer chain started with an Ivocerin PI radical, while species **2** match a recombination reaction between a thiyl radical induced growing polymer chain and a thiyl radical. Particularly interesting is that no Ge-based species, which would originate from the PI decay can be found in the MS spectra.

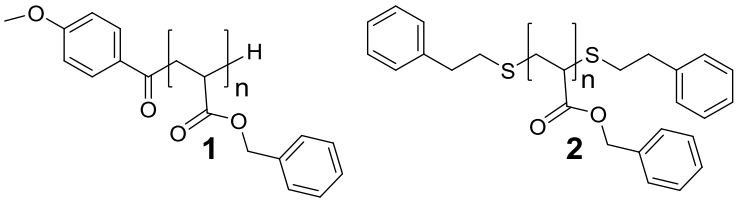

Figure 84: Other species found in the mass spectrum

However, it has to be mentioned that, even though regulated, radical polymerization possesses the potential to undergo a variety of side reactions leading to additional signals in the mass spectrum.

3.3 Regulating acrylates *via* β-allyl sulfones

β-Allyl sulfone ester ASEE has already been used in studies for modifying MA-based networks. Here, the regulating ability of different β-allyl sulfone (ASEE) concentrations (5, 10, 20, and 35 mol%) towards ACs were investigated in the photoreactor. After ^{1}H NMR spectroscopy, GPC measurements of the NMR samples taken after 30, 100, and 500 s of irradiation were conducted. Additionally, Maldi-TOF-MS analysis of the sample containing 20 mol% of ASEE was carried out.

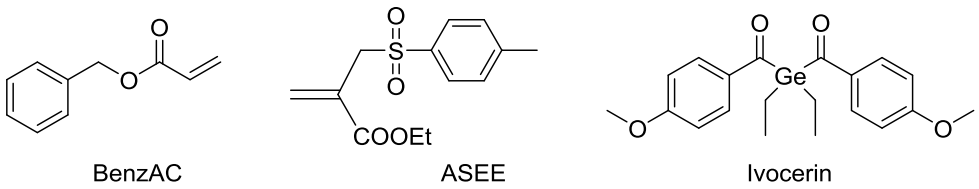

Figure 85: Monomer BenzAC, AFCT reagent ASEE, and PI Ivocerin

In order to evaluate the key parameters for characterizing photopolymerization speed and co-reactivity properties of ASEE in BenzAC, regression curves were calculated for the first 8 measuring points. The slopes of these curves were then used to calculate r_{total} and r_{co}.

Starting with an ASEE content of 5 mol% in the AC formulation, a clear retardation of the AFCT-regulated reaction compared to homopolymerization can be observed (r_R = 0.71, r_{DBC} = 0.90). Moreover, Figure 86 illustrates that the β-allyl sulfone is preferably consumed leading to an f_{co} of 1.82 and an f_{DBC} of 1.12.

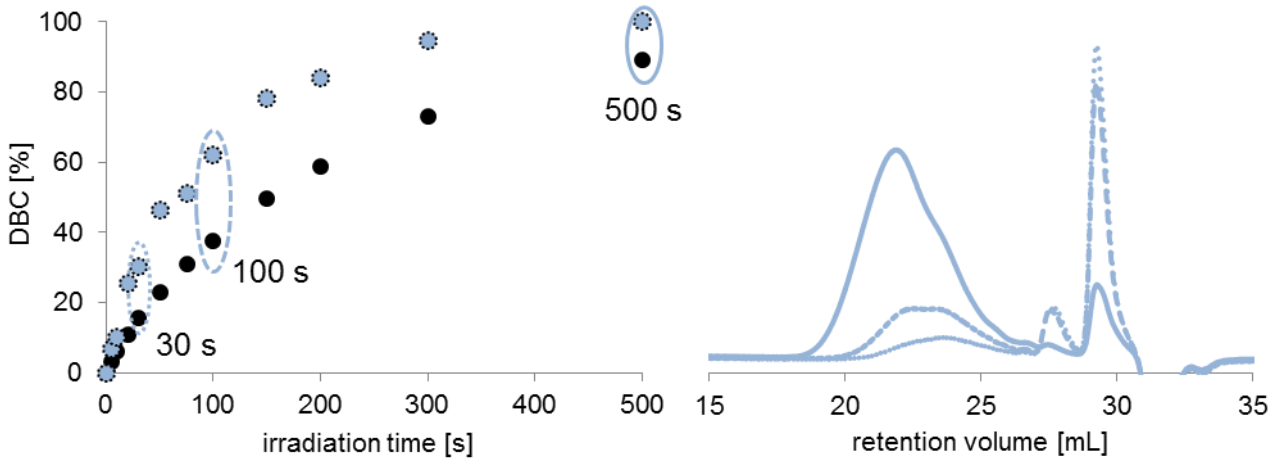

Figure 86: Conversion curve and molecular weight distribution for 30 s (⋯), 75 s (– –), and 500 s (—) for AC formulation consisting of 95 mol% BenzAC (●) and 5 mol% ASEE (◌)

This has a huge impact on the regulating abilities. Results in Table 15 indicate that Đ values are changing from ~1.8 to ~2.1 and the M_ns are increasing from ~1,300 to ~2,600 Da during polymerization. These findings can be explained by the exhaustion of the AFCT reagent in the later stage of photopolymerization. At the beginning of the polymerization ASEE is preferably consumed and therefore, exhibits better regulation. The faster consumption of ASEE in comparison with BenzAC leads to a surplus of AC in the end phase of the photopolymerization. During this phase, the lack of AFCT reagent leads to poor regulation of the photopolymerization and hence, Đ and M_n values are increasing.

Table 15: Results for BenzAC 95 mol% and ASEE 5 mol%

irradiation time	**conversion**		**GPC**	
	BenzAC [%]	ASEE [%]	M_n [Da]	Đ
30 s	15	30	1,350	1.83
100 s	38	62	1,700	1.91
500 s	89	100	2,600	2.11

Similar results can be found for the formulation containing 10 mol% of ASEE. Reaction speed of the photopolymerization is even slower (r_R = 0.55, r_{DBC} = 0.79). Figure 87 shows the preferred consumption of AFCT reagent (f_{co} = 1.64, f_{DBC} = 1.25).

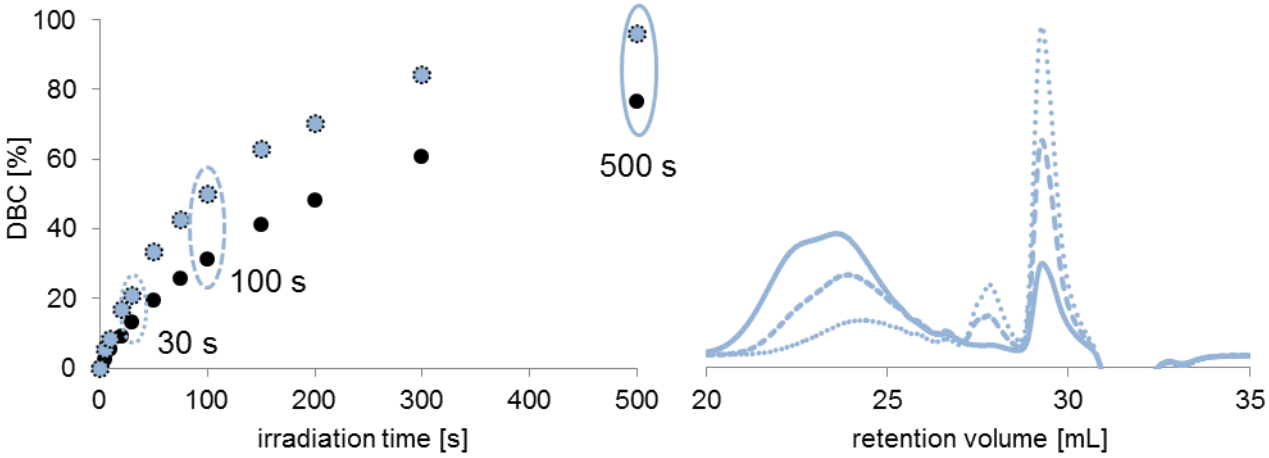

Figure 87: Conversion curve and molecular weight distribution for 30 s (), 75 s (), and 500 s () for AC formulation consisting of 90 mol% BenzAC () and 10 mol% ASEE ()

As found for thiols, the increase of ASEE concentration in the formulation leads to narrower molecular weight distribution manifesting in lower Đ and M_n values. Besides that, the effect of the exhaustion of β-allyl sulfone modifier explained for the 5 mol% ASEE formulation before is still clearly observable (Table 16).

Table 16: Results for BenzAC 90 mol% and ASEE 10 mol%

irradiation time	**conversion**		**GPC**	
	BenzAC [%]	ASEE [%]	M_n [Da]	Đ
30 s	13	21	1,000	1.48
100 s	31	50	1,200	1.59
500 s	77	96	1,500	1.76

The addition of 20 mol% to the AC formulation (Figure 88) delays photopolymerization even more (r_R = 0.46, r_{DBC} = 0.67). On the other hand, the co-reactivity parameter f_{co} of 1.33 is lowered approaching 1, but finally DBC_{ASEE} is significantly higher than DBC_{BenzAC} (f_{DBC} = 1.29).

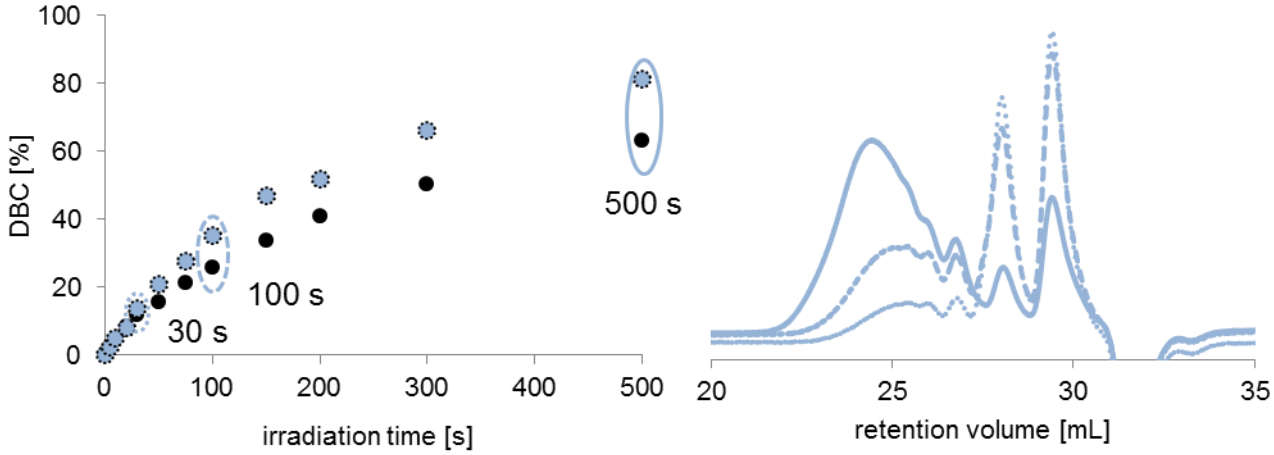

Figure 88: Conversion curve and molecular weight distribution for 30 s (·····), 75 s (– – –), and 500 s (——) for AC formulation consisting of 80 mol% BenzAC (●) and 20 mol% ASEE (●)

Even though increasing with irradiation time, the values characterizing AFCT regulation Đ and M_n become lower and the difference of Đ and M_n after 30 and 500 s is not that big anymore compared to lower ASEE concentrations (Table 17). This makes perfect sense, since the co-reactivity parameter value approaches 1.

Table 17: Results for BenzAC 80 mol% and ASEE 20 mol%

irradiation time	**conversion**		**GPC**	
	BenzAC [%]	ASEE [%]	M_n [Da]	Đ
30 s	12	14	650	1.28
100 s	26	35	700	1.32
500 s	63	81	850	1.43

The last examined formulation contained an ASEE amount of 35 mol%. Concerning photopolymerization rate, the increase in ASEE concentration obviously results in retardation (r_R = 0.45, r_{DBC} = 0.66). In case of co-reactivity, Figure 89 illustrates nearly homogeneous consumption of ASEE and BenzAC. This can be confirmed by taking a look at the co-reactivity parameter f_{co} of 1.07 and f_{DBC} of 0.99.

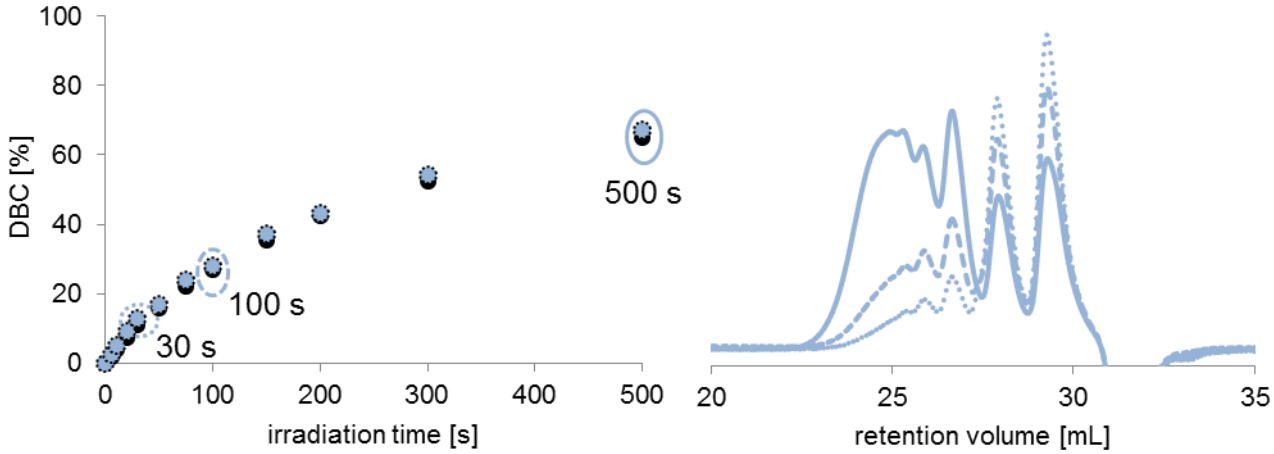

Figure 89: Conversion curve and molecular weight distribution for 30 s (·····), 75 s (– – –), and 500 s (——) for AC formulation consisting of 65 mol% BenzAC (●) and 35 mol% ASEE (✺)

This homogeneous consumption also leads to more constant Đ ~1.25 and M_n ~550-650 Da values throughout the whole photopolymerization (Table 18).

Table 18: Results for BenzAC 65 mol% and ASEE 35 mol%

irradiation time	**conversion**		**GPC**	
	BenzAC [%]	ASEE [%]	M_n [Da]	Đ
30 s	11	13	550	1.23
100 s	27	28	600	1.24
500 s	65	67	650	1.30

Eventually, all collected key parameters for ASEE regulation in BenzAC were plotted in diagrams to investigate the dependency of different ASEE concentrations on photopolymerization speed, co-reactivity, and regulation.

Figure 90 pictures the development of the photopolymerization speed parameters r_R and r_{DBC} with increasing β-allyl sulfone concentrations. An increase in AFCT reagent ratio in the AC formulation leads to a decrease of DBC_{end} of the AFCT-regulated reaction. Moreover, the reaction rate parameter r_R indicates already a significantly slower reaction upon the addition of 5 mol% ASEE. Raising the amount of ASEE in BenzAC even leads to more retardation.

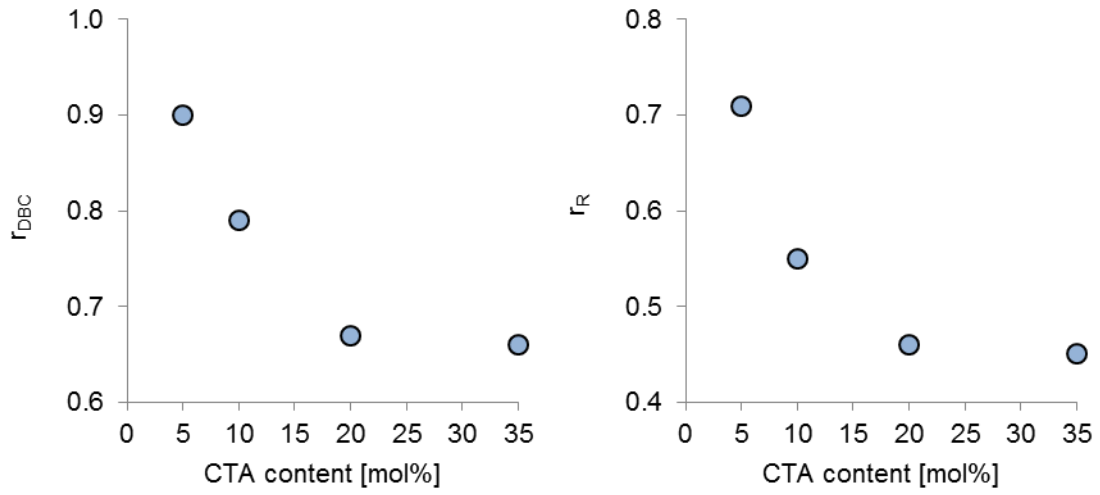

Figure 90: Photoreactor key figures characterizing photopolymerization relative reactivity of ASEE (●) at different concentrations

Co-reactivity plots in Figure 91 are particularly interesting. For concentrations of 5, 10, and 20 mol% ASEE in BenzAC, the AFCT reagent is preferably consumed resulting in f_{co} >1.3. Even though f_{co} values decrease approaching 1 with increasing ASEE concentration meaning better co-reactivity, the difference in the DBC_{end} of BenzAC and ASEE become bigger. However, for an ASEE concentration of 35 mol% the co-reactivity parameter f_{co} is close to 1 also leading to a f_{DBC} ~1, which is an indicator for good co-reactivity.

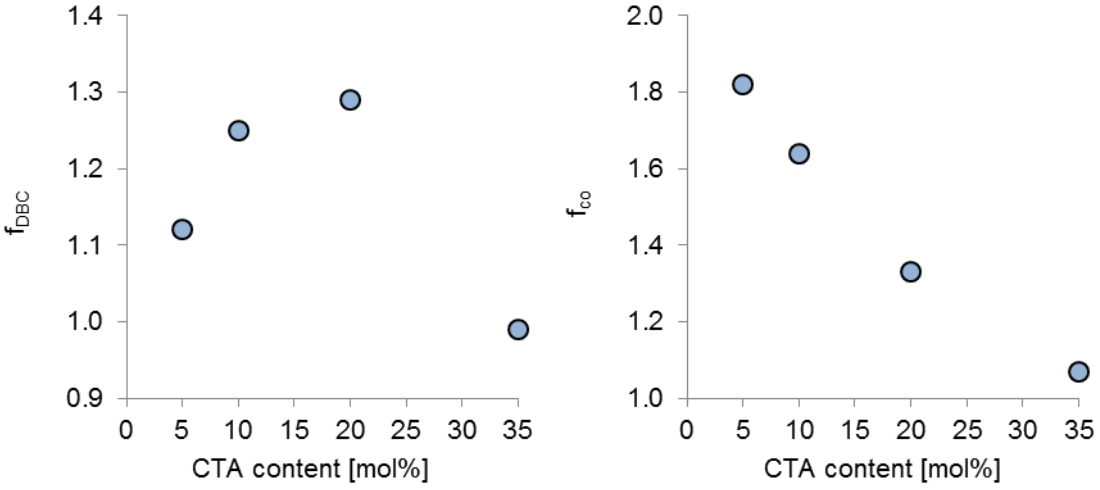

Figure 91: Photoreactor key figures characterizing co-reactivity of ASEE (●) at different concentrations;

GPC measurements delivered the Đ values characterizing the molecular weight distribution. Even 5 mol% of ASEE enable a significant narrowing of the molecular weight distribution in comparison with homopolymerization (Figure 92). As expected, Đ values decrease with increasing β-allyl sulfone concentration in the BenzAC formulation.

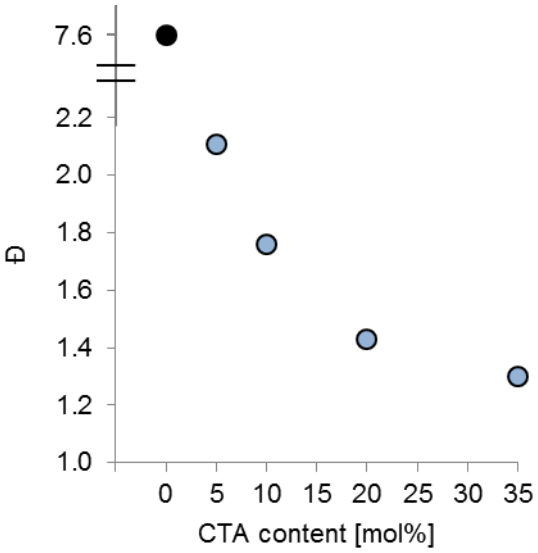

Figure 92: Development of Đ after 500 s of irradiation with increasing ASEE concentration [homopolymerization (●), ASEE (●)];

Summarizing, β-allyl sulfone ASEE in ACs can regulate photopolymerization. This regulation is accompanied by a rather poor co-reactivity and a significant retardation compared to homopolymerization. With respect to these issues the β-allyl sulfone ASEE is not the proper choice for regulating AC networks.

Table 19: Collected results for ASEE-regulated BenzAC

Formulation	***Homopolym. vs. total DBC***					***DBC of monomer and CTA***			
BenzAC : ASEE	**DBC_{end}** [%]	**r_{DBC}** [ ]	**R** [DBC s^{-1}]	**r_R** [ ]	Monomer CTA	**DBC_{end}** [%]	**f_{DBC}** [ ]	**r** [DBC s^{-1}]	**f_{co}** [ ]
100% : 0%	100	-	0.654	-	BenzAC	100	-	0.654	-
95% : 5%	90	0.90	0.462	0.71	BenzAC ASEE	89 100	1.12	0.444 0.807	1.82
90% : 10%	79	0.79	0.362	0.55	BenzAC ASEE	77 96	1.25	0.340 0.560	1.64
80% : 20%	67	0.67	0.300	0.46	BenzAC ASEE	63 81	1.29	0.282 0.373	1.33
65% : 35%	66	0.66	0.298	0.45	BenzAC ASEE	67 66	0.99	0.290 0.312	1.07

Particularly interesting in case of β-allyl sulfones are the Maldi-TOF-MS analysis results. As already mentioned in the State of the art, β-allyl sulfones provide more possible reaction pathways, since the elimination of the tosyl (**Ts**) radical comes along with the formation of new DBs, which are able to undergo further reactions with radicals. Thus, ASEE MS spectrum is expected to contain more oligomeric species than the spectrum of MT or VE4.

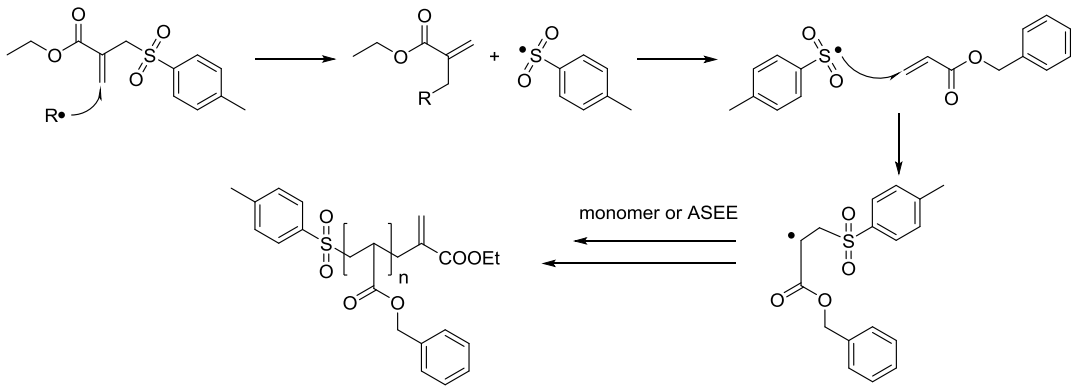

Figure 93: ASEE regulation mechanism ending up with the most expected oligomer species

Figure 93 illustrates the reaction mechanism of ASEE leading to the main regulation product. As can be seen in Figure 94, the mass spectrum proves the formation of the expected sodium adduct.

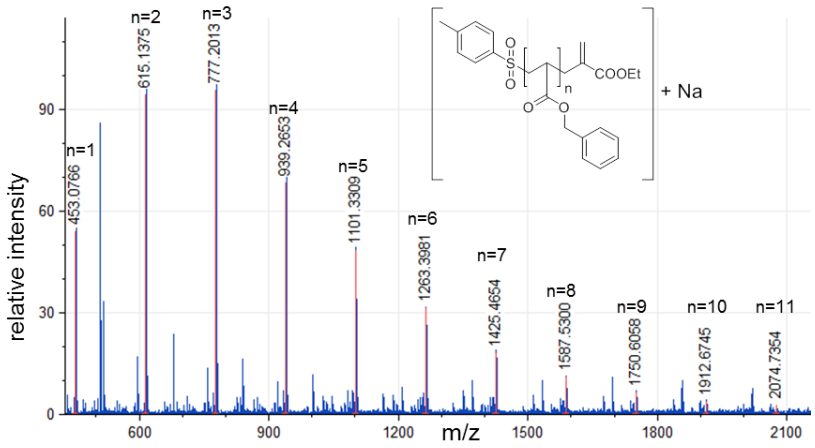

Figure 94: Maldi-TOF spectrum highlighting the main sodium adduct of ASEE regulated BenzAC;

Comparing the most intensive peaks of the mass spectrum with the M_n determined by means of GPC measurements, it can be seen that M_n ~850 Da from GPC is a bit higher in value than the most intensive mass peaks at 615 and 777 Da.

Moreover, a variety of other formed species was found in the mass spectrum (Figure 95).

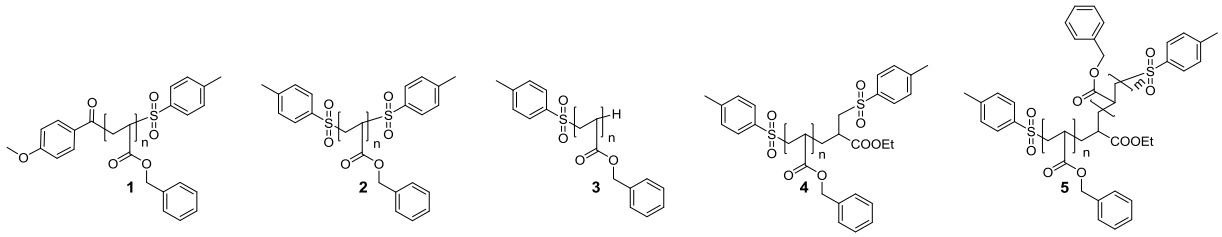

Figure 95: Other species found in the mass spectrum

Particularly interesting, are oligomeric species 4 and 5, which result in the same molecular mass. Since β-allyl sulfone elimination mechanism of the sulfonyl group leads to the formation of new DBs, the mass spectrum shows that these DBs are able to react with other sulfonyl leaving groups or growing polymer chains. Once again, no Ge-based species were found.

3.4 Regulating acrylates *via* α-vinyl sulfonates

Finally, the best performing AFCT reagent in ACs from the photoreactor study was tested. α-Vinyl sulfonate VE4 was the only screened AFCT reagent that did not slow down photopolymerization rate compared to homopolymerization and also exhibited the desired co-reactivity properties.

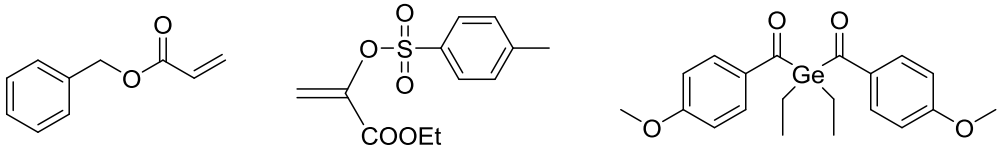

BenzAC VE4 Ivocerin

Figure 96: Monomer BenzAC, AFCT reagent VE4, and PI Ivocerin

In order to determine the regulating ability of different vinyl sulfonate ester (VE4) concentrations towards ACs, photoreactor experiments with vinyl sulfonate ester concentrations of 5, 10, 20, and 35 mol% were carried out. After ^{1}H NMR spectroscopy, GPC measurements of the NMR samples taken after 30, 75, and 500 s of irradiation were conducted. Additionally, Maldi-TOF-MS analysis of the sample containing 20 mol% of VE4 was carried out.

Starting with 5 mol% VE4 in the BenzAC formulation, the reaction rate of the AFCT-regulated photopolymerization is with an r_R of 0.95 nearly as fast as BenzAC homopolymerization. Also a DBC_{reg} of 99% nearly reaches DBC_{homo} of 100%. Figure 97 pictures the co-reactivity of BenzAC and VE4. As can be seen, the consumption of VE4 is slightly preferred, which can

be confirmed by an f_{co} of 1.27. The DBC_{end} of BenzAC and VE4 is with 100% and 99% nearly equivalent.

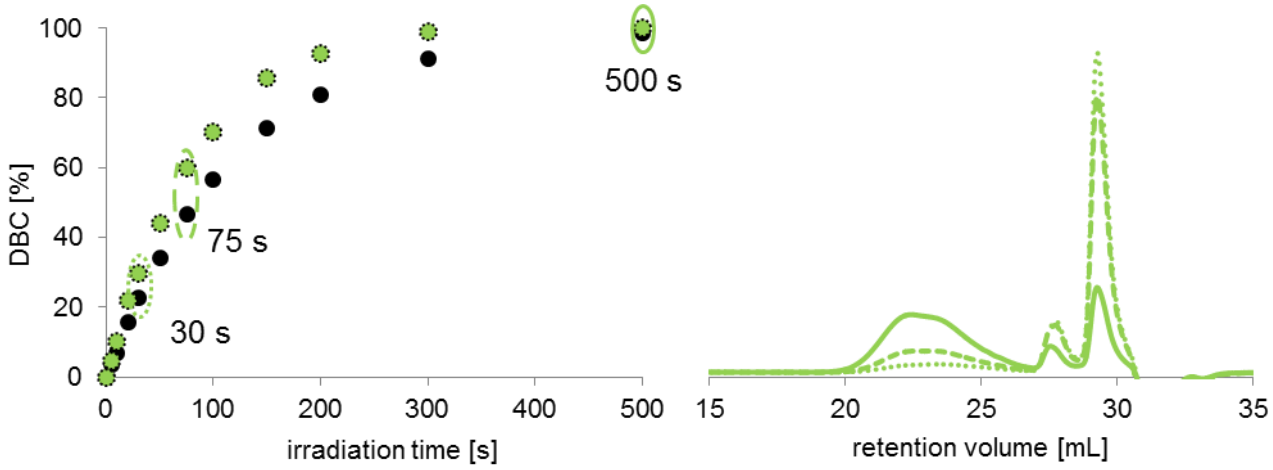

Figure 97: Conversion curve and molecular weight distribution for 30 s (·····), 75 s (– – –), and 500 s (——) for AC formulation consisting of 95 mol% BenzAC (●) and 5 mol% VE4 (●)

GPC results show that regulation of BenzAC is with Đ values ~1.8 rather constant (Table 20). However, M_n is slightly raised from 1,500 to 1,850 Da.

Table 20: Results for BenzAC 95 mol% and VE4 5 mol%

irradiation time	**conversion**		**GPC**	
	BenzAC [%]	VE4 [%]	M_n [Da]	Đ
30 s	23	30	1,500	1.85
75 s	47	60	1,700	1.78
500 s	99	100	1,850	1.77

Increasing the VE4 content in the AC formulation to 10 mol%, slightly accelerates the photopolymerization when compared to 5 mol% VE4 in BenzAC. The AFCT-regulated reaction is as fast as homopolymerization (r_R = 1.00, r_{DBC} = 0.99). Co-reactivity key figure f_{co} with 1.23 indicates a slightly preferred consumption of VE4. Nevertheless, f_{DBC} with 0.97 confirms similar DBC_{end}s of BenzAC and VE4 after 500 s of irradiation (Figure 98).

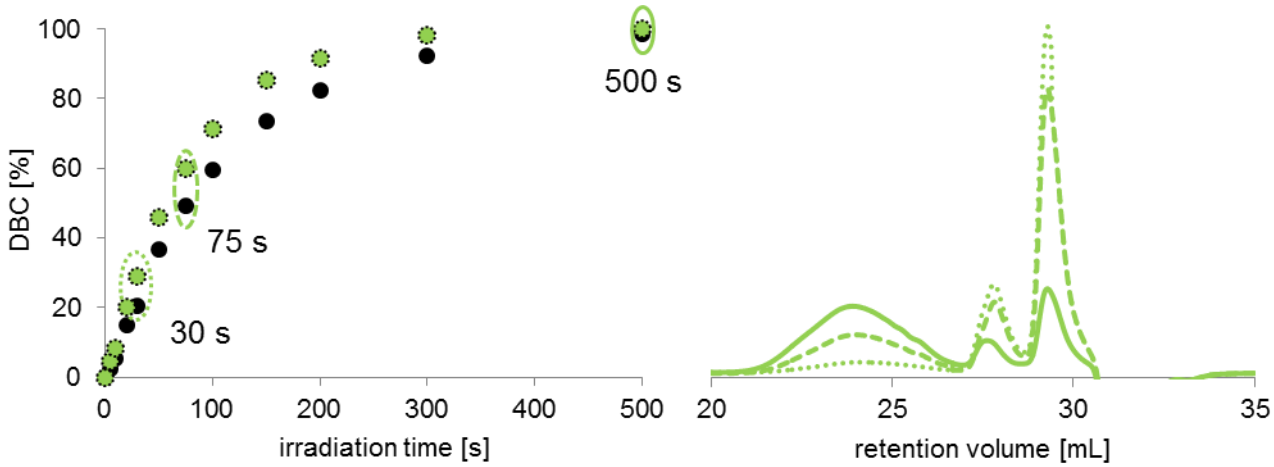

Figure 98: Conversion curve and molecular weight distribution for 30 s (▪▪▪▪▪▪), 75 s (▬▬▬), and 500 s (▬▬▬) for AC formulation consisting of 90 mol% BenzAC (●) and 10 mol% VE4 (●)

The rather homogeneous and equal consumption of BenzAC and VE4 also leads to constant Đ values ~1.5 and M_ns between 1,100 and 1,250 Da, which are proving the good regulation abilities (Table 21).

Table 21: Results for BenzAC 90 mol% and VE4 10 mol%

irradiation time	**conversion**		**GPC**	
	BenzAC [%]	VE4 [%]	M_n [Da]	Đ
30 s	20	29	1,100	1.47
75 s	49	60	1,200	1.46
500 s	99	100	1,250	1.49

Adding 20 mol% VE4 to a BenzAC formulation keeps the reaction speed of AFCT-regulated photopolymerization in the range of homopolymerization (r_R = 1.01, r_{DBC} = 0.97). In Figure 99 homogeneous consumption of AFCT reagent and BenzAC can be observed (f_{co} = 1.08) resulting in an f_{DBC} of 1.01.

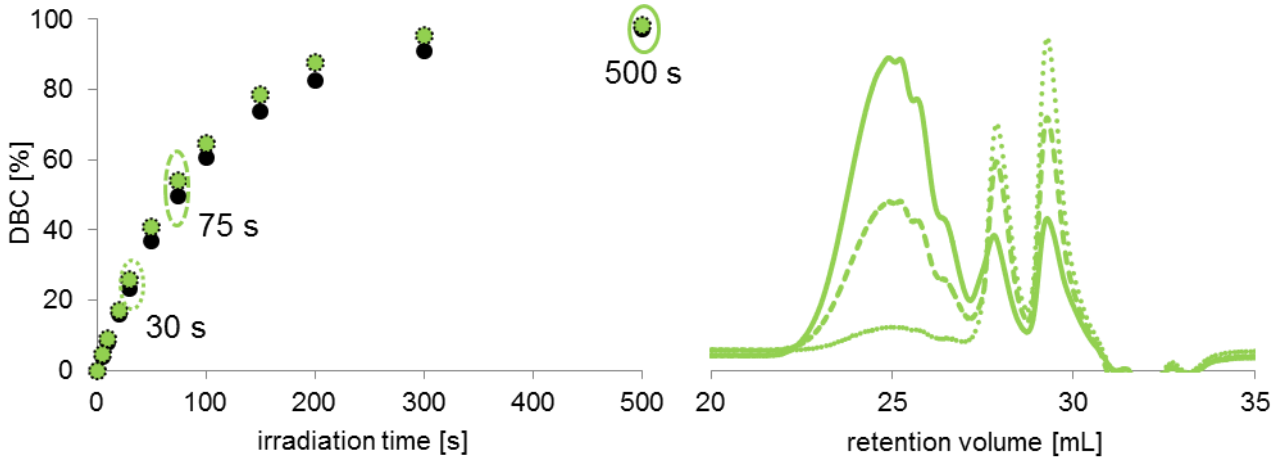

Figure 99: Conversion curve and molecular weight distribution for 30 s (▪▪▪▪▪▪), 75 s (▬▬▬), and 500 s (▬▬▬) for AC formulation consisting of 80 mol% BenzAC (●) and 20 mol% VE4 (●)

GPC measurements revealed very constant Đ values of 1.28 and M_n ~800 Da.

Table 22: Results for BenzAC 80 mol% and VE4 20 mol%

irradiation time	conversion		GPC	
	BenzAC [%]	VE4 [%]	M_n [Da]	Đ
30 s	23	26	800*	1.28
75 s	50	54	800*	1.29
500 s	97	98	850*	1.28

*outside of calibration range (890 – 177,000 Da)

Eventually, a formulation with 35 mol% vinyl sulfonate ester was measured. In terms of reaction speed the increase to 35 mol% comes along with a slight increase in photopolymerization speed (r_R = 1.08, r_{DBC} = 0.98). In Figure 100 the co-reactivity between BenzAC and VE4 is imaged. The consumption of AFCT reagent and BenzAC is very homogeneous, which can be confirmed by an f_{co} of 0.92 and an f_{DBC} of 1.01.

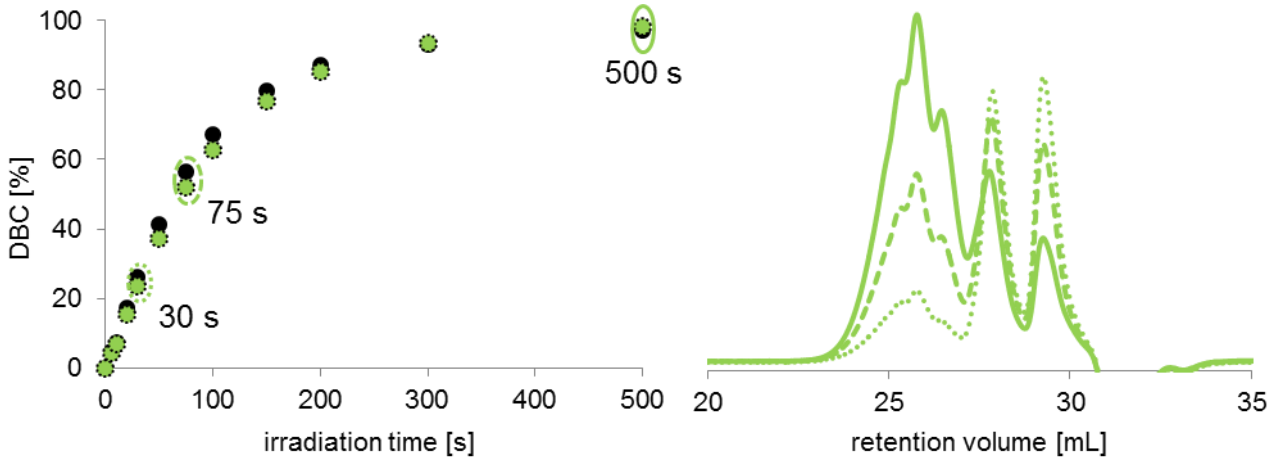

Figure 100: Conversion curve and molecular weight distribution for 30 s (⋯⋯), 75 s (– – –), and 500 s (——) for AC formulation consisting of 65 mol% BenzAC (●) and 35 mol% VE4 (●)

Table 23 shows again the exceptionally good regulating abilities of VE4 resulting in constant Đ ~1.16 and M_n values ~600 Da during the whole polymerization.

Table 23: Results for BenzAC 65 mol% and VE4 35 mol%

irradiation time	conversion		GPC	
	BenzAC [%]	VE4 [%]	M_n [Da]	Đ
30 s	26	24	650*	1.17
75 s	56	52	650*	1.16
500 s	97	98	600*	1.16

*outside of calibration range (890 – 177,000 Da)

In order to discuss the influence of concentration of VE4 in BenzAC on AFCT reaction, plots with the most important key figures were created.

Figure 101 deals with the photopolymerization speed of AFCT-regulated reaction compared to homopolymerization. Concerning DBC_{end}, r_{DBC} values remain constant and close to 1 throughout the whole concentration range indicating a similar DBC_{reg} and DBC_{homo}. The photopolymerization speed factor r_R (~1 for all concentrations) even increases a little bit with rising VE4 ratio in the formulation. Thus, VE4-regulated photopolymerization exhibits no retardation in comparison with BenzAC homopolymerization.

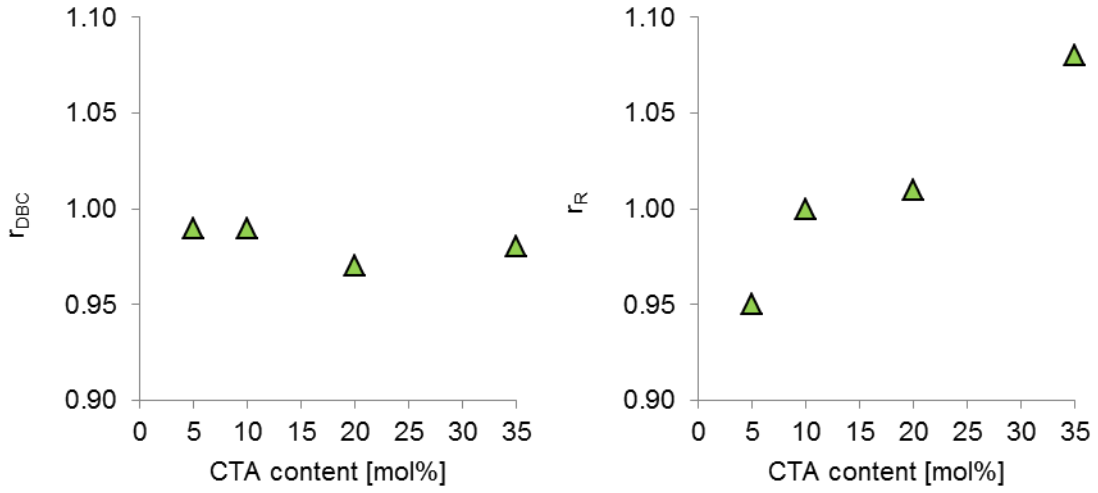

Figure 101: Photoreactor key figures characterizing photopolymerization relative reactivity of VE4 (▲) at different concentrations;

Discussing co-reactivity, it can be seen, that the DBC_{end} of BenzAC and VE4 reaches always ~100% (f_{DBC} ~1). On the other hand, the co-reactivity factor f_{co}, beginning with an f_{co} of 1.27 at low VE4 concentration, decreases with increasing VE4 concentration in ACs. However, the values for f_{co} are close to 1 for the whole concentration range and therefore good co-reactivity of VE4 in BenzAC can be stated.

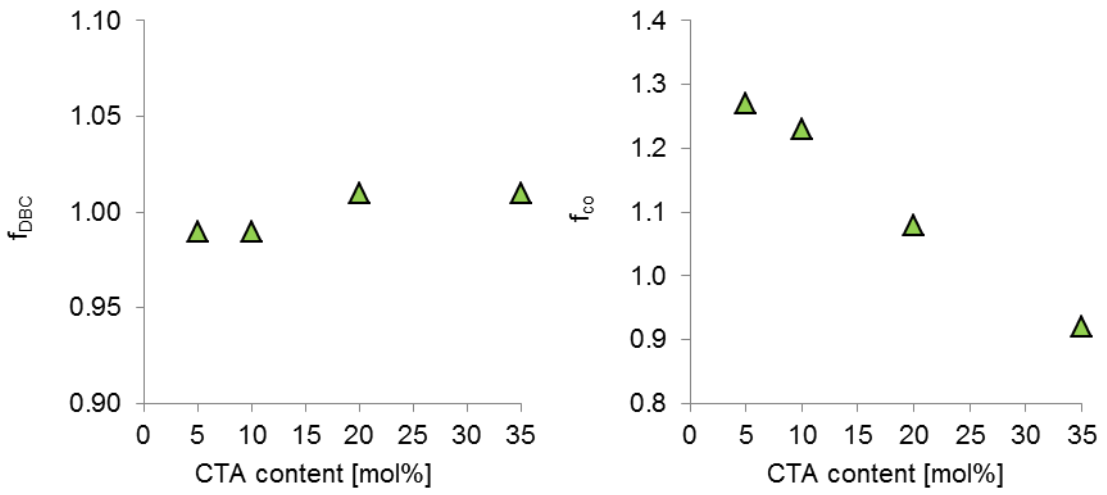

Figure 102: Photoreactor key figures characterizing co-reactivity of VE4 (▲) at different concentrations;

Eventually, the regulating abilities of vinyl sulfonate ester VE4 in BenzAC were investigated by means of GPC providing information about the molecular weight distribution. Figure 103 displays the distinct narrowing of molecular weight distribution when adding small amounts of VE4 compared with homopolymerization. Again, a rising VE4 concentration in the AC formulation leads to lower Đ values testifying better regulation.

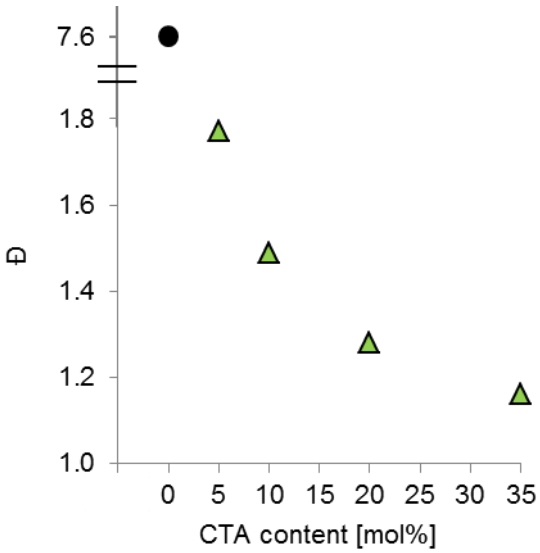

Figure 103: Development of Đ after 500 s of irradiation with increasing VE4 (▲) concentration [homopolymerization (●)];

Summarizing, vinyl sulfonate ester VE4 represents an AFCT reagent with a good co-reactivity towards ACs. Moreover, good regulation was discovered without sacrificing

polymerization speed. Due to these properties, AFCT reagent VE4 commend itself as potential candidate for modifying ACs

Table 24: Collected results for VE4-regulated BenzAC

Formulation	***Homopolym. vs. total DBC***					***DBC of monomer and CTA***			
BenzAC : VE4	**DBC_{end}** [%]	**r_{DBC}** [ ]	**R** [DBC s^{-1}]	**r_R** [ ]	Monomer CTA	**DBC_{end}** [%]	**f_{DBC}** [ ]	**r** [DBC s^{-1}]	**f_{co}** [ ]
100% : 0%	100	-	0.654	-		100	-	0.621	-
95% : 5%	99	0.99	0.619	0.95	BenzAC VE4	100 99	0.99	0.611 0.775	1.27
90% : 10%	99	0.99	0.652	1.00	BenzAC VE4	100 99	0.99	0.637 0.783	1.23
80% : 20%	97	0.97	0.662	1.01	BenzAC VE4	97 98	1.01	0.651 0.705	1.08
65% : 35%	98	0.98	0.709	1.08	BenzAC VE4	97 98	1.01	0.728 0.673	0.92

From all three samples (30, 75, and 500 s), Maldi-TOF-MS measurements were performed. Again, no additional or vanishing mass peaks were observed. In Figure 104 the regulating mechanism of VE4 is depicted leading to the main oligomer arising from AFCT mechanism.

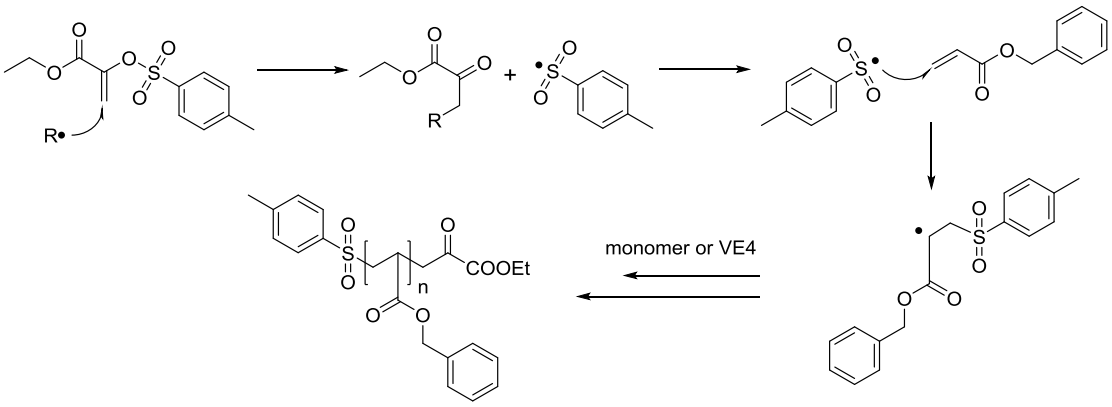

Figure 104: VE4 regulation mechanism ending up with the most expected oligomer species

Once again, the mass spectra proves the existence of the sodium adduct of this oligomer (Figure 105).

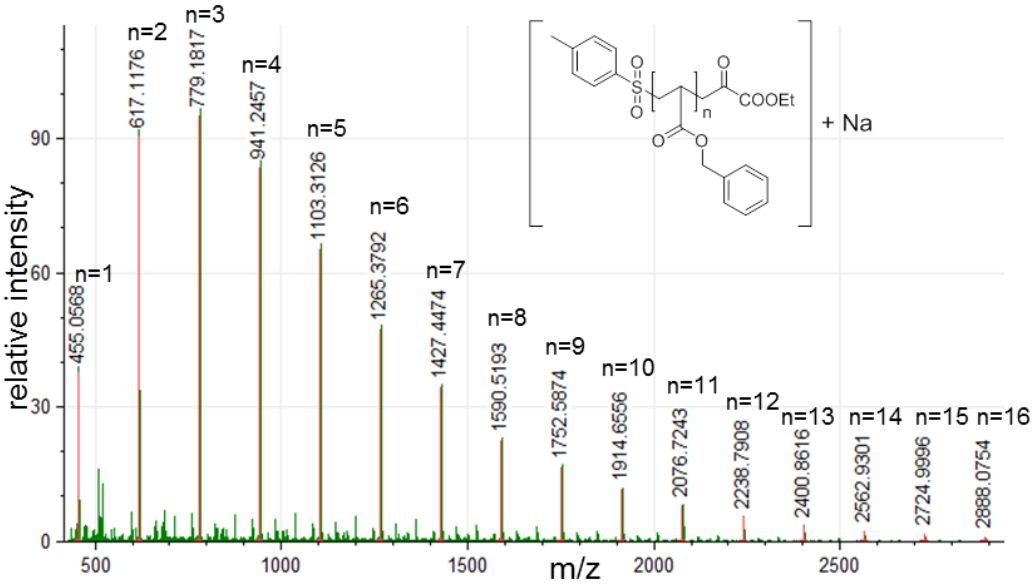

Figure 105: Maldi-TOF spectrum highlighting the main sodium adduct of VE4 regulated BenzAC;

For VE4 regulated BenzAC formulations, the M_n from GPC ~800 Da and corresponds well with the most intensive peak from the mass spectrum at 779 Da.

Additionally, the oligomeric species containing the starting radical of PI Ivocerin was found in the mass spectrum (Figure 106).

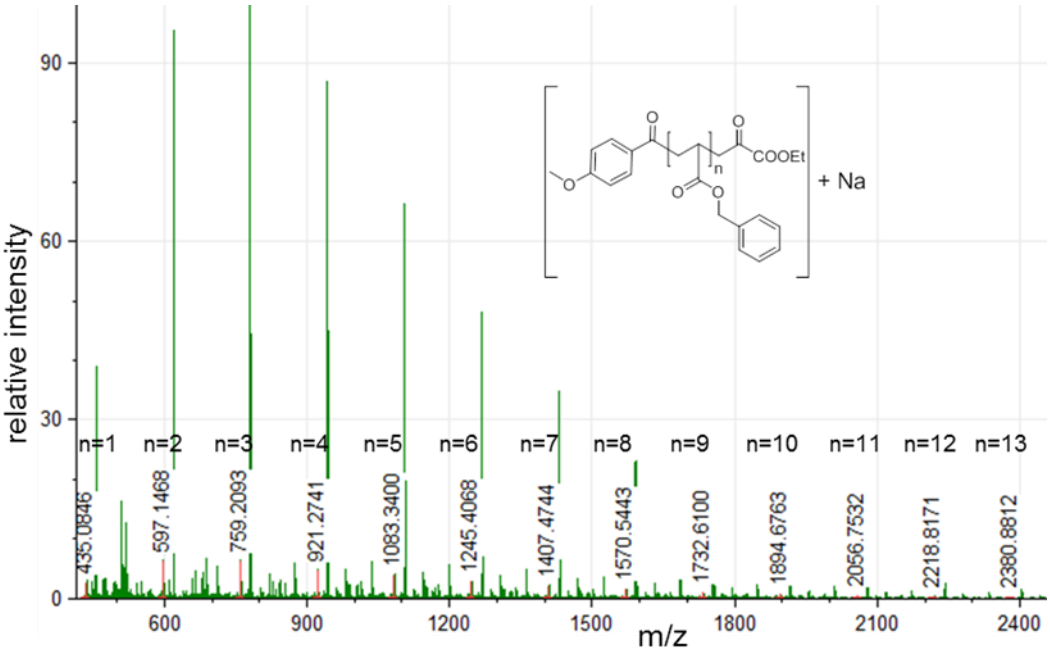

Figure 106: Maldi-TOF spectrum highlighting the sodium adduct of PI-initiated oligomer chain with VE4 activating group as end group;

Apart from that, traces of following species showed signals in the MS spectrum (Figure 107).

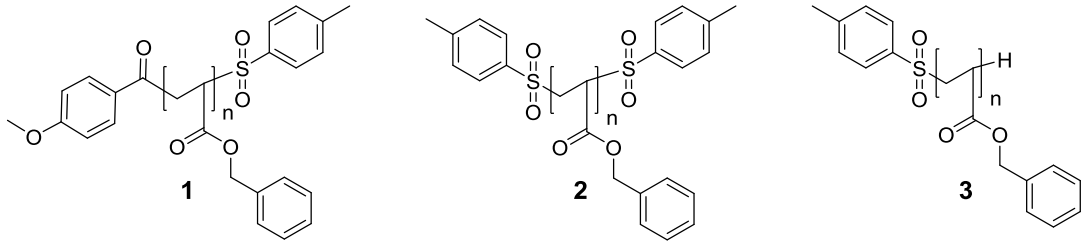

Figure 107: Other species found in the mass spectrum

Also the VE4-regulated sample exhibited no mass peaks originating from Ge-based PI oligomeric species.

3.5 Comparing thiol, β-allyl sulfone, and α-vinyl sulfonate regulation in acrylates

During analyzing thiols, β-allyl sulfones, and α-vinyl sulfonates for regulating acrylates, a lot of data about photopolymerization speed, co-reactivity, and regulation of radical photopolymerization was collected and has already been interpreted in the chapters before. In order to compare the properties of the different CTAs, plots containing information about this recorded data were prepared.

Beginning with relative reactivity (Figure 108), ASEE exhibits significant retardation increasing with β-allyl sulfone content in the AC formulation. One explanation for that could be the formation of a DB after β-scission of the sulfonyl radical. As already discussed in detail in General Part 1, these formed DBs can react again with a sulfonyl radical, which finally delays photopolymerization. However, thiols and α-vinyl sulfonates show much better results, which can stand comparison with the reaction speed of BenzAC homopolymerization over the whole tested CTA concentration range. Nevertheless, concentration-depending trends can be observed. While r_R of thiols slightly drops with increasing thiol content, r_R for VE4 slightly increases with rising VE4 concentration in BenzAC. Comparing thiol-regulation with α-vinyl sulfonate with respect to photopolymerization speed, it can be concluded that both CTAs do not delay photopolymerization.

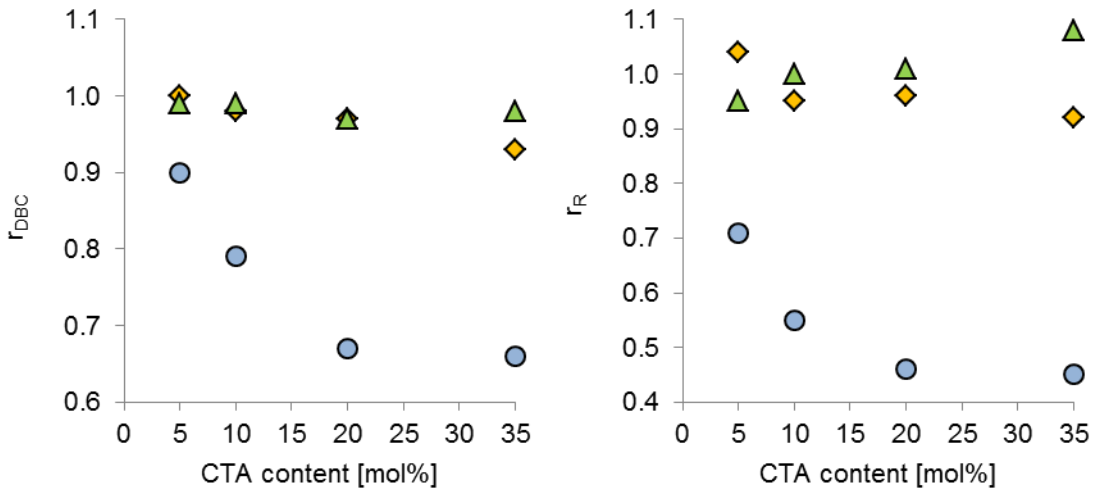

Figure 108: Photoreactor key figures characterizing photopolymerization relative reactivity of CTA at different concentrations [thiol (◆), ASEE (●), VE4 (▲)];

In terms of co-reactivity, β-allyl sulfone ASEE shows higher DBC_{end}s for ASEE than DBC_{BenzAC}. The difference in consumption of ASEE and BenzAC becomes greater until 20 mol% of ASEE in the formulation and then suddenly drops to an f_{DBC} ~1. This is particularly interesting, since f_{co} indicates an improvement of co-reactivity with increasing AFCT reagent ratio in the formulation, which should usually come along with f_{DBC} tending towards 1. Nonetheless, ASEE does not show good co-reactivity in ACs and thus is not the ideal candidate for regulating AC-based networks.

More important is the comparison between thiol and VE4. As can be seen in Figure 109, f_{DBC} of VE4 remains constant ~1.0 at all tested concentrations, while thiol-regulated formulations exhibit a decrease of f_{DBC} from 1.0 to 0.8 with increasing thiol amount. The co-reactivity parameter plot demonstrates that an increase of CTA content in ACs lead to a decrease in f_{co} value. In case of thiols, an almost ideal co-reactivity factor close to 1 at 5 mol% thiol declines to an f_{co} value of 0.65 at 35 mol% thiol. These findings show that homopolymerization of BenzAC becomes favored at higher thiol content. On the other hand, the consumption of vinyl sulfonate ester VE4 in BenzAC is slightly preferred at low concentration (f_{co} ~1.25 for 5 and 10 mol% VE4) and leads to f_{co} close to 1 at 20 and 35 mol% improving co-reactivity. Summarizing, it can be stated that co-reactivity of VE4 in BenzAC, considering the concentration range of 5 to 35 mol% CTA, is better than co-reactivity of thiols in BenzAC.

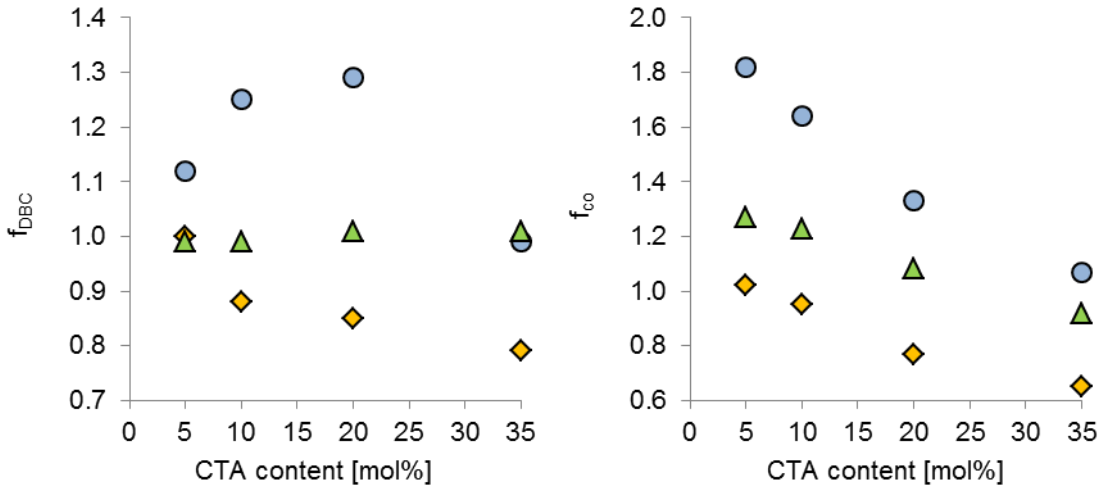

Figure 109: Photoreactor key figures characterizing co-reactivity of CTA at different concentrations [thiol (◆), ASEE (●), VE4 (▲)];

In order to prove the better co-reactivity of VE4 with ACs, GPC results investigating molecular weight distribution can be used. Since a good co-reactivity of a CTA with a monomer results in uniform and equal consumption rates during the whole polymerization process, this should also effect the regulation of formed polymer chain. Applied to the tested CTAs, one would expect a better molecular weight regulation of AC chains with VE4 than with thiols and ASEE.

Figure 110 illustrates that all tested CTAs manage already at low CTA concentration to significantly narrow the molecular weight distribution compared with homopolymerization. As expected, ASEE shows the worst regulation for all concentrations (highest Đ values). This can be attributed to the poor co-reactivity with ACs. Comparing thiol regulation with vinyl sulfonate ester regulation, Figure 110 shows lower Đ values for VE4 regulation for all investigated CTA concentrations. This provides evidence of the better regulating abilities of vinyl sulfonate ester in ACs.

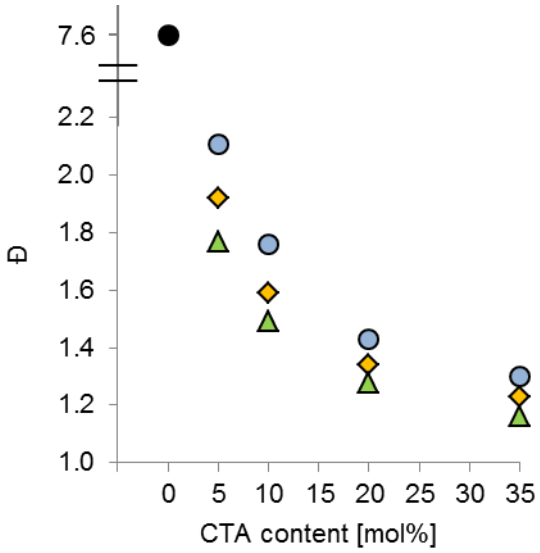

Figure 110: Development of Đ after 500 s of irradiation with increasing CTA concentration [homopolymerization (●), thiol (◆), ASEE (●), VE4 (▲)];

As conclusion of this chapter, it may be stated that the vinyl sulfonate ester VE4 was proven to efficiently regulate monofunctional BenzAC in photopolymerization. Particularly striking is that regulation does not come along with retardation. Compared with the state-of-the-art thiol regulation, vinyl sulfonate ester AFCT regulation shows better co-reactivity with ACs and a better regulation yielding narrower molecular weight distributions.

Considering all this factors, vinyl sulfonate ester represents the most promising candidate for regulating AC networks.

4 Comparison of vinyl sulfonate esters as AFCT reagents with dithiols for modifying diacrylate networks

4.1 Formulations and test specimens

As a result of the kinetic and mechanistic studies, the vinyl sulfonate ester VE4 was found to be the best regulating AFCT reagent for ACs. From its equal and steady consumption with ACs in the photoreactor, a C_{tr} ~1 can be derived. Moreover, no retardation compared with homopolymerization of ACs was observed.

These promising results tipped the scale in favor of a network study with difunctional ACs to highlight the possibilities of AFCT network regulation by performing a variety of different mechanical tests. Besides that, all experiments should be compared with a thiol that is comparable in structure with the AFCT reagent.

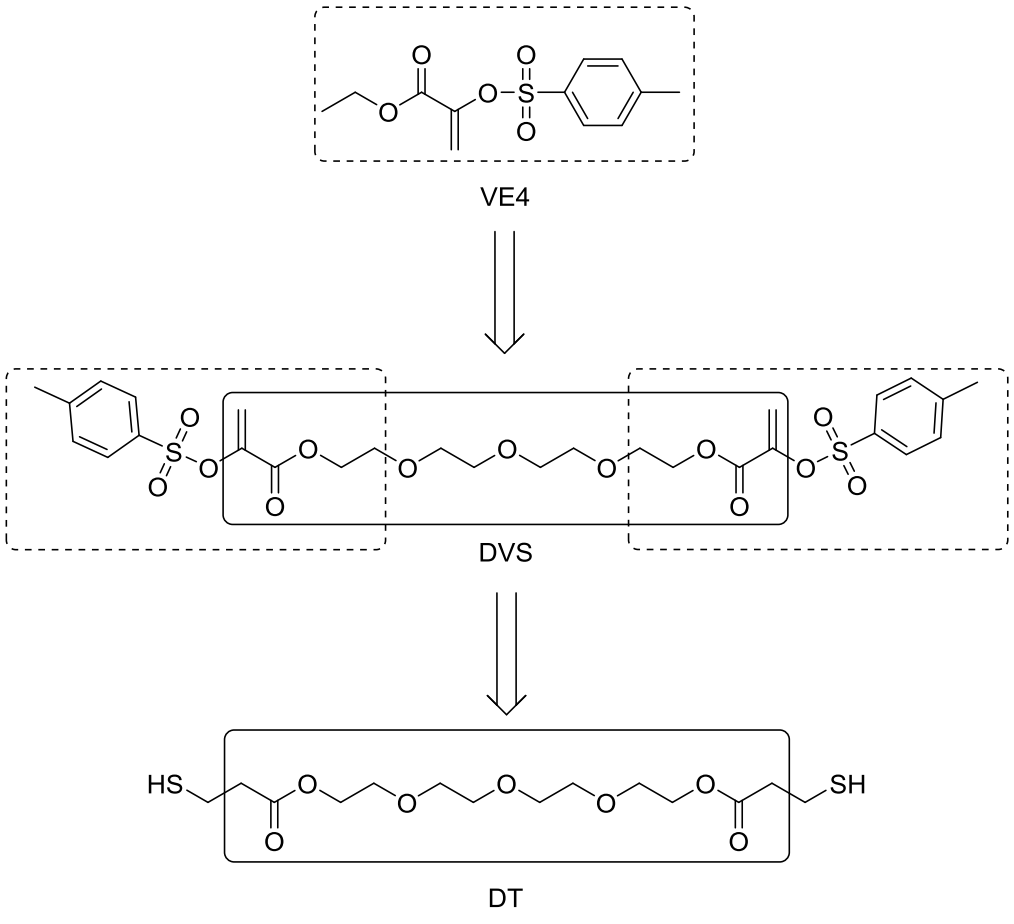

Figure 111: VE4 was found to efficiently regulate monofunctional ACs. For difunctional AC network studies, DVS was used and a dithiol DT similar in structure was selected to compare the AFCT with thiol-ene regulation.

In order to guarantee better crosslinking, a difunctional AFCT reagent **DVS** was tested, which is based on the structural pattern of VE4. For better comparison, the dithiol **DT** was chosen as it has a similar spacer.

As polymer matrix 1,6-hexanediol diacrylate (**HDDA**) was picked. HDDA finds broad application as a standard monomer in photopolymerization and is also available under the brand name Sartomer SR238.[81] For initiating polymerization, germanium-based PI Ivocerin was used.

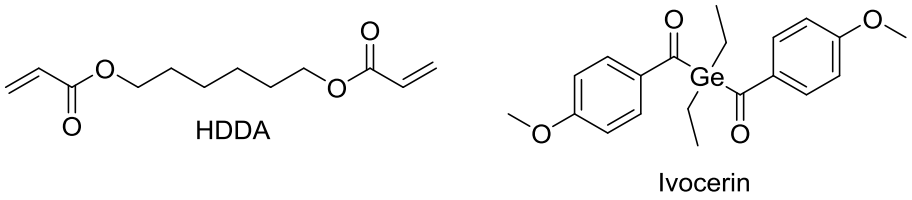

Figure 112: Monomer 1,6-hexanediol diacrylate (HDDA) and PI Ivocerin

For observing the influence on network regulation, the following formulations for later analysis were mixed:

Table 25: Overview of all tested formulations and their composition

formulation	**HDDA** [mol%]	**DT** [mol%]	**DVS** [mol%]
M	100	-	-
DT5	95	5	-
DT10	90	10	-
DT20	80	20	-
DT35	65	35	-
DVS5	95	-	5
DVS10	90	-	10
DVS20	80	-	20
DVS35	65	-	35

To all formulation 0.3 w% of PI were added. The formulations were then used for analysis or to cure test specimens for mechanical tests.

4.2 Real time-near infrared photorheology

RT-NIR-photorheology provides a powerful tool to investigate chemical and rheological behavior of formulations during a photocuring process. By coupling RT-NIR with photorheology important parameters, like time until gelation ($\mathbf{t_{gp}}$), double bond conversion at gel point ($\mathbf{DBC_{gp}}$), the time until 95% of the final double bond conversion is reached ($\mathbf{t_{DBC95\%}}$), final double bond conversion ($\mathbf{DBC_{final}}$), the time until 95% of the final storage modulus is reached ($\mathbf{t_{G'end95\%}}$), the final storage modulus ($\mathbf{G'_{end}}$), and the shrinkage stress (normal force measurements ($\mathbf{F_N}$)) can be evaluated.

Table 26: Summarized results of RT-NIR photorheology

Formulation	t_{gp} [s]	DBC_{gp} [%]	$t_{DBC95\%}$ [s]	DBC_{final} [%]	$t_{G'end95\%}$ [s]	G'_{end} [MPa]	F_N [N]
M	1.0 ± 0.1	8 ± 1	30	89	143	0.96	46
DT5	1.6 ± 0.1	18 ± 1	22	92	139	0.90	45
DT10	2.2 ± 0.1	33 ± 1	12	96	157	0.88	40
DT20	1.7 ± 0.1	38 ± 1	7	100	88	0.70	33
DT35	2.7 ± 0.1	55 ± 2	6	100	79	0.58	25
DVS5	3.8 ± 0.1	31 ± 1	26	91	153	0.96	41
DVS10	4.8 ± 0.1	37 ± 1	20	93	177	0.89	36
DVS20	5.8 ± 0.1	47 ± 2	19	97	224	0.81	25
DVS35	7.3 ± 0.2	70 ± 2	18	100	265	0.77	18

A very meaningful parameter, which can be extracted from the RT-NIR photorheology results, is the gel point, which is defined as the intersection of loss modulus (**G''**) and storage modulus (**G'**).[82] By using rheology data, the t_{gp} can be determined. Parallel recorded DBC from RT-NIR can then be used to evaluate the DBC_{gp}. At the gel point the liquid monomer formulation turns into a solid gel. This transformation in aggregate phase leads to the formation of shrinkage stress in the network. As already mentioned in the introduction, CTAs can shift the gel point to higher DBC. A higher DBC_{gp} means that solidification takes place later in the polymerization process and therefore, more homogeneous networks are formed and a decrease in shrinkage stress can be observed.[36]

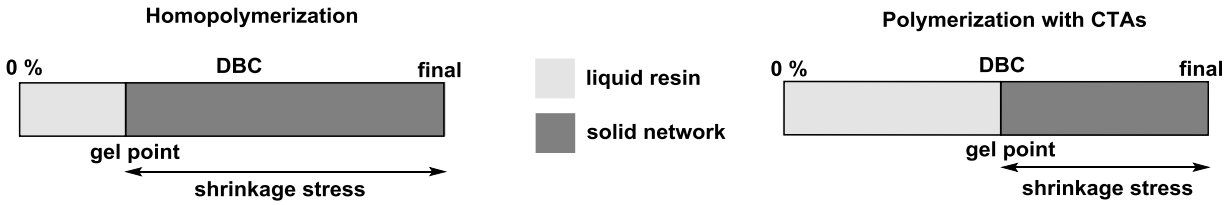

Figure 113: Shift of gel point to higher DBC yielding in reduced shrinkage stress in the material

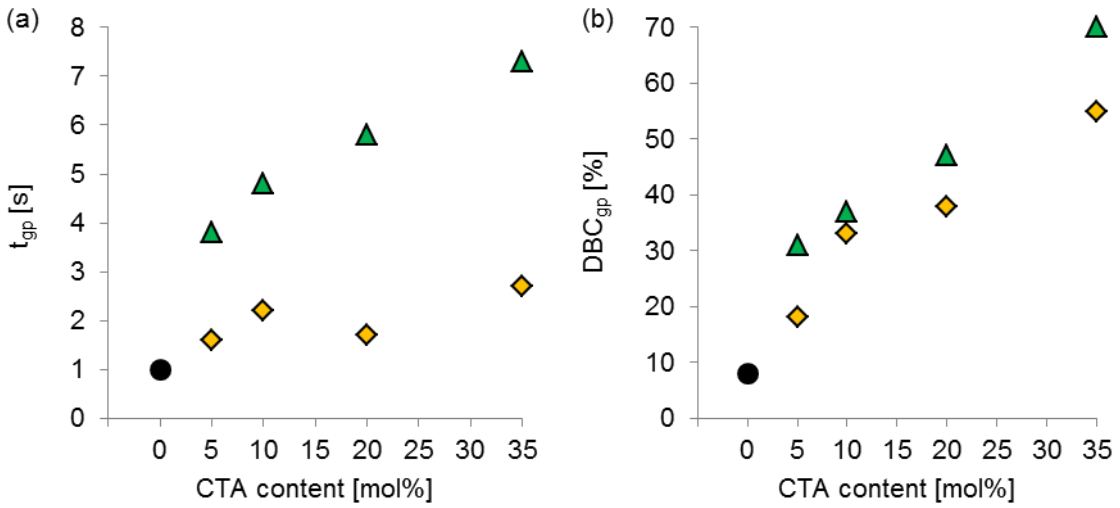

Figure 114: (a) Change of t_{gp} and (b) DBC_{gp} with increasing CTA content (M ●, DT ◆, and DVS ▲);

Regarding Figure 114 a, an increasing in thiol content in the AC-based photo-resin leads to longer t_{gp}s delaying gelation. For the homopolymer M gelation takes place after 1.0 s, while thiol-regulated samples lead to slightly longer t_{gp}s (1.6-2.7 s). Same applies for DVS-regulated formulations, where DVS5 already delays gelation to a t_{gp} of 3.8 s. The following delay of t_{gp} is almost linear increasing with increasing the DVS amount. Compared to thiols, DVS-regulated formulations show longer t_{gp}s. Already 5 mol% of DVS in the AC formulation delays gelation more than 35 mol% of DT.

Concerning DBC_{gp} in Figure 114 b, thiols show a clear increase of DBC_{gp}. The homopolymerization exhibits early gelation at 8 % DBC. The addition of small amounts of thiols of 5 and 10 mol% shifts the gel point to 18% and 33% DBC. Higher thiol ratios result in a DBC_{gp} of more than 50%. A similar development can be observed for DVS-regulated formulations. Low vinyl sulfonate ester concentrations of 5 and 10 mol% in the AC resin shift the DBC_{gp} to 31% or 37%. A DVS concentration of 35 mol% leads to a DBC_{gp} of even 70%. Comparing thiol with DVS formulations of same concentration show that the DBC_{gp} values of DVS-regulated formulations are always significantly higher than for thiol formulations.

Another interesting parameter for determining the speed of the curing is the $t_{DBC95\%}$ value, which describes the time until 95% of the final DBC after 300 s of irradiation is reached. The $t_{DBC95\%}$ value can be used as a measure for the speed of photopolymerization. Homopolymerization needs 30 s to reach 95% of DBC_{final} (Figure 115 a). The addition of thiols leads to a clear reduction of $t_{DBC95\%}$ values. However, the trend shows that small amounts of thiols reduce the $t_{DBC95\%}$ rather fast. The difference between DT20 (7 s) and DT35 (6 s) is only marginal. DVS regulation of diacrylates also lead to faster reactions.

Nevertheless, it can be seen that the change of $t_{DBC95\%}$ in the range of 10-35 mol% DVS is negligible. Comparing thiol- and vinyl sulfonate ester-regulated formulations of same concentrations shows that thiols lead to faster reactions than DVS in the HDDA resin. From the evaluated data, it can be stated that the photopolymerization is accelerated until a certain concentration of CTA in the resin is reached. After reaching this concentration, $t_{DBC95\%}$ remains almost constant. However, DVS35 is with a $t_{DBC95\%}$ of 18 s much slower than DT35 with a $t_{DBC95\%}$ of 6 s.

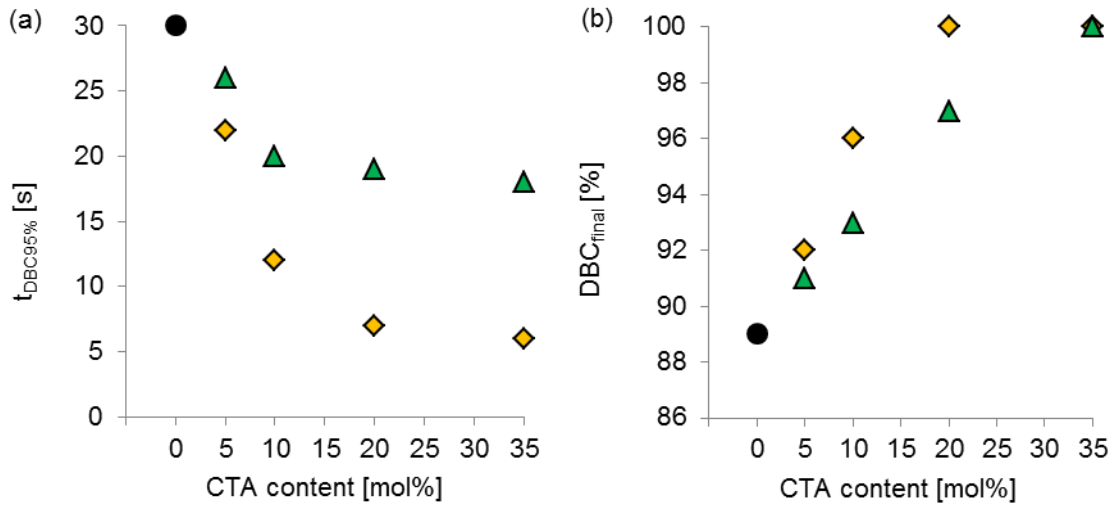

Figure 115: (a) $t_{DBC95\%}$ and (b) DBC_{final} values for different CTA content (M ●, DT ◆, and DVS ▲);

The last key figure dealing with the DBC is DBC_{final}. DBC_{final} is a measure for the completeness of the photopolymerization. Figure 115 b illustrates that the homopolymerization M results in a rather high DBC_{final} of 89%. As expected, the addition of DT raises the DBC_{final}. With 20 mol% DT 100% DBC_{final} can be achieved. The same development can be observed for DVS-regulated formulations. Again, the addition of AFCT reagent raises the DBC_{final} until reaching 100% at 35 mol% DVS. Comparing DT and DVS formulations of same concentrations, thiol formulations always exhibit a slightly higher DBC_{final} than vinyl sulfonate ester formulations, reaching 100% DBC at lower CTA concentrations. In this context, it has to be emphasized that all DBC measurements concerning DVS formulations refer to the DB of the monomer HDDA and the DB of the AFCT reagent DVS, while measurements for DT formulations only comprise the DB of the monomer HDDA. This means that no information about the thiol conversion is included. In terms of thiol conversion it makes sense to use results, which have been already discussed in General part 3.2. The photoreactor study proved that a low thiol content of 5 mol% leads to thiol conversions close to 100%, while higher concentrations (10, 20, and 35 mol%) exhibited thiol conversion < 90%. Therefore, it can be assumed that formulations with > 10 mol% DT ratio do not show 100% thiol conversion.

Another parameter is the time until 95% of final storage modulus is reached $t_{G'end95\%}$ (Figure 116 a). For DT formulations, the $t_{G'end95\%}$s for low thiol concentrations remain in the range of the homopolymer ~145 s. For DT20 and DT35, $t_{G'end95\%}$s are reached after a shorter time periods of 88 and 79 s. In contrast, DVS-regulated formulations need longer time periods to reach 95% of the final G'. Moreover, $t_{G'end95\%}$ is considerably increasing with the DVS content.

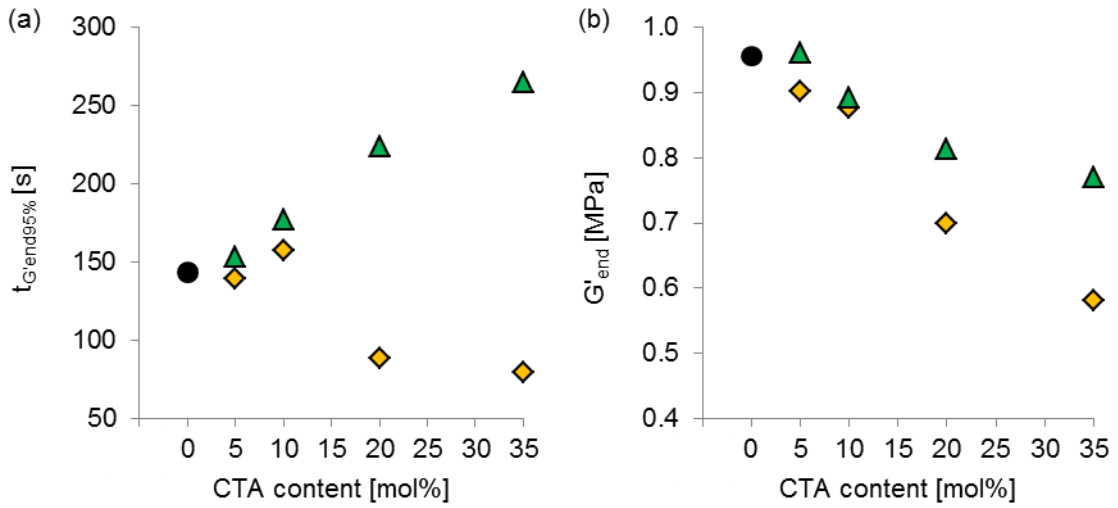

Figure 116: (a) Plot of $t_{G'end95\%}$ and (b) G'_{end} with increasing CTA content (M ●, DT ◆, and DVS ▲);

G'_{end} describes the storage modulus after 300 s of irradiating the formulation (Figure 116 b). The neat HDDA formulation reaches the highest G'_{end} value of 0.96 MPa. DT5 and DT10 formulations only slightly decrease G'_{end} (0.90 and 0.88 MPa), while higher thiol concentrations lead to a significant decrease in G'_{end} (0.70 and 0.58 MPa). This can be attributed to the formation of flexible thio-ether bridges lowering the G'. Applying DVS to AC resins also results in a decrease of G'_{end}, especially at higher AFCT reagent content. However, while at low CTA content the G'_{end}s of DT- and DVS-regulated formulations remain in the same range, thiol-regulated networks exhibit significantly lower G'_{end} values than DVS-regulated networks at higher CTA concentrations.

As already pointed out in Figure 113, a shift of DBC_{gp} usually comes along with a decrease in shrinkage stress. In order to prove this theory, F_N measurements were conducted. Considering the DT-regulated formulations, Figure 117 clearly shows that thiol-regulated curing emerges in a reduction of shrinkage stress. Low thiol concentrations (5 and 10 mol%) only lead to a slight reduction of F_N (45 and 40 N) compared to the homopolymer (46 N). As expected, DT20 and DT35 lead to a greater reduction of F_N (33 and 25 N). Regarding DVS-regulation similar results can be seen in Figure 117. The addition of 5 and 10 mol% DVS results in a slight decrease of F_N (41 and 36 N). DVS20 and DVS35 already show a decrease of F_N of 45 and 61% (25 and 18 N) when compared to homopolymerization. The comparison between DT and DVS formulations of same concentrations clearly points out that the

application of vinyl sulfonate esters comes along with a greater reduction of shrinkage stress. These findings can be put into relation with the DBC_{gp} values. As already discussed above, DVS regulation in HDDA is able to shift the gel point to higher DBCs than DT regulation. Consequently, the later transition from the liquid to the solid aggregate state mitigates the formation of polymerization-induced shrinkage stress in the material.

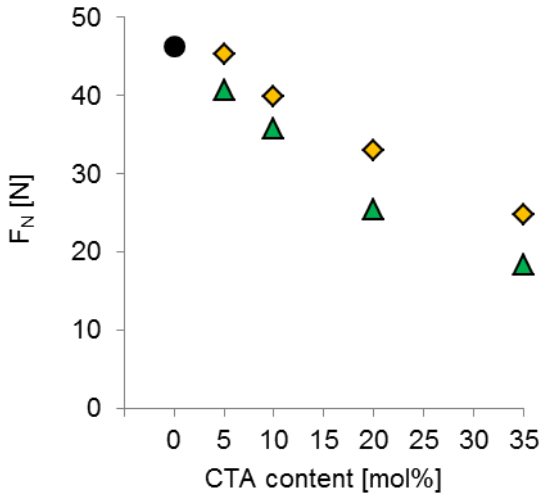

Figure 117: Plot of F_N development with increasing CTA content (M ●, DT ◆, and DVS ▲);

4.3 Dynamic mechanical thermal analysis

For gathering information about mechanical and thermal properties of the cured material, dynamic mechanical thermal analysis (**DMTA**) measurements were performed. DMTA is a very useful tool to analyze the viscoelastic behavior of cured photopolymers. Therefore, a polymer specimen is exposed to a sinusoidal stress, while passing through a temperature program. By recording the temperature depending storage modulus (**G'**) and loss modulus (**G''**), parameters like the glass transition temperature (**T_g**), loss factor (**tan δ=G''/G'**), and full width at half maximum (**FWHM**) of the glass transition area, which can be regarded as a measure for the regulating ability of CTAs, can be extracted. Moreover, the storage modulus at 20 °C (**G'_{20}**) can be determined. This value is important, since network regulation should not lead to a decrease of G'_{20}. Important information can also be gained about the crosslinking density by evaluating the modulus at rubber elasticity state (**G'_r**).

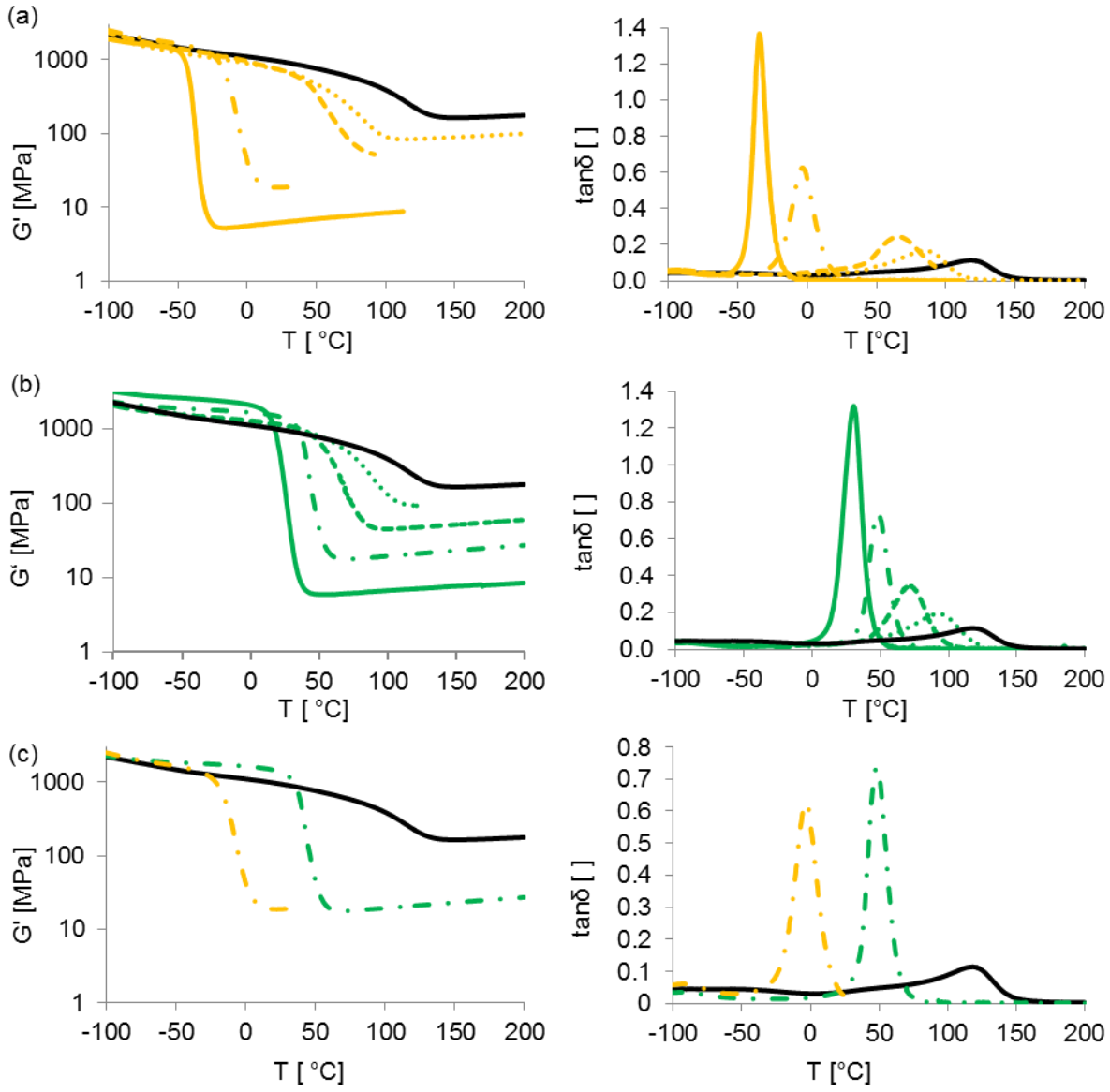

Figure 118: Diagrams of temperature-depending G' and tanδ for (a) thiol-based networks, (b) AFCT-regulated networks, and (c) comparison between M, DT20, and DVS20 [M (▬), DT5 (▪▪▪▪), DT10 (▪ ▪ ▪), DT20 (▪ ▪ ▪), DT35 (▬), DVS5 (▪▪▪▪), DVS10 (▪ ▪ ▪), DVS20 (▪ ▪ ▪), and DVS35 (▬)];

As can be seen in Figure 118 and Figure 119, the glass transition becomes sharper with increasing CTA content, which emerges in a sudden drop of G' and the narrowing of the loss factor curve (quantified as the full width at half maximum of the loss factor curve FWHM) indicating better regulated and more homogeneous networks. Concerning T_g, CTA network regulation comes along with a shift of T_g to lower temperatures. While at low CTA concentrations (5 and 10 mol%) DVS- and DT-regulated networks exhibits T_gs in the same temperature range, DT-regulated networks show significantly lower T_gs at higher DT concentrations (20 ad 35 mol%) than the DVS analog. From the FWHM values similar network regulating abilities for diacrylate networks can be stated for DT and DVS.

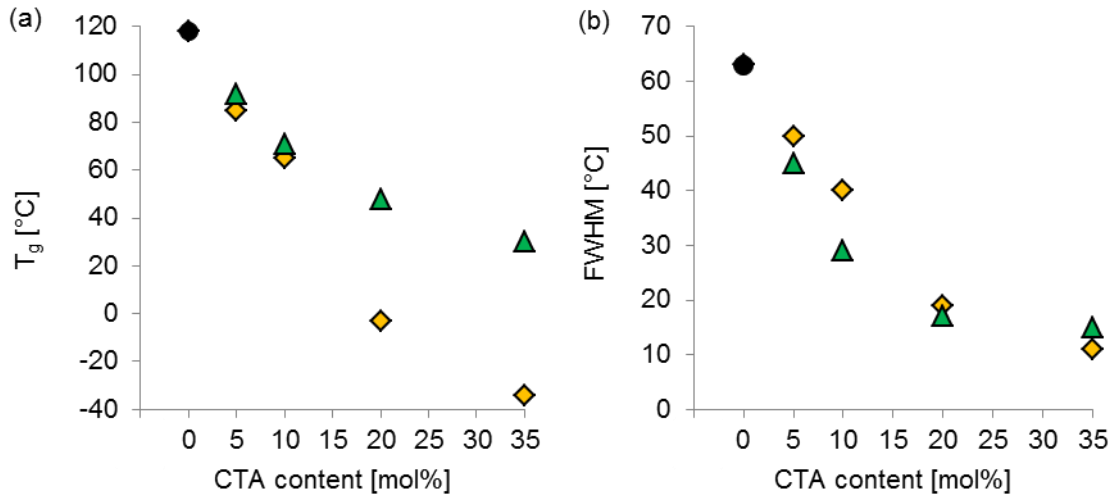

Figure 119: (a) T_g and (b) FWHM values with increasing CTA content (M ●, DT◆, and DVS ▲);

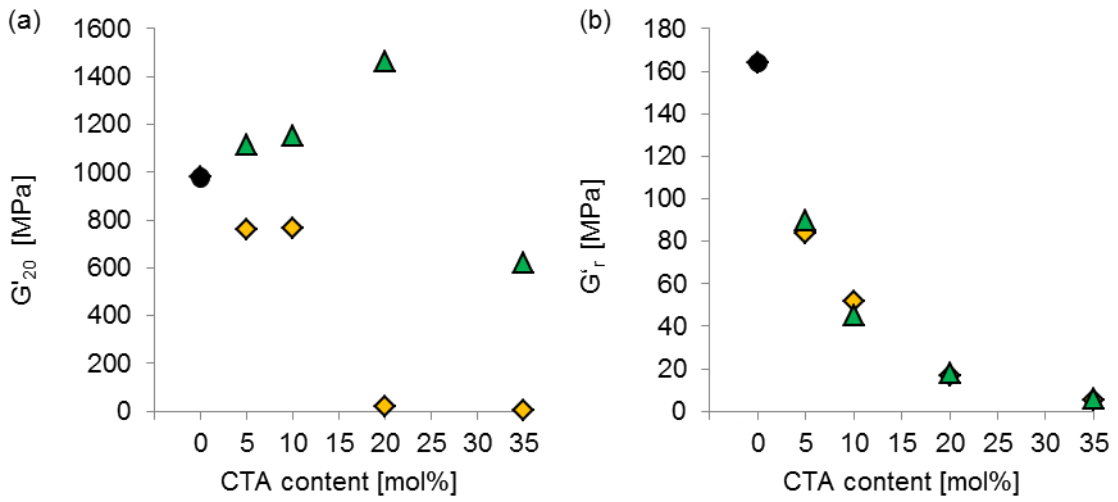

Figure 120: (a) G'$_{20}$ and (b) G'$_r$ values with increasing CTA content (M ●, DT ◆, and DVS ▲);

Figure 120 proves that AFCT-regulated specimens show higher G'$_{20}$ than the neat HDDA specimen, while thiol-ene-regulated networks exhibit a decrease in G'$_{20}$. This is not surprising, considering the formation of flexible thio-ether bridges, which are softening the material.

The G'$_r$s values are decreasing with increasing CTA amount in the specimen. This is not surprising since regulation should lead to a lower crosslinking density. G'$_r$s values for DVS networks are in the range of DT networks, which usually is an indication for similar crosslinking density in the networks. However, it has to be emphasized that even the formation of flexible thio-ether bridges or the existence of pendant thiol groups in the network

could lead to a decrease of G'_r values in comparison with AFCT-regulated networks even though in reality possessing higher crosslinking density.

Table 27: Overview of the most important DMTA data

specimen	G'_{20} [MPa]	T_g [°C]	G'_r [MPa]	FWHM [°C]
M	979	118	164	66
DT5	759	85	84	50
DT10	768	65	52	40
DT20	19	-3	17	19
DT35	6	-34	5	11
DVS5	1112	92	90	45
DVS10	1151	71	45	29
DVS20	1465	48	18	17
DVS35	619	30	6	15

4.4 Tensile test

Tensile test is one of the most utilized tests for materials. This quasi-static test is carried out to make a statement about the strength and the plasticity of materials resulting in a stress-strain curve. As specimens dog chew bone-shaped samples are casted, fixed between two clamps and strained with a constant velocity. At the same time a stress-strain plot is recorded.

In case of photopolymers mostly brittle polymers are expected. However, it has to be mentioned that stress-strain curves are naturally depending on ambient temperatures and so the T_g of photopolymers is decisive for the curve shape, since DMTA results have already enlightened the correlation between CTA concentration in a network and decrease of T_g and especially G'_{20}.

In Figure 121 and Figure 122 the results of the tensile test for DT- and DVS-regulated specimens are illustrated. The reference polymer M shows rather brittle behavior with a maximum stress ($\boldsymbol{\sigma_M}$) of ~37 MPa and an elongation at break ($\boldsymbol{\varepsilon_B}$) of 7%, while the DT samples react with a significant decrease in σ_M upon DT in the material. At higher DT concentration the materials exhibit a very low modulus and ε_B slightly increases. The addition of thiols leads to a loss of material strength.

A different behavior can be observed for samples DVS5-DVS20. These specimens show an increase of σ_M up to 51.5 MPa with increasing DVS content, while $\boldsymbol{\varepsilon_B}$ remains in the same range. The steeper slope in the linear region also indicates an increase in modulus. On the other hand, DVS35 represents an exception. By reaching a σ_M of only 15 MPa, material

strength is lowered. However, with a ε_B of ~110% it exhibits an even elastomer-like curve shape. This is not surprising since DVS35 already exhibits a rather low T_g and G'_{20} value.

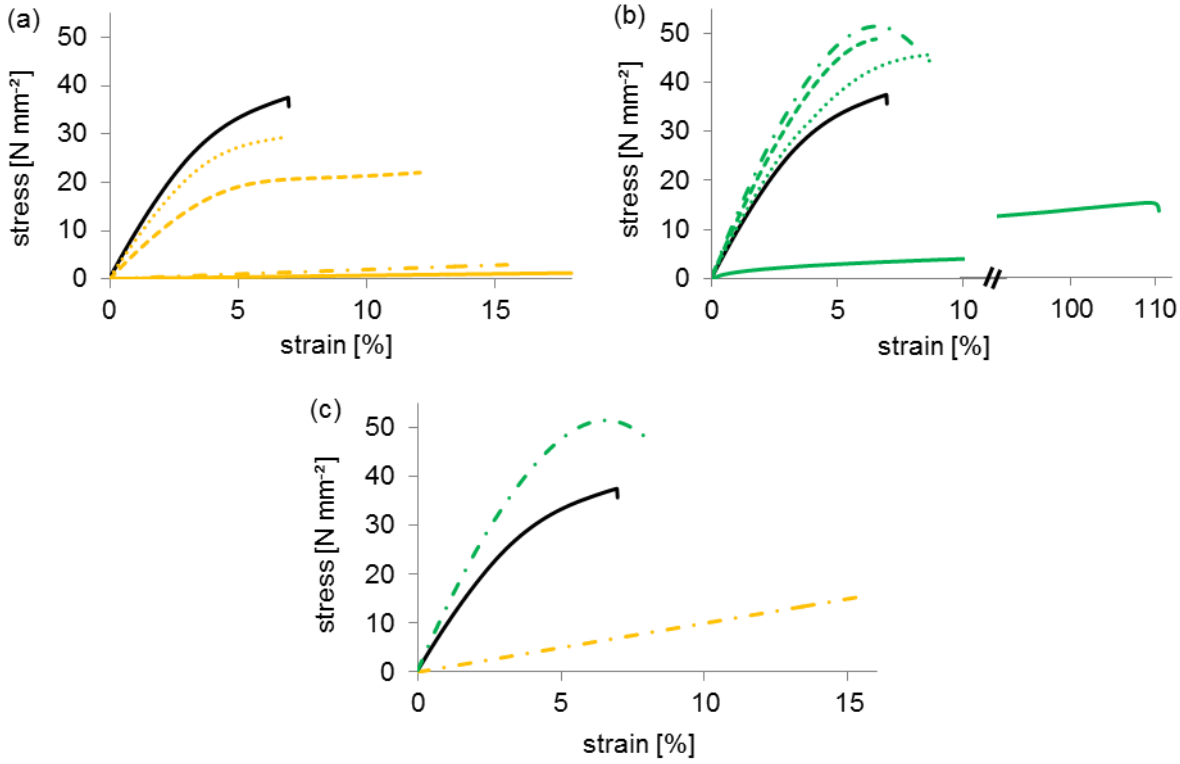

Figure 121: Stress-strain diagram of (a) thiol-regulated specimens, (b) AFCT-regulated samples, and (c) comparison between M, DT20, and DVS20 [M (——), DT5 (·····), DT10 (– – –), DT20 (– · –),DT35 (——), DVS5 (·····), DVS10 (– – –), DVS20 (– · –), and DVS35 (——)];

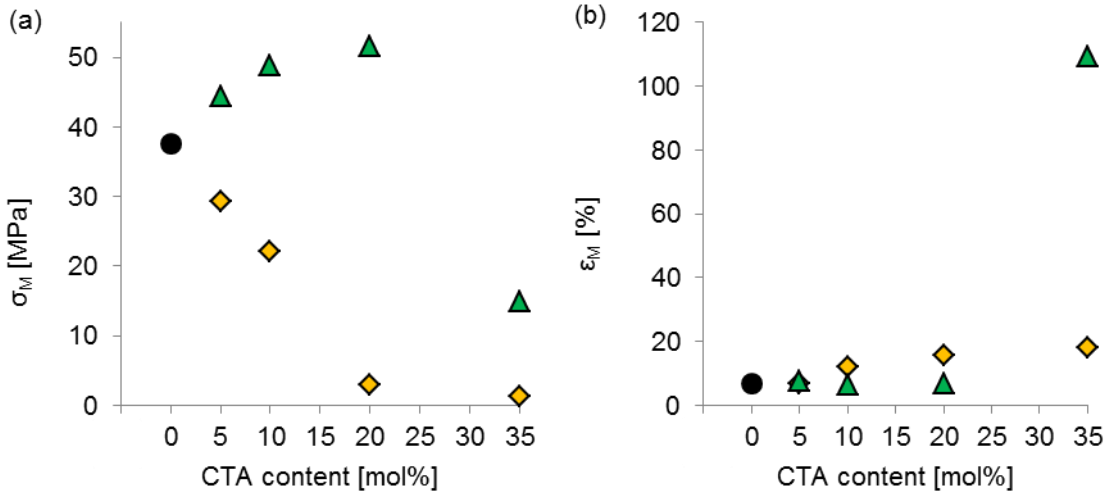

Figure 122: (a) Plot of σ_M values and (b) ε_M values with increasing CTA content (M ●, DT ◆, and DVS ▲);

Comparing thiol-regulated with AFCT-regulated specimens, DVS-regulated specimens clearly outperform DT-regulated specimens in terms of material strength.

Summarizing, a clear connection between the curve shapes of the tested specimens and the beforehand determined DMTA G'_{20} values can be realized. Higher G'_{20} values (DVS5-DVS20) show materials of higher strength, while specimens with lower G'_{20} values (DT5-DT35, DVS35) exhibit material of lower strength.

Table 28: Overviews of most important tensile test figures and G'_{20} from DMTA

specimen	σ_M [MPa]	ε_M [%]	G'_{20} (DMTA) [MPa]
M	37.6	6.9	979
DT5	29.3	6.7	759
DT10	22.0	12.0	768
DT20	3.0	15.5	19
DT35	1.3	17.9	6
DVS5	44.4	7.4	1112
DVS10	48.9	6.5	1151
DVS20	51.5	6.6	1465
DVS35	14.9	109.2	619

4.5 Dynstat impact resistance

Generally, impact resistance is a measure for the toughness of a material. Toughness itself is defined as ability of a material to absorb energy through plastic deformation before fracture and at the same time exhibit high strength. It has to be mentioned that ductile materials show plastic deformation as well, but they are lacking in material strength. So for making a statement about material toughness, a combination of Dynstat impact resistance results and G'_{20} values from DMTA measurements were used.

As can be seen in Figure 123, impact resistance of CTA-regulated networks increase with rising CTA content. While the unregulated homopolymerized network M exhibits a rather poor impact resistance of ~ 5 kJ m^{-2}, 5 mol% of DVS (~11 kJ m^{-2}) double, 10 mol% of DVS (~15 kJ m^{-2}) triple and 20 mol% of DVS (~20 kJ m^{-2}) even quadruple the impact resistance. This can be explained by the better regulation during the network formation of the photopolymers, leading to more homogeneous networks. DVS35 even increases the impact resistance by eightfold, but it has to be mentioned that only two out of four samples provided results for Dynstat impact resistance. The reason for that is the ductile nature of the DVS35 network. The rather low T_g of ~30 °C and a G'_{20} of 619 MPa already alter the properties of the initial network. Much greater significance can be extracted from the tensile test results. In comparison with the networks DVS5-DVS20, which exhibit a steep slope of the curve and a high σ_M and rather low ε_B, DVS35 clearly represents a ductile behavior with a rather flat slope

and a considerable plastic deformation. Therefore, the hammer was not able to break two of the samples.

Also thiol-regulated specimens exhibit an increase in toughness, which is slightly lower than the increase of AFCT-regulated samples. Nevertheless, the gain in toughness comes along with a loss in G'_{20}, which can be attributed to the formed flexible thio-ether bridges in the network, while DVS-regulated samples maintain high G'_{20}.

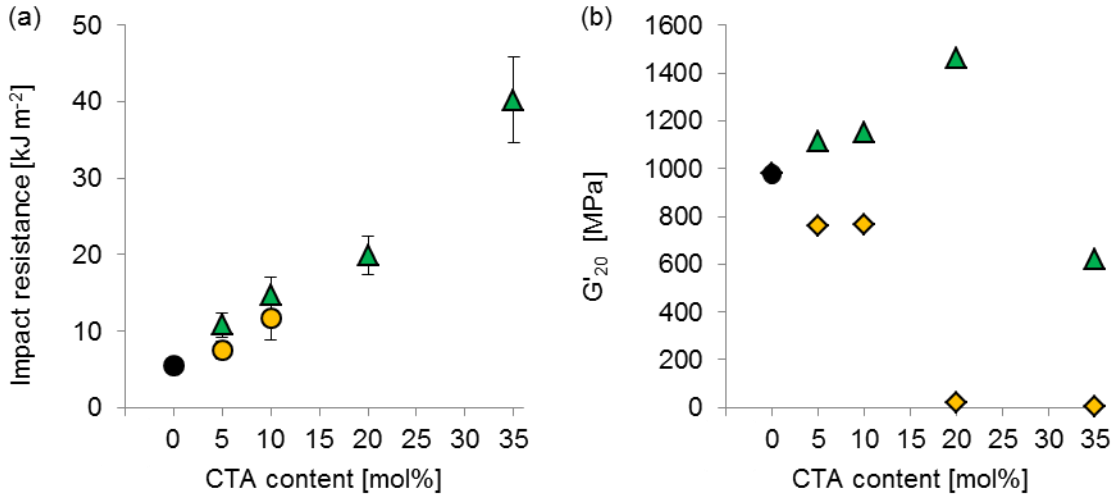

Figure 123: (a) Dynstat impact resistance values and (b) G'_{20}(DMTA) values with increasing CTA content (M ●, DT ◆, and DVS ▲);

Besides, it has to be mentioned that for networks DT20 and DT35 the Dynstat experiment could not be executed successfully. This can be explained by taking a closer look on the G'_{20} values from DMTA analysis. While networks DT5 and DT10 possess G'_{20} ~750 MPa, network DT20 and DT35 show G'_{20} values ~10 MPa. These low G'_{20} values are characteristic for ductile materials. This can be confirmed by before conducted tensile tests. In this special case, the deformation of DT20 and DT35 material was so strong that the hammer of the Dynstat setup was not able to break the samples and thus no results for impact resistance could be obtained.

Summarizing, AFCT-regulated specimens show a slightly higher increase in impact resistance than thiol-regulated samples without sacrificing G'_{20}, whereas the increase of impact resistance in thiol-regulated networks comes along with a significant loss of G'_{20}.

Table 29: Results of Dynstat impact resistance with G'_{20} values from DMTA

specimen	impact resistance [kJ m^{-2}]	G'_{20} (DMTA) [MPa]
M	5.5 ± 0.7	979
DT5	7.5 ± 1.2	759
DT10	11.7 ± 2.9	768
DT20	-	19
DT35	-	6
DVS5	10.8 ± 1.6	1112
DVS10	14.6 ± 2.5	1151
DVS20	20.0 ± 2.5	1465
DVS35	40.2 ± 5.6	1170

4.6 Nanoindentation

In order to gain information about the material hardness, nanoindentation experiments were performed. From the recorded data, values for the indentation hardness (H_i) and the reduced modulus (E_r) could be extracted.

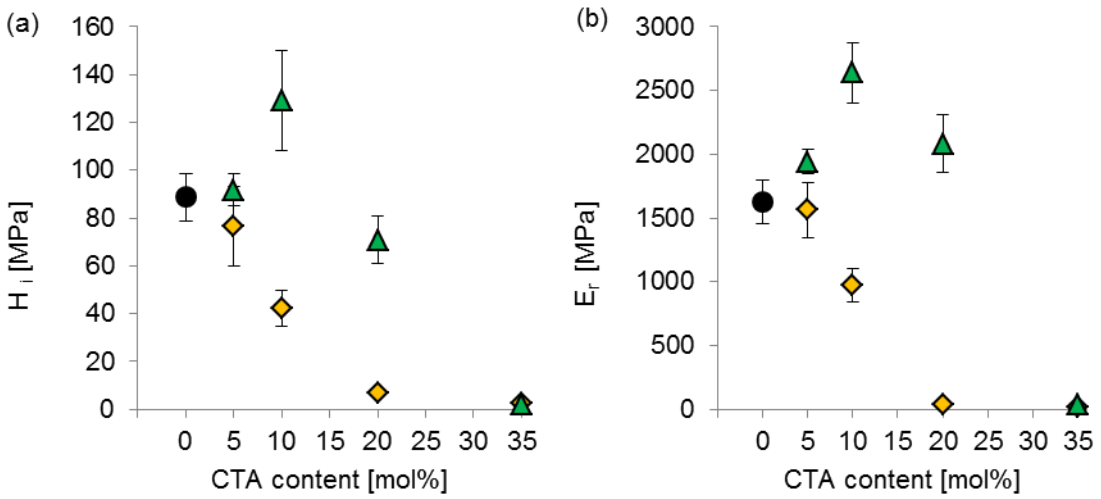

Figure 124: (a) H_i values and (b) E_r values with increasing CTA content [M ●, DT ◆, and DVS ▲];

Generally, diacrylate networks possess a rather good hardness and high modulus at room temperature. As depicted in Figure 124, the addition of small amounts of AFCT reagent (< 20 DB%) can even increase hardness values, while larger amounts lead to a sudden decrease in hardness. At the same time, the increase in hardness of DVS-regulated specimens comes along with an increase in E_r, while a decrease in hardness of AFCT-regulated samples results in a decrease of E_r.

On the other hand the regulation of AC networks with thiols exhibits a constant loss of hardness and modulus declining with increasing DT amount in the networks. The decrease in

modulus with increasing dithiol ratio in the samples has already been confirmed by DMTA measurements and tensile tests and can be contributed to the formation of flexible thio-ether bridges softening the material.

Table 30: Results of nanoindentation experiments

specimen	H_i [MPa]	E_r [MPa]
M	88.8 ± 9.9	1628 ± 173
DT5	76.7 ± 16.5	1566 ± 216
DT10	42.2 ± 7.7	975 ± 129
DT20	6.8 ± 0.4	37 ± 1
DT35	2.3 ± 0.2	13 ± 1
DVS5	91.8 ± 6.5	1939 ± 95
DVS10	129.0 ± 21.0	2641 ± 236
DVS20	70.7 ± 9.9	2082 ± 224
DVS35	1.8 ± 0.1	38 ± 3

4.7 Swellability

Swellability tests represent an easy way to determine the network density of polymers. Therefore, polymer disks were swollen in ethanol at 25 °C and weighted before swelling ($\mathbf{m_{start}}$), after swelling ($\mathbf{m_{swollen}}$), and after drying ($\mathbf{m_{dry}}$) the swollen disks until constant weight was reached. From that data, the swellability (**S**) and gel fraction (**G**) could be calculated.

The standard deviation for S and for G were <0.8 w% and <0.3 w%, respectively, for all measurements.

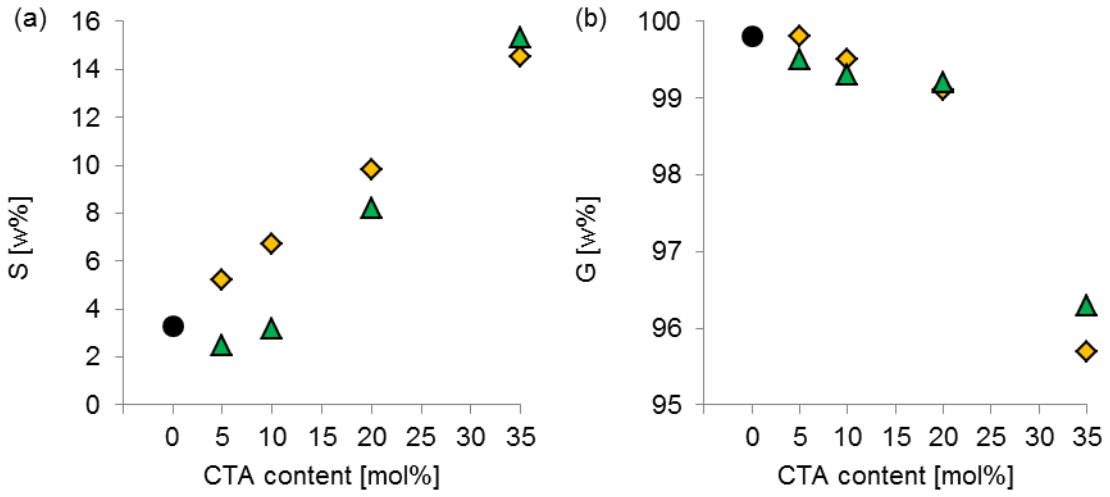

Figure 125: (a) Swellability S and (b) gel fraction G with increasing CTA content [M ●, DT ◆, and DVS ▲];

As can be seen in Figure 125 and Table 31, the homopolymer M exhibits with an S of 3.3 w% and a G of 99.8 w% a rather dense network. Adding small amounts of AFCT reagent (DVS5 and DVS10) does not change the network density significantly. At higher DVS concentrations S increases for DVS20 to ~8 w% and for DVS35 to ~15 w%. For DVS35 the G decreases significantly compared to the other DVS-regulated matrices.

Regarding thiol-regulated networks, small amounts of thiols lead to a moderate increase of S (DT5 and DT10), while DT20 and DT35 show an increase of S and a decrease of G in the range of DVS20 and DVS35. The low G values for DVS35 and DT35 can be explained by the migration of unreacted CTA due to a less crosslinked network.

Table 31: Results of swellability compared with T_g

pellet	swellability S [w%]	gel fraction G [w%]	T_g [°C]
M	3.3	99.8	118
DT5	5.2	99.8	85
DT10	6.7	99.5	65
DT20	9.8	99.1	-3
DT35	14.5	95.7	-34
DVS5	2.5	99.5	92
DVS10	3.2	99.3	71
DVS20	8.2	99.2	48
DVS35	15.3	96.3	30

4.8 Storage stability

Storage stability was measured by means of rheometry. Therefore, the viscosity of the formulations was determined after 0 days and after 120 days storage in the dark at 37 °C.

As can be seen in Table 32, the viscosity for the neat monomer is the lowest one (~ 8 Pa s). The addition of CTAs leads to an increase in viscosity, whereas the AFCT reagent DVS is more viscous than the thiol. As expected, the not stabilized thiol formulations are prone to gelation. The thiol formulation with 35 mol% DT gelled already after 5, the formulation with 20 mol% gelled after 10, and the formulation with 10 mol% after 80 days. For DT5 a slightly raised viscosity was measured after 120 days.

Table 32: Results for viscosity measurements after 0 and 120 days

sample	viscosity (0 days) [mPa s]	viscosity (120 days) [mPa s]
M	7.9	7.6
DT5	8.5	9.0
DT10	9.7	gelation after 80 days
DT20	12.8	gelation after 10 days
DT35	32.9	gelation after 5 days
DVS5	11.4	11.2
DVS10	17.0	16.7
DVS20	35.0	37.2
DVS35	102.2	114.3

Concerning AFCT formulations, DVS5 and DVS10 show no change of viscosity after 120 days of storage. For higher DVS concentrations a slight increase in viscosity was observed. It can be concluded that AFCT formulations show better storage stability than thiol formulations.

Experimental Part

2 Kinetic studies of addition-fragmentation chain transfer reagents

2.1 Screening addition-fragmentation chain transfer reagents in the photoreactor

Basically, a photoreactor consists of a 10 mL two necked round bottom flask with a small magnetic stir bar, a quick-fit that is closed with a special quartz glass, a clamp and a septum for sampling (Figure 126).

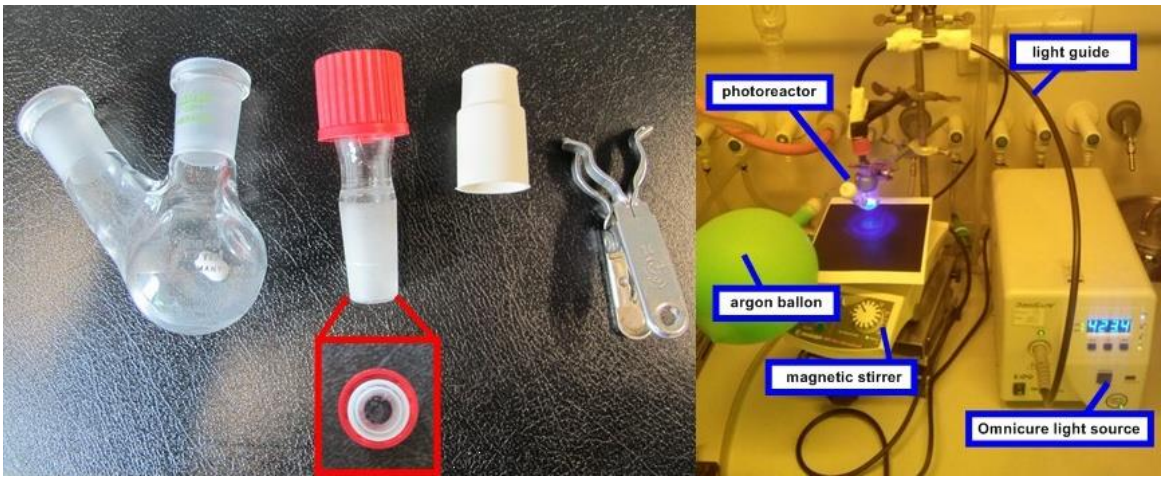

Figure 126: Typical photoreactor setup

As a light source an Exfo OmniCureTM 2000 with a broadband Hg-lamp (400-500 nm, 500 mW cm^{-2} at the tip of the light guide, ~ 3 mW cm^{-2} on the sample surface measured with an Ocean Optics USB 2000+ spectrometer) was used. The light guide was an OmniCure liquid light guide 3 mm tip diameter and 1500 mm length with a wavelength range from 320-500 nm, which was fixed with clamps to avoid movement of the light guide during the measuring period. The tip of the light guide was placed directly on the quartz glass bottom of the quick-fit. Under the photoreactor a magnetic stirrer and a black paper sheet to avoid reflection of the light were placed. Moreover, every measurement was carried out under Ar.

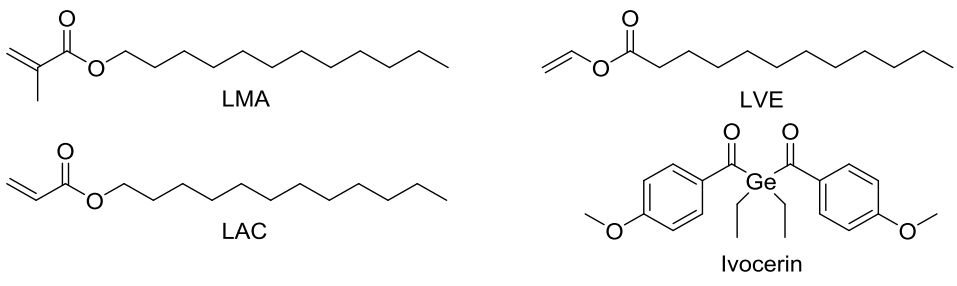

Figure 127: Model monomers used for photoreactor screening study: Lauryl methacrylate (LMA), Vinyl laurate (LVE), Lauryl arcylate (LAC) and Ivocerin as PI;

For every measurement a test solution was prepared. The total monomer and chain transfer reagent (**CTA**) mass of the test solution was specified to be 400 mg. The mixture ratio of these 400 mg was chosen in such a way that the received formulation contained the desired DB ratio between monomer and CTA. Additionally, 3 mol% of photoinitiator Ivocerin were added to the formulation, before it was dissolved in 2 mL deuterated benzene and thoroughly bubbled with Ar for at least 10 min.

Depending on the chemical nature of the tested model monomers (Figure 127), different total irradiation and sampling times were chosen.

Table 33: Different sampling times for used model monomers in photoreactor screening (total irradiation time in bold print)

measuring point	**sampling time [s]**		
	LMA	LVE	LAC
1	0	0	0
2	50	50	25
3	100	100	50
4	200	200	75
5	300	300	100
6	450	450	150
7	600	600	200
8	900	900	300
9	1200	1200	450
10	1800	1800	600
11	-	-	900

Before irradiating the test solution the first time, a sample at 0 s was taken with a syringe and transferred to a brown NMR tube, which guaranteed UV/Vis-light protection. Immediately after the transfer, the test solution was quenched with 0.6 mL of deuterated chloroform. Then the test solution was irradiated for a desired time of x seconds. The irradiation periods were manually adjusted and triggered off at the OmniCure® 2000 system. After the irradiation stopped, another sample was taken with a syringe, transferred to a brown NMR tube and quenched with deuterated chloroform again. This procedure was repeated for all beforehand selected sampling times. The average sample volume taken from the photoreactor was ~50 µL.

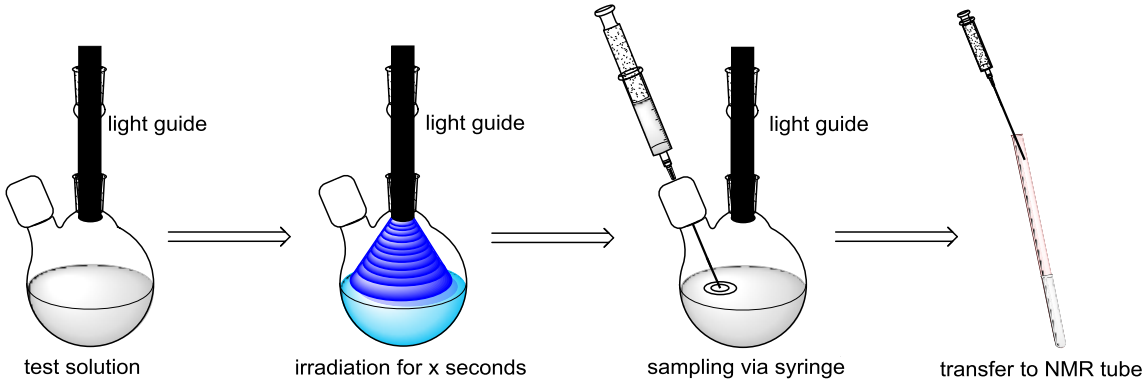

Figure 128: Sampling procedure in photoreactor study

Within two days all collected NMR tubes were analyzed with a Bruker Avance 400 MHz NMR device (^{1}H NMR 16 scans). The measured spectra were processed and evaluated by means of Bruker Topspin 2.1 software.

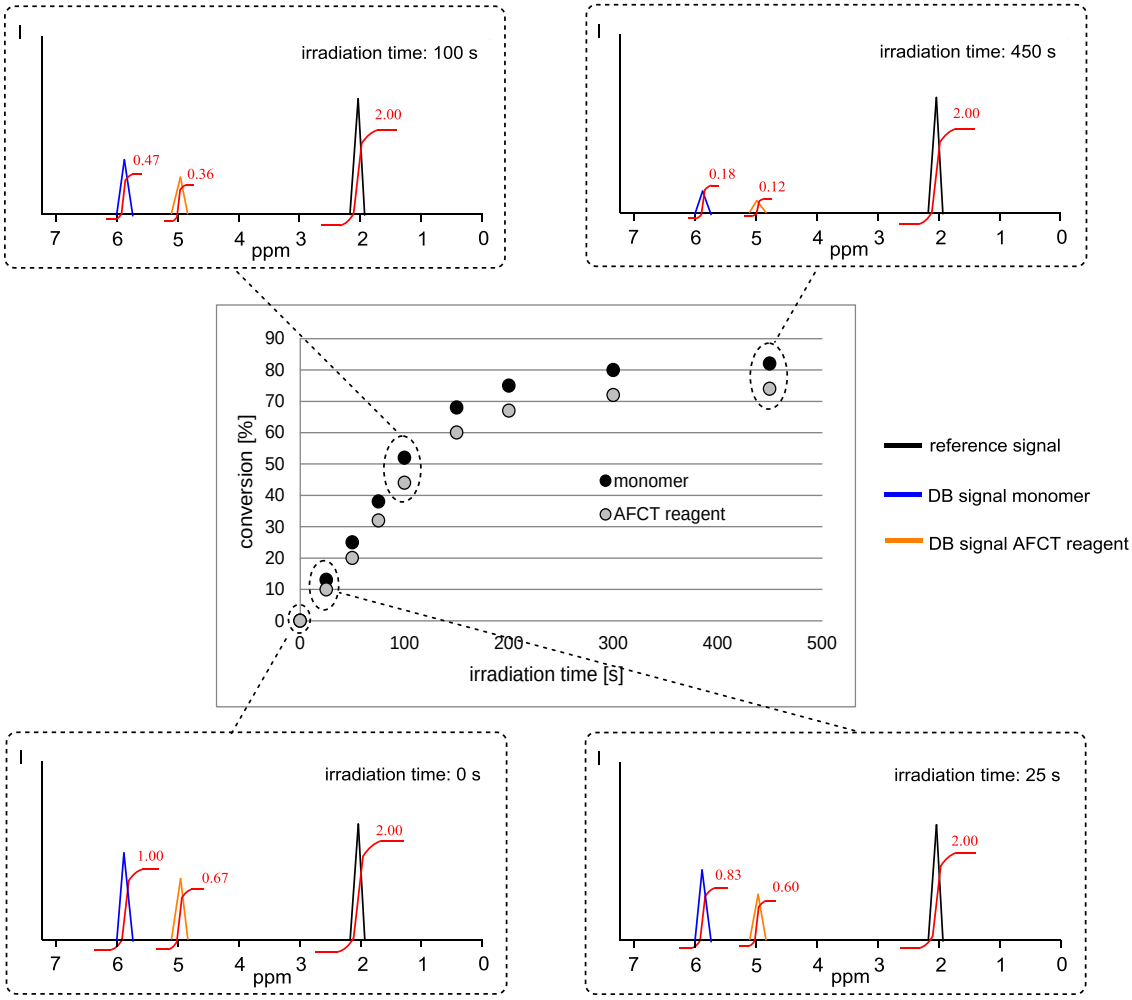

Figure 129: Schematic ^{1}H NMR spectra taken after different irradiation times and the so generated conversion-time diagram

As can be seen in Figure 129, in the ^{1}H NMR spectra the double bond (**DB**) signals of the monomer and the AFCT reagent can be seen. By irradiating the formulation, the PI forms

radicals and polymerization starts, which means that the DBs are turned into aliphatic polymer backbones. In the ^{1}H NMR spectra this leads to a decrease of DB signals of the monomer and of the AFCT reagent and new aliphatic signals are formed instead. The decrease of the ene signals can be determined by integration over the peak area and directly corresponds with the double bond conversion (DBC) of the observed ene species. Moreover, a reference signal that is not changing its peak area during polymerization is needed as internal standard. Ideally, this reference signal should be from the monomer or the AFCT reagent itself, so that no additional substances that may influence polymerization have to be added.

In order to determine parameters for describing the *relative reactivity* (**r_R**) of photopolymerization and the *co-reactivity factor* (**f_{co}**) of a monomer/ AFCT reagent system, some key figures were defined. As key figures for the photopolymerization speed, the conversion-time curve of the homopolymerization is compared to the conversion-time curve of the AFCT-regulated polymerization comprising the total amount of DBs (monomer and AFCT reagent) in the formulation (Figure 130 a).

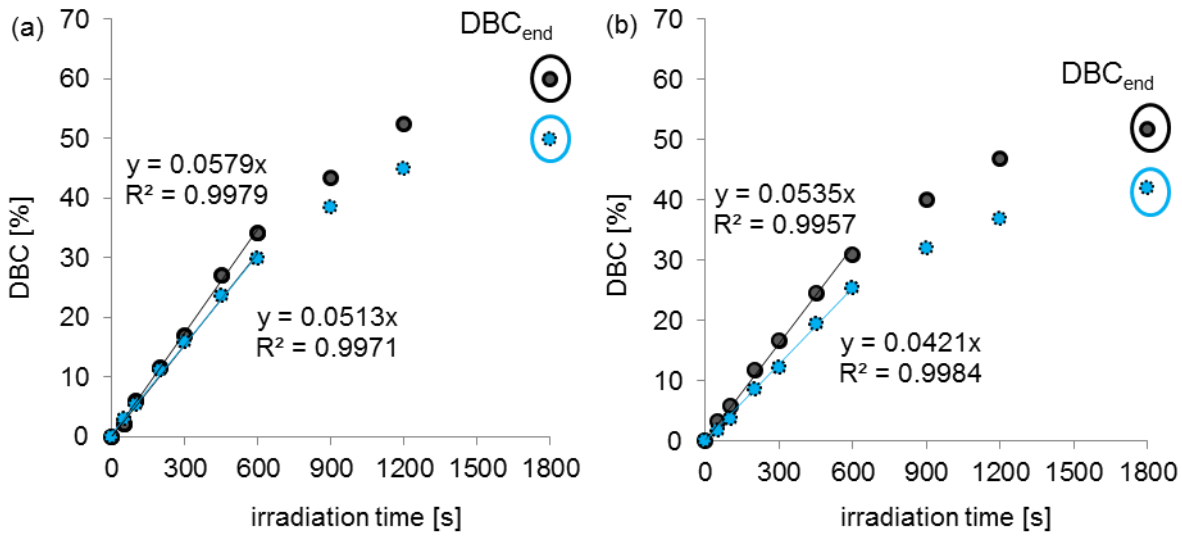

Figure 130: Regression curves for the calculation of the parameters relative reactivity r_R (a) and co-reactivity factor f_{co} (b)

Thus, the first measuring points are taken and a regression curve is calculated. The slope of this regression curve conforms to the conversion rate [% s^{-1}]. To generate a dimensionless key figure (r_R), the slope of the AFCT-regulated reaction (R_{reg}) is divided by the slope of the homopolymerization (R_{homo}) (Eq. 5). This parameter describes, whether the AFCT-regulated reaction is faster (r_R >1) than homopolymerization, as fast as (r_R =1) homopolymerization, or shows retardation (r_R <1) compared to homopolymerization.

$$r_R = \frac{R_{reg}}{R_{homo}} \ (Eq. 5)$$

Since r_R only comprises the first measuring points of the conversion-time curve potential changes of DBC at higher conversions are neglected. Consequently, a second dimensionless key figure the *relative double bond conversion* (**r_{DBC}**) is introduced, which reflects the relation between AFCT-regulated polymerization and homopolymerization at the end of the photoreactor experiment by dividing the DBC_{end} of the AFCT-regulated reaction DBC_{reg} by the DBC_{end} of the homopolymerization (DBC_{homo}) (Eq. 6).

$$r_{DBC} = \frac{DBC_{reg}}{DBC_{homo}} \ (Eq. 6)$$

Same applies for the co-reactivity (Figure 130 b). The slope of the regression curve describes the conversion rate [% s^{-1}] of consumption of the corresponding DBs. By setting the rate of AFCT-regulated reaction (r_{AFCT}) in relation to the rate of the monomer ($r_{monomer}$), the *co-reactivity factor* (**f_{co}**) can be calculated (Eq. 7). In case of co-reactivity factor, an f_{co} of 1 means a homogeneous and equal consumption of monomer and AFCT reagent, while an f_{co} >1 leads to a preferred consumption of AFCT reagent and an f_{co} <1 results in a preferred consumption of the monomer.

$$f_{co} = \frac{r_{AFCT}}{r_{monomer}} \ (Eq. 7)$$

In order to describe the co-reactivity at higher conversions the DBC_{end}s of AFCT reagent and the monomer curve are proportioned to give the *double bond conversion factor* (**f_{DBC}**) (Eq. 8).

$$f_{DBC} = \frac{DBC_{AFCT}}{DBC_{monomer}} \ (Eq. 8)$$

Taking all above defined key figures into account, makes it possible to make a statement about the applicability of an AFCT reagent in a monomer resin.

It has to be mentioned that every photoreactor experiment was carried out at least twice to ensure accuracy of the photoreactor measurement. Most measuring points of the first and the second measurement were congruent or exhibited only a slight deviation ≤ 2%.

2.1.1 Regulating methacrylates *via* addition-fragmentation chain transfer

In order to analyze the regulating abilities of AFCT reagents (Figure 131), photoreactor experiments were carried out. The ratio was determined to be 80 mol% LMA and 20 mol% AFCT reagent with 3 mol% PI Ivocerin. The exact procedure of the photoreactor study and the calculation of the key figures were conducted according to Experimental part 2.1.

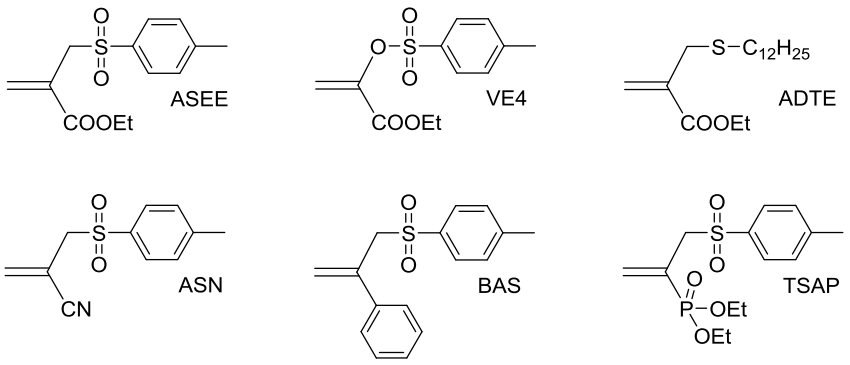

Figure 131: Tested AFCT reagents in the photoreactor screening study

As already mentioned, an appropriate model monomer provides a chemical group whose signal in the ^{1}H NMR spectrum does not change during the photopolymerization process. This chemical group can then be used as internal standard to calculate the DBC. In order to prove the stability of the reference signal, dimethyl terephthalate was used as internal standard, which did not take part in the photopolymerization and gave a signal at 8.01 ppm.

For LMA the methyl group at the end of the aliphatic chain was used as internal reference. Signal stability was proved by integration of the singlet at 8.01 ppm and the triplet at 0.80 ppm. Over time no significant change of the signal was observed.

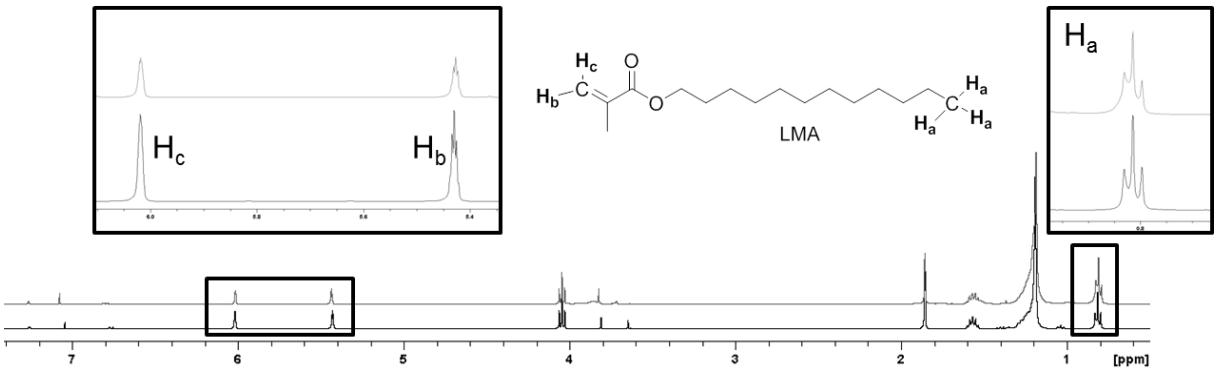

Figure 132: ^{1}H NMR spectrum of LMA after 0 and 1800 s of irradiation highlighting the DBs of the MA group and the reference peak occurring from the methyl group of the aliphatic chain

In Figure 132 LMA and its ^{1}H NMR signals are depicted. It can be seen that the reference peak (H_a) remains stable, while the signals of the DB (H_b and H_c) decrease over time. In case of LMA both DB signals can be used for integration.

2.1.2 Regulating vinyl esters *via* addition-fragmentation chain transfer

In order to analyze the regulating abilities of AFCT reagents (Figure 133), photoreactor experiments were carried out. The ratio was determined to be 80 mol% LVE and 20 mol% AFCT reagent with 3 mol% PI Ivocerin. The exact procedure of the photoreactor study and the calculation of the key figures were conducted according to Experimental part 2.1.

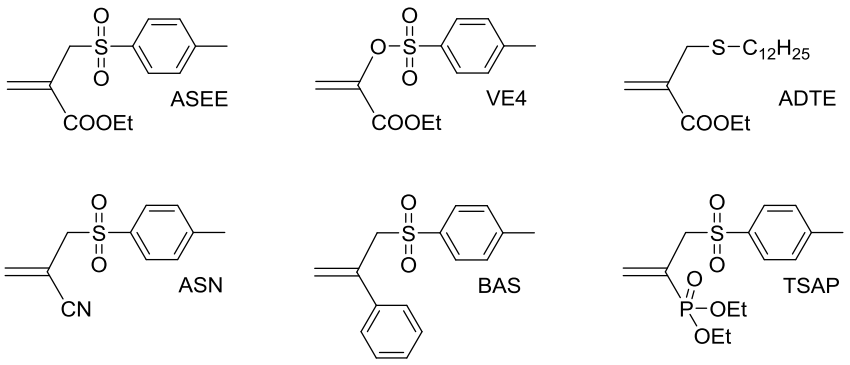

Figure 133: Tested AFCT reagents in the photoreactor screening study

Regarding LVE in Figure 134, the reference signal H_a shows also no alteration during photopolymerization. The DB signals H_b and H_d also exhibit an decrease without overlapping with other signals occurring from chemical groups, which are built during polymerization. However, it has to be considered that the $CDCl_3$ solvent peak as well as aromatic protons from the AFCT reagent may overlap with the signal. As can be seen in Figure 134, the signal for H_c interferes with another signal of unknown origin manifesting in an uneven baseline and cannot be used for determining the DBC of LVE.

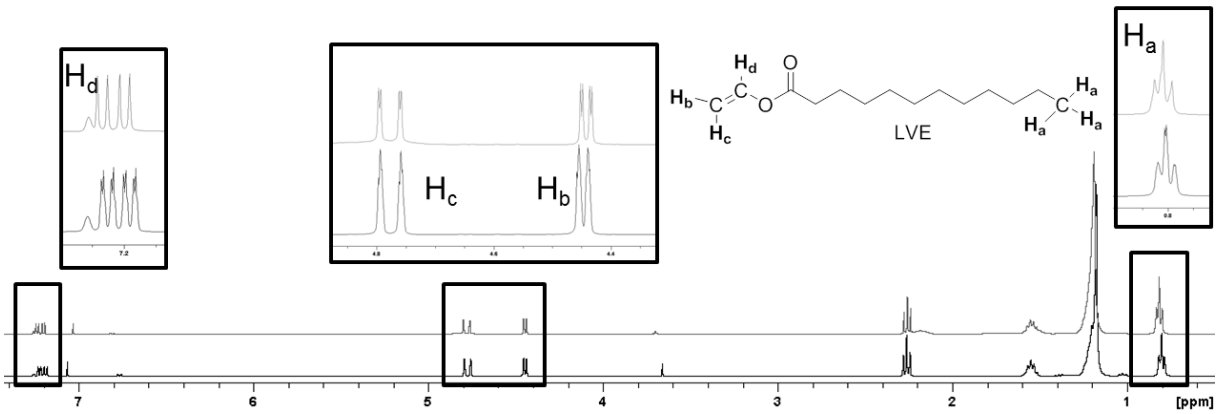

Figure 134: ^1H NMR spectrum of LVE after 0 and 1800 s of irradiation highlighting the DBs of the VE group and the reference peak occurring from the methyl group of the aliphatic chain

2.1.3 Regulating acrylates *via* addition-fragmentation chain transfer

In order to analyze the regulating abilities of AFCT reagents (Figure 135), photoreactor experiments were carried out. The ratio was determined to be 80 mol% LAC and 20 mol% AFCT reagent with 3 mol% PI Ivocerin. The exact procedure of the photoreactor study and the calculation of the key figures were conducted according to Experimental part 2.1.

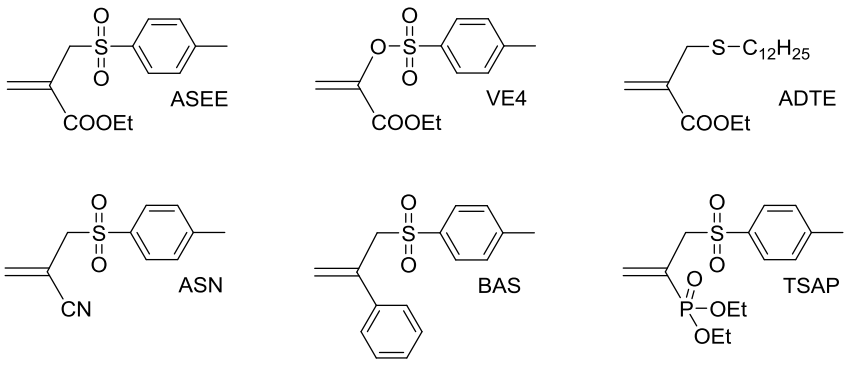

Figure 135: Tested AFCT reagents in the photoreactor screening study

^{1}H NMR spectrum of LAC shows a constant reference signal over time. Moreover, all three DB signals (H_b, H_c, and H_d) can be used for determining the DBC. Due to the high reactivity of ACs, LAC DBs are fully consumed during photopolymerization. Therefore, the DB signals vanish (Figure 136).

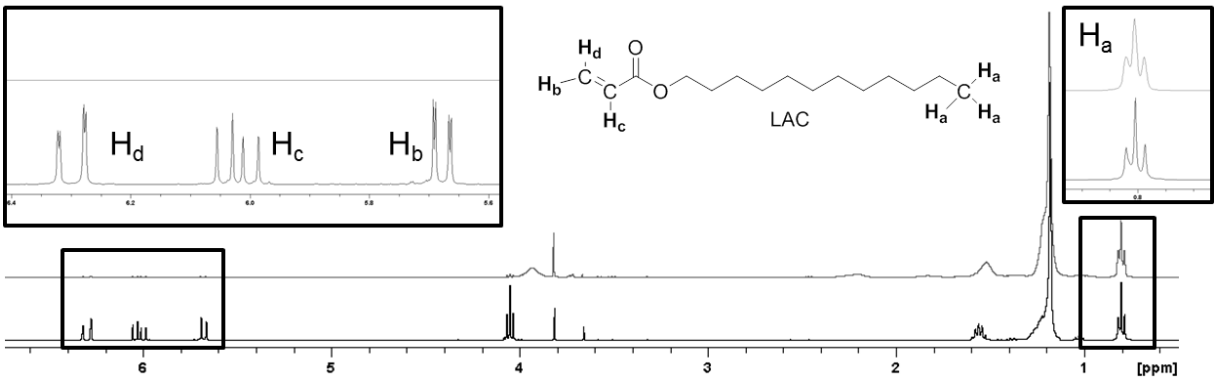

Figure 136: ^{1}H NMR spectrum of LAC after 0 and 900 s of irradiation highlighting the DBs of the AC group and the reference peak occurring from the methyl group of the aliphatic chain

2.2 New addition-fragmentation chain transfer reagents for vinyl esters and acrylates

2.2.1 3-(phenylsulfonyl)prop-1-en-2-yl acetate (BVE)

2.2.1.1 Synthesis of 3-(phenylsulfonyl)prop-1-en-2-yl acetate (BVE)

2.2.1.1.1 Synthesis of (phenyl(prop-2-yn-1-yl)sulfane[77]

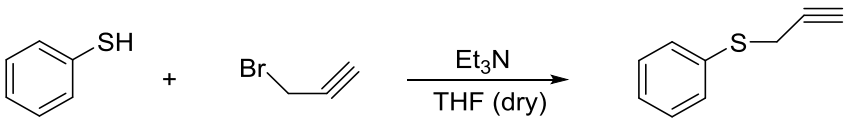

[110.17] [118.96] [148.22]

chemicals	M_W [g/mol]	[mmol]	[eq.]	[g]	[mL]
thiophenol	110.17	10.0	1.0	1.101	-
propargyl bromide	118.96	10.0	1.0	0.952	-
triethylamine	153.32	1.4	0.14	0.142	-
THF (dry)	-	-	-	-	12.0

An equimolar amount of thiophenol and triethylamine was dissolved in 9 mL dry THF under Ar atmosphere. Then a solution of propargyl bromide in 3 mL dry THF was added dropwise, which led to the formation of a white precipitate. The solution was stirred for another hour and then quenched by adding 20 mL brine. The yellowish organic layer was washed 3 times with brine and then dried over sodium sulfate. Finally, the solvent was evaporated to give yellowish liquid oil as product.

Yield: 1.39 g (94% theoretical yield, 94% yield of literature[77]), yellowish liquid

RI: n^{20}_D = 1.590 (n^{22}_D = 1.6001 in literature[83])

^{1}H NMR (400 MHz, $CDCl_3$, δ, ppm): 7.62 (d, 2H; Ar-H), 7.48 (m, 3H; Ar-H), 3.76 (d, ^{4}J= 2.9 Hz, 2H; -CH_2-), 2.38 (t, ^{4}J= 2.3 Hz, 1H; -C≡CH);

^{13}C NMR (400 MHz, $CDCl_3$, δ, ppm): 130.29 (-$\underline{C}_6H_5$-), 129.5 (-$\underline{C}_6H_5$-), 127.7 (-$\underline{C}_6H_5$-), 125.5 (-$\underline{C}_6H_5$-), 80.6 (-$\underline{C}$≡CH), 72.3(-C≡$\underline{C}$H), 23.3 (-$\underline{C}H_2$-);

2.2.1.1.2 Synthesis of (prop-2-yn-1-ylsulfonyl)benzene

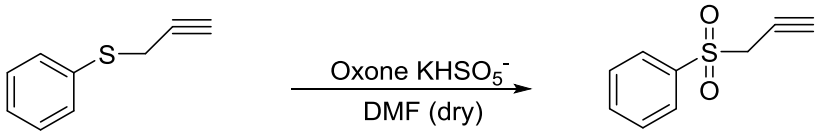

[148.22] [180.22]

chemicals	M_W [g/mol]	[mmol]	[eq.]	[g]	[mL]
(2-propynylthio)benzene	148.22	4.5	1.0	0.66	-
Oxone®	307.38	12.6	2.8	3.88	-
DMF (dry)	-	-		-	10

Oxone® ($KHSO_5$ x 0.5 $KHSO_4$ x 0.5 K_2SO_4) was suspended in 10 mL dry DMF and thoroughly bubbled with Ar. Then 3 mL of a (2-propynylthio)benzene solution in dry DMF were added dropwise to the Oxone® and were stirred for 15 h. The slightly yellowish solution turned transparent overnight. As a work up, the reaction solution was filtrated and afterwards diluted with water. Subsequently, the DMF/water phase was extracted 3 times with 40 mL Et_2O. The combined organic layers were twice washed with brine and dried over sodium sulfate. Finally, the solvent was evaporated yielding in white crystalline product.

Yield: 0.73 g (90% theoretical yield), white powder

m.p.: 90-92 °C (92-93 °C in literature[84])

^{1}H NMR (400 MHz, $CDCl_3$, δ, ppm): 8.01 (d, 2H; Ar-H), 7.72 (t, 1H; Ar-H), 7.61 (t, 2H; Ar-H), 3.97 (d, ^{4}J= 2.6 Hz, 2H; -CH_2-), 2.38 (t, ^{4}J= 2.6 Hz, 1H; -C≡CH);

^{13}C NMR (400 MHz, $CDCl_3$, δ, ppm): 138.5 (C$_6$H$_5$-), 135.2 (C$_6$H$_5$-), 130.1 (C$_6$H$_5$-), 129.8 (C$_6$H$_5$-), 77.1 (-C≡CH), 72.5 (-C≡CH), 49.3 (-CH_2-);

2.2.1.1.3 Synthesis of 3-(phenylsulfonyl)prop-1-en-2-yl acetate (BVE)[78]

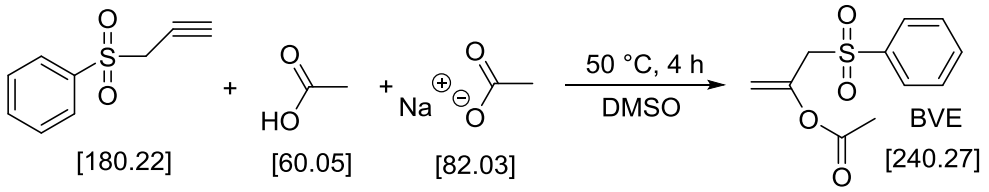

chemicals	M_W [g/mol]	[mmol]	[eq.]	[g]	[mL]
(prop-2-yn-1-ylsulfonyl)benzene	180.22	5.0	1	0.90	-
sodium acetate	82.03	90.0	18	7.39	-
acetic acid	60.05	24.0	4.8	1.45	1.3
DMSO	-	-		-	25

Sodium acetate and acetic acid were suspended in 25 mL DMSO and 12 mL of a (prop-2-yn-1-ylsulfonyl)benzene solution were added dropwise under Ar protection. The reaction was stirred 12 h at r.t. and afterwards quenched with 50 mL water. Then the aqueous phase was extracted 3 times with 30 mL of ether. The combined ether phases were twice washed with 25 mL saturated $NaHCO_3$ solution and twice with brine. The ether phase was dried over sodium sulfate and evaporated. After some time white crystals precipitated from the concentrated solution. The white crystals were filtrated and washed with cold ether to be finally dried in the desiccator.

Yield: 0.76 g (63% theoretical yield, 85% yield of literature[78]), white powder

m.p.: 94-95 °C (90-91 °C in literature[78])

^{1}H NMR (400 MHz, $CDCl_3$, δ, ppm): 7.92 (d, ^{3}J= 7.4 Hz, 2H; Ar-H), 7.69 (t, ^{3}J= 7.4 Hz, 1H; Ar-H), 7.59 (t, ^{3}J= 7.4 Hz, 2H; Ar-H), 5.06 (d, ^{2}J= 2.0 Hz, 1H; C=CH_2), 4.85 (d, ^{2}J= 2.0 Hz, 1H; -C=CH_2), 4.03 (s, 2H; -CH_2-), 1.97 (s, 3H; -OCO-CH_3);

^{13}C NMR (400 MHz, $CDCl_3$, δ, ppm): 168.6 (-OCO-CH_3), 144.1 (C=CH_2), 138.4 (C_6H_5-), 134.0 (C_6H_5-), 129.1 (C_6H_5-), 128.6 (C_6H_5-), 110.1 (C=CH_2), 60.3 (-CH_2-), 20.7 (-OCO-CH_3);

2.2.1.2 Reactivity evaluation in photoreactor

The photoreactor procedure was conducted according to Experimental Part 2.1.

2.2.2 Ethyl 2-((4-methylphenyl)sulfonamido)acrylate (TAA)

2.2.2.1 Synthesis of ethyl 2-((4-methylphenyl)sulfonamido)acrylate (TAA)[79]

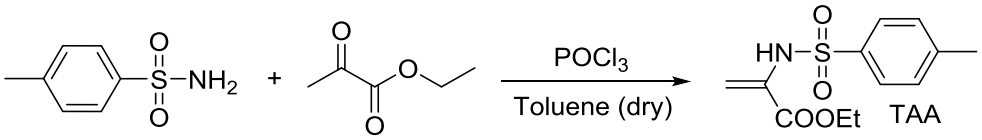

[171.21] [116.12] [269.32]

chemicals	M_W [g/mol]	[mmol]	[g]	[mL]
p-toluenesulfonamide	171.21	7.0	0.198	-
ethyl pyruvate	116.12	7.0	0.813	-
phosphorus oxychloride	153.32	1.1	0.183	0.3
toluene (dry)	92.14	-	-	12.0

p-Toluenesulfonamide and ethyl pyruvate were suspended in dry toluene. Then phosphorus oxychloride was added dropwise to the solution. The suspension was heated to 80 °C for 20 h. After cooling down, the solution was diluted with 10 mL of saturated $NaHCO_3$ and the solid residues were filtrated. The organic layer was afterwards washed twice with 20 mL water and twice with 20 mL brine. Finally, the toluene layer was dried over Na_2SO_4 and evaporated to give orange viscous liquid (Y= 1.53 g). The crude product was diluted with 3 drops of Et_2O. After 72 h in the refrigerator at -20 °C white crystals precipitated in the crude product. The white crystals were washed in 50 mL cold ether, filtrated and dried in the desiccator.

Yield: 0.91 g (48% theoretical yield, 94% of literature[79]), white powder

m.p.: 74-75 °C (76-77 °C in literature[79])

^{1}H NMR (400 MHz, $CDCl_3$, δ, ppm): 7.75 (d, 2H; Ar-H), 7.30 (d, 2H; Ar-H), 7.09 (s, 1H; NH), 5.62 (bs, 2H; =C$\underline{H_2}$), 4.23 (q, ^{3}J= 7.1 Hz, 2H; COO-C$\underline{H_2}$-), 2.40 (s, 3H; Ar-C$\underline{H_3}$), 1.27 (t, ^{3}J= 7.1 Hz, 3H; -O-CH_2-C$\underline{H_3}$);

^{13}C NMR (400 MHz, $CDCl_3$, δ, ppm): 163.1 ($\underline{C}$OO-CH_2-), 144.3 ($\underline{C}$=CH_2), 135.5 (-$\underline{C}_6H_4$-), 131.0 (-$\underline{C}_6H_4$-), 129.7 (-$\underline{C}_6H_4$-), 127.6 (-$\underline{C}_6H_4$-), 106.7 (C=$\underline{C}H_2$), 62.5 (COO-$\underline{C}H_2$-), 21.6 (-C_6H_4-CH_3), 14.0 (COO-CH_2-$\underline{C}H_3$);

2.2.2.2 Reactivity evaluation via photo-DSC

Photo-DSC measurements were performed at a Netzsch DSC 204 F1 with autosampler. Analyzed monomer formulations (10 ± 1 mg) were irradiated with filtered UV-light (400-500 nm) with an Exfo OmiCureTM series 2000 broadband Hg-lamp at 25 °C under constant N_2 flow (20 mL min^{-1}). The light intensity was set to 1 W cm^{-2} at the tip of the light guide corresponding ~20 mW cm^{-2} on the surface of sample and the heat flow of polymerization reaction was recorded as a function of time. The neat BenzMA monomer formulation and the monomer/ AFCT reagent formulation were measured three times each.

3 In depth kinetic and mechanistic studies of thiols, β-allyl sulfones, and vinyl sulfonate esters in acrylates

3.1 Free radical homopolymerization of acrylates

In order to gain more detailed information about the regulating abilities of thiols, β-allyl sulfones, and vinyl sulfonate esters in acrylates a comparative study with different CTA concentrations was performed. This time photoreactor, GPC, and Maldi-TOF-MS were used as analytical tools.

First of all, homopolymerization of the used monomer BenzAC with Ivocerin as PI was conducted (Figure 137). However, the photoreactor procedure including evaluation was carried out according to Experimental Part 2.1.

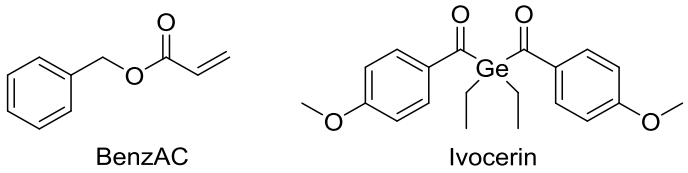

Figure 137: Structure of Benzyl acrylate (BenzAC) and PI Ivocerin

In Figure 138 the ^{1}H NMR spectrum for BenzAC is pictured. As can be seen, the DB signals H_b, H_c, and H_d can be used for evaluating the DBC, since no overlapping occurs. The reference signal H_a is shifted during polymerization and gives a broad signal H_e between 4.6 and 5.1 ppm. This shift can be attributed to the formation of the polymer backbone resulting in a different chemical environment. In order to include all signals arising from the methylene group of BenzAC, the integration area has to be adapted.

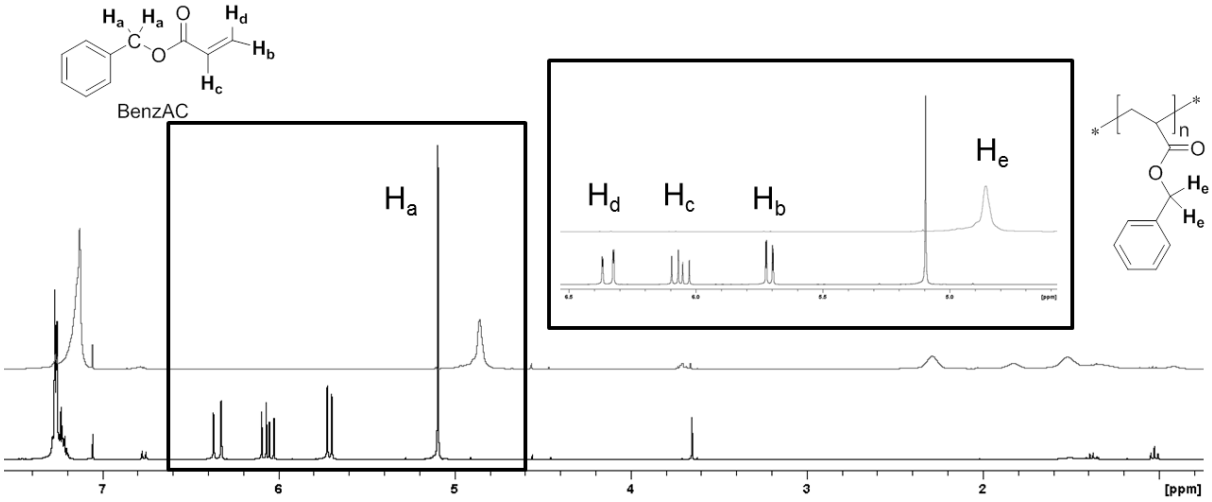

Figure 138: ^{1}H NMR spectrum of BenzAC after 0 and 500 s of irradiation highlighting the DBs of the BenzAC group and the reference peak occurring from the methylene group linking the acrylic moiety with the phenyl group

To provide equally distributed measuring points for the conversion-time plots, the irradiation times shown in Table 34 were chosen. Altogether, two photoreactor measurements were conducted.

Table 34: Different sampling times for BenzAC in photoreactor (total irradiation time in bold print)

measuring point	**sampling time [s]** BenzAC
1	0
2	5
3	10
4	20
5	30
6	50
7	75
8	100
9	150
10	200
11	300
12	**500**

After ^{1}H NMR spectroscopy, samples of one photoreactor measurement after 30, 75, and 500 s of irradiation were transferred to GPC vials and the deuterated chloroform residues were removed under vacuum at 30 mbar overnight at room temperature without removing the monomer. Then the remaining oligomers were dissolved in 0.5 mL of dry THF and transferred through a syringe filter in an amber glass GPC vial. The GPC device was a Waters GPC with 3 columns connected in series (Styragel HR 0.5, Styragel HR 3 and Styragel HR4) and a Waters 2410 RI detector was used for peak detection. The flow rate was set to be 1.0 mL min^{-1} and the column temperature was kept constant at 40 °C throughout the whole measuring period. For calibration, polystyrene standards (890-177,000 Da) in THF were used. The recorded data were analyzed with the software tool OmniSEC 4.5.

In case of homopolymerization no Maldi-TOF-MS experiments were performed, since Maldi-TOF-MS measurements require a narrow molecular weight distribution.

3.2 Regulating acrylates *via* thiols

For evaluating the regulating abilities of thiols in ACs, MT (phenylethyl mercaptane) was chosen as a model thiol for regulating BenzAC. In the photoreactor, four different MT concentrations (5 mol%, 10 mol%, 20 mol%, 35 mol%) were measured (two measurements per concentration). Basically, the photoreactor procedure was conducted according to Experimental Part 2.1.

As can be seen in Figure 139, the methylene group next to the sulfur of the thiol was used to determine the thiol conversion. The formation of thioether bridges shift the H_d signal to lower ppms leading to a decrease of the original signal. This decrease enables the calculation of the thiol conversion.

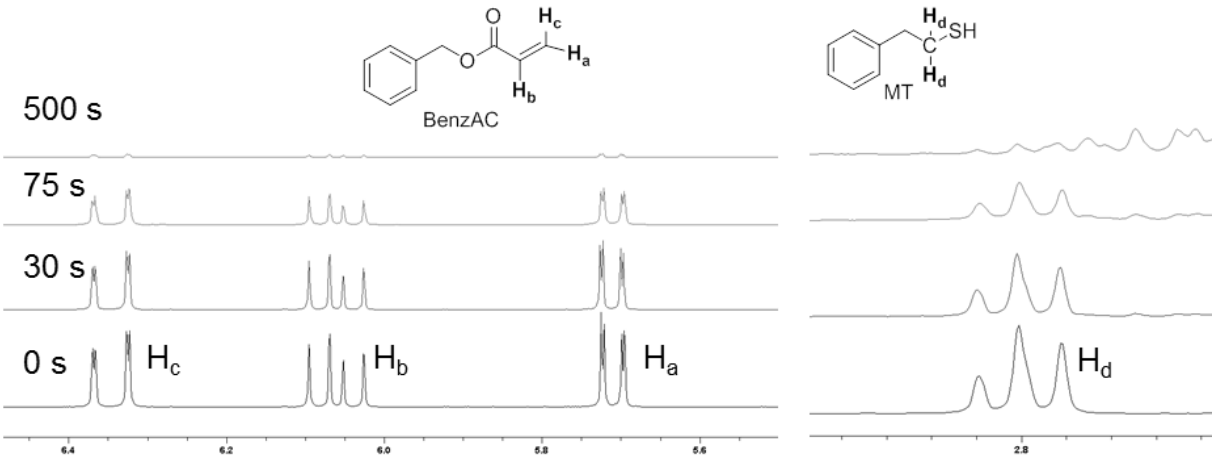

Figure 139: Representative ^{1}H NMR spectra of samples consisting of BenzAC 80 mol% and MT 20 mol% taken from photoreactor after 0, 30, 75, and 500 s of irradiation illustrating the regions with signals of analytical interest and their decrease over time

After the photoreactor analysis, the samples after 30, 75, 500 s of irradiation were analyzed by means of GPC according to Experimental Part 3.1.

Finally, Maldi-TOF-MS measurements of the sample containing 80 mol% BenzAC and 20 mol% MT were measured. Therefore, ^{1}H NMR samples after 30, 50, and 500 s of irradiation from photoreactor study were collected for Maldi-TOF measurements. The samples were transferred from the NMR tubes in small 2 mL glass vials and the deuterated chloroform and benzene residues were evaporated. Then the oligomeric samples were dissolved with an exact volume of a methanol-chloroform solution (1:1) to give a solution of defined concentration of 20 mg/mL. As matrix dithranol and as cationizer sodium trifluoroacetate (**Na TFA**) were used. Stock solutions of 10 mg/mL dithranol in methanol-chloroform (1:1) and 2 mg/mL Na TFA in methanol-chloroform (1:1) were prepared. Subsequently, 2 µL of oligomer solution, 15 µL of dithranol solution and 5 µL of cationizer solution were pipetted with an Eppendorf pipette in a 2 mL Eppendorf tube and thoroughly mixed. Finally 1 µL of the beforehand mixed analytic solution were pipetted on a waters

Maldi-TOF sample carrier and the solvent was evaporated. The whole procedure was performed in the orange light lab, where all wavelengths below 520 nm are filtered (adhesive foils of the company IFOHA).

Finally, Maldi-TOF measurements were carried out by means of a MALDI MS: Synapt G2 HDMS (Waters, UK) in positive ion and V mode. The laser firing rate was adjusted to 1 kHz with laser energy of 270 (parameter setting on the machine). Calibration of the device was performed with a peptide mix up to 3,500 Da. The mass region measured was set to be 430-4,000 Da to exclude the peaks originating from the monomer, CTA, and the PI Ivocerin, which would impair the sensitivity of the measurement in the higher molecular weight region.

3.3 Regulating acrylates *via* β-allyl sulfones

As a result of the photoreactor screening, the second best choice for regulating ACs was found to be β-allyl sulfone ASEE. Such as thiols, four different ASEE concentrations (5 mol%, 10 mol%, 20 mol%, 35 mol%) were measured in the photoreactor (two measurements per concentration). The photoreactor procedure was performed according to Experimental Part 2.1. Regarding the ^{1}H NMR spectrum of ASEE in BenzAC in Figure 140, there is a slight overlapping of the signals H_b from BenzAC and H_e from ASEE. Hence, signals H_a for BenzAC and H_d for ASEE were used to monitor the DBC.

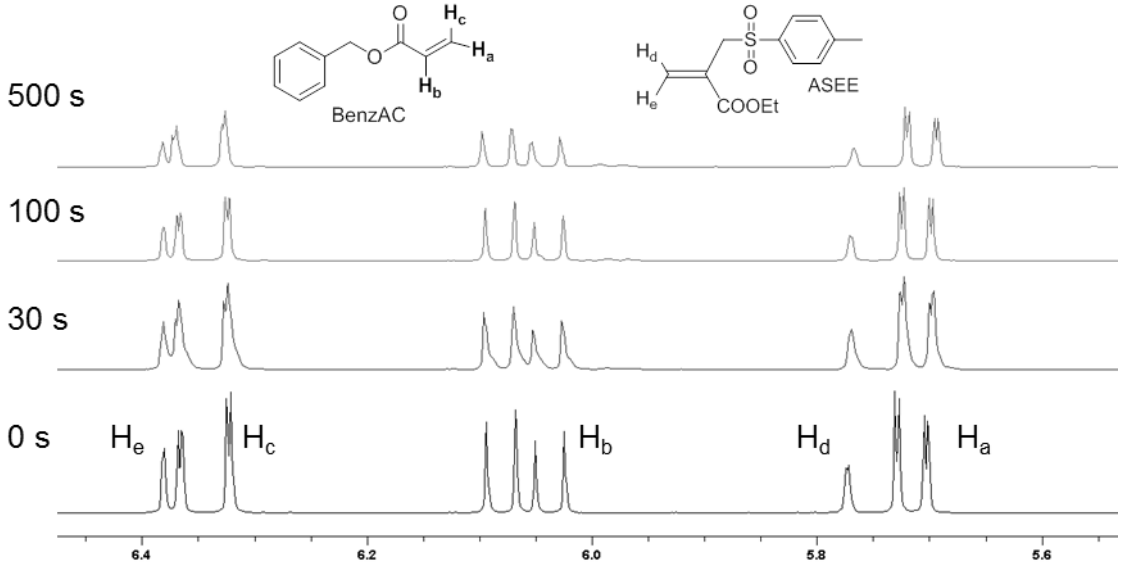

Figure 140: Representative ^{1}H NMR spectra of samples consisting of BenzAC 80 mol% and ASEE 20 mol% taken from photoreactor after 0, 30, 100, and 500 s of irradiation illustrating the regions with signals of analytical interest and their decrease over time

The collected photoreactor samples after 30, 100, and 500 s were used to perform GPC measurements according to Experimental Part 3.1. Moreover, the same samples were used for Maldi-TOF-MS analysis, which was conducted according to Experimental Part 3.2.

3.4 Regulating acrylates *via* vinyl sulfonate ester

Finally, the most promising AFCT reagent from the photoreactor screening (vinyl sulfonate ester VE4) was measured together with BenzAC in the photoreactor. Again, four different VE4 concentrations (5 mol%, 10 mol%, 20 mol%, 35 mol%) were measured in the photoreactor. The photoreactor procedure was performed according to Experimental Part 2.1. All photoreactor measurements were conducted twice to ensure the accuracy of the measurement.

As can be seen in Figure 141, there is a slight overlapping of the signals H_b from BenzAC and H_e from VE4. Hence, signals H_a for BenzAC and H_d for VE4 were used to monitor the DBC.

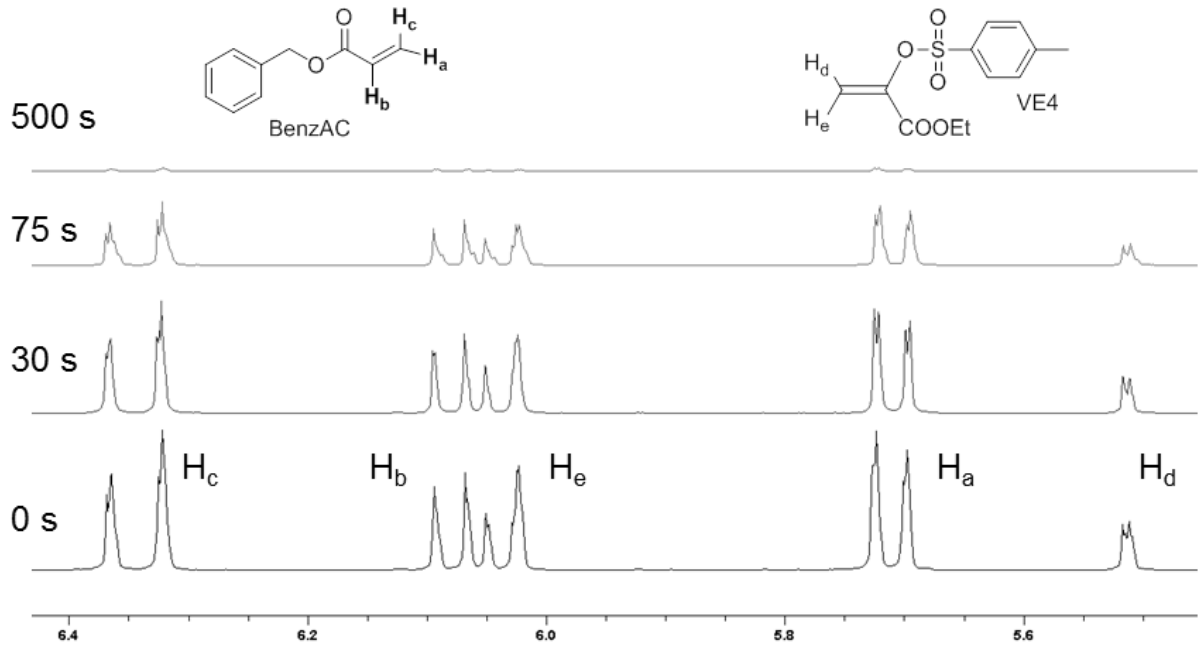

Figure 141: Representative ^{1}H NMR spectra of samples consisting of BenzAC 80 mol% and VE4 20 mol% taken from photoreactor after 0, 30, 75, and 500 s of irradiation illustrating the regions with signals of analytical interest and their decrease over time

GPC procedures for the photoreactor samples after 30, 75, and 500 s of irradiation were carried out according to Experimental Part 3.1. Maldi-TOF-MS procedure was conducted according to Experimental Part 3.2.

4 Comparison of vinyl sulfonate esters as addition-fragmentation chain transfer reagents with dithiols for modifying diacrylate networks

4.1 Formulations and test specimens

HDDA was chosen to be the matrix for the mechanical study. As PI Ivocerin® was used. For guaranteeing network regulation, DVS was applied as AFCT network modifier and the dithiol DT was used as thiol-ene regulator.

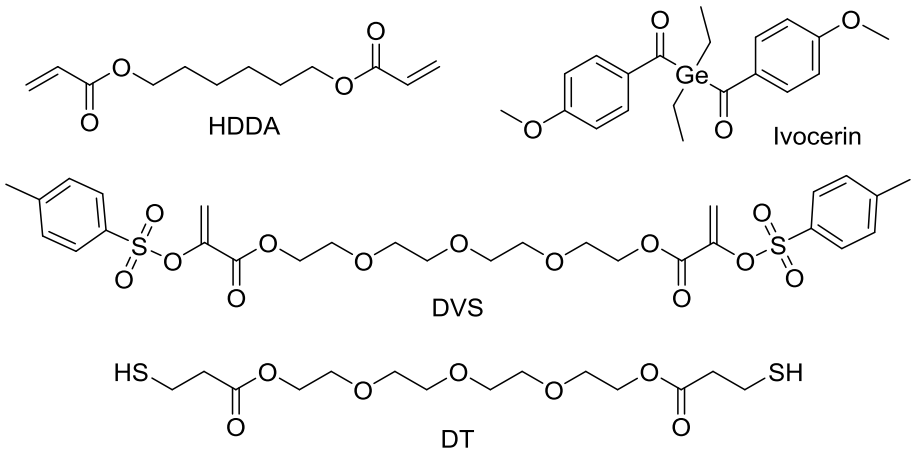

Figure 142: Used substances for AC study: 1,6 hexanediol diacrylate as monomer matrix, Ivocerin® as PI, DVS as AFCT reagent, and DT as dithiol

In order to compare the influence of AFCT- and thiol- CTAs on network regulation, formulations with different CTA DB ratios were mixed (Table 35). All substances were weighted in a 20 mL brown glass flask and 0.3 w% of PI were added. Then the substances were vortexed and homogenized in the ultrasonic bath for at least 30 min at 40 °C before being measured or cured.

Table 35: Overview of all tested formulation and their composition

formulation	HDDA [mol%]	DT [mol%]	DVS [mol%]
M	100	-	-
DT5	95	5	-
DT10	90	10	-
DT20	80	20	-
DT35	65	35	-
DVS5	95	-	5
DVS10	90	-	10
DVS20	80	-	20
DVS35	65	-	35

Parts of the formulations were directly used for RT-NIR photorheology and storage stability measurements. For mechanical tests, test specimens were cured in silicon molds by filling the molds with formulation and curing them in a Lumamat 100 light oven provided by Ivoclar Vivadent AG. The light oven was equipped with 6 Osram Dulux L Blue lamps (18 W, 400-580 nm). The light intensity of ~20 mW cm^{-2} was determined with an Ocean Optics USB 2000+ spectrometer at the position of the silicone molds. The total curing time was 600 s, whereby the specimens were turned after 300s and the backside was irradiated for another 300 s. Finally, the cured specimens were sanded and polished to comply with the required specification.

4.2 Real time-near infrared photorheology

The real time-near infrared-photorheometer consisted of an Anton Paar MCR 302 WESP with a P-PTD 200/GL Peltier glass plate and a disposable PP25 measuring system coupled with a Bruker Vertex 80 FTIR spectrometer. For measuring IR spectra, external mirrors guided the IR beam from the spectrometer through the flat glass plate and the sample to the flat rheology plate, where the beam was reflected. Then the reflected IR beam was led to an external MCT detector (Figure 143).

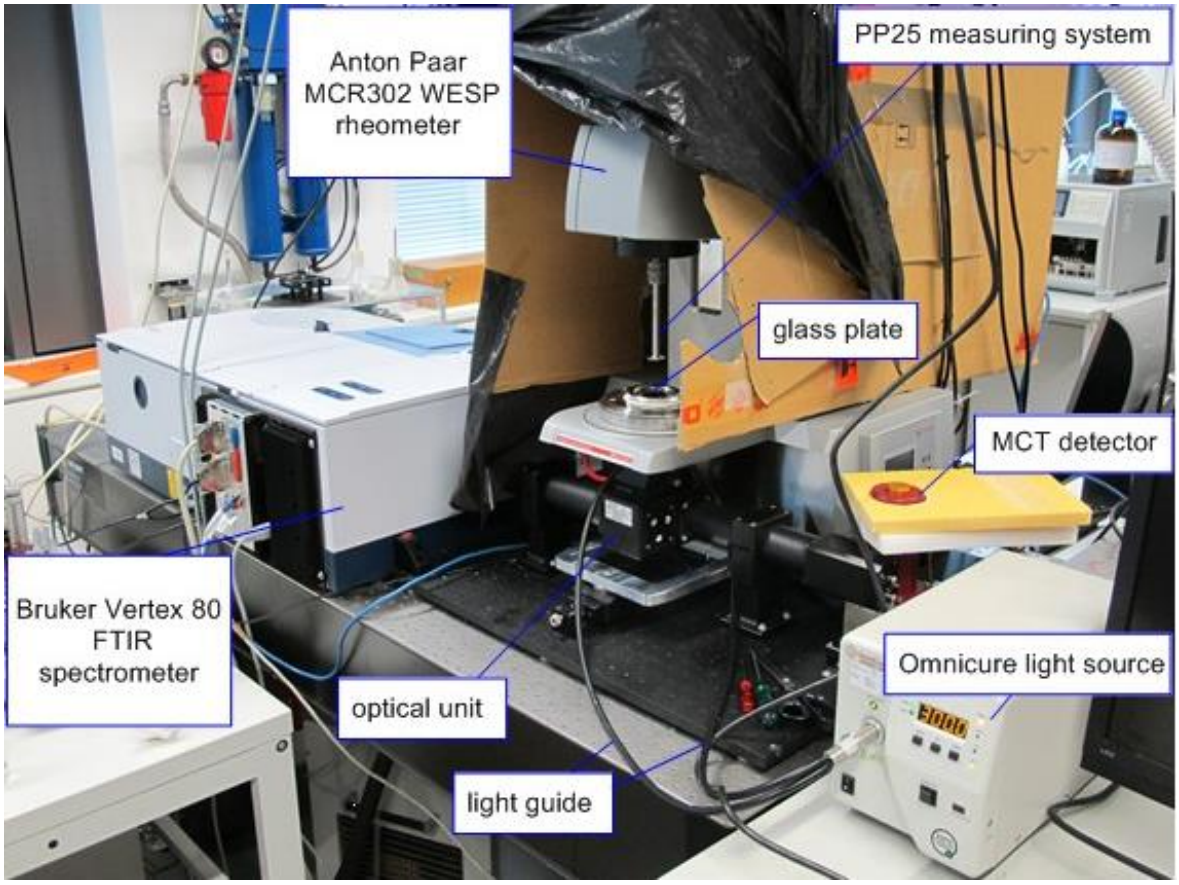

Figure 143: Setup of RT-NIR photorheometer

For every monomer formulation, 130 µL were placed on the glass plate. The measuring temperature was 20 °C and the gap between glass plate and a stainless steel PP25 plate was 200 µm. The measurements were conducted in oscillation mode with a strain of 1 % and a frequency of 1 Hz. For irradiating the samples, an Exfo OmniCure TM 2000 with a broad band Hg-lamp was used. The light with a wavelength between 400-500 nm was led through a dual leg light guide, whose tips were located directly under the glass plate. The irradiation intensity was 10 mW cm^{-2} at the surface of the sample. Every formulation was measured at least three times.

During the measurement the storage modulus (**G'**), the loss modulus (**G''**) and normal force ($\mathbf{F_N}$) were recorded. At the beginning of the measurement a period of 60 s with 1 measurement point per second without irradiation was measured. Then the sample was irradiated for altogether 5 min. The first 60 s of irradiation 0.2 measurement points per s were recorded. The last 4 min 1 measurement point per s was determined. In order to monitor the double bond conversion (**DBC**) RT-NIR analysis was applied. Therefore, every ~0.2 s a single spectrum was recorded. An OPUS 7.0 software tool was used to process the spectra and to integrate the relevant DB bands at ~6160 cm^{-1}.

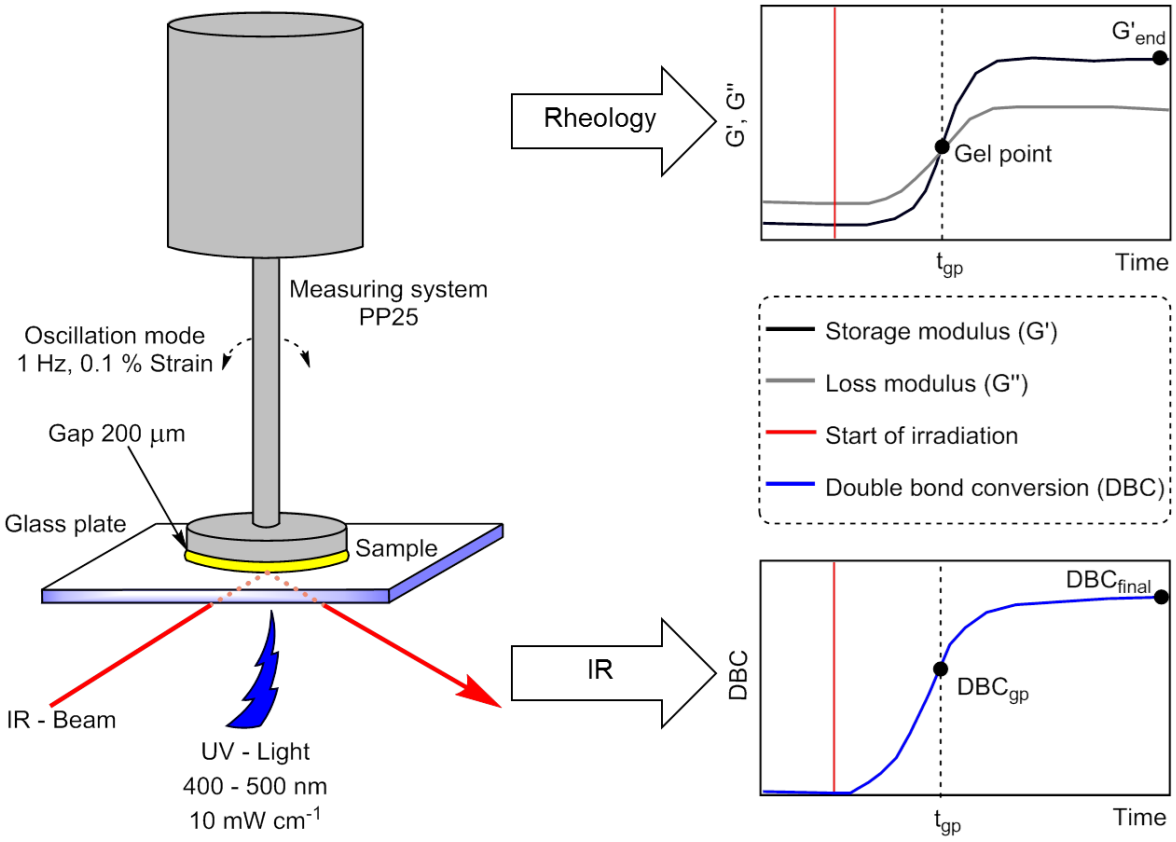

Figure 144: Schematic setup of RT-NIR photorheology and evaluated data

As depicted in Figure 144, the gel point can be extracted from the recorded rheology data. The definition of the gel point is the intersection of G' and G'', while a G'/G''< 1 exhibits liquid

and a G'/G''> 1 exhibits solid (gel) behavior of the cured material. Hence, the time until gelation ($\mathbf{t_g}$) can be determined. In parallel, IR spectra are recorded. Combining rheology and IR data enables to determine the DBC at the gel point ($\mathbf{DBC_g}$). Moreover, values for the final storage modulus ($\mathbf{G'_{end}}$), and the final DBC ($\mathbf{DBC_{final}}$) can be extracted. Another parameter of interest, which was gained from the rheology data, was the development of F_N as a measure for shrinkage stress during photopolymerization. Therefore, the rheometer recorded the force that is necessary to maintain the gap of 200 µm between glass and steel plate.

4.3 Dynamic mechanical thermal analysis

For DMTA tests rectangular samples (~ 5 x 2 x 40 mm^3) were cured according to Experimental Part 4.1. Every sample was polished and the exact geometries were determined before measurement. After sample preparation, DMTA measurements were performed by means of an Anton Paar MCR 301 with a CTD 450 oven and a SRF 12 measuring system. The measured temperature range reached from -100 to 200 °C with a heating rate of 2 °C min^{-1}. The prepared polymer specimens (~ 5 x 2 x 40 mm^3) were tested in torsion mode with a frequency of 1 Hz and 0.1% strain. Rheoplus/32 V3.40 from Anton Paar was used as software tool to evaluate and process the recorded data (G', G'', tanδ). In order to provide reliable results, two DMTA specimens were measured for each network.

4.4 Tensile test

Tensile test specimens were casted according to Experimental Part 4.1. The dog chew bone-shaped samples (~ x x y x z mm^3) met the requirements for ISO 527 test specimen 5b.

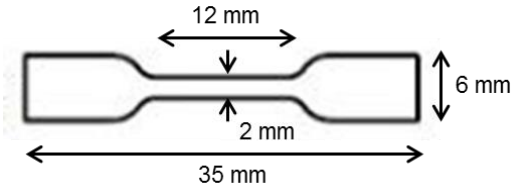

Figure 145: Dimensions of tensile test samples (thickness: 2 mm)

The tests themselves were performed on a Zwick Z050 with a maximum test force of 50 kN. The specimens were fixed between two clamps and strained with a traverse speed of 5 mm min^{-1}. At the same time a stress-strain plot is recorded. This quasi-static test was carried out to make a statement about the strength and the plasticity of material resulting in a stress-strain curve. Tensile stress (σ) and tensile strain (ε) can be calculated with following equations:

$$tensile\ stress: \sigma = \frac{F}{A_0}$$

$$tensile\ strain: \varepsilon = \frac{\Delta L}{L_0} \times 100\%$$

$$F \ldots force\ [N], A_0 \ldots initial\ cross\ section\ [mm^2], \Delta L \ldots elongation\ [m], L_0 \ldots initial\ lenght\ [m]$$

Altogether five specimens were measured for each network.

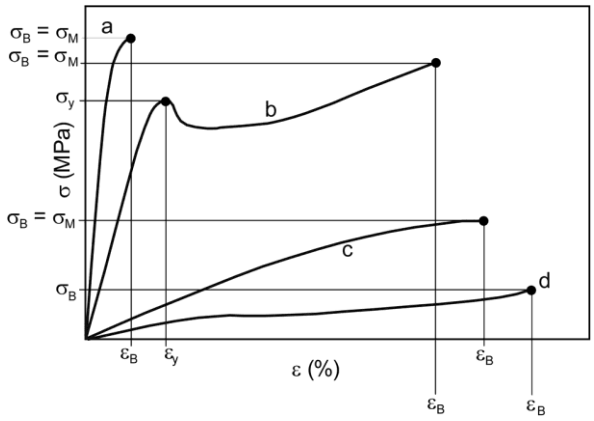

Figure 146: Examples for stress-strain curves for (a) brittle polymers, (b) tough material with yield point, (c) tough material without yield point, and (d) elastomeric material

Figure 146 gives several examples of how a stress-strain curve for a polymer could look like. In case of photopolymers mostly brittle polymers (a) are expected.

4.5 Dynstat impact resistance

For Dynstat impact resistance tests rectangular samples (~ 10 x 2 x 15 mm³) were cured and prepared according to the procedure in Experimental Part 4.1. The Dynstat tests were carried out with a 10 kpcm hammer. Sample DVS35 (HDDA 65 mol% DVS 35 mol%) was measured with a 20 kpcm hammer, because of the significantly higher impact resistance of the material. Finally the results were converted from kpcm to kJ and divided by the area of fracture in m². A schematic setup of a Dynstat impact resistance test is depicted in Figure 147. The hammer breaks the test specimen and the absorbed energy is recorded.

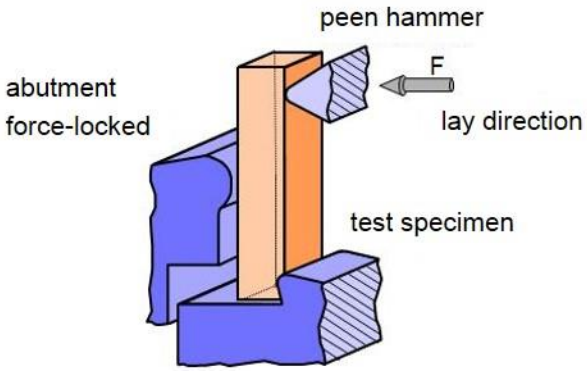

Figure 147: Schematic setup of a Dynstat impact resistance test

For every sample four different specimens were measured. The sample DVS35 was so tough that only two of four specimens were destroyed. Therefore, only two values for impact resistance were recorded. Besides that, it was not possible to receive results for the DT20 and DT35 sample, because the hammer was not able to break the too soft specimens at all.

For calculating the impact resistance (a_n), the following equation was used:

$$a_n = \frac{w_n}{h \times b}$$

$$w_n \dots impact\ energy\ absorbed\ by\ specimen\ [kJ], h \dots height\ of\ specimen\ [m],$$

$$b \dots width\ of\ specimen\ [m]$$

4.6 Nanoindentation

Nanoindentation experiments were carried out by means of a Hysitron TI 750L. The polymer specimens were indented with a loading rate of 0.1 mN s^{-1} and then held for 30 s at the maximum load of 1 mN. Finally, the load was released with an unloading rate of 0.2 mN s^{-1}. Altogether, five measurements per network were performed.

4.7 Swellability

For swelling tests, polymer pellets (3 pellets per polymer network) with a diameter of 2 mm and a height of 1 mm were cured according to Experimental Part 4.1. These pellets were weighted (m_{start}) and subsequently submerged in ethanol with 200 ppm hydroquinone monomethyl ether for 14 day at 25 °C. The ethanol was changed after 1, 5, 8 and 11 days. Afterwards, the polymer disks' surfaces were dried with a paper towel to remove excessive ethanol and were then weighed ($m_{swollen}$). Finally, the polymer pellets were dried in a 60 °C

vacuum drying oven until constant weight was reached (m_{dry}). From that data, the swellability (S) and gel fraction (G) can be calculated by means of the following equations:

$$S = \frac{m_{swollen}}{m_{dry}}$$

$$G = \frac{m_{dry}}{m_{start}}$$

$m_{start} \ldots mass\ of\ pellets\ after\ curing, m_{swollen} \ldots mass\ of\ swollen\ pellets, m_{dry} \ldots mass\ of\ dried\ pellets$

4.8 Storage stability

For comparing storage stability, the prepared monomer formulations were analyzed on a modular compact rheometer MCR 300 Physica Anton Paar. The viscosity measurements were carried out at 20 °C with a CP-25 measuring system (diameter 25 mm). The distance from the tip to peltier plate was set to 48 µm and a shear rate was specified to be 100 s^{-1}. The overall measuring time was set to be 100 s and every 5 s a measuring point was recorded (20 measuring points per formulation). The collected data was analyzed by means of a Rheoplus/32 V3.40 software tool from Anton Paar. Subsequently, the formulations were stored in an amber 20 mL vial at 37 °C in the dark for 120 days. After storage, viscosity was measured once again the same way as described above and compared with the initial results. Samples DT10, DT20, and DT35 were already gelled after 120 days of storage and so no rheology measurements were possible.

Summary

Nowadays, photopolymers based on (meth)acrylates find broad use in industry. Typical applications are coatings, inks, adhesives, photoresists, medical applications (e.g. biomaterials, dental fillings), and stereolithography. The advantages of radical cured (meth)acrylate photopolymers are their fast curing, solvent-free curing conditions, the possibility of 3D structuring, and their mechanical properties such as high hardness, rigidity, and heat deflection temperature. Nevertheless, the uncontrolled free radical curing mechanism comes along with drawbacks like the formation of inhomogeneous networks leading to shrinkage stress in the material and yielding materials of low toughness.

These disadvantages generate a demand for regulation techniques of free radical photopolymerization. The state-of-the-art method is represented by thiol-ene chemistry, which enables the regulation of radical photopolymerization leading to more homogeneous networks and materials of improved toughness. However, thiol-ene chemistry also has some drawbacks like strong odor of the thiol compounds, low storage stability of the formulations, and the formation of flexible thio-ether bridges softening the material.

Recently, addition-fragmentation chain transfer (AFCT) reagents (β-allyl sulfones and vinyl sulfonate esters) have been reported to represent a new technique to regulate dimethacryle networks in photopolymerization.

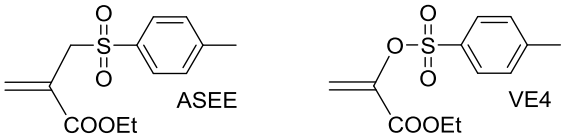

β-allyl sulfone vinyl sulfonate ester

The scope of this diploma thesis was to find new AFCT reagents, which are able to regulate methacrylates, vinyl esters, or acrylates. In order to find new AFCT reagents, a photoreactor study was carried out to investigate the co-reactivity of monofunctional monomers with monofunctional AFCT reagents, which were characterized by a double bond conversion (DBC)-time curve measured in a photoreactor. To guarantee regulation during the whole photopolymerization process, an equal and steady consumption of the monomer and the AFCT reagent is necessary. In the first section, a broad screening of different β-allyl sulfones, allyl sulfides, and α-vinyl sulfonates in model methacrylate, vinyl ester, and acrylate resins was carried out.

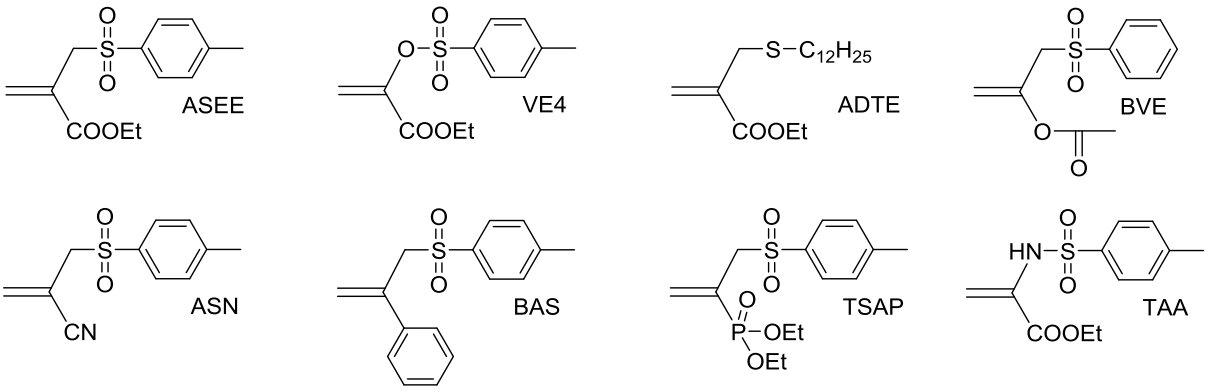

Besides the already published excellent regulating abilities of ASEE and VE4 towards methacrylates, the vinyl sulfonate ester VE4 was discovered to show promising co-reactivity with acrylates without delaying the photopolymerization.

Therefore, an extensive photoreactor study covering different vinyl sulfonate ester concentration and including the comparison with a thiol was conducted. Moreover, the photoreactor samples at different conversions were analyzed by means of GPC and Maldi-TOF-MS for providing in depth information about AFCT regulation and mechanism.

The study revealed that the vinyl sulfonate ester VE4 shows equal and steady consumption in acrylic resins without delaying photopolymerization. This equal consumption leads to constant molecular weight distributions during the whole photopolymerization process.

Moreover, Maldi-TOF-MS measurements certified the presence of the main oligomeric species arising from AFCT mechanism of vinyl sulfonate ester VE4. Additionally, M_n from GPC measurements corresponds with the highest peak in the mass spectrum.

The good co-reactivity of thiols in acrylates leads to a very equal and steady consumption of the CTA and the monomer at low concentrations (f_{co} (co-reactivity factor) ~ 1) and significantly drops with increasing thiol concentration in the formulation ($f_{co} < 1$). On the other hand, vinyl sulfonate ester VE4 in acrylates is slightly preferred consumed ($f_{co} > 1$) at low concentrations and more equally consumed at concentrations ~ 20 mol% ($f_{co} \sim 1$). However, the molecular weight distribution is for all tested concentrations narrower for AFCT regulation than for thiol regulation, which indicates better regulation abilities of vinyl sulfonate ester VE4.

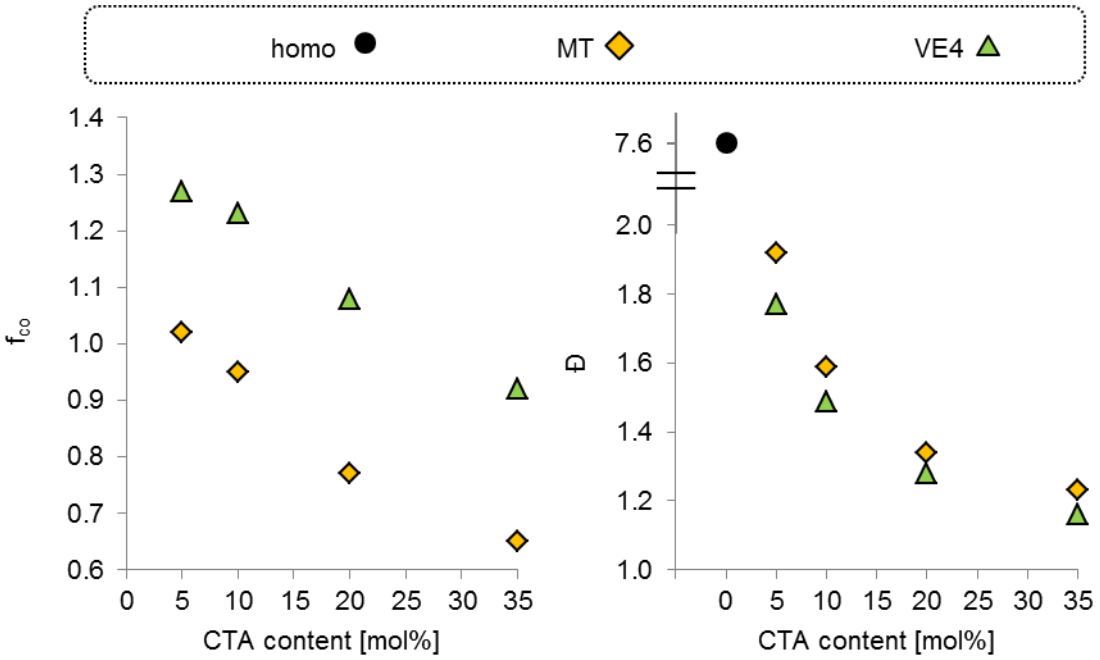

These promising findings tipped the scale in favor of network study exploring the regulating ability of divinyl sulfonate ester (DVS) in a diacrylate matrix using different analytical methods (e.g. RT-NIR photorheology, DMTA, tensile test, Dynstat impact resistance, nanoindentation, and storage stability). Moreover, a dithiol (DT) was used in order to compare AFCT with state-of-the-art thiol-ene regulation.

RT-NIR photorheology exhibited that the regulation of acrylate formulations with DVS and DT leads to a shift of gel point to higher DBC (**DBC_{gp}**) delaying gelation (time until gel point is reached (**t_{gp}**)). In comparison with thiols, DVS can move the gel point to even higher DBCs. This results in a greater reduction of shrinkage stress in the AFCT-regulated acrylate matrix compared with the thiol-regulated.

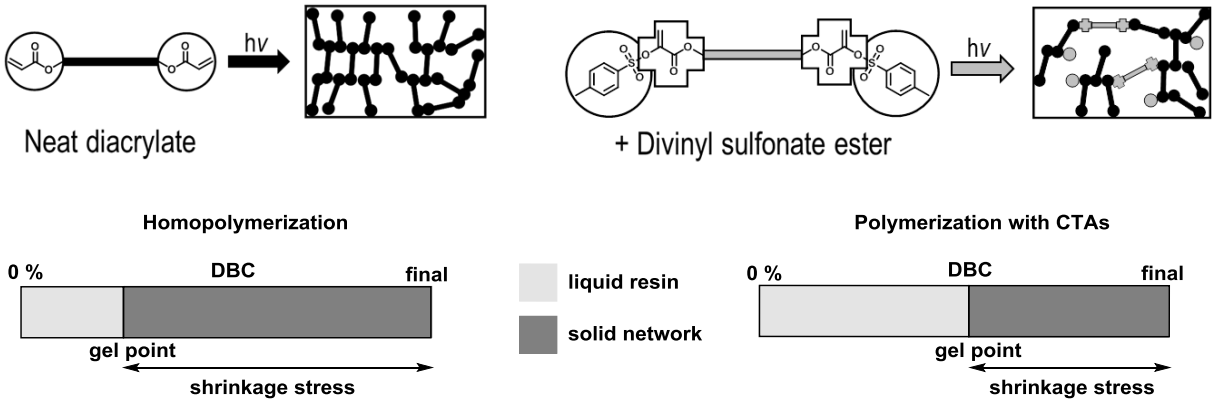

DMTA measurements showed a sharpening in glass transition with increasing DVS content in the acrylic resin. Moreover, the glass transition temperature (T_g) was significantly shifted to lower temperatures. Compared to thiols, the storage modulus at room temperature G'_{20} for

AFCT-regulated networks remained in the range of the homopolymer, while the presence of thiols as CTAs in an acrylic network led to a drop in G'_{20} due to the formation of flexible thio-ether bridges. Tensile test confirmed these results.

At the same time, Dynstat impact resistance test exhibited that DVS-regulated acrylate networks show a significant increase in toughness in the range of thiol-regulated acrylate networks. Even tough toughness increases, G'_{20} determined by DMTA remains in the range of the homopolymer, while for the increase in toughness of thiol-regulated samples modulus has to be sacrificed. The loss in modulus also leads to a loss in hardness, while AFCT-regulated networks even show a slight increase at low DVS concentrations.

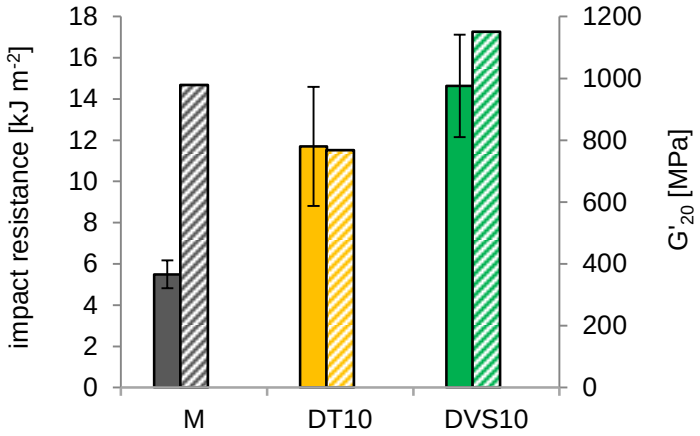

Finally, storage stability experiments clearly highlighted the superior storage properties of acrylate formulation with AFCT reagent additives compared with acrylate/ thiol formulations. While acrylate/ thiol formulations are prone to gelation after rather short storage periods, acrylate/ DVS formulations did not show an increase in viscosity after 120 days storage at 37 °C.

Summarizing, the collected results indicate the great potential of vinyl sulfonate esters as AFCT reagents to regulate the curing of acrylate-based photoresins. Compared to the state-of-the-art thiol-ene chemistry, AFCT regulation in acrylates leads to equally well regulated networks exhibiting an increase in toughness in the same range. The great benefits of AFCT-regulated networks are the higher modulus at room temperature, the higher hardness, and the better storage stability of the formulations.

Materials, Devices, and Analyses

Table 36: Reagents and substances used with corresponding distributer

Reagents	Distributer
1,6-Hexanediol diacrylate (HDDA)	Alfa Aesar
Benzyl acrylate (BenzAC)	ABCR
Benzyl methacrylate (BenzMA)	Aldrich
Deuterated benzene (C_6D_6)	Eurisotop
Deuterated chloroform ($CDCl_3$)	Eurisotop
Dimethyl terephthalate	Aldrich
Ethyl pyruvate	TCI
Ivocerin	Ivoclar Vivadent
Lauryl acrylate (LAC)	CONDEA
Lauryl methacrylate (LMA)	Aldrich
Oxone	ABCR
Phenylethyl mercaptane (MT)	Aldrich
Phosphorus oxychloride	Fluka
Propargyl bromide (80% in toluene)	ABCR
p-Toluenesulfonamide	Fluka
Sodium acetate	Aldrich
Sodium bicarbonate ($NaHCO_3$)	Merck
Sodium sulfate (Na_2SO_4)	Donau Chemie
Tetraethylene glycol bis(3-mercaptopropionate) (DT)	Wako
Thiophenol	Merck
Triethyl amine (Et_3N)	ACROS Organics
Vinyl laurate (LVE)	Aldrich

^{1}H-NMR and **^{13}C-NMR** spectra were measured with a BRUKER Avance DRX-400 FT-NMR spectrometer. The chemical shift was reported in ppm (s = singlet, d = doublet, t = triplet, q = quartet, m = multiplet, dd = doublet on doublet, bs = broad singlet). The solvents used were deuterated chloroform ($CDCl_3$, 99.5 % deuteration).

For **thin layer chromatograms** (TLC) TL–aluminum foils coated with silica gel 60 F245 from Merck were used.

Column chromatography was conducted on Merck silica gel 60 (0.040–0.063 mm). The silica gel chromatography was performed with a Büchi MPLC-system equipped with the control unit C-620, fraction collector C-660, and UV-photometer C-635.

Polymer specimens for DMTA, swellability, nanoindentation, Dynstat impact resistance, and tensile test measurements were photocured in a Lumamat 100 light oven (provided by VIAG) (400-500 nm) with 6 Osram Dulux L Blue 18 W lamps.

Photo-DSC polymerizations were conducted on a DSC 204 F1 device from Netzsch.

GPC measurements were performed with a Waters GPC using three columns connected in series (Styragel HR 0.5, Styragel HR 3 and a Styragel HR 4) and a Waters 2410 RI detector.

The coupled **RT-NIR photorheology** experiments were performed on an Anton Paar MCR 302 WESP with a P-PTD 200/GL Peltier glass plate and a disposable PP25 measuring system. The rheometer was additionally coupled with a Bruker Vertex 80 FTIR spectrometer.

DMTA measurements were performed with an Anton Paar MCR 301 with a CTD 450 oven and a SRF 12 measuring system.

A modular compact rheometer MCR 300 by Physica, Anton Parr (disc-plate rheometer) was used for **storage stability** tests.

For **nanoindentation** experiments a Hysitron TI 750L was used.

Dynstat impact tests were performed on a Karl Frank GmbH Dynstat device, Type 573 using a 0.5 J hammer (and a 2 J hammer for the DVS35 specimens).

The preparation of photoreactive formulations and substances was carried out in a **yellow light laboratory**. The laboratory had adhesive foils of the company IFOHA attached to all windows and the fluorescent lamps were type Osram lumilux with chip control light colour 62 (wavelengths below 480 nm are filtered).

Tensile tests were performed by means of a Zwick Z050 with Zwick Z050 with a maximum test force of 50 kN. TestXpert II software was used to process and evaluate the recorded data.

Abbreviations

ΔH	Enthalpy
2M	2 mix consisting of UDMA and D3MA (molar ratio 1:1)
3D	Three-dimensional
AC	Acrylate, acrylic
ADTE	Ethyl 2-((dodecylthio)methyl)acrylate
AFCT	Addition-fragmentation chain transfer
ASA	N-Methyl-N-propyl-2-(tosylmethyl)acrylamide
ASEE	2-Ethyl-2-(tosylmethyl)acrylate
ASN	2-(Tosylmeth)acrylonitrile
ATRP	Atom transfer radical polymerization
BAPO	Benzoyl phosphine oxide
BAS	2-(Tosylmethyl)styrene
BenzAC	Benzyl acrylate
BenzMA	Benzyl methacrylate
BVE	3-(Phenylsulfonyl)prop-1-en-2-yl acetate
CQ	Campherquinone
CTA	Chain transfer reagent
C_{tr}	Chain transfer constant
D3MA	1,10-Decane dimethacrylate
DA	Diacrylate
DAS	((Oxybis(ethane-2,1-diyl))bis(oxy)bis(ethane-2,1-diyl)bis(2-(tosylmethyl)acrylate)
DB	Double bond
DBC	Double bond conversion
DBC_{AFCT}	Final DBC of AFCT curve (photoreactor)
DBC_{final}	Final double bond conversion (at the end of experiment)
DBC_{gp}	Double bond conversion at gel point
DBC_{homo}	Final DBC of homopolymerization (photoreactor)
$DBC_{monomer}$	Final DBC of monomer curve (photoreactor)
DBC_{reg}	Final DBC of AFCT-regulated reaction (photoreactor)
DMA	Dimethacrylate
DMA	Dynamic mechanical analysis
DMAB	Dimethylaminobenzoic acid ethyl ether
DMTA	Dynamic mechanical thermal analysis
DSC	Differential scanning calorimetry
DT	Dithiol
DTT	Dithiothreitol
DVS	Divinyl sulfonate ester
e.g.	For example
EBPADMA	Ethoxylated bisphenol-A dimethacrylate
EDT	Tetra(ethylene glycol) dithiol
E_r	Rubber elasticity modulus
f_{co}	Co-reactivity factor (photoreactor)
f_{DBC}	Double bond conversion factor (photoreactor)
FWHM	Full wide at half maximum
G’	Storage modulus
G’’	Loss modulus
G'_{20}	Storage modulus at 20 °C (room temperature)
GPC	Gel permeation chromatography
HDDA	1,6-hexanediol diacrylate
k_{add}	Rate constant of addition reaction
k_{CT}	Rate constant of chain transfer

k_{frag}	Rate constant of fragmentation reaction
k_p	Rate constant of propagation
k_{tr}	Rate constant of transfer reaction
LFP	Laser flash photolysis
M	HDDA (1,6-hexanediol diacrylate)
MA	Methacrylate, methacrylic
MAC	Methylacrylate
Maldi	Matrix-assisted laser desorption/ionization
MAS	2-(2-Ethoxyethoxy)ethyl 2-(toylmethyl)acrylate
MDTVE	
MMA	Methyl methacrylate
MS	Mass spectrum
MT	Model thiol (phenylethyl mercaptane)
NMR	Nuclear magnetic resonance
PEGDA	Polyethylene glycol diacrylate
PETMP	Pentaerythritol tetrakis(3-mercapto-propionate)
PI	Photoinitiator
r_{AFCT}	Conversion rate of AFCT curve (photoreactor)
RAFT	Reversible addition fragmentation chain transfer
r_{DBC}	Relative double bond conversion (photoreactor)
R_{homo}	Conversion rate of homopolymerization (photoreactor)
$r_{monomer}$	Conversion rate of monomer curve (photoreactor)
r_R	Relative reactivity of photopolymerization (photoreactor)
R_{req}	Conversion rate of AFCT-regulated polymerization (photoreactor)
RT-NIR	Real time near infrared
TAA	Ethyl 2-((4-methylphenyl)sulfonamido)acrylate
tanδ	Loss factor
$t_{DBC95\%}$	Time until 95% of the final double bond conversion is reached
T_g	Glass transition temperature
$t_{G'end95\%}$	Time until 95% of the final storage modulus is reached
t_{gp}	Time until gel point
TMPMP	Trimethylolpropane tris(3-mercaptopropionate)
TOF	Time of flight
Ts	Tosyl group
TSAP	
UDMA	Urethane dimethacrylate
UV	Ultraviolett light
VE	Vinyl ester
VE4	Ethyl 2-(tosyloxy)acrylate
Vis	Visible light
z.B.	zum Beispiel

References

1. Studer, K., UV-curing: worth investing in a prosperous green technology. *Coating* **2007,** *40 (9)*, 33-37.
2. Jacobs, P. F., A brief history of rapid prototyping & manufacturing: The growth years. *P/M Sci. Technol. Briefs* **2001,** *3* (5), 13-16.
3. Abe, Y., Current status and updates on the radiation curing technology for polymers for coatings. *DIC Tech. Rev.* **2005,** *11*, 1-20.
4. Fouassier, J. P.; Allonas, X.; Burget, D., Photopolymerization reactions under visible lights: principle, mechanisms and examples of applications. *Prog. Org. Coat.* **2003,** *47* (1), 16-36.
5. Zheng, X., The composition and application of UV-curable adhesive. *Adv. Mater. Res. (Durnten-Zurich, Switz.)* **2014,** *955-959* (Advances in Environmental Technologies III), 70-73, 5 pp.
6. Roßhaupter, E.; Hundt, D., Photolacke. *Chemie in unserer Zeit* **1971,** *5* (5), 147-153.
7. Dworak, C.; Koch, T.; Varga, F.; Liska, R., Photopolymerization of biocompatible phosphorus-containing vinyl esters and vinyl carbamates. *J. Polym. Sci. Part A: Polym. Chem.* **2010,** *48* (13), 2916-2924.
8. Mautner, A.; Qin, X.; Wutzel, H.; Ligon, S. C.; Kapeller, B.; Moser, D.; Russmueller, G.; Stampfl, J.; Liska, R., Thiol-ene photopolymerization for efficient curing of vinyl esters. *J. Polym. Sci., Part A: Polym. Chem.* **2013,** *51* (1), 203-212.
9. Husar, B.; Heller, C.; Schwentenwein, M.; Mautner, A.; Varga, F.; Koch, T.; Stampfl, J.; Liska, R., Biomaterials based on low cytotoxic vinyl esters for bone replacement application. *J. Polym. Sci., Part A: Polym. Chem.* **2011,** *49* (23), 4927-4934.
10. Cushing, M. C.; Anseth, K. S., Hydrogel Cell Cultures. *Science* **2007,** *316* (5828), 1133-1134.
11. Moszner, N.; Salz, U., New developments of polymeric dental composites. *Prog. Polym. Sci.* **2001,** *26* (4), 535-576.
12. Moszner, N.; Hirt, T., New polymer-chemical developments in clinical dental polymer materials: Enamel-dentin adhesives and restorative composites. *J. Polym. Sci., Part A: Polym. Chem.* **2012,** *50* (21), 4369-4402.
13. Fedorovich, N. E.; Swennen, I.; Girones, J.; Moroni, L.; van Blitterswijk, C. A.; Schacht, E.; Alblas, J.; Dhert, W. J. A., Evaluation of Photocrosslinked Lutrol Hydrogel for Tissue Printing Applications. *Biomacromolecules* **2009,** *10* (7), 1689-1696.
14. Zhang, A. P.; Qu, X.; Soman, P.; Hribar, K. C.; Lee, J. W.; Chen, S.; He, S., Rapid Fabrication of Complex 3D Extracellular Microenvironments by Dynamic Optical Projection Stereolithography. *Adv. Mater.* **2012,** *24* (31), 4266-4270.
15. Wood coating: http://6iee.com/data/uploads/50/753317.jpg. (accessed 07/06/16).
16. Glass fiber: http://www.wiretechworld.com/good-forecasts-for-global-fiber-optic-connectors-market/. (accessed 07/07/16).
17. 3D structure: https://www.vismath.eu/documents/image/27/277/277-05-2310-21.jpg. (accessed 07/07/16).
18. Microchip: http://images.wisegeek.com/integrated-circuit-on-motherboard.jpg. (accessed 07/07/16).
19. Dental filling: http://atlantacenterforcosmeticdentistry.com/services-we-offer/restorative-services/tooth-colored-fillings/. (accessed 07/07/16).
20. Tripp, E. P.; Weisman, J., *Modern Paint and Coatings* **1982**, 51.
21. Pasternack, G., *Radiation Curing* **1980,** *8*, 14.
22. Fouassier, J. P., *Photoinitiatior, Photopolymerization, and Photocuring*. Hanser/Gardner: **1995**.
23. Davidson, R. S., *Radiation Curing*. RAPRA REVIEW REPORTS: **2001**; Vol. 12.
24. Schnabel, W., *Polymers and Light*. Wiley-VCH: **2007**.
25. Arthur Green, W., *Industrial Photoinitiators: A Technical Guide*. Taylor & Francis Group: **2010**.

26. Moszner, N.; Fischer, U. K.; Ganster, B.; Liska, R.; Rheinberger, V., Benzoyl germanium derivatives as novel visible light photoinitiators for dental materials. *Dent. Mater.* **2008,** *24* (7), 901-907.
27. Husár, B.; Ligon, S. C.; Wutzel, H.; Hoffmann, H.; Liska, R., The formulator's guide to anti-oxygen inhibition additives. *Progress in Organic Coatings* **2014,** *77* (11), 1789-1798.
28. Ligon, S. C.; Husár, B.; Wutzel, H.; Holman, R.; Liska, R., Strategies to Reduce Oxygen Inhibition in Photoinduced Polymerization. *Chem. Rev.* **2014,** *114* (1), 557-589.
29. Schwalm, R., *UV Coatings: Basics, Recent Developements, New Application*. Elsevier Science: **2006**.
30. Liska, R.; Schuster, M.; Inführ, R.; Turecek, C.; Fritscher, C.; Seidl, B.; Schmidt, V.; Kuna, L.; Haase, A.; Varga, F.; Lichtenegger, H.; Stampfl, J., Photopolymers for rapid prototyping. *J. of Coating. Tech. and Res.* **2007,** *4* (4), 505-510.
31. Chandra, R.; Thapliyal, B. P.; Sehgal, B.; Soni, R. K., Studies on the kinetics of photo-initiated radical polymerisation of modified epoxy resin. *Polym. Int.* **1992,** *29* (3), 185-190.
32. Qin, X.-H.; Gruber, P.; Markovic, M.; Plochberger, B.; Klotzsch, E.; Stampfl, J.; Ovsianikov, A.; Liska, R., Enzymatic synthesis of hyaluronic acid vinyl esters for two-photon microfabrication of biocompatible and biodegradable hydrogel constructs. *Polym. Chem.* **2014,** *5* (22), 6523-6533.
33. Colombani, D., Chain-growth control in free radical polymerization. *Prog. Polym. Sci.* **1997,** *22* (8), 1649-1720.
34. Gauss, P.; Ligon-Auer, S. C.; Griesser, M.; Gorsche, C.; Svajdlenkova, H.; Koch, T.; Moszner, N.; Liska, R., The influence of vinyl activating groups on β-allyl sulfone-based chain transfer agents for tough methacrylate networks. *J. Polym. Sci., Part A: Polym. Chem.* **2016,** *54* (10), 1417-1427.
35. Lu, H.; Stansbury, J. W.; Bowman, C. N., Towards the elucidation of shrinkage stress development and relaxation in dental composites. *Dent. Mater.* **2004,** *20* (10), 979-986.
36. Gorsche, C.; Koch, T.; Moszner, N.; Liska, R., Exploring the benefits of β-allyl sulfones for more homogeneous dimethacrylate photopolymer networks. *Polym. Chem.* **2015,** *6* (11), 2038-2047.
37. Sultan, J. N.; McGarry, F. J., Effect of rubber particle size on deformation mechanisms in glassy epoxy. *Polym. Eng. Sci.* **1973,** *13* (1), 29-34.
38. Hillmyer, M. A.; Lipic, P. M.; Hajduk, D. A.; Almdal, K.; Bates, F. S., Self-Assembly and Polymerization of Epoxy Resin-Amphiphilic Block Copolymer Nanocomposites. *J. Am. Chem. Soc.* **1997,** *119* (11), 2749-2750.
39. Liu, J.; Thompson, Z. J.; Sue, H.-J.; Bates, F. S.; Hillmyer, M. A.; Dettloff, M.; Jacob, G.; Verghese, N.; Pham, H., Toughening of Epoxies with Block Copolymer Micelles of Wormlike Morphology. *Macromolecules (Washington, DC, U. S.)* **2010,** *43* (17), 7238-7243.
40. Zhang, H.; Tang, L. C.; Zhang, Z.; Friedrich, K.; Sprenger, S., Fracture behaviours of in situ silica nanoparticle-filled epoxy at different temperatures. *Polymer* **2008,** *49* (17), 3816-3825.
41. Hazot, P.; Pichot, C.; Maazouz, A., Synthesis of hairy acrylic core-shell particles as toughening agents for epoxy networks. *Macromol. Chem. and Phys.* **2000,** *201* (6), 632-641.
42. Szczepanski, C. R.; Pfeifer, C. S.; Stansbury, J. W., A new approach to network heterogeneity: Polymerization induced phase separation in photo-initiated, free-radical methacrylic systems. *Polymer* **2012,** *53* (21), 4694-4701.
43. Jansen, J. F. G. A.; Dias, A. A.; Dorschu, M.; Coussens, B., Fast Monomers: Factors Affecting the Inherent Reactivity of Acrylate Monomers in Photoinitiated Acrylate Polymerization. *Macromolecules* **2003,** *36* (11), 3861-3873.
44. Yakacki, C. M.; Shandas, R.; Safranski, D.; Ortega, A. M.; Sassaman, K.; Gall, K., Strong, tailored, biocompatible shape-memory polymer networks. *Adv. Funct. Mater.* **2008,** *18* (16), 2428-2435.
45. Phelan, M.; Aldabbagh, F.; Zetterlund, P. B.; Yamada, B., Mechanism and kinetics of the free radical ring-opening polymerization of cyclic allylic sulfide lactones. *Polymer* **2005,** *46* (26), 12046-12056.

46. Kharasch, M. S.; Nudenberg, W.; Mantell, G. J., REACTIONS OF ATOMS AND FREE RADICALS IN SOLUTION. XXV. THE REACTIONS OF OLEFINS WITH MERCAPTANS IN THE PRESENCE OF OXYGEN1. *J. Org. Chem.* **1951,** *16* (4), 524-532.
47. McNair, O. D.; Brent, D. P.; Sparks, B. J.; Patton, D. L.; Savin, D. A., Sequential Thiol Click Reactions: Formation of Ternary Thiourethane/Thiol–Ene Networks with Enhanced Thermal and Mechanical Properties. *ACS Applied Materials & Interfaces* **2014,** *6* (9), 6088-6097.
48. Hoyle, C.; Cole, M.; Kuang, W.; Jonsson, S.; Nason, C.; Ishijima, T.; Kess, R.; Viswanathan, K.; Lee, T. Y.; Ng, R.; Miller, C., Photocuring in the presence of oxygen always a consideration. *RadTech Rep.* **2002,** *16* (6), 47-56.
49. Hoyle, C. E.; Lee, T. Y.; Roper, T., Thiol–enes: Chemistry of the past with promise for the future. *Journal of Polymer Science Part A: Polymer Chemistry* **2004,** *42* (21), 5301-5338.
50. Hoyle, C. E.; Bowman, C. N., Thiol–Ene Click Chemistry. *Angew. Chem. Int. Ed.* **2010,** *49* (9), 1540-1573.
51. Cramer, N. B.; Reddy, S. K.; O'Brien, A. K.; Bowman, C. N., Thiol−Ene Photopolymerization Mechanism and Rate Limiting Step Changes for Various Vinyl Functional Group Chemistries. *Macromolecules* **2003,** *36* (21), 7964-7969.
52. Lecamp, L.; Houllier, F.; Youssef, B.; Bunel, C., Photoinitiated cross-linking of a thiol–methacrylate system. *Polymer* **2001,** *42* (7), 2727-2736.
53. O'Brien, A. K.; Cramer, N. B.; Bowman, C. N., Oxygen inhibition in thiol–acrylate photopolymerizations. *J. Polym. Sci. Part A: Polym. Chem.* **2006,** *44* (6), 2007-2014.
54. Becka, E.; Podgorski, M.; Bowman, C. In *Ester-free thiol-X resin: A new material with enhanced mechanical properties*, American Chemical Society: **2015**; pp POLY-518.
55. Esfandiari, P.; Ligon, S. C.; Lagref, J. J.; Frantz, R.; Cherkaoui, Z.; Liska, R., Efficient stabilization of thiol-ene formulations in radical photopolymerization. *J. Polym. Sci., Part A: Polym. Chem.* **2013,** *51* (20), 4261-4266.
56. Moad, G.; Rizzardo, E.; Thang, S. H., Radical addition-fragmentation chemistry in polymer synthesis. *Polymer* **2008,** *49* (5), 1079-1131.
57. Yagci, Y.; Reetz, I., Addition–fragmentation reactions in polymer chemistry. *React. Funct. Polym.* **1999,** *42* (3), 255-264.
58. Moad, G.; Rizzardo, E.; Thang, S. H., Living Radical Polymerization by the RAFT Process: A Third Update. *Aust. J. Chem.* **2012,** *65* (8), 985-1076.
59. Matyjaszewski, K., Atom Transfer Radical Polymerization (ATRP): Current Status and Future Perspectives. *Macromolecules* **2012,** *45* (10), 4015-4039.
60. Park, H. Y.; Kloxin, C. J.; Scott, T. F.; Bowman, C. N., Stress Relaxation by Addition-Fragmentation Chain Transfer in Highly Cross-Linked Thiol-Yne Networks. *Macromolecules (Washington, DC, U. S.)* **2010,** *43* (24), 10188-10190.
61. Gorsche, C.; Griesser, M.; Gescheidt, G.; Moszner, N.; Liska, R., β-Allyl Sulfones as Addition–Fragmentation Chain Transfer Reagents: A Tool for Adjusting Thermal and Mechanical Properties of Dimethacrylate Networks. *Macromolecules* **2014,** *47* (21), 7327-7336.
62. Ligon-Auer, S. C.; Schwentenwein, M.; Gorsche, C.; Stampfl, J.; Liska, R., Toughening of photo-curable polymer networks: a review. *Polym. Chem.* **2016,** *7* (2), 257-286.
63. Meijs, G. F.; Rizzardo, E., Chain transfer by an addition-fragmentation mechanism. The use of α-benzyloxystyrene for the preparation of low-molecular-weight poly(methyl methacrylate) and polystyrene. *Die Makromolekulare Chemie, Rapid Communications* **1988,** *9* (8), 547-551.
64. An, L.; Gao, C.; Yan, X.; Fu, Z.; Yang, W.; Shi, Y., Emulsion polymerization of styrene using irreversible addition–fragmentation chain transfer agents: effect on the course of the polymerization and molecular weight. *Colloid and Polymer Science* **2012,** *290* (8), 719-729.
65. Meijs, G. F.; Rizzardo, E.; Thang, S. H., Preparation of controlled-molecular-weight, olefin-terminated polymers by free radical methods. Chain transfer using allylic sulfides. *Macromolecules* **1988,** *21* (10), 3122-3124.

66. Gorsche, C.; Seidler, K.; Knaack, P.; Dorfinger, P.; Koch, T.; Stampfl, J.; Moszner, N.; Liska, R., Rapid formation of regulated methacrylate networks yielding tough materials for lithography-based 3D printing. *Polym. Chem.* **2016,** *7* (11), 2009-2014.
67. Hutson, L.; Krstina, J.; Moad, C. L.; Moad, G.; Morrow, G. R.; Postma, A.; Rizzardo, E.; Thang, S. H., Chain Transfer Activity of ω-Unsaturated Methacrylic Oligomers in Polymerizations of Methacrylic Monomers. *Macromolecules* **2004,** *37* (12), 4441-4452.
68. Sato, E.; Uehara, I.; Horibe, H.; Matsumoto, A., One-Step Synthesis of Thermally Curable Hyperbranched Polymers by Addition-Fragmentation Chain Transfer Using Divinyl Monomers. *Macromolecules (Washington, DC, U. S.)* **2014,** *47* (3), 937-943.
69. Sato, E.; Zetterlund, P. B.; Yamada, B., Macromonomer Synthesis Using Oligomers of ω-Unsaturated Methacrylate as Addition-Fragmentation Chain Transfer Agents: Increased Efficiency by Manipulation of Steric Hindrance. *Macromolecules* **2004,** *37* (7), 2363-2370.
70. Tanaka, K.; Yamada, B., Reactions of bifunctional addition-fragmentation chain transfer agents for synthesis of polymer bearing unsaturated moieties at both ends. *Macromol. Chem. Phys.* **2000,** *201* (14), 1565-1573.
71. Park, H. Y.; Kloxin, C. J.; Scott, T. F.; Bowman, C. N., Covalent adaptable networks as dental restorative resins: Stress relaxation by addition-fragmentation chain transfer in allyl sulfide-containing resins. *Dent. Mater.* **2010,** *26* (10), 1010-1016.
72. Cramer, N. B.; Bowman, C. N., Kinetics of thiol-ene and thiol-acrylate photopolymerizations with real-time fourier transform infrared. *J. Polym. Sci., Part A: Polym. Chem.* **2001,** *39* (19), 3311-3319.
73. Wei, H.; Senyurt, A. F.; Jonsson, S.; Hoyle, C. E., Photopolymerization of ternary thiol-ene/acrylate systems: film and network properties. *J. Polym. Sci., Part A: Polym. Chem.* **2007,** *45* (5), 822-829.
74. Senyurt, A. F.; Wei, H.; Hoyle, C. E.; Piland, S. G.; Gould, T. E., Ternary Thiol−Ene/Acrylate Photopolymers: Effect of Acrylate Structure on Mechanical Properties. *Macromolecules* **2007,** *40* (14), 4901-4909.
75. Park, H. Y.; Kloxin, C. J.; Fordney, M. F.; Bowman, C. N., Stress Reduction and Tg Enhancement in Ternary Thiol-yne-Methacrylate Systems via Addition-Fragmentation Chain Transfer. *Macromolecules (Washington, DC, U. S.)* **2012,** *45* (14), 5647-5652.
76. Alfrey, T.; Price, C. C., Relative reactivities in vinyl copolymerization. *J. Poly. Sci.* **1947,** *2* (1), 101-106.
77. Yoshimatsu, M.; Matsuura, Y.; Gotoh, K., A Novel 3,4-Bis(sulfenyl)- or 4-Selenenyl-3-sulfenylpenta-2,4-dienylation of Aldehydes Using 4-Ethoxy-1,2-bis(sulfenyl)- or 1-Selenenyl-2-sulfenyl-buta-1,3-dienyl Lithiums. *Chem. Pharm. Bull.* **2003,** *51* (12), 1405-1412.
78. Appleyard, G. D.; Stirling, C. J. M., Elimination-addition. Part XIV. Addition of carboxylate ions to allenes and acetylenes and use of the adducts in acylation. *Journal of the Chemical Society C: Organic* **1967,** (0), 2686-2691.
79. Yonezawa, Y.; Shin, C.-g.; Ono, Y.; Yoshimura, J., Dehydrooligopeptides. I. The Facile Coupling of α-Amino Acids with α-Dehydroamino Acids to Dehydrodipeptides. *Bull. Chem. Soc. Jpn.* **1980,** *53* (10), 2905-2909.
80. Brandrup, J., *Polymer handbook*. Wiley: New York, **1999**; Vol. 4.
81. http://emea.sartomer.com/en/products/acrylates/acrylate-monomers/. **08/03/2016**.
82. Winter, H. H.; Chambon, F., Analysis of linear viscoelasticity of a crosslinking polymer at the gel point. *J. Rheol. (N. Y.)* **1986,** *30* (2), 367-82.
83. Yoon, N. M.; Choi, J.; Ahn, J. H., Convenient Synthesis of Phenyl Sulfides by a Borohydride Exchange Resin-Phenyl Disulfide System in Methanol. *J. Org. Chem.* **1994,** *59* (12), 3490-3493.
84. Russell, G. A.; Ngoviwatchai, P.; Wu, Y. W., Electron-transfer processes. 46. Allylic and propargylic substitution reactions involving radicals generated from alkylmercury halides. *JACS* **1989,** *111* (13), 4921-4927.